CR-1999-209487

THE U.S. SPECTRUM X GAMMA COORDINATION FACILITY

NASA Contract NAS5-32779

Final Report

For the Period 11 October 1994 through 30 April 1999

Principal Investigator

Dr. William R. Forman

August 1999

Prepared for:

National Aeronautics and Space Administration
Goddard Space Flight Center
Greenbelt, MD 20771

Smithsonian Institution
Astrophysical Observatory
Cambridge, Massachusetts 02138

The Smithsonian Astrophysical Observatory
is a member of the
Harvard-Smithsonian Center for Astrophysics

Contents

List of Figures

1 Spectrum X Gamma Observatory

Spectrum-X-Gamma (SXG) provides for US participation in a first-class international x-ray mission. Despite launch delays, SXG will provide unique scientific opportunities due to its capability for all-sky monitoring, polarimetry, high resolution spectroscopy, and broad wavelength range – from the ultraviolet (TAUVEX and FUVITA), through the x-ray (SODART and JET-X), to the hard x-ray (MART), and gamma-ray burst detectors. Before describing our completed work, we review the unique properties of SXG and the provide some examples of the scientific importance of SXG in the Chandra, XMM, and ASTRO-E era.

1.1 US Participation and Mission Status

The US participation in the mission includes both instrument development and data rights. The US provided instruments are the Stellar X-ray Polarimeter (SXRP) and Monitoring X-ray Experiment (MOXE), an all-sky monitor. Also, the US has agreed to provide equipment for archiving the data for both Russia and Denmark, in exchange, for shares of the observing time from both these countries.

While the SXG launch has been delayed due to unexpected funding difficulties, progress has continued. There is modest Russian funding for the project, and present work in Russia includes completion of the engineering mock-up of the spacecraft by the end of this year. It is also planned to begin tests of the electric, telemetry, and command interfaces of the spacecraft and scientific payload. The sub-contractors are working on the production of the parts of the flight spacecraft.

1.2 Unique Features of SXG

The key feature of SXG is the large area SODART telescope (see Fig. 1). SXG is equipped with a pair of approximately 1000 cm^2 telescopes having moderate angular resolution (HPBW= 2′) with large 1°FOV's. The telescopes are deployed in space, using a jack-knife mechanism, to produce an 8m focal length optical system with subsequent good efficiency at high x-ray energies.

The uniqueness of SXG derives from its instrument complement which allows broad wavelength coverage from the UV (TAUVEX at 3000Åwith 6-8 arc-sec resolution) to hard X-rays (MART up to 150 keV with $\sim$ 0.5°angular resolution). The instruments operate simultaneously and hence provide multi-wavelength observations over a broad wavelength band. In addition, the high earth orbit targeted for the observatory will provide long continuous viewing, critical for studying source variability over periods of hours to days.

Individual instruments provide further unique capabilities. In particular, the US-provided Stellar X-ray Polarimeter (SXRP) can perform sensitive polarimetric observations of both galactic and extra-galactic objects at energies of $E = 2.6$ and 5.2 keV, using a thin graphite crystal, and at energies above 5 keV, using a metallic lithium target. It is the first x-ray polarimeter scheduled to fly on a long-lived space mission and the only polarimeter planned in the near future. It will be used extensively in studying x-ray polarization of galactic X-ray binaries as a function of pulse and binary phase.

Another unique instrument is the Silicon X-ray Array (SIXA) which can obtain temporally resolved ($\delta t = 12 \times 10^{-6}$ sec) spectra of bright (several times the Crab) galactic sources with CCD-like energy resolution ($\sim$ 200 eV). The Joint European X-ray Telescope (JET-X) provides another

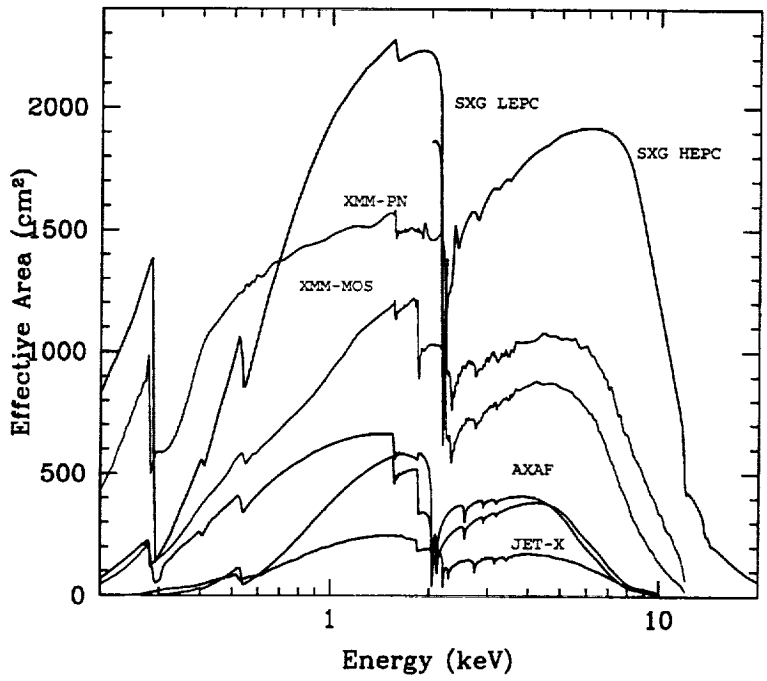

Figure 1: A comparison of the major missions and typical instruments is shown. The large area of SODART is apparent compared to ROSAT, ASCA, and Chandra. The XMM effective areas shown are for a single XMM telescope, with either the PN or MOS cameras. Including all XMM telescopes gives a total imaging effective area approximately 70% larger than that shown, comparable to SXG.

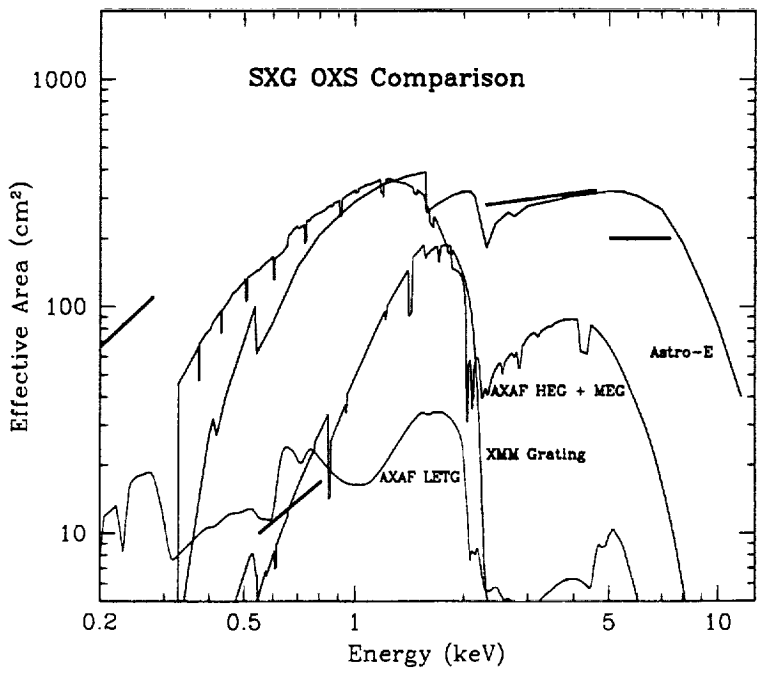

Figure 2: The effective area of the OXS is compared to other instruments. Although the OXS requires multiple observations to cover a given wavelength region, its large FOV compensates for this relative inefficiency when mapping limited energy bands (e.g., iron line) over solid angles of order 1 square degree.

unique capability. Jet-X is an entire separate telescope system, built by UK and Italy, with CCD detectors similar to those on XMM. Above 2 keV, JET-X has an effective area at least 30% that of Chandra, with a modest angular resolution of 20″ over the 40′ diameter FOV.

High resolution spectroscopy aboard SXG is provided by the Objective X-ray Spectrometer (OXS), a front-mounted panel of Bragg crystals optimized for spectroscopy in four narrow energy bands. This spatially resolved high resolution spectroscopy capability is significant, even in light of the capabilities of the Chandra, XMM, and ASTRO-E spectrometers (see Fig. 2 for a comparison of OXS with these instruments). The unique feature of the OXS is its ability to yield spatially resolved high resolution spectra (albeit in narrow energy bands) over a large field of view. For large, low surface brightness extended sources, e.g. clusters and supernova remnants, the Chandra and XMM gratings cannot yield model-independent high resolution spectra for the entire field. ASTRO-E does provide such a capability and has the advantage that the entire spectrum is observed simultaneously. However, for some applications (see sections 1.3.2 and 1.3.3 below) , the large FOV of the OXS compensates for the multiplexing capability of ASTRO-E. Finally, ASTRO-E has no capability at the lowest energies. In conclusion, for extended sources, the OXS complements the capabilities of the other major observatories, and is unchallenged at the lowest energies.

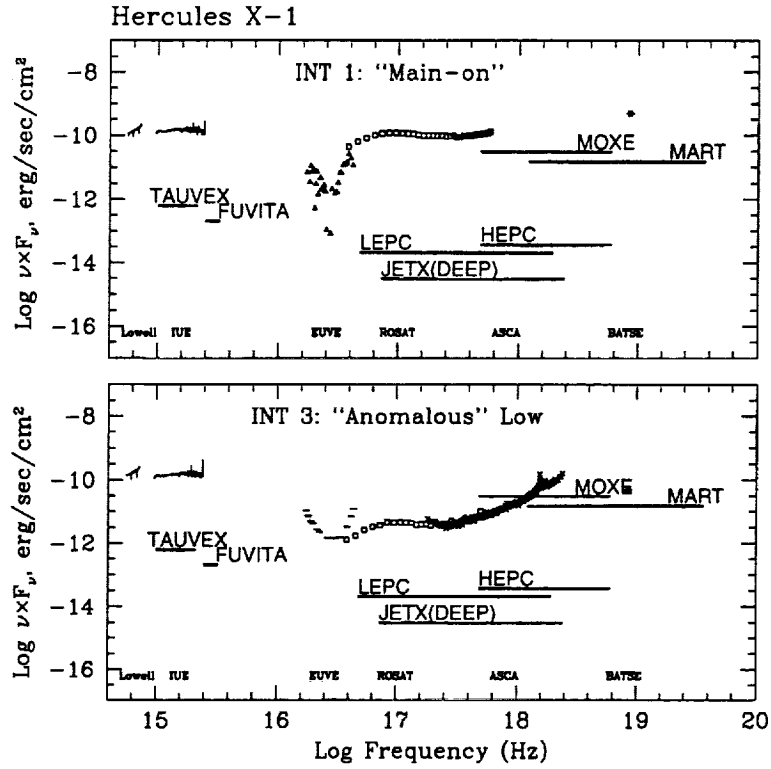

Figure 3: The sensitivities of the SXG instruments is compared to the observed spectra of Hercules X-1. The SXG instruments have the sensitivity to easily study many galactic sources as well as the brighter extra-galactic sources.

1.3 SXG Fundamental Science Capabilities

In this section we describe three of the unique science capabilities which SXG provides. We discuss simultaneous broad band studies, X-ray polarimetry, and high resolution spectroscopy as applied to clusters of galaxies.

1.3.1 Simultaneous Multi-wavelength Observations

One key approach to understanding the complex behavior of both galactic and extra-galactic compact objects and their surrounding accretion disks is simultaneous, multi-wavelength monitoring. Fig. 3 shows the results of such monitoring for Hercules X-1 (Vrtilek et al. 1994; ApJ, 436, L9), but the arguments apply equally well to extra-galactic objects, although they are significantly fainter.

On the most fundamental level, broad band monitoring will enable us to understand the origin of the different spectral components arising from compact objects. By observing time delays as a function of wavelength we can learn how energy is processed from one band to another. We can understand the origin of the components by understanding the importance of re-processing, Compton up-scattering, and disk viscosity in producing the overall observed spectrum.

Other scientific goals of long term, broad band monitoring are the behavior of the gravitational

and Doppler broadened iron K-alpha line from black holes (e.g., MCG 6-30-15) and the pulse and long term behavior of galactic sources (e.g., Her X-1).

SXG is ideally suited to these types of studies because of its instrument complement and high earth orbit. The instrument complement provides broad wavelength coverage from almost the optical to the hard X-rays. The high earth orbit allows long uninterrupted views to determine the detailed variability behavior as a function of wavelength. The sensitivities of the SXG instruments are shown in Fig. 3, and indicate that SXG can extend broad band monitoring capabilities to sources 2–4 orders of magnitude fainter than Her X-1.

1.3.2 High Resolution Spectroscopy of Cluster Mergers

One of the exciting discoveries from combined ROSAT and ASCA X-ray observations was that the effects of cluster formation can be seen both in the surface brightness distributions of clusters and in their temperature maps. For example, Fig. 4 shows the ASCA temperature map of the cluster Cygnus A (provided by M. Markevitch) in color, with the ROSAT surface brightness map superposed (solid contours). One sees both the distorted surface brightness distribution with a second peak to the north-west of the main cluster and a hot (red) shocked region between the two surface brightness maxima.

Study of these mergers in X-rays is perhaps the approach to understanding the physics of the virialization process as small scale systems merge to form clusters. Large merger events such as that shown for Cygnus A are remarkably energetic. In fact, *massive mergers are the most energetic events in the Universe since the Big Bang*, dissipating $\mathbf{10^{63-64}}$ ergs. By studying in detail the hot gas, the dominant baryonic component in clusters, we can map the dark matter distribution and better understand how energy is distributed among the mass components.

The OXS is the best instrument available to study the detailed merger process. With its large FOV, it can readily map an entire cluster like Cygnus-A to measure line widths and velocity shifts around the strong 6.7 keV iron line complex. For comparison, Fig. 5 shows the expected ASTRO-E iron spectrum of a typical $2' \times 2'$ region of Cygnus-A for a 100 ksecond observation. With a field of view of only 8 square arc-minutes, over 100 separate ASTRO-E pointings would be required to map the interesting dynamics of just this one cluster. This would require roughly 2/3 of a year (given the 50% efficiency of ASTRO-E's low earth orbit), occupying a full 30% of the expected 2 year lifetime of ASTRO-E's microcalorimeter. The OXS, however, with comparable effective area to ASTRO-E's microcalorimeter (see Fig. 2), could step through the energy band covering the iron line emission in roughly 20 energy steps (concentrating on the regions around the strong lines) in just 4 weeks.

The ASTRO-E microcalorimeter and OXS provide complementary capabilities. ASTRO-E provides a broad band spectrum over a small solid angle, while the OXS covers a larger solid angle, but only over a limited wavelength band. Both capabilities are required to fully understand the formation of large scale structure and spectacular cluster mergers.

1.3.3 Large Angular, High Resolution Spectroscopy Investigations

As noted above, the key capability of the OXS is large solid angle studies over a limited energy band. Other investigations require such a capability. For example, the OXS, with its unique low energy response (see Fig. 2) can spatially resolve cluster cooling flows to detect cooling gas in the

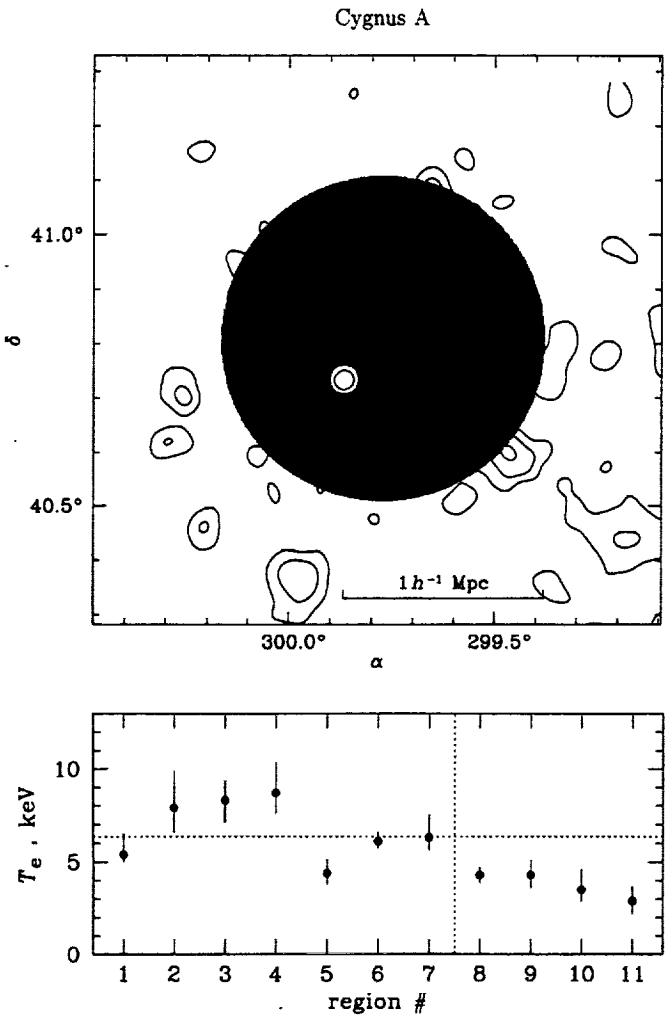

Figure 4: The ASCA temperature map (color) with the ROSAT surface brightness superposed shows the need for mapping the entire $0.5 \times 0.5°$cluster to understand the physics of cluster mergers and the virialization process. The hot (red) gas is seen lying between the two surface brightness peaks. Together the surface brightness and temperature maps suggest that the north-west surface brightness peak is falling into the main cluster and that the merger has shock heated gas lying in front of the in-falling sub-cluster. The lower portion of the figure shows the numerical values of the best fit temperatures in each cluster region.

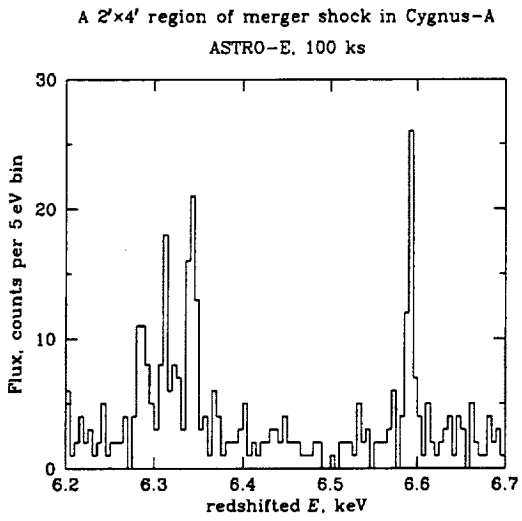

Figure 5: Simulated iron line spectrum for a $2 \times 2'$ region of Cygnus-A as observed with ASTRO-E for 100 ksec. Covering the entire 0.5×0.5 sq. deg. cluster would require approximately 2/3 of a year. Alternatively, one could observe the entire cluster, 100 times the solid angle by stepping through the iron line energy band with the OXS in 20 energy steps of 100 ksec each in about 1 month.

inhomogeneous intra-cluster medium. For Perseus, the brightest nearby cluster, with a cooling radius of $r_{cool} = 5'$, one could determine the location of the coolest components and possibly determine the fate of the cooling gas. The OXS can use clusters as background sources and map the cool gas in cluster outskirts to determine the baryon fraction in the Universe, map the gas in filaments around clusters to study the effects of large scale structure on the growth of collapsed systems, and find/detect the "missing" baryons, expected to be "warm" which are predicted to exist from Big Bang nucleosynthesis calculations, but are not yet observed.

One particularly interesting application of the OXS is to map a many square degree region around our own galactic center in the energy band around the 6.4 keV iron fluorescent line. This allows one to determine the activity history of the black hole in the Galactic Center (as suggested by Sunyaev and collaborators). Thus, one could for the first time perform "astroarchaeology" of our own central black hole.

1.3.4 Polarimetry with SXG

The Stellar X-ray Polarimeter (SXRP) allows sensitive polarimetric observations of compact X-ray sources, both galactic and extra-galactic (see Fig. 6).

Sensitive polarimetry of black hole disks (e.g., Cyg X-1) can differentiate between emission from the optically thick outer region of the disk (emission polarized parallel to the plane of the disk) and emission from the optically thin inner region (polarized perpendicular to the plane of the disk). Polarization measurements can be used to determine the viscosity parameter in the disk.

For X-ray pulsars (e.g., Cen X-3 and Her X-1), polarization observations can differentiate be-

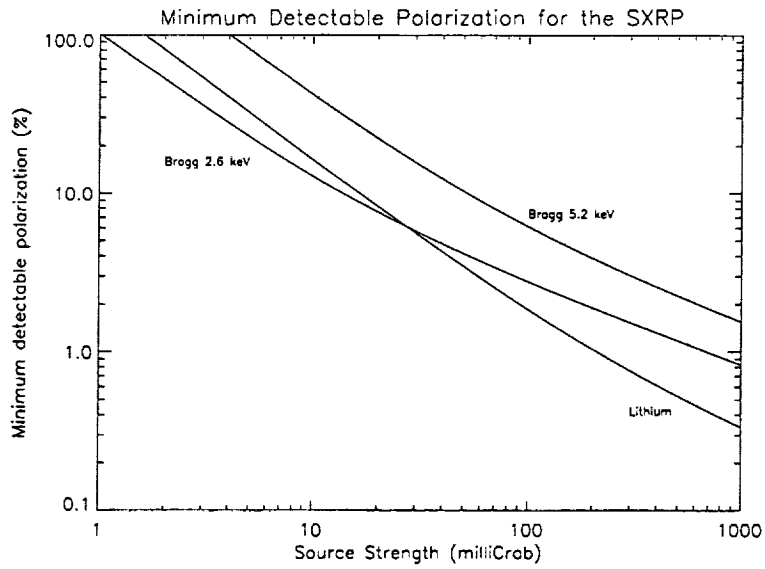

Figure 6: Sensitivity for SXRP for the two Bragg energy bands and for the Lithium crystal (> 5keV) for a 100ksec observation. SXRP allows polarization measurements of galactic sources (at the 1% level in 100ksec). In 100ksec, 10% polarization can be detected for the brighter extra-galactic sources. For bright, compact, galactic X-ray sources, polarizations can be measured as a function of pulse and binary orbital phases.

tween different beaming models. A fan beam is produced when matter falls onto the magnetic pole in an accretion column while a pencil is produced as matter falls onto the magnetic pole along the stellar surface (i.e., slab accretion geometry). These two different models yield quite different polarization signatures as a function of pulse phase.

These fundamental investigations of collapsed objects are only possible with the SXRP on SXG. No other missions are planned to carry out X-ray polarimetry.

2 Activities for US Observers

In this section we summarize our accomplishments and progress in supporting US observers in preparing proposals and deriving the capabilities of the SXG Observatory.

2.1 WWW Site

We have established a WWW site

`http://hea-www.harvard.edu/SXG/sxg.shtml`

where observers can obtain current documentation on SXG instruments, scientific programs of SXG institutions, useful software for preparing SXG proposals and analyzing SXG data, and calibration data needed for estimating SXG count rates and spectra.

The WWW site includes a searchable index to support interested users and links to all other participating institutions. The site points to tools developed by others that are of general interest and contains simple on-line programs in support of AO preparation (see below).

Various standard software tools are on-line to support users. For example, we provide an on-line version of PIMMS (Portable, Independent, Multi-Mission Simulator developed by HEASARC) with current versions of effective areas for the SXG instruments. In addition, the SXG WWW site points to generally useful tools (e.g., *IRAF*, *XSPEC*, *SAOtng*) for X-ray data analysis.

We have maintained links to the SXG participating institutions with their own WWW sites.

2.2 Calibration Data

We have collected telescope/instrument effective areas for SODART, HEPC, LEPC, OXS, SXRP, and SIXA, and made them available both on our Web site and through anonymous-ftp. We have also delivered the data to HEASARC for incorporation in the official PIMMS distribution.

We have collected predicted instrument background rates and response matrices. The response matrices have been converted to *XSPEC* (standard HEASARC spectral fitting program) format. Directions for generating simulated spectra have been prepared and are part of the AO. Needed software and response files are available over the WWW and via anonymous ftp.

2.3 AO Materials and Activities

The Spectrum X Gamma Announcement of Opportunity was prepared and submitted to NASA Headquarters (see attached). In addition, the Technical Appendix to accompany the AO was prepared and thoroughly proofed. The AO materials include flux conversions, observation windows and sensitivity calculations. It was reviewed by DSRI staff and formed the basis of the current DSRI observatory guide.

We worked with the Russian team to define the merging process for US observations with overall SXG program. Also, we developed a draft proposal for allocation of secondary time. This gives the US additional data from the SODART telescope when the observatory pointing is controlled by another telescope (e.g., JET-X).

We have developed and tested a simple e-mail-based electronic proposal submission system, including a web-based interface. To assist scientific planning, the SXG Electronic Proposal Ingestion Software was thoroughly tested and debugged. A WWW interface to that software was added. The system was deliberately flooded with several hundred mock proposals submitted from a remote site in rapid succession. We verified that our software was able to sustain this load, parse the proposals, and populate the database. With minor modifications, this package has been adopted for use at the Danish Space Research Institute (DSRI).

We have acquired the target visibility program for SXG from the JET-X project. We currently do not plan to make this tool widely available, but have provided figures showing regions of the sky that are available for each month of the year. Similar plots are available for viewing with the OXS which views the sky in a direction perpendicular to the pointing direction of the JET-X and SODART telescopes. A newly available tool which we have tested has been made available by IKI via the WWW. At present it is rather slow and we plan to look into 1) improving the performance of this program and 2) providing a mirror site here in the US.

Table 1: Hardware Components of the IKI Archive

Archive Component	Major Hardware Elements
Archive Generation	Computers, CD Writers, Disks
Archive Software	Server, Computers, Disks
IKI On-line Storage	Servers, Disks, Jukeboxes
Ancillary Data	Computer, Disks
On-line Catalog	Servers, Disks
Calibration Data Archive	Computers, Disks, CD Writer, Jukebox
Test and Development	Computer, Disk
Firewall Protection	Computers, Disks, Routers
Archive Network Management	Computer, Disk, Ethernet Switch

Finally, we have discussed with IKI detailed mechanisms for allocating collaborative US/IKI observing time. Our discussions have resulted in an increase in time available to US observers for selecting targets, with such observations being the focus of collaborative studies with Russian scientists. Fostering such collaborations is a primary goal of the US SXG program.

3 Support to Archive and Software Development

One of the key elements in SXG is the US support for data archives at IKI (Space Research Institute, Moscow) and computer support at DSRI (Danish Space Research Institute). In exchange for this archival support, the US receives the Russian and Danish archival data which comprises the vast bulk of the mission data. This final agreement arose during discussions at the Moscow manager's meeting (1995). It was agreed that the US will receive the entire Russian share of the SXG data. This includes Tauvex, JET-X, EUVITA, and MART-LIME.

One key feature of the archive development to date has been hardware compatibility between DSRI, IKI, and the SXGCF. With compatible computers (SUN workstations) it has been agreed to share all software in common. Hence, the US receives an important added benefit in the assured accessibility of software developed at IKI and DSRI. The detailed activities completed to support development of the archives are described below.

3.1 IKI Archival Hardware

In support of development of a scientific archive at IKI, we have helped to define the hardware needed to support the establishment of a scientific archive which can provide access to scientific users. We purchased and tested a set of computer hardware suitable for a prototype archive system. One feature of our approach has been to ensure that the US and IKI

The procurement of IKI archive hardware has been a continuing major activity during the first phase of the project The components of the archive were defined during a visit by W. Forman to Moscow and in collaboration with E. Churazov and M. Gilfanov. Subsequently, SAO hosted the visit of M. Boiarskii to the US to define the actual hardware elements that will comprise each component. The archive cost as defined below remains fully within the budget allocated by NASA for the archive. Table 1 lists the archive elements.

The hardware components were procured and shipped in three separate installments. The first order was purchased and shipped to IKI with the assistance of the Smithsonian Office of International Affairs (Dr. L. Hirsch, SI Washington) and the US State Department (Dr. M. Pifer) in conjunction with the June 1995 Gore-Chernomyrdin meeting before the official protocols allowing duty-free shipping were signed. This shipment included approximately $100K of hardware. Major components included: printer, 100 CD Jukebox, CD recorder (with blank CDROM's), Pentium PC, Tape backup unit (with tapes), disks, 3 computers, and 1 X-terminal. As part of this hardware shipment to IKI, we worked with the Smithsonian Office of International Affairs and the Department of State to prepare material for the Vice President's visit to Moscow which was used by the President's science advisor, Dr. John Gibbons, in his statement at the ceremonies concluding the visit to Moscow.

Remaining components of the archive, allowing prototype development for all archive subsystems, were all shipped successfully to Moscow through the US Embassy with the help of the NASA representative.

3.2 DSRI Hardware Procurement

In addition to support for IKI, we have purchased 4 SUN SPARC computers and a CD writer for DSRI as part of the US/Danish collaboration. This hardware was successfully shipped to DSRI. As with IKI, DSRI has purchased SUN workstations which are in use at SAOcf and hence all DSRI software will also be fully compatible with hardware at SAOcf.

The CD writer, purchased from Young Minds in California, is not functioning properly. We have been assisting DSRI in resolving the problem. Initially, it was believed that the model of the CD writer purchased purchased for DSRI would only write on a particular brand of CDROM. That brand was unavailable in Denmark and we searched for a dealer locally. Several samples were obtained and provided to DSRI. Unfortunately, these new CDROM's did not resolve the issue. Young Minds has agreed to replace the CD Writer which appears to be defective and we are assisting DSRI in the exchange.

3.3 Software Development Support

As mentioned in Sec. 2, we have provided support for spectral analysis of SXG data with *XSPEC*, the most widely-used x-ray spectral analysis program. We have also identified a number of other existing software tools that can be used for SXG data analysis, and have developed a prototype interface for some of them to the existing and popular image display program *SAOtng*. For example, The *ZHTOOLS* analysis toolkit, developed by A. Vikhlinin for JET-X data analysis, contains a number of generally applicable x-ray spatial and spectral analysis tools, which we have researched extensively. We have developed *SAOtng* interfaces to *ZHTOOLS* tasks for smoothing, radial profiling and image statistics. Our results are displayed in Fig. 7. Additional tools have been identified through our monitoring of the software development efforts of other x-ray astronomy groups such as the Chandra Science Center, HEASARC, and BeppoSAX, as well as individual developers. Examples of *SAOtng* interfaces to a number of tools useful for x-ray image background estimation are shown in Fig. 8.

Our goal is to provide an image-oriented analysis package built around *SAOtng* and incorporating existing analysis tools, which can be used both for quick quantitative assessment of archival data by archival researchers as well as detailed analysis of SXG data by US guest observers.

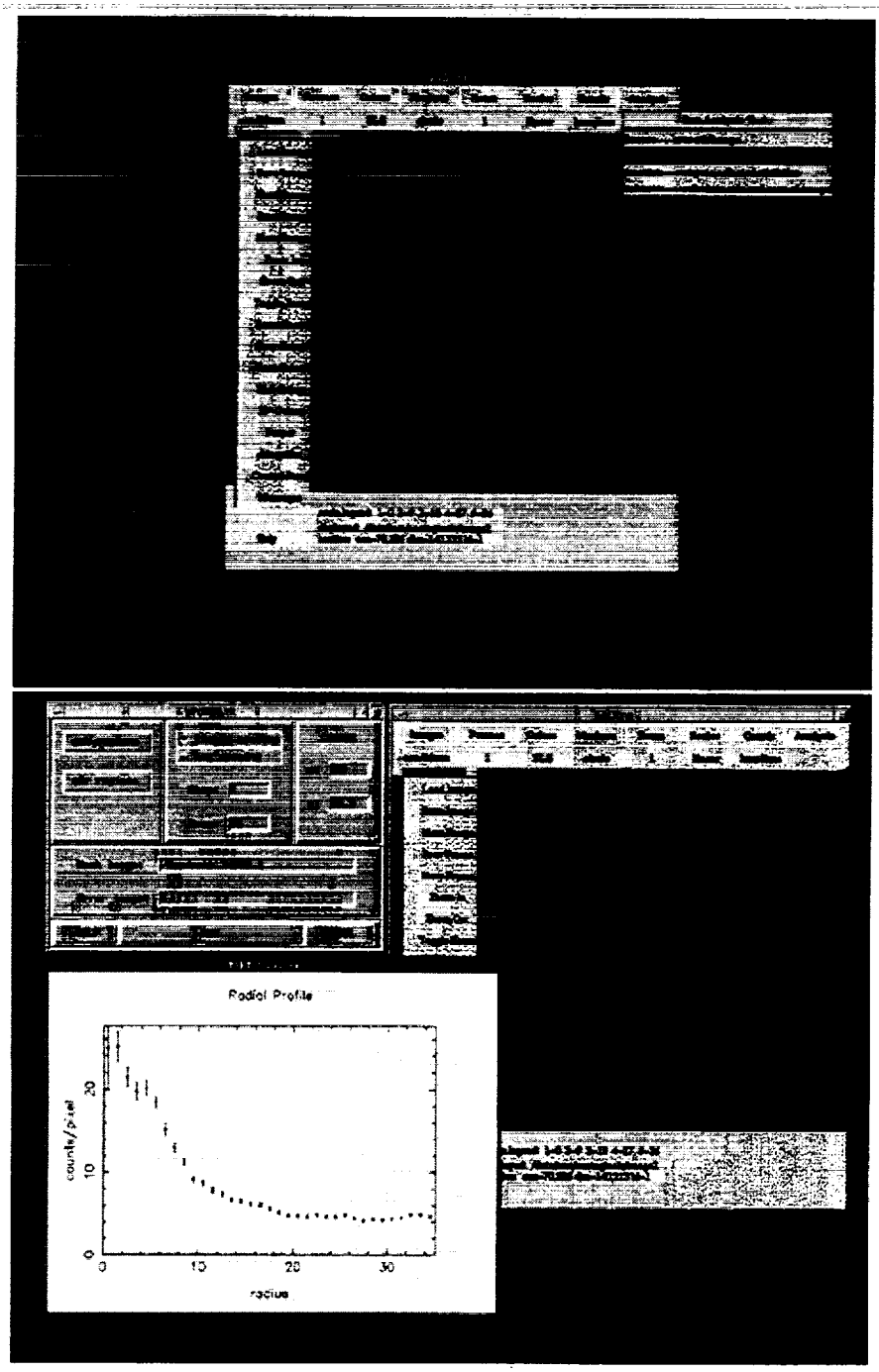

Figure 7: The merging of image processing/display and scientific analysis tools. The first figure shows a menu of several analysis tasks e.g., smoothing, generating a radial profile. The second panel shows the setup window after the radial profile option has been selected as well as the resulting profile for an extended source which is generated from the graphically selected region and user-defined radial bins.

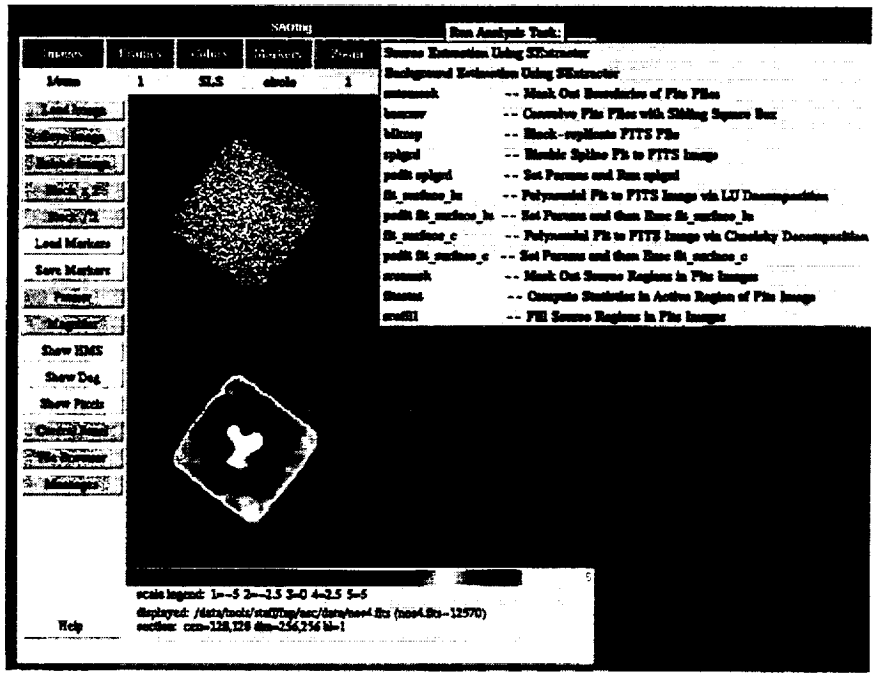

Figure 8: An *SAOtng* interface to tools useful for background estimation in x-ray images. The tools include the optical source extraction code *SExtractor* (Bertin & Arnouts 1996, A&AS, 117, 393), as well as a number of tools developed for the CSC, all of which can be executed by *SAOtng*. The upper panel displays a simulated Chandra HRC image. The lower left displays the fitted background, using the *fit_surface_lu* task, and the lower right panel displays the residuals. All three panels have the same scale and colormap.

4 Support to Spectrum X Gamma Project

We have supported NASA by reviewing drafts of agreements and protocol statements. For example we reviewed the Astrophysics MOU for the US Russia Executive Joint Working Group and commented on the SXG Implementing Agreement in relation to scientific issues and access to data. We reviewed and provided inputs to the Gore-Chernomyrdin Goals/Objectives statement as related to Spectrum X Gamma.

Throughout the project, we have supported the Spectrum X Gamma Project by attending and organizing meetings.

In November 1994, we hosted a visit by DSRI which included discussions of plans for the development and operation of the US SRG coordinating facility, archiving method (for the SRG data) defined, availability of archiving software/procedures, CD-ROM writing/archiving, implementation of the Danish RDF format in PROS, NASA support to DSRI (hardware/software), choice of common Raw File Format for the US instruments on board SRG. As an outgrowth of the meeting, DSRI agreed to use CDROMS for archiving purposes and use of common software tools for data analysis.

Meetings we have supported include the ISC meetings in London (September 1995) and Zurich (May 1996). In Zurich, we presented the planned use of CDROM's to archive the "raw" data. The CDROM's will be supplied by NASA and IKI will generate two copies of the data on CDROM's to ensure a secure archive. We supported the TIC meeting in Helsinki (December 1994).

We organized and hosted the October 1995 meeting of the SXG Technical Interchange Committee (TIC), the technical arm of the SXG International Science Committee (ISC). This Ninth TIC Meeting included visitors from Italy, UK, Russia, and Hungary. The US team provided demos of SAO developed tools.

We supported the 1996 June 17/18 Data Center Meeting organized by HEASARC. We presented our plans for utilizing software developed by others and storing data in FITS format with ASCII data bases. More importantly we familiarized ourselves with activities of other groups – especially HEASARC and SAX.

At the request of the TIC chairman, A. Hornstrup, we organized an in-flight calibration meeting (March 1997) involving all the SXG instruments. Representatives from a half dozen countries attended. In addition to making arrangements for all visitors, we also organized a panel of external reviewers to examine the in-flight calibration plans for each instrument. The goal is to have a complete calibration, but at the same time, hold to a minimum the total calibration time which otherwise will subtract from the available scientifically useful observing program.

On April 7-8, 1998, we attended a MOXE Software Review at LANL. The purpose of the review was to determine the status of all components of MOXE software and develop plans for completing those parts not yet done. Of particular interest to SAO were LANL plans to create two archive data paths, one delivering short-term results to SAO, and a second delivering a longer term archive to HEASARC. Both SAO and HEASARC representatives at the review felt that the two-archive approach was a duplication of effort, and recommended rather that SAO and HEASARC jointly develop a plan for a single archive that maximized scientific usefulness while minimizing duplication. SAO will be the point of contact with MOXE for this effort. This plan will be part of the overall Data Management Plan discussed below.

As part of work on the TIC, we have provided inputs as required. For example, we reviewed and commented on the file formats and data products as proposed by instrument teams and the

TIC. We have made available, to DSRI, the Optical and Infrared Division generated database - STARBASE.

We attended the Nordic Symposium on "The use of SRG and INTEGRAL" (September 14-16, 1997) to discuss the scientific uses of SXG in the context of the Chandra and XMM missions. The unique features of SXG were emphasized. A communique to then Prime Minister Chernomyrdin was prepared requesting support for an early launch of SXG.

5 Conclusion

SXG remains a viable mission despite its delays. Even in the era of Chandra, XMM, and ASTRO-E, SXG provides some unique capabilities as well as much-needed reserve observing capacity for these heavily over-subscribed missions. Much progress has been made on collaborative approaches to archiving, software development, and analysis tools for SXG. AO materials have been prepared and agreements reached on time allocation and procedures for secondary time utilization. The launch of SXG will provide US investigators both unique capabilities and opportunities for international collaboration.

A SXG Research Announcement

RESEARCH ANNOUNCEMENT

SPECTRUM-X-GAMMA
(SXG)
GENERAL OBSERVER PROGRAM

Cycle 1

DRAFT June 26, 1998

June 1998 Rev 1.1

Contents

A Spectrum-X-Gamma Program Description

A.1 Overview

Spectrum-X Gamma (SXG) is a large, satellite-borne astronomical observatory, with scientific instrumentation spanning the energy range from extreme ultraviolet to gamma-ray. It is being developed under the auspices of the Russian Space Agency, with instruments contributed by research groups in a number of European countries and the US. The estimated launch date is June, 2000.

One of the main pointed instruments on-board SXG is SODART, a moderate spatial resolution, high-throughput x-ray telescope. Through bilateral agreements with the Russian Space Research Institute (IKI) and the Danish Space Research Institute (DSRI), a limited amount of observing time from SODART will be made available to US observers, both directly and through collaborations with observers at IKI and DSRI. This NRA solicits proposals for such observations, to be carried out during the first year of SXG operation.

A.2 Instrument Description

The SODART system consists of twin, co-aligned, thin-foil, high-throughput x-ray telescopes, FM1 & FM2. Each telescope has a spatial resolution of $\sim 3'$ (HPD) and an on-axis effective area of $\sim$800 cm^2 at $\sim$6 keV. FM1 and FM2 operate independently, and are each supported by four focal plane instruments mounted in movable sleds.

The instrumentation includes three imaging proportional counters – the Low Energy (0.2 – 8 keV) Proportional Counter (LEPC) and High Energy (2 – 25 keV) Proportional Counter (HEPC), developed by DSRI, and the Focal Plane X-ray Detector (FRD), a $\sim$2 – 25 keV detector developed by IKI. These detectors will be useful for joint spatial/spectral studies of extended sources such as clusters of galaxies. They offer an overall spatial resolution of $\sim 3'$ (limited by the telescopes) and spectral resolution ranging from $\sim$33% at 1 keV to $\lesssim$10% at 20 keV. LEPC, HEPC, and FRD detectors are available for both FM1 and FM2.

Higher-resolution spectroscopy may be accomplished with the Silicon X-ray Array (SIXA), an array of 19 solid state detectors, each similar to the Einstein SSS, arranged in a hexagonal pattern. SIXA is sensitive to x-rays from 0.5 – 20 keV and has an energy resolution of $\sim$3% at 6 keV. Since each array element corresponds to a single pixel with a diameter of $\sim 4'$, SIXA is more appropriate to studies where detailed spatial information is not required. Examples include, but are not limited to, spectroscopic studies of isolated point sources or large extended sources including nearby clusters of galaxies and supernova remnants. SIXA is part of the focal plane instrumentation for FM1.

X-ray polarization studies of bright, accretion-powered x-ray sources, radio pulsars, and supernova remnants may be carried out with the Stellar X-Ray Polarimeter (SXRP), developed by Columbia University. SXRP is part of the focal plane instrumentation for FM2.

Finally, the Objective Crystal Spectrometer (OXS) may be maneuvered in front of FM2. The OXS is a large, flat Bragg crystal panel that will allow high-resolution spectroscopy ($E/\Delta E \sim 100 - 1000$) in four energy ranges, from 0.2 – 0.285 keV, 0.6 – 1.2 keV, 2.5 – 5.0 keV, and 5.0 – 10.0 keV. The OXS is intended for mapping spectral line emission in extended sources. The OXS is developed by DSRI, the Max-Planck-Institut für Extraterrestrische

Physik, Aussenstelle Berlin, and IKI.

Additional details about the SODART instrument may be found in the SXG SODART Observer's Guide, available via the World-Wide Web, from the US SXG Coordination Facility (SXGCF) at SAO (**http://hea-www.harvard.edu/SXG/sxg.shtml**).

A.3 Mission Operation

SXG will be placed into Earth orbit by a Russian Proton-2 launch vehicle. The initial orbit will be highly eccentric, with a 4 day period, ~500 km perigee, and ~200,000 km apogee. Useful x-ray observing time will be ~3 days per orbit. Circularization of the orbit will lead to an ~40,000 km perigee after 2 years.

After the various operational and viewing constraints are taken into account, it is expected that ~80% of the sky will be accessible at any time. However, there will be a region of the sky never accessible to SODART. This region will be $\sim 30^\circ \times 30^\circ$, and will change slightly as the orbit evolves. It will be located at $-40^\circ \leq \delta \leq -10^\circ$, and, depending on the choice of launch parameters, may be placed at any Right Ascension.

SXG operations will be managed by the Lavochkin Association, Moscow, and IKI. There will be one ground station contact every 18 to 30 hours, with a maximum of 10 separate pointings between contacts. However, fewer pointings between contacts are anticipated during the first months of operation. In addition, there will be a limited ability to execute raster scans during single pointings. It is expected that the absolute pointing accuracy will be $\lesssim 2'$ in R.A. and Declination, with a pointing stability of $\pm \sim 2.5''$ per minute. The accuracy of the reconstructed attitude solution will be $\lesssim 35''$.

After ground station capture, data will be transmitted to IKI for processing and distribution. Observation data products will include instrument science and engineering data sets, satellite orbital elements, attitude solution, instrument command timeline, and a sub-set of the spacecraft engineering data relevant to the instrument in question. Data products will be provided in FITS format. Observers can expect to receive their data within ~3 weeks of the observation. Data will be distributed to US observers by the SXGCF. After one year, the data will be transferred to a public archive, created and maintained by the SXGCF.

A.4 Summary of Proposal Policies

SXG observing time is divided into two categories - primary and secondary time. During primary observing time, the observer's target(s) and choice of instruments determine the pointing direction of the entire observatory. During secondary time, the observatory pointing direction is determined by another instrument, but the secondary observer has access to the data of a non-controlling instrument. For the US, primary and secondary observing time comes in two "flavors". The first is US-only time and the second is collaborative time in which the observations and analyses are carried out with Russian SXG colleagues.

A.4.1 Prime Observing Time - US Only and Collaborative

The US has been alloted 2.5% of the primary time available to SODART using both SODART telescopes. Since the total SODART time comprises 45% of the total observing time, US

observing time will amount to 1.125% of the total SXG primary time, or $\sim 2.7 \times 10^5$ seconds per year, assuming a useful pointing time of $\sim 2.4 \times 10^7$ seconds per year.

An additional 1.5% of the total SODART primary time ($\sim 1.6 \times 10^5$ seconds) will be made available for US/Russian collaborations. US observers may propose for half of this time as lead PI's (US/Russian program). They may name specific Russian co-PI's if they choose, or have them assigned by IKI. Russian scientists will propose for the remaining half, under a similar collaborative program managed by IKI (Russian/US program). US co-PI's may be either named in the original proposal or selected by subsequent US peer review.

A.4.2 Collaborative Time

In addition to the primary time noted above, the US also has available SODART secondary time but only as collaborative time with Russia. This time consists of 2.5% of the total SODART secondary time ($\sim 3.3 \times 10^5$ seconds) for US/Russian collaborations. Up to half of this time will be used to recover any US or US/Russian primary time proposals accepted by the US peer review but ultimately rejected in generating the final Cycle 1 timeline. Similarly, up to half will be used by IKI to recover similar Russian/US primary time proposals. Any remaining collaborative secondary time will be filled with approved Russian secondary time observations, for which US observers may propose to collaborate, once the final Cycle 1 timeline has been determined. Since this timeline will be known prior to the Cycle 2 proposal review, proposals for this secondary time, as well as for successful Russian/US primary time observations with unnamed US co-PI's, should be submitted for the Cycle 2 program.

US/Danish collaborations also may be possible. However, the details of this program are unknown at the time of release of this NRA. Such collaborations will therefore be the subject of a separate announcement.

A.4.3 Targets of Opportunity

The final SXG policy for Targets of Opportunity (TOO's) has not yet been defined or approved by the International Scientific Committee. Preliminary plans limit TOO's to less than 5% of the total observing time per year, and assign data rights to the observer whose time was appropriated for the TOO. TOO observations will be allocated only in observing slots already assigned to a PI. The Spectrum-X-Gamma project leader will decide on the suitability of possible Targets of Opportunity in consultation with the project investigators of each main instrument. A majority of instrument PI's must agree to the suspension of the observing program for the Target of Opportunity. Depending on the details of how the TOO observation is inserted into the existing observation timeline, the time to acquire the TOO will range from $\sim$5 – 7 days.

Individual observers will not be able to propose for generic TOO's (for example, the first transient to be detected in the observing cycle) in advance.

A.5 The US Spectrum-X Gamma Coordination Facility

The US Spectrum-X Gamma Coordination Facility is operated by the Smithsonian Astrophysical Observatory. The SXGCF will assist NASA HQ in executing this general observer

program by:

- managing the US proposal review,
- communicating US observing programs to IKI,
- distributing and archiving US SXG data covered by this program,
- creating and maintaining a US public archive for SXG data,
- making available to GO's data reduction and analysis software developed by other parties,
- providing SXG documentation to US observers.

Additional information about the SXG mission may be obtained electronically via the World-Wide Web at **http://hea-www.harvard.edu/SXG/sxg.shtml** or via anonymous ftp at **ftp://sao-ftp.harvard.edu/pub/sxg**. The SXGCF may be contacted by e-mail at **sxg@cfa.harvard.edu**.

B Instructions for Responding to NASA Research Announcements

TO BE PROVIDED BY NASA

C Additional Proposal Information

The information contained in Appendix C augments and supersedes Appendix B and applies only to this NRA.

C.1 Proposal Preparation and Submission

C.1.1 General Observing Parameters

There are no restrictions on the amount of observing time or number of targets requested in proposals. However, exposures for individual pointings cannot be longer that the time between two ground station contacts ($\sim 10^5$ s.). There is no lower limit on exposure time, but the limited number of pointings between ground station contacts ($\sim$10) make it unlikely that many short pointings can be scheduled between any two ground station contacts. Multiple, short pointings during a single observation can, however, be made by specifying a raster scan. At most, a single raster scan observation will be performed between two ground contacts.

Current plans limit TOO's to less than 5% of the total observing time per year, and assign data rights to the observer whose time was appropriated for the TOO. TOO observations will be allocated only in observing slots already assigned to a PI. The Spectrum-X-Gamma project leader will decide on the suitability of possible Targets of Opportunity in consultation with the project investigators of each main instrument. A majority of instrument PI's must agree to the suspension of the observing program for the Target of Opportunity. The turn-around time to acquire a TOO is $\sim$ 5 – 7 days. There is no provision to apply for generic TOO's in advance.

For each observation, proposers should give a minimum exposure time, below which the scientific goals cannot be achieved, and a maximum exposure time, above which operational considerations such as on-board storage limitations could compromise the observation.

At any given time, $\sim$80% of the sky is available for observation with SODART. However, due to constraints on satellite orientation with respect to the Sun, and the availability of suitable guide stars for the star sensors, specific targets will, in general, be visible only during specific "viewing windows" during the year. Proposers who wish to observe particular targets at particular times should confirm target visibility, using the JMAN viewing tool (see SXG SODART Observer's Guide). Proposals for such "time-critical" observations may be made by specifying either a begin and end time for the viewing window, an epoch, period and phase interval, or a desired time interval since the last observation of the target.

Proposals submitted in response to this announcement should specify simultaneous use of both FM1 and FM2. Any detector available to FM1 can be matched with any detector available to FM2. Except for observations with OXS, which views the sky 90° from the viewing direction of FM1, it is in the proposer's best interest to plan observations which make efficient use of both telescopes.

C.1.2 Who May Propose

Every SXG proposal must identify a Principal Investigator (PI), who assumes full responsibility for the scientific study and the budget. The intent of this program is to enhance U.S.-Russian and U.S.-Danish scientific cooperation, in keeping with bilateral agreements between

the U.S. and Russia and the U.S. and Denmark. Thus, only individuals affiliated with U.S. institutions and located in the U.S. are eligible to propose for this AO through NASA. The requirement of affiliation with a U.S. institution does not extend to co-investigators.

Following selection, the mission timeline team will deal only with the person identified as Principal Investigator. It will be the Principal Investigator's duty to respond to any questions about detector usage or observational modes.

C.1.3 Letters of Intent

Interested observers are requested to send an electronic "Letter of Intent" to propose. Although not required, submission of such letters is to the PI's advantage, since updates to the technical and programmatic information contained in this NRA will likely occur before the deadline for proposal submissions, and such updates may prove useful to PI's in preparing their proposals. Letters of Intent will provide a list of likely PI's to whom new information regarding the mission can be forwarded as soon as it becomes available. Proposers not submitting Letters of Intent will themselves be responsible for learning of any relevant new information through the SXGCF WWW Home page.

To ensure proper processing, the email letter of intent should include the phrase "SXG Letter of Intent NRA-TBD" in the Subject field, and should contain the PI's name, institution, address, phone number, and email address in the body of the letter.

The letter of intent should be e-mailed to **sxg-intent@cfa.harvard.edu**. Notification of receipt will be communicated electronically.

C.1.4 Selecting US or Collaborative Time

US proposers may increase their chances of selection by agreeing to have their proposals considered for collaborative time. Proposers may indicate their preference for US or US/Russian time. The choice of either or both is allowed, and no preference will be interpreted as selecting both. It will not be necessary to name collaborating PI's although proposers are free to do so. Proposals of both types will be reviewed by the US peer review (i.e., the US SXG National Level selection) and proposal type will not affect the ranking of the proposal.

C.1.5 Technical and Budget Proposals

The proposal review procedure will be conducted in two stages. During the first stage, the scientific and technical merits of the proposed investigation will be reviewed by panels of science peers. Based upon the criteria listed in Section C.3.1.1 of this NRA, a set of proposals will be recommended for selection by the SXG Program Scientist at NASA Headquarters. These proposals will be forwarded to the Telescope Level and Observatory Level Time Allocation Committees, where they will be merged with proposals from other SXG instruments and national programs (see section C.3.1.3). PI's of proposals which survive these reviews will then be asked to submit a budget proposal for the second stage review.

Only technical proposals should be submitted in response to this NRA.

C.1.6 Submission of Proposals

Fifteen copies of the proposal, including a signed original, should be mailed to the following address:

Smithsonian Astrophysical Observatory
attn: SXGCF, NRA-TBD
General Investigator Program
60 Garden Street
Cambridge, MA 02138

In addition, the information contained in the Cover and Target pages must be submitted electronically, as specified in Appendix D.

Budget proposals also should be sent to the above address.

C.1.7 Where to Go for Help

If you require more information or have questions regarding the proposal process, access to information, forms, etc., please call **617 496-7914** or email **sxg-help@cfa.harvard.edu**. Information about the SXG mission can be obtained electronically at **http://hea-www.harvard.edu/SX**

C.2 Proposal Format and Content

C.2.1 Technical Proposal Format

The proposal should include the following pages in the following order:

Section	Page Limits	Comments
Cover Page	1	Includes abstract; No other cover required
Signature Page	1	Administrator and PI signatures
Proposal Body	2	Scientific justification and technical feasibility
Figures and Tables	2	
Target Pages	as needed	
Other relevant material	2	References, CV, and required institutional material

C.2.1.1 Page Limits - Proposals should be concisely written to facilitate the overall evaluation process. The total length of the science and technical section of the proposal text (proposal body) is 2 single-spaced pages (equivalently 1 double-sided sheet of paper) of textual material. Figures and tables may include up to 2 additional pages (equivalently 1 double-sided sheet of paper). References and material required by the proposers institution should also be included and should not exceed 2 single-spaced, double-sided, typewritten sheets of paper.

C.2.1.2 Format – All material should be in point size 10 or larger, with 1 inch margins. Single-spaced copy is acceptable and proposers are encouraged to use double-sided sheets of paper. The enclosure of additional materials such as reprints or preprints is discouraged. To facilitate the recycling of proposals after review, proposals should be submitted on plain, white paper only. This precludes the use of cardboard stock, plastic covers, colored paper, etc.

C.2.2 Technical Proposal Content

The proposal body should include two sections. The first section (estimated length 1 page) should clearly state the scientific problem to be addressed, with relevant background and references to previous work. Sufficient details should be provided so that reviewers can determine the significance of the planned research and the contribution to the field that the intended research will make. The second section (estimated length 1 page) should describe the feasibility of the proposed investigation. Assumptions should be clearly stated. Source strengths should be given and the calculations used to draw conclusions regarding feasibility should be clearly defined. The feasibility section should discuss previous observations of the proposed target(s), if they are relevant.

The two pages of text can be supported with two pages (1 double-sided sheet) of tables and figures. These should be of sufficient size and clarity and should be clearly labeled.

C.2.3 Cover Page, Target Pages and Electronic Submission

The Cover and Target pages identify the proposers, describe the technical details of the proposed observation (instrument, position, time) and include an abstract summarizing the investigation.

Example and blank versions of the cover page and target pages are available via anonymous ftp as noted in Appendix D. When filled out, these pages may be used as cover and target pages for the paper version of the proposal. The single file which combines both the cover page and target page must be e-mailed (see below) as the electronic submission.

Additional target pages should be included if more than one target is to be observed. These additional pages should occur for both the electronic submission and the printed version of the proposal.

Each proposal must be identified as to type by filling in the appropriate Observing Program on the Cover Page (US, US/Russian, or no preference). Each proposal, regardless of type, must identify one primary research area. Secondary research areas may be selected, but should be kept to a minimum. NASA reserves the right to reassign a proposal to different primary or secondary research areas. The research areas are:

1	Stars
2	Cataclysmic Variables
3	X-ray Binaries
4	SNR's and Galactic Diffuse Emission
5	Normal Galaxies
6	AGN
7	Clusters and Superclusters
8	Cosmic XRB, Deep Surveys
9	Other

C.2.4 Budget Proposals

Approximately 30 days after the final target list (see section 3.1.3) has been released (which serves as notification of the tentative acceptance of a Technical proposal), successful proposers will be requested to submit Budget proposals. A suggested budget form is available via anonymous ftp as noted in Appendix D of this NRA. Alternatively, the cost section may be prepared according to the guidelines of the institution submitting the proposal, but it must contain:

- The name of the corresponding scientific proposal, the name of the Principal Investigator, and the proposal number (assigned by the SXGCF). Copies of the scientific proposal should NOT be resubmitted.
- Cost estimates for direct labor, including individual person-months and rates for the personnel involved.
- Estimated costs for equipment, materials, and computer services, including type of computer and number of hours of mainframe computer use. Itemize items over $500.
- Travel costs – itemize trips, including travel to data analysis centers. In general, only one trip per team member to a professional society meeting will be supported.
- Overhead rates and costs.
- Other costs, with explanation.
- Contributions from any cost-sharing plan.
- Total cost of support being requested from NASA.
- A detailed breakdown of the responsibilities of the various investigators who are requesting funding.
- For all co-investigators at different institutions for which budget support is being sought, a separate budget summary must be included. A brief (less than one page) justification for the submitted budget, providing the rationale for the various cost items and amounts requested.

A review team comprised of a subset of the Technical peer review panel will then review the Budget proposals and, based upon overall consideration of both scientific and cost factors, will recommend funding levels to the Selecting Official for final selection and award.

C.2.4.1 Workstation Request – As has been the policy in recent years, NASA may provide some investigators with the computational resources needed for the analysis selected under this NRA. The objective is not to enhance general computing capability, but rather to support SXG data analysis at the investigator's home institution.

The analysis of SXG data typically requires a workstation with at least 1 Gbyte of disk space and more than 32 Mbyte of memory. Typical software would include SAOTNG, IRAF, FTOOLS, and XSPEC, which are currently fully supported for Sun/SunOS, Sun/Solaris, DEC/ULTRIX, DEC/OSF, and SGI/IRIX. Limited support for these tools is available for VMS workstations.

Requests for workstations should briefly describe the computing capabilities which are expected to exist at the proposer's institution during the period in which the research will be performed. The proposer must also explain the scientific impact, if the request for the workstation is declined. The budget request for workstations should be included in the budget form.

C.2.4.2 Budgets for Multiple Proposals – Proposers with multiple accepted proposals may submit a single budget proposal. Those doing so should clearly indicate all proposals covered by their budget. In their justifications, proposers should break down the overall budget into the amounts for the various investigations to be carried out.

C.3 Proposal Evaluation and Selection

C.3.1 Technical Proposal

C.3.1.1 Evaluation Criteria The following criteria replace the criteria given in Appendix B. They apply only to the evaluation of proposals submitted in response to this NRA and are shown in descending order of priority.

1. The overall scientific merit of the investigation.

2. The suitability of using the SXG observatory and data products for the proposed investigation, the degree to which the investigation uses SXG's unique capabilities and recognizes SXG's observing constraints, the feasibility of accomplishing the objectives of the investigation within the time proposed, and the feasibility of the analysis techniques.

3. The relevance of the proposed research to NASA's Astrophysics program and the potential for international collaborations, especially for those proposals that fall in the collaborative category.

4. The competence and relevant experience of the principal investigator and any collaborators as an indication of their ability to carry the investigation to a successful

conclusion within the requested resources, including the timely publication of refereed scientific journal papers.

C.3.1.2 Selection of US Proposals – Both US and US/Russian proposals will be evaluated by peer review panels, using the criteria mentioned above, and a single prioritized list will be generated. To allow for the elimination of selected proposals in the merging process (see below) an oversubscription of ~50% is anticipated.

C.3.1.3 Merging U.S. Proposals with Those from Other SXG Programs – The observation planning sequence for SXG is complex because of the simultaneous operation of multiple telescopes by different countries, each having different access to the observatory resources.

There will be three selection levels for the main telescopes (SODART, Jet-X, MART-LIME, FUVITA): National Level, Telescope Level, & Observatory Level. At the National Level, the main task is to select and prioritize the primary and secondary observing time proposals with no duplication. Selection of proposals in response to this NRA corresponds to selection at the US National Level. At the Telescope Level, duplication of targets from competing national proposal lists is eliminated. At the Observatory Level, a merged target list is assembled and conflicts between different telescopes are resolved by assigning primary and secondary time according to a prescription approved by the SXG International Science Committee.

It is possible that some US or US/Russian proposals that were approved at the US National Level, but eliminated at either the Telescope or Observatory Level, may be recovered by being assigned secondary rather than primary observing time.

Final selection of proposals submitted to this NRA will be made by the Director, Astrophysics Division, NASA Office of Space Science.

C.3.2 Budget Proposals

A subset of the original peer review panel will review the Budget proposals and, based upon overall consideration of both scientific and cost factors, will recommend a set of proposals to the Selecting Official for funding. The second review will take place ~8 weeks after the release of the merged target list. Following the second review, those proposers selected for award will be notified of the funding level for their investigation.

In addition to the overall scientific/technical rating of the proposal from the Technical review, the primary criterion used in the Budget evaluation will be the cost of the investigation, including cost reasonableness (in the context of the anticipated level of effort required to carry out the investigation successfully) and total proposed cost in relation to available funds. It should be noted that, once approved by the Technical review and international merging process, proposed observations will take place (barring unforeseen difficulties) regardless of funding level.

C.4 Implementation

All of the proposals approved by the merging process will be entered into an observation database. It is likely that observational details will need to be worked out with the PI prior to the observation. Each observation will be assigned a unique identifying (sequence) number. It is the responsibility of the mission planning and operations team at IKI to produce a mission timeline out of all approved observation requests.

Investigators should be aware that observations of their targets will, under most circumstances, be carried out contiguously: once an observation begins, the satellite will not be moved until the observation has been completed. Some exceptions are observations that specifically request discontinuity, for monitoring or phase coverage, and observations requiring use of high bit rate telemetry.

An observation will be considered compete if 90% of the required stable on-source exposure time has been achieved.

Investigators whose proposals are selected will have proprietary use of their data for 12 months after receipt of the data in usable form, after which time the data will be made available to other interested investigators.

C.5 Schedule

Included below is the schedule for the review and selection of proposals for the first SXG AO.

DATE	EVENT
Launch - 14 months	AO1 Announced
Launch - 11 months	AO1 Proposals Due
Launch - 9 months	US Target Selection Complete
Launch - 3 months	Merged Target List and Time Line Complete
Launch + 2 months	Activation Complete
Launch + 2 months	AO1 Observations Begin

Proposals may be submitted at any time prior to proposal deadline. Those received after that date will be held for the next review cycle, planned for approximately one year after the present cycle.

C.6 Education/Public Outreach

C.6.1 Opportunities within the SXG Program

Partners in Education: A Strategy for Integrating Education and Public Outreach Into NASA's Space Science Programs (released in March 1995) describes the Office of Space Science's (OSS) approach for making education at all levels and the enhancement of the public understanding of science integral parts of space science research activities.

Education and public outreach are now expected to be a part of each flight program and research discipline. This will be implemented through a mixture of mission/project-specific outreach activities, plus education/outreach activities conducted by those individual

researchers/general observers who wish to do so. NASA encourages those researchers who have relevant expertise or inclination to engage in education outreach. Therefore, interested SXG proposers are encouraged to include a modest program of educational/public outreach activities as part of their research proposals.

More information on **Partners in Education** may be obtained by visiting the web site **http://www.hq.nasa.gov/office/oss/edu/educov.htm**. For more information on OSS and Astrophysics education policies and programs, contact Dr. Jeffrey D. Rosendhal, Astrophysics Division, Code SZ, NASA Headquarters, Washington, DC, 20546.

C.6.2 Other Educational Opportunities

We also call your attention to the **Initiative to Develop Education through Astronomy and Space Science** (IDEAS) program. The IDEAS program, administered by the Hubble Space Telescope (HST) Science Institute, specifically provides small grants (typically $6000) to enhance the participation of research astronomers in pre-college or public outreach activities.

For more information on the IDEAS program, send e-mail to **ideas@stsci.edu**, visit the web page **http://www.stsci.edu/pubinfo/edugroup/ideas.html**, or contact the program's manager, Ms. Anne Kinney at **410 338-4831 (kinney@stsci.edu)** or ST ScI's Education Coordinator Mr. Flavio Mendez at **410 338-4977 (mendez@stsci.edu)**.

D Proposal Forms

All proposers are required to complete and submit certain forms. These include

Cover Page
Signature Page
Target Pages
Budget Summary (Budget Proposals only)

Simple ASCII forms are provided for this purpose. They may be edited with any text editor. Blank forms may be obtained from the anonymous ftp site **sao-ftp.harvard.edu** in the sub-directory /pub/sxg/nra. The complete commands for accessing these files are (using the Cover/Target Page form as an example):

ftp sao-ftp.harvard.edu
login as "anonymous" with email address as password
cd pub/sxg/nra/forms
get blank_cover_form
get blank_target_form
get blank_signature_form
get blank_budget_form
quit

In addition, proposers are required to submit the information in the Cover and Target pages electronically. The completed cover and target pages should be e-mailed, as a single file, to **sxg-proposal@cfa.harvard.edu**. The completed forms may also be used *as* the Cover and Target Pages for the printed proposal.

Alternatively, proposers may submit the Cover and Target Page information electronically by completing the form at **http://hea-www.harvard.edu/SXG/wwwprop.shtml.**

B SXG SODART Observer's Guide

SPECTRUM-X-GAMMA

SODART OBSERVER'S GUIDE

VERSION 1.0 August 3, 1999

U.S. Spectrum-X-Gamma Coordination Facility
Smithsonian Institution Astrophysical Observatory
60 Garden St., Cambridge, MA 02138

Contents

List of Figures

List of Tables

Editor's Note

Most of the material in this document has been extracted from the Mission Operations Report of the SXG Technical Implementation Committee. Additional information may be found in Vol. 2279 of the SPIE Proceedings Series. At this time, much of the technical information is based on theoretical calculations rather than actual measurement. This is changing rapidly as the flight models of the telescopes and their instrumentation are calibrated. Proposers are urged, therefore, to check for updates to the information contained here, as the launch of SXG approaches. These updates are likely to appear first in electronic form at the various SXG WWW sites. Useful sites to check are **http://hea-www.harvard.edu/SXG/sxg.html** at the U.S. SXG Coordination Facility, **http://uhuru.dsri.dk/srg/srg.html** at DSRI, and **http://hea.iki.rssi.ru/Welcome.html** at IKI.

1 Introduction

This document provides detailed technical information about the Spectrum-X Gamma Observatory and the scientific instruments available to U.S. astronomers who wish to propose for SXG observations. This information is intended to allow proposers to identify sources appropriate for scientific study with SXG, determine when specific sources can be observed, and assess the feasibility of proposed observations.

Spectrum–X–Gamma, or SXG, (also known as Spectrum–Röntgen-Gamma or SRG) is a large, multi-wavelength, orbiting astronomical observatory, developed under the sponsorship of the Russian Academy of Sciences, with instruments contributed by a number of European countries and the US. The SODART X-ray Telescope System is one of the main SXG facilities. It consists of twin, thin–foil, conical X–ray telescopes (hereafter called FM1 and FM2), developed by DSRI, and several focal plane instruments. A set of UV telescopes, TAUVEX, are co–aligned with SODART. The SXG spacecraft is shown in Figure 1.

Moveable sleds allow the selection of four different focal plane instruments for each telescope.

The focal plane instruments that may be selected with FM1 are:

- Low Energy (0.2 - 8 keV) Proportional Counter (LEPC–1), an imaging proportional counter with a circular FOV with diameter 30 ′, 13% energy resolution at 6 keV and $\sim 0.5'$ position resolution. Developed by DSRI.

- High Energy (2 - 25 keV) Proportional Counter (HEPC–1) with a circular FOV with diameter 60 ′ and other properties similar to the LEPC. Developed by DSRI.

- Silicon X–ray Array (SIXA), an array of solid state detectors for moderate resolution spectroscopy from 0.5 - 20 keV. Each detector is circular with a FOV of 3.9 ′ and the array is hexagonal with a total FOV diameter of 25′. Developed by the University of Helsinki and the Russian Space Research Institute (IKI).

- Focal Plane X–ray Detector (FRD–A), a high energy (2 - 25 keV) imaging proportional counter with a circular FOV with diameter 50′, 17% energy resolution at 6 keV and $\sim 0.5'$ position resolution. Developed by IKI.

The focal plane instruments that may be selected with FM2 are:

- LEPC–2, HEPC–2 and FRD–2 (duplicates of LEPC–1, HEPC–1 and FRD–A1).

- X–ray Polarimeter (SXRP), developed by Columbia University.

- Objective Crystal Spectrometer (OCS), allowing high energy spectroscopy ($E/\Delta E \sim 100 - 1000$ in four energy ranges: 0.20 - 0.285 keV, 0.60 - 1.2 keV, 2.50 - 5.0 keV and 5.0 - 10.0 keV. OCS is developed by DSRI, the Max–Planck–Institute and IKI.

The SODART system with all the telescopes and instruments is represented in Fig. 2.

SXG will be launched into a deep, highly eccentric orbit with a period of approximately four days. This choice of orbit enables long duration ($\lesssim 80$ hours) observations to be made.

Semimajor axis	106000 km
Eccentricity	0.935
Inclination	51.6°
Longitude of Ascending Node	190°
Argument of Perigee	317°
Orbital Period	96 hours
Altitude at Perigee	~500 km
Altitude at Apogee	~199,000 km

Table 1: SXG Initial Orbital Parameters

The orbital parameters at the beginning of the mission are listed in Table 1. It is expected that orbital circularization will lead to an ~40,000 km altitude at perigee after 2 years.

Ground station operations will take place every 18 to 30 hours. As experience grows, it should be possible to plan for at least 10 re–orientations of the spacecraft per 24 hour period. With all the operational and pointing constraints (see below) taken into account, $\sim$ 80% of the celestial sphere should be visible during any orbit.

The spacecraft pointing is controlled by a sun sensor, which stabilizes one axis, and two star sensors, one of which stabilizes a second axis. The star sensors are sensitive to only a small set of $\sim$ 15 bright stars. The pointing system provides an absolute pointing accuracy of $\sim$ 2′ in each coordinate (at a probability level of 90%). A proposed feedback system using TAUVEX could improve the pointing accuracy to $\sim$ 3″, but implementation of this system has not yet been agreed upon. The settling time after a slew is at most 5 minutes. The pointing stability is $\lesssim$ 5″ over a one minute interval with a limit cycle of 30″ from the nominal attitude. The maximum drift rate is 1.0×10^{-4} ″ per second during pointing mode and the slew rate is at least 0.35° per second. The post-facto aspect reconstruction will be $\lesssim$ 35″ for the spacecraft. Additional aspect information will be provided by the TAUVEX UV telescope which is co-aligned with SODART and mounted to the SODART tube. The details of the aspect solution to be provided by TAUVEX are not yet specified.

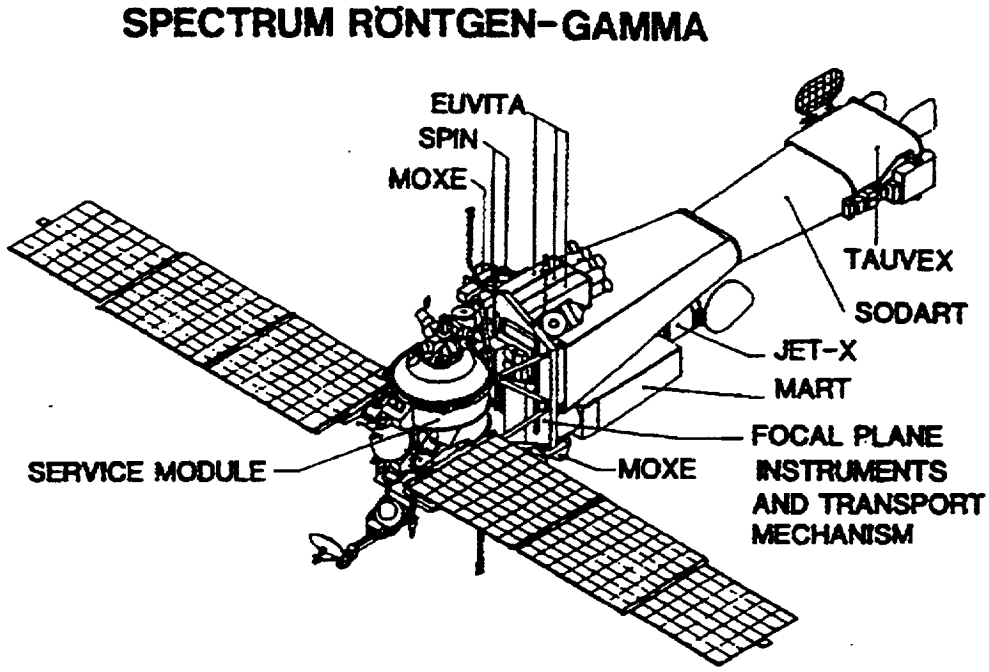

Figure 1: The Spectrum–X–Gamma Satellite

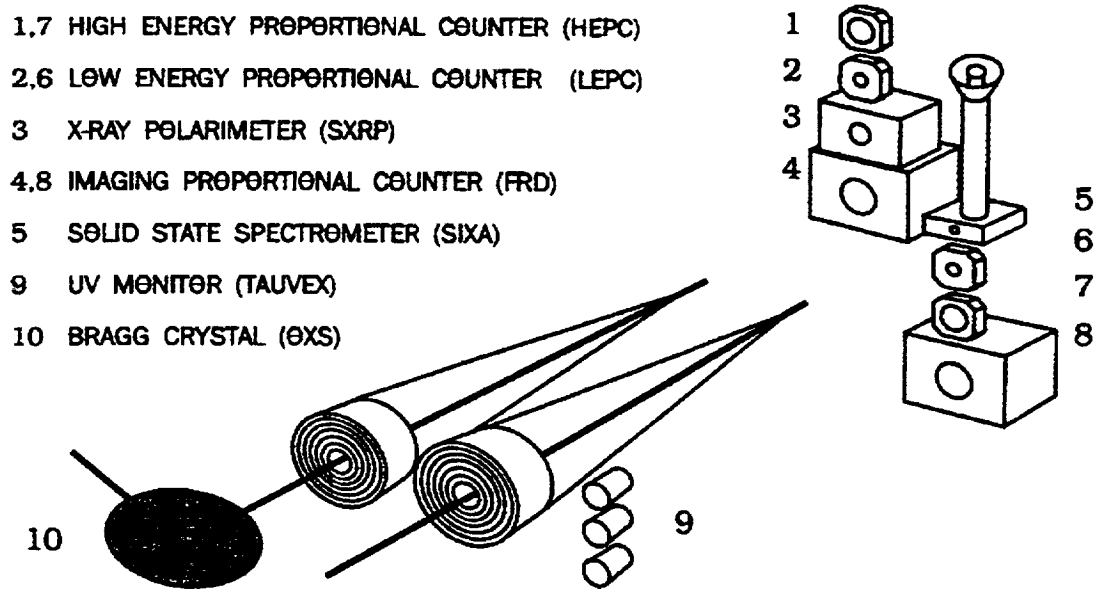

Figure 2: The SODART X-ray Telescope System

2 Observing constraints

The Spectrum-X-Gamma Observatory is a very complex system because of the large instrument complement. In addition, the spacecraft itself is derived from a generic spacecraft that has been used for a large number of missions. In the next sections, we describe constraints which may be relevant to US observers.

2.1 Limitations on Targets of Opportunity

Targets of opportunity can be proposed. The maximum time allocation per year for TOO's from all participants is 5% of the total time. TOO's will be approved by the national selection process and follow the same acceptance procedure as other observations. Upon notification of a TOO, the SXGCF will notify the the SXG project leader who will decide on the suitability of possible TOO's in consultation with the project scientist of each instrument. More than half the instrument PIs must agree to the suspension of the observing program for the TOO since other instrument observing programs will be interrupted to allow observation of the TOO.

2.2 Satellite constraints

Exposure times for individual pointings can not exceed the time between ground station contacts, which are expected to occur every 18 – 30 hours. Although, in principle, there is no lower limit to the duration of individual observations, the number of satellite pointings between ground station contacts will be limited to $\sim$ 10, so only a small number of very short pointings can be accomodated between any two ground station contacts. It will be possible, however, to make raster scans of short duration within a single pointing.

2.3 Instrument Constraints

2.3.1 Stellar X-ray Polarimeter Constraints

The SXRP lies on one of the two sleds (Sled 1) and has no user commandable inputs. The data are stored in a 96 Mbyte capacity memory. Typically, a 24 hour observation interval will utilize 60 Mbytes of memory (equivalently TBD detected events). Polarimetry observations will be most effective if coordinated observations with SIXA (and MART-LIME) are obtained to monitor the time-variability of the source spectrum (e.g., Hercules X-1). Note that aspect information from TAUVEX is critical to obtaining the best performance from SXRP.

2.3.2 Silicon X-ray Array Constraints

SIXA has six different observing modes which can be selected by the observer: three different SEC (single event characterization) modes, Energy-Spectrum Mode (ESM), Window-Counting Mode (WCM), and Time-Interval Mode (TIM). The control over the modes is shared between two processors, so that one DPU (SEC DPU) runs the SEC modes, and the other DPU (EGY DPU) the three other modes. The ESM, WCM and TIM can be run in parallel with one SEC mode (maximum of four modes simultaneously), and any of the

modes can be switched off independently. The starting and ending times of each spectrum are stored with a 10 ms timing accuracy. The time resolution in SEC, ESM and WCM is about 30.5 microseconds, and in TIM it is 12.21 microseconds.

The storage capacity of SIXA is 44Mbytes between observing sessions. For the Crab Nebula, the count rate is 6000 cts s^{-1} which will fully fill the 44Mbyte memory in 3 hours (in raster scan mode). For the Perseus cluster with a count rate of 2.4, 1.4, and 0.5 cts s^{-1} in the central element, 6 inner circle elements, and 12 outer circle elements respectively, the data will consume 6Mbytes of memory (4Mbytes for EGY spectra and 2Mbytes for SEC data).

2.4 Attitude Pointing Constraints

A limitation on the number of pointings arises from the limited on-board memory. Current specifications allow for at least 10 pointings between ground contacts (nominally every 16-30 hours between telemetry sessions). In addition, there may be a reduced number of pointings allowed during the first six months of the mission. Ground contacts last for 4-5 hours during which time no new data is taken. Raster scans can be accomplished over moderate areas of approximately 100 sq. degrees. When in use, the OXS (Objective X-ray Spectrometer) will view the sky 90 degrees from the pointing direction of the other pointed instruments. Scanning in wavelength, will require approximately 10 spacecraft attitude changes of magnitude 5-15 arcminutes for a single pointing. These attitude changes will occur no more frequently than once every 10^4 seconds.

2.5 Viewing Constraints

The following discussion is taken from the User's Manual for JMAN, a program for determining viewing opportunities for the JET-X instrument (M. Ricketts, Rutherford Appleton Laboratory, JET-X(93)RAL-150.1). Since the Jet-X and SODART telescopes are co-aligned, it is generally applicable to the SODART instruments as well.

The orientation of the Spectrum-X-Gamma platform is constrained by several factors. If one defines the telescope pointing direction as the X axis and the solar panel pointing direction as the -Z axis , then the sun must be within 10° of the XZ plane and within 40° of the YZ plane. Further, the two star sensors, which can only use stars brighter than about magnitude 1.0, view in planes 20° from XY plane towards -Z, and between 70° and 140° from the X axis. These constraints are illustrated in Figure 3.

When the OXS instrument is operating, The X-axis is constrained to view along an arc 90° from the OXS target and between 50° and 130° from the Sun. The precise location of the arc depends on the Sun position, as is shown in Figure 4. In ecliptic coordinates the Sun is in the horizontal plane, and the OXS can view a point at ecliptic latitude lat. when the sun is between S1 and S2, and again 6 months later.

As the Sun direction changes from S1 to S2, the arc the telescope can view changes ; the total accessible arc is approximately 80° + 20 Sin(lat). The OXS can view the ecliptic pole at any time, and the telescope can view any point in the ecliptic plane if the date is chosen appropriately.

The above is, of course, subject to a star being available for the star sensor in a suitable position.

2.5.1 Determining SXG Viewing Opportunities

JMAN can be used to determine areas of the sky visible for a given time interval, or dates that a given target position can be observed. In the following example, JMAN is used to determine the visible regions of the sky for SODART observations during the interval from 1-Jan-1999 to 31-Dec-1999 (MJD 51179.00–51210.0). User responses to program prompts appear at the far right.

```
> jman
  Data dir:/proj/sxg/soft/jman/dat

     Jet-X Observation Constraints vsn 1.05 16 Oct 96

     1 - Jet-X visibility, 1 orbit
     2 - Jet-X visibility, period
     3 - Jet-X Point dates
     4 - Jet-X vis, OXS on, any date
     5 - Jet-X Point check, OXS on
     6 - OXS visibility
     7 - Update Parameters
     8 - Subsidiary plots
     9 - Close current plot device
    10 - Help
    11 - Return/Exit
Option\1 [integer]:                                                    2
Orbit data spans MJD 51162.3 to 51894.3
Enter Start of period, either MJD or dd.d/mm/yy, default 20.31/12/98
Date\51167.31 [character]:                                       51179.0
Orbit data spans MJD 51162.3 to 51894.3
Enter End of period,   either MJD or dd.d/mm/yy, default  1/01/99
Date\51179.00 [character]:                                       51210.0
Visible any time (else all time)\T [logical]:                          T
Graphics device/type (? to see list, default /NULL):                   ?
PGPLOT v5.0.3 Copyright 1994 California Institute of Technology
Device types available:
/GIF   (Graphics Interchange Format file, landscape orientation)
/VGIF  (Graphics Interchange Format file, portrait orientation)
/NULL  (Null device, no output)
/PPM   (Portable Pixel Map file, landscape orientation)
/VPPM  (Portable Pixel Map file, portrait orientation)
/PS    (PostScript file, landscape orientation)
/VPS   (PostScript file, portrait orientation)
```

```
 /CPS   (Colour PostScript file, landscape orientation)
 /VCPS  (Colour PostScript file, portrait orientation)
 /TEK4010 (Tektronix 4010 terminal)
 /GF    (GraphOn Tek terminal emulator)
 /RETRO (Retrographics VT640 Tek emulator)
 /XTERM (XTERM Tek terminal emulator)
 /TK4100 (Tektronix 4100 terminals)
 /VT125 (DEC VT125 and other REGIS terminals)
 /WD    (X Window Dump file, landscape orientation)
 /VWD   (X Window Dump file, portrait orientation)
 /XDISP (pgdisp or figdisp server)
 /XWINDOW (X window window@node:display.screen/xw)
 /XSERVE  (A /XWINDOW window that persists for re-use)
 Graphics device/type (? to see list, default /NULL):                /PS
Calculating constraint, MJD 51180.3
Calculating constraint, MJD 51184.3
Calculating constraint, MJD 51188.3
Calculating constraint, MJD 51192.3
Calculating constraint, MJD 51196.3
Calculating constraint, MJD 51200.3
Calculating constraint, MJD 51204.2
Calculating constraint, MJD 51208.2

     Options

     1 - Another device
     2 - Return/Exit
 Device_option\2 [integer]:                                           2

     Jet-X Observation Constraints vsn 1.05 16 Oct 96

     1 - Jet-X visibility, 1 orbit
     2 - Jet-X visibility, period
     3 - Jet-X Point dates
     4 - Jet-X vis, OXS on, any date
     5 - Jet-X Point check, OXS on
     6 - OXS visibility
     7 - Update Parameters
     8 - Subsidiary plots
     9 - Close current plot device
    10 - Help
    11 - Return/Exit
 Option\11 [integer]:                                                11
>
```

The selection of **/PS** for graphics device directs the output to a postscript file named **pgplot.ps**, in the directory from which the program was executed.

Example plots of areas of the sky visible to the SODART telescopes or the OXS are shown in Figures 5 – 10 and Figures 11 – 16, respectively. JMAN can be obtained from the SXGCF via the WWW (**http://hea-www.harvard.edu/SXG/jman_sxg.html**) or directly from RAL via anonymous ftp (**ftp://sdcjx2.bnsc.rl.ac.uk/pub/jetx/jman/**).

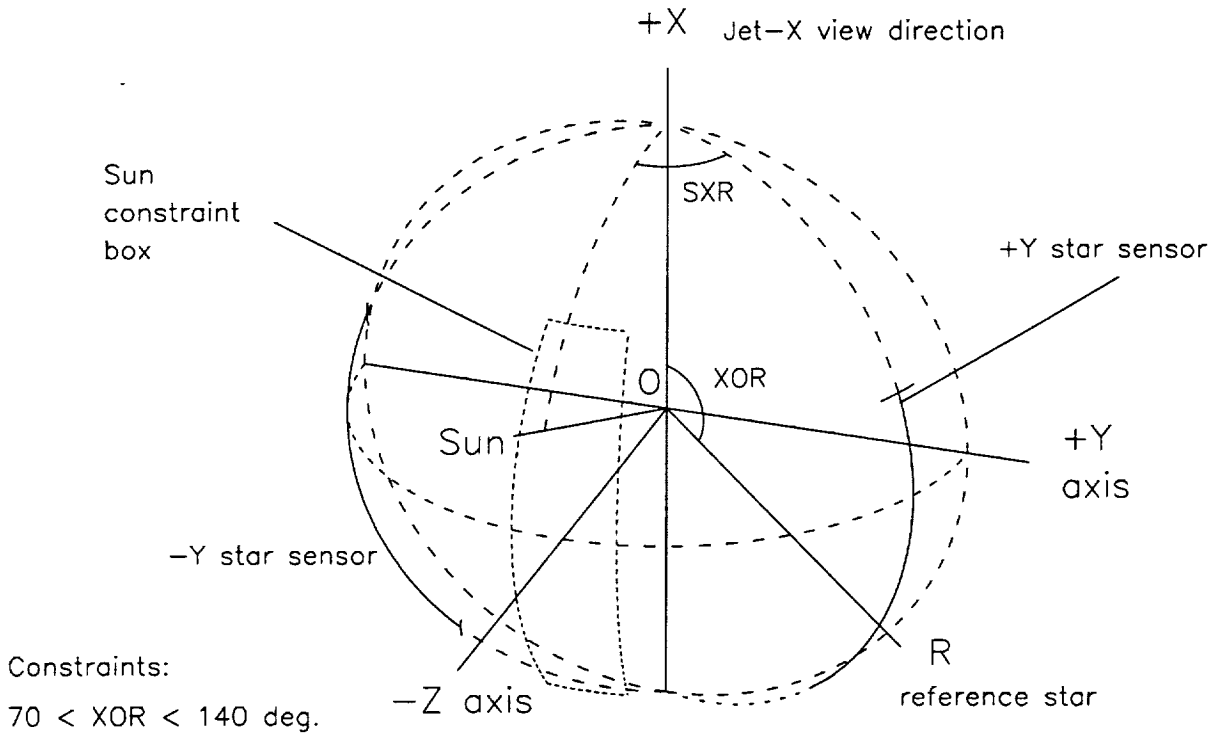

Constraints:

$70 < XOR < 140$ deg.

$-40 <$ Sun $-$ ZY plane < 40 deg.

$60 < SXR < 80$ deg.

Figure 3: Guide Star and Sun Constraints on SXG Viewing Direction

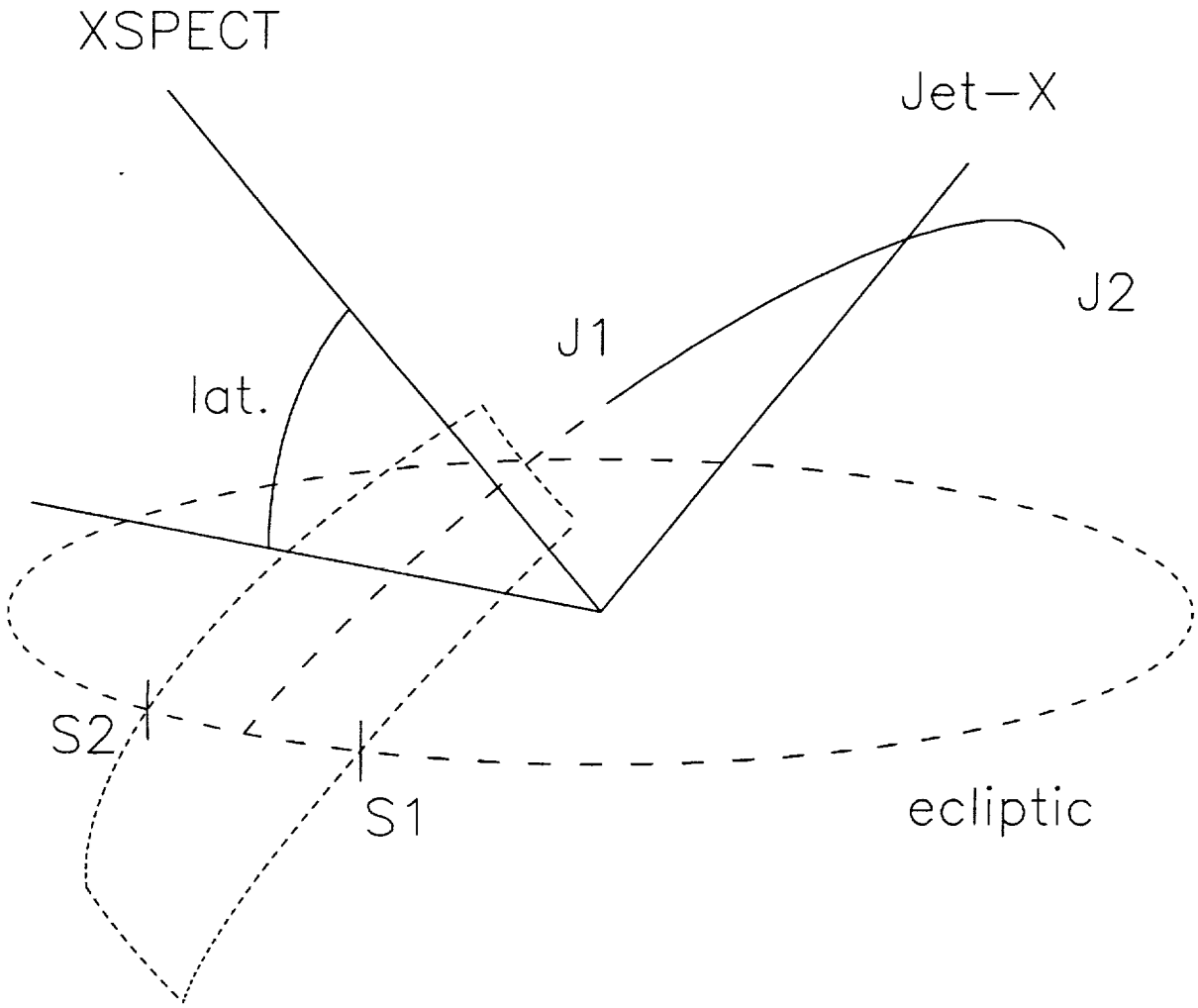

Figure 4: OXS Viewing Constraints

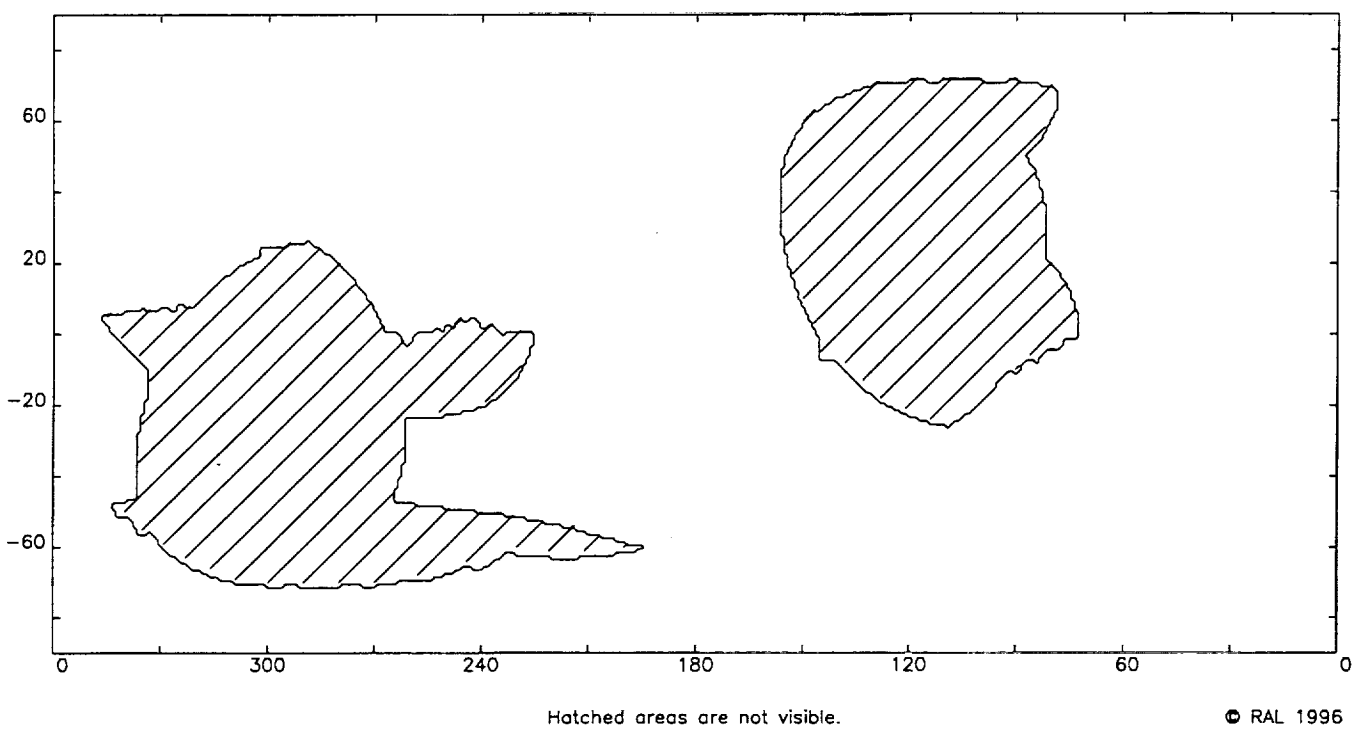

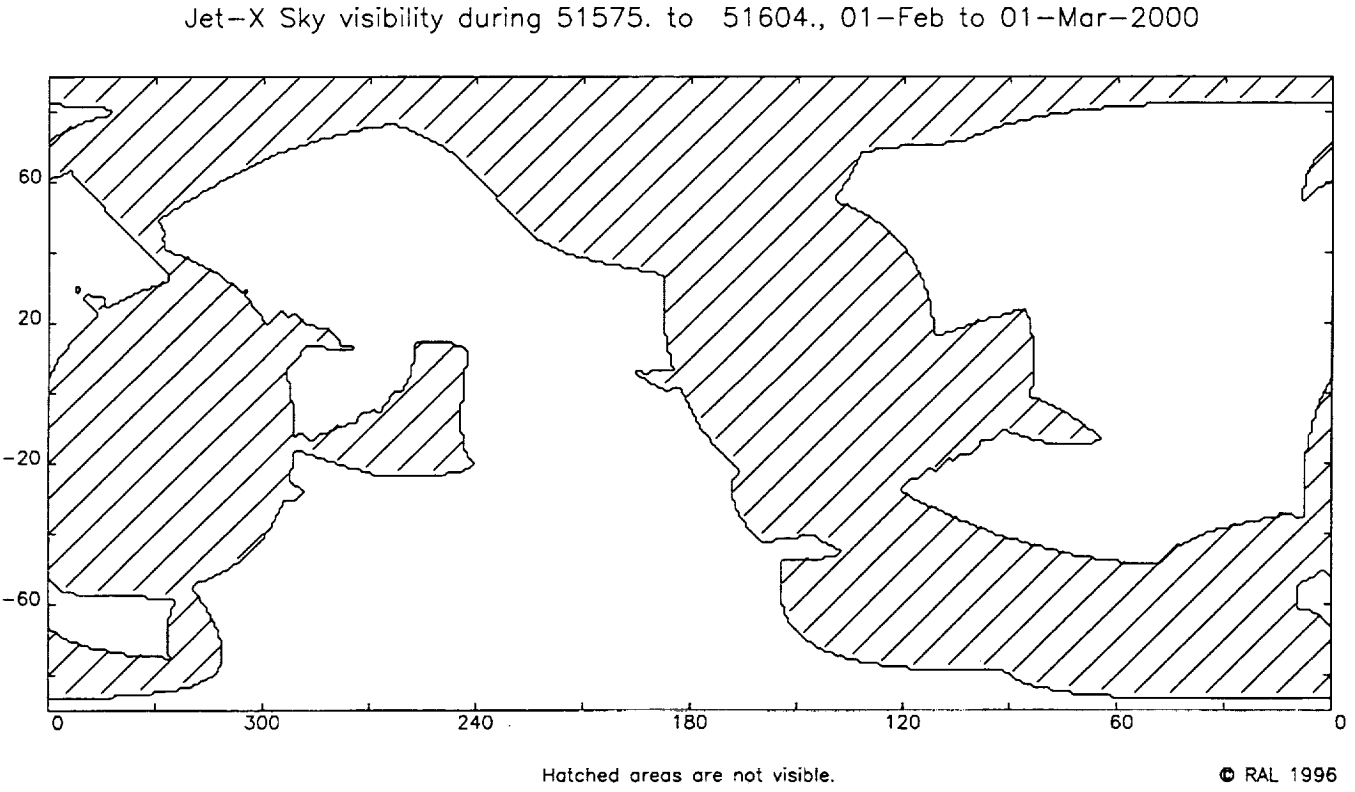

Figure 5: SODART Telescope Viewing Opportunities for Jan. & Feb. 2000 Figures 5 – 10 show visible areas of the sky (RA vs. Dec.) at one-month intervals. Here, "Jet-X" refers to the pointing direction of the Jet-X and (co-aligned) SODART telescopes.

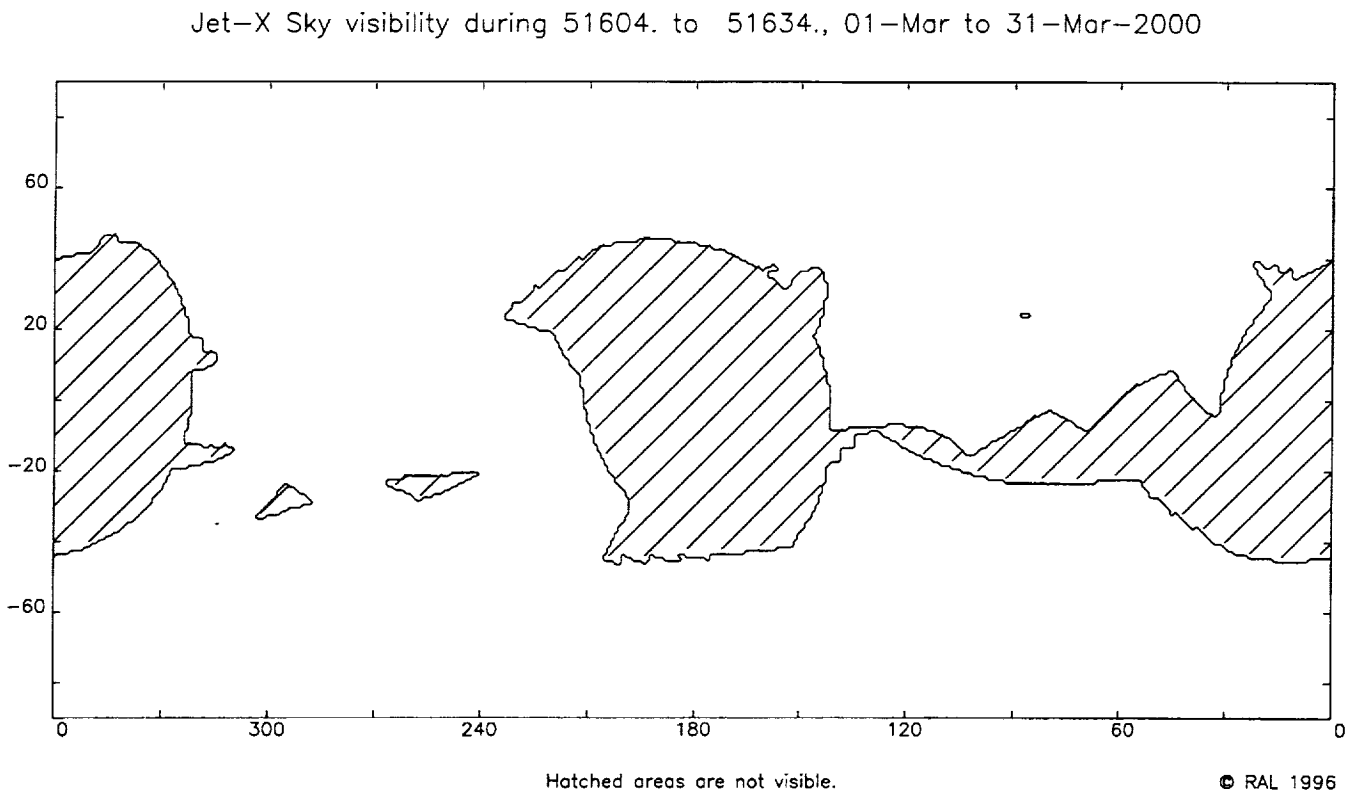

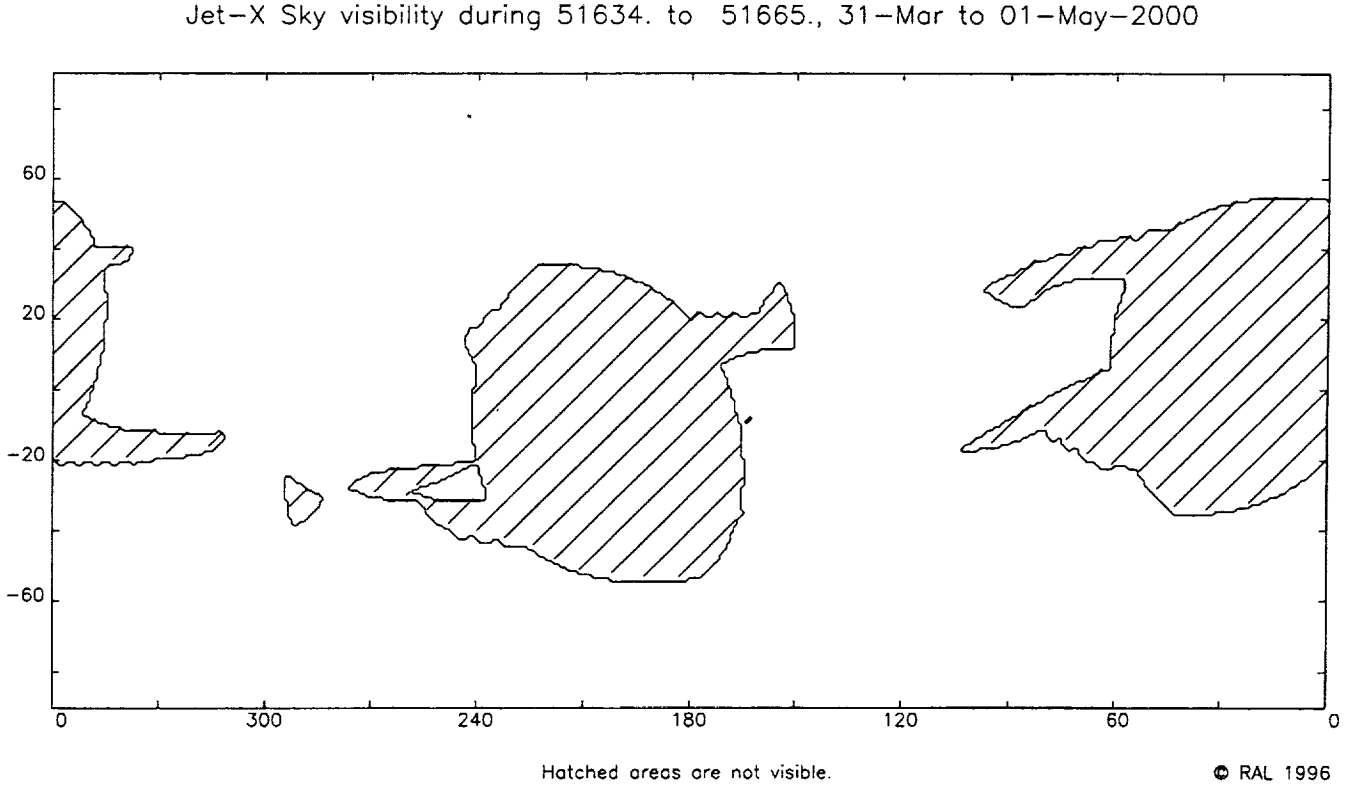

Figure 6: SODART Telescope Viewing Opportunities for March & April 2000

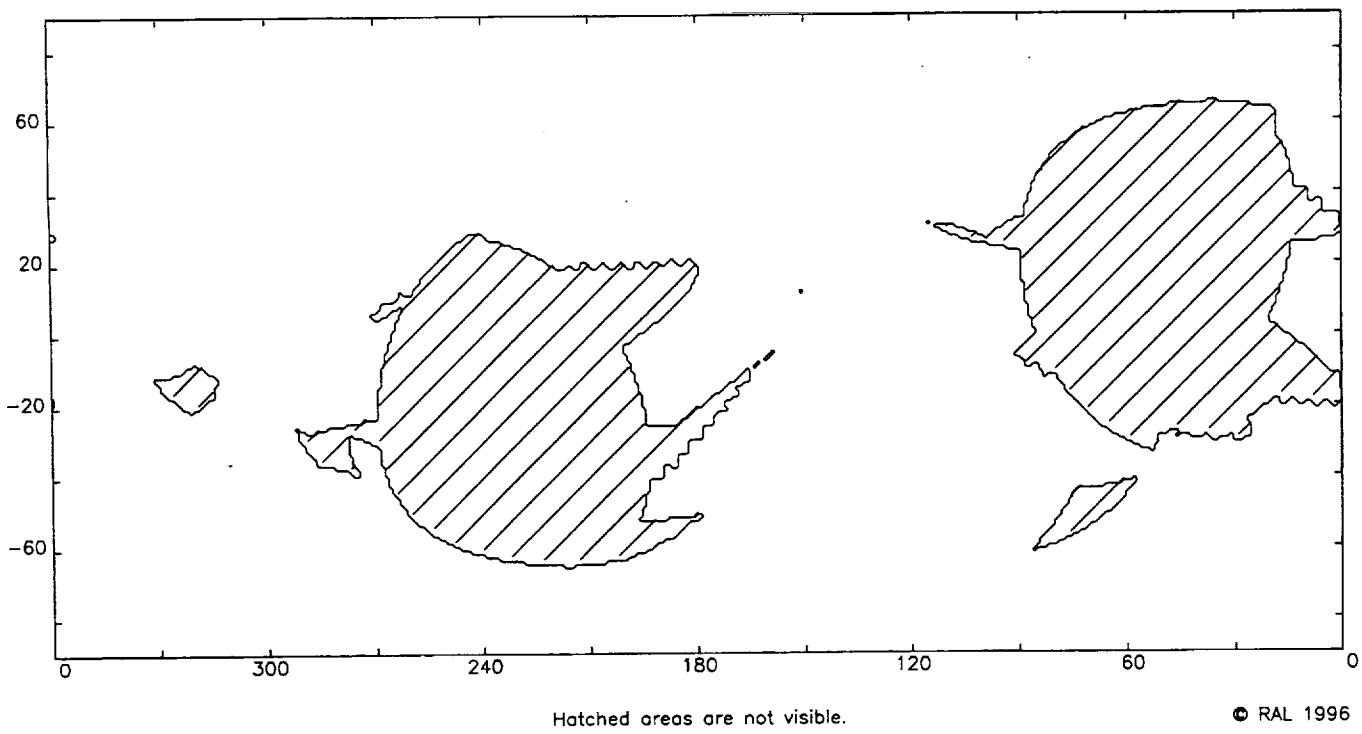

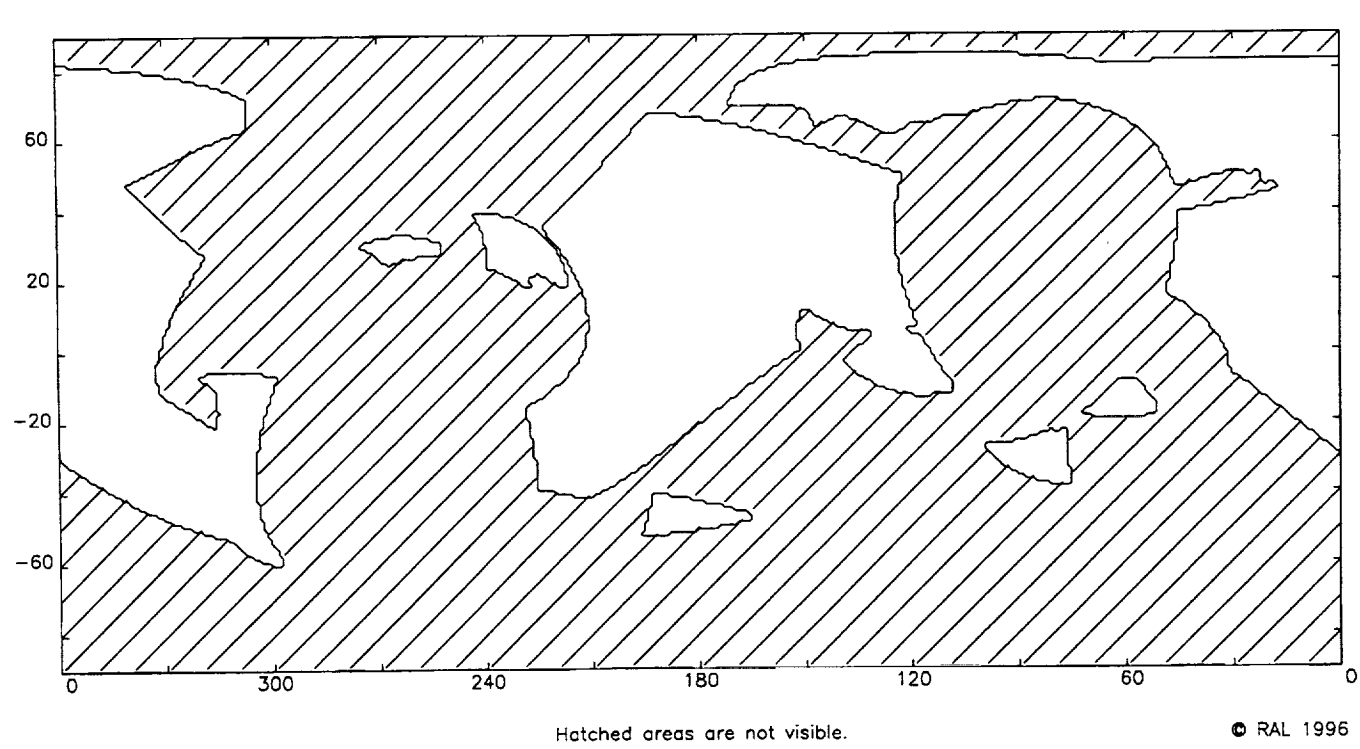

Figure 7: SODART Telescope Viewing Opportunities for May & June 2000

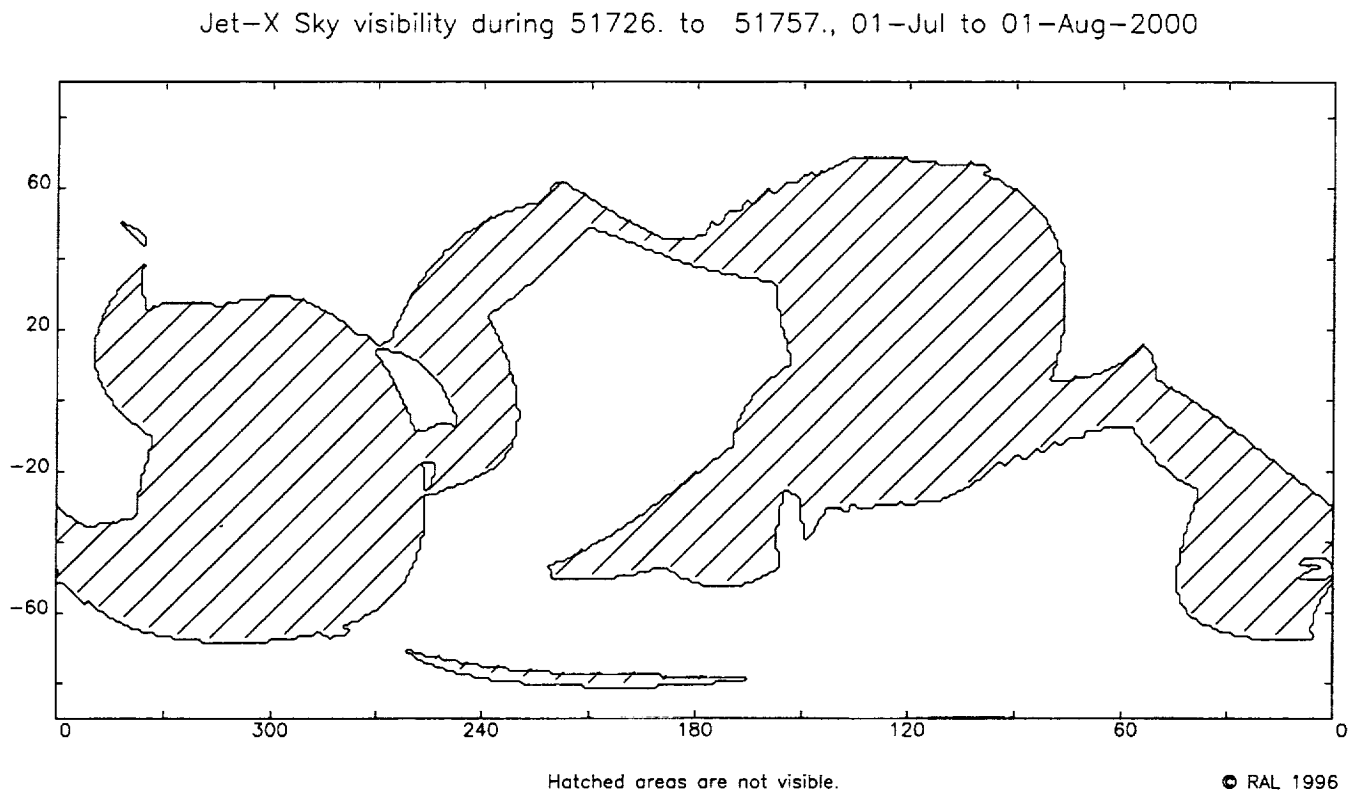

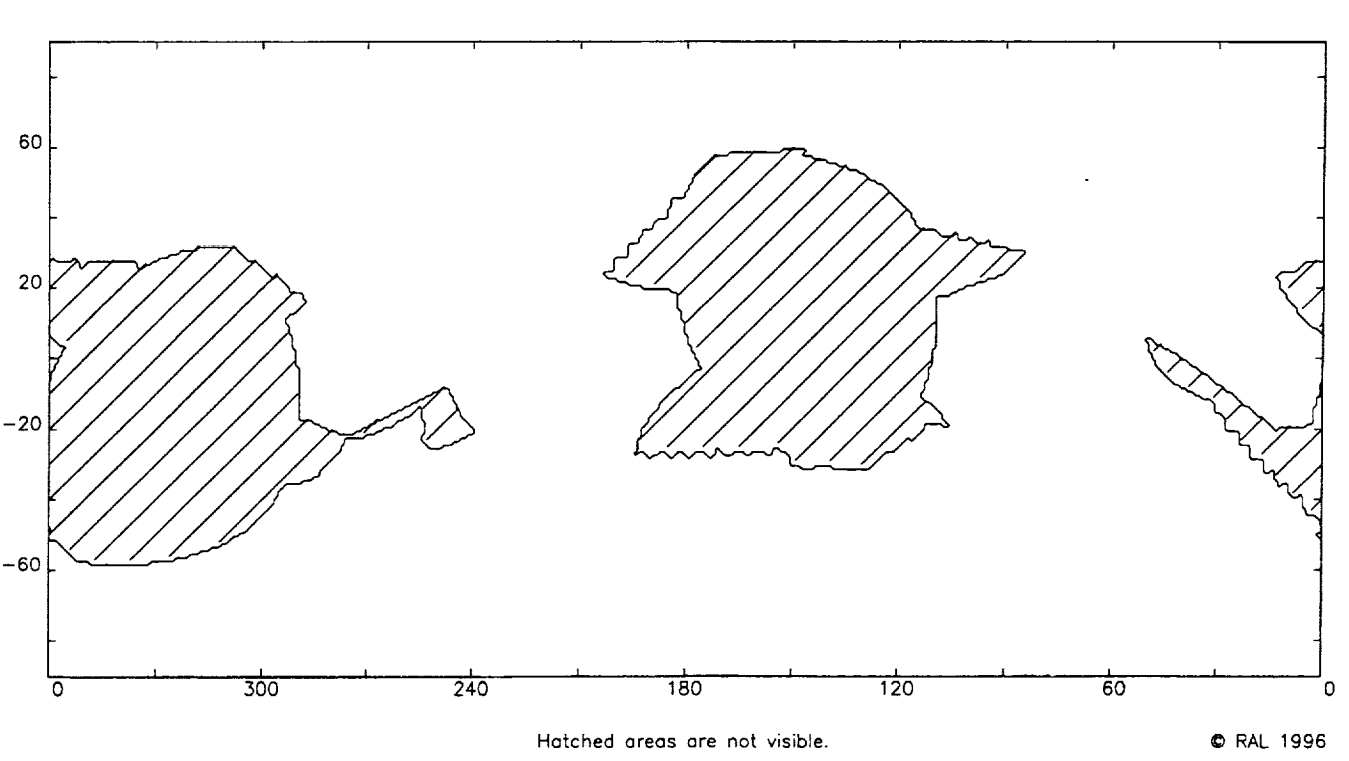

Figure 8: SODART Telescope Viewing Opportunities for July & Aug. 2000

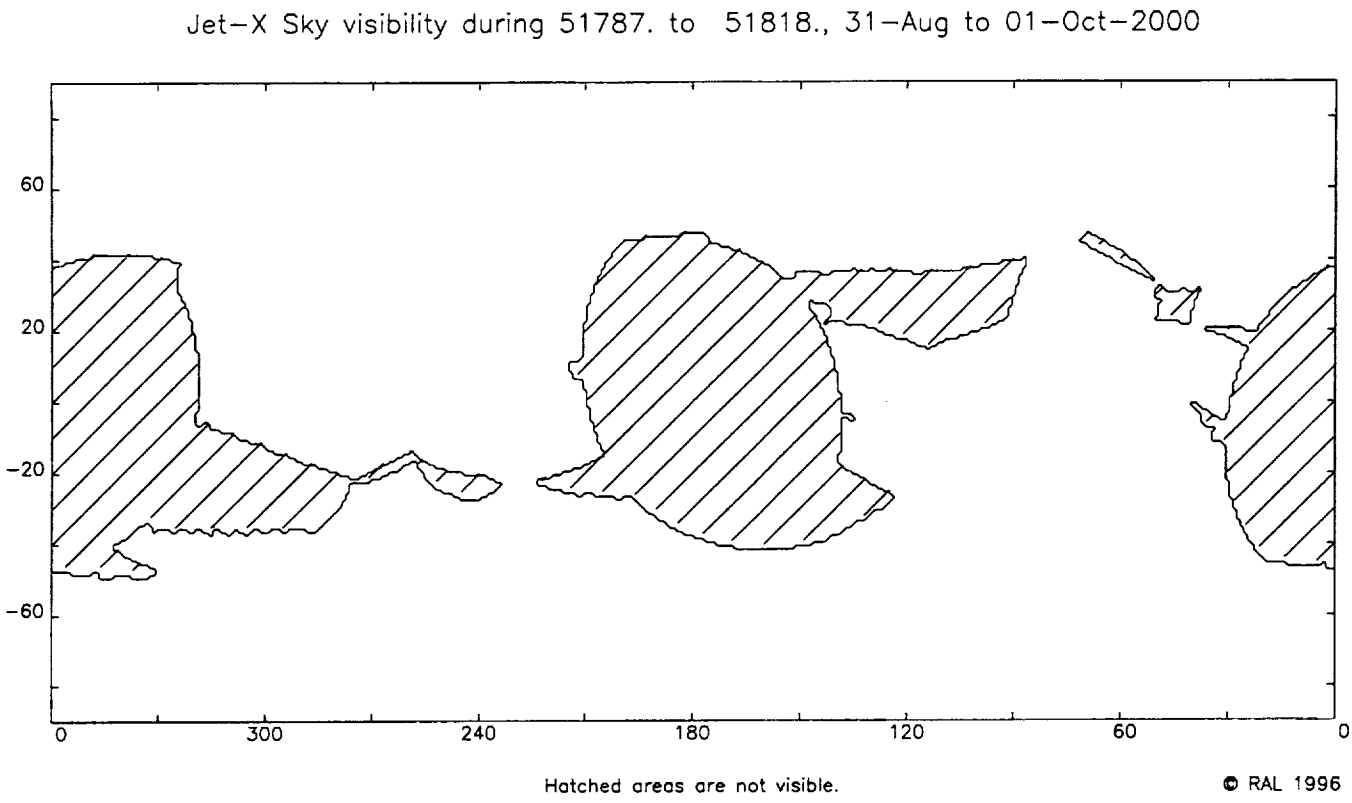

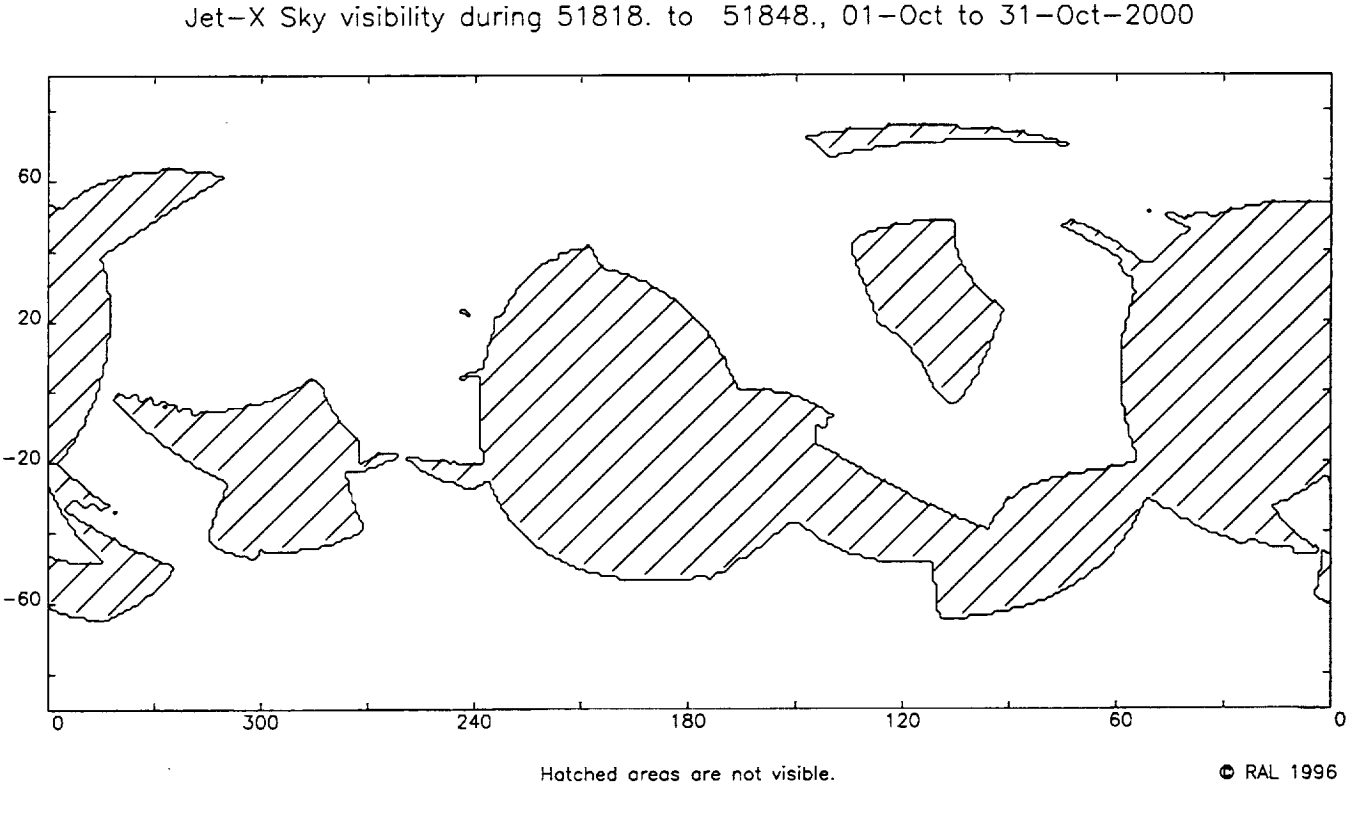

Figure 9: SODART Telescope Viewing Opportunities for Sept. & Oct. 2000

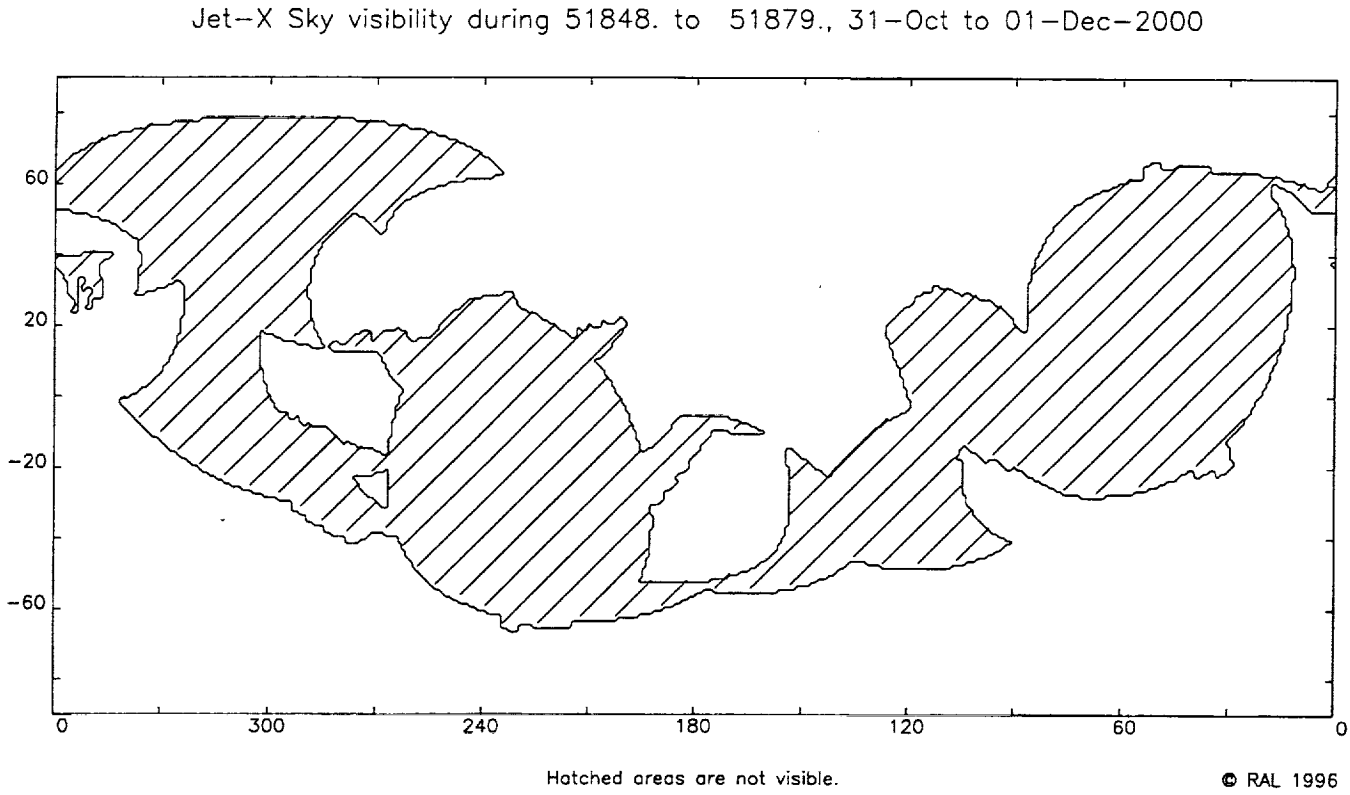

Figure 10: SODART Telescope Viewing Opportunities for Nov. & Dec. 2000

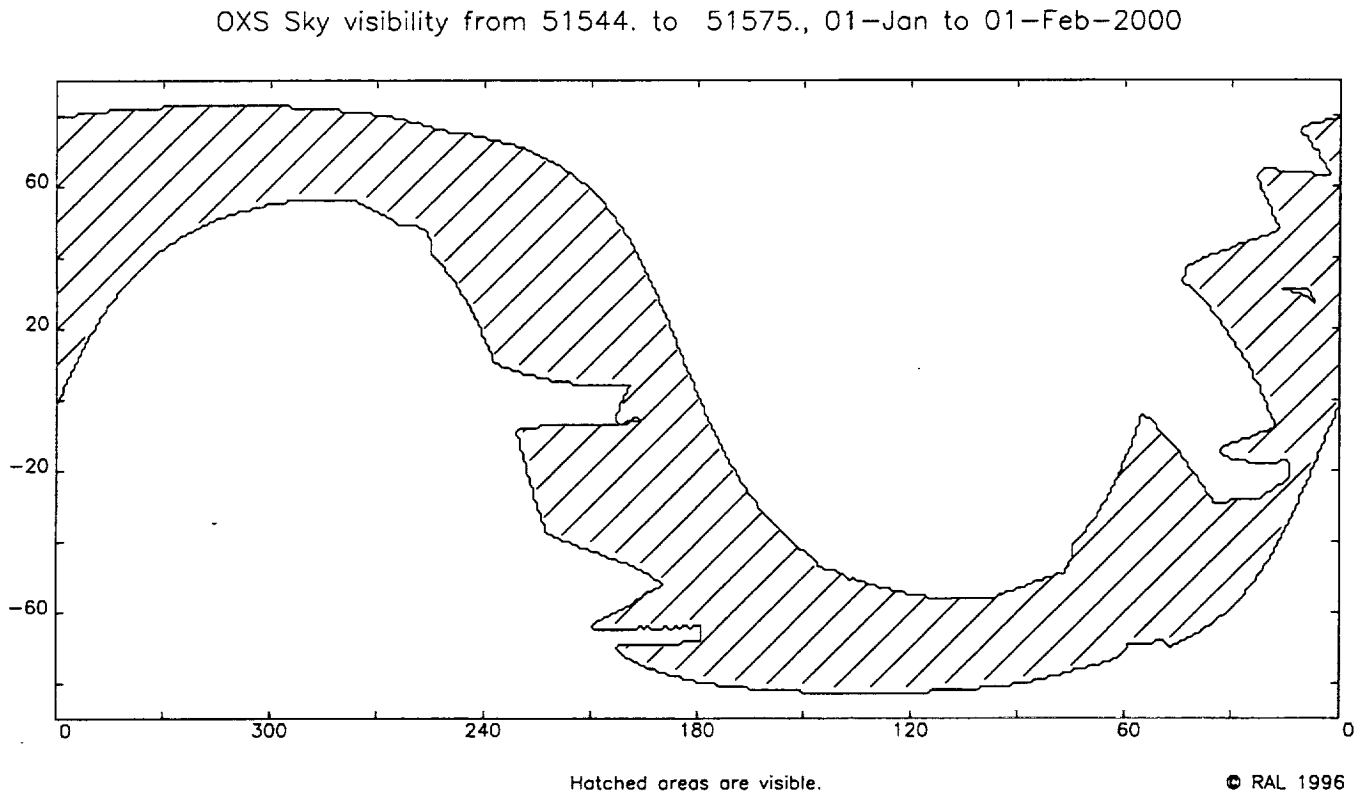

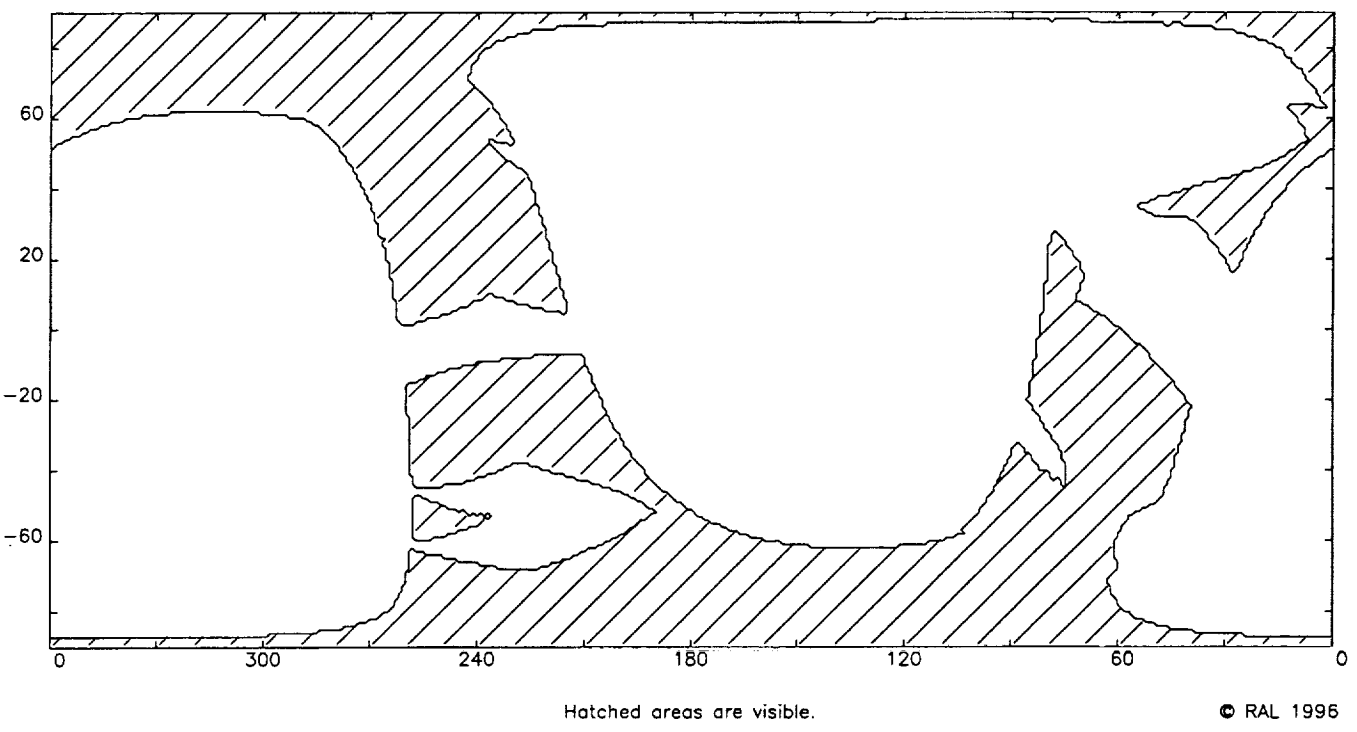

Figure 11: OXS Viewing Opportunities for Jan. & Feb. 2000 Figures 11 – 16 show visible areas of the sky (RA vs. Dec.) at one-month intervals.

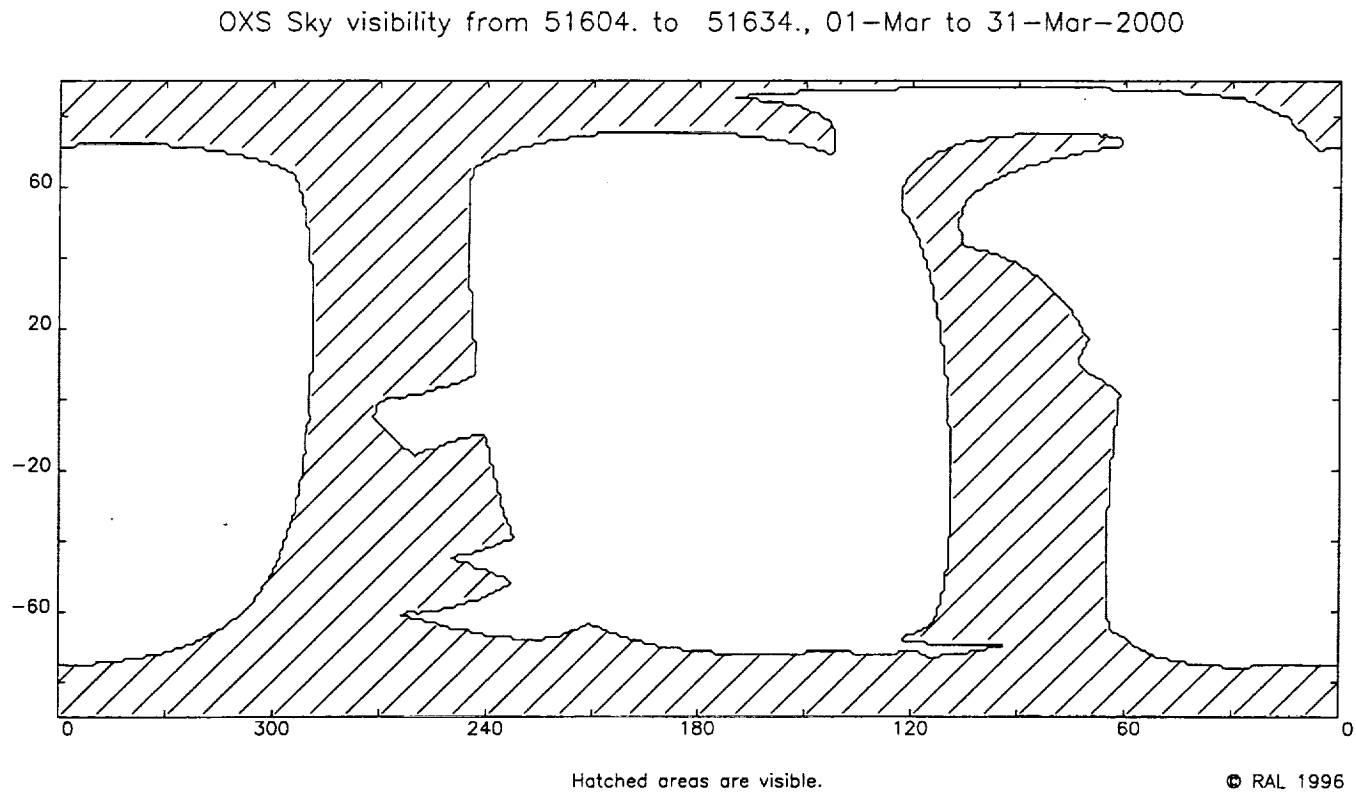

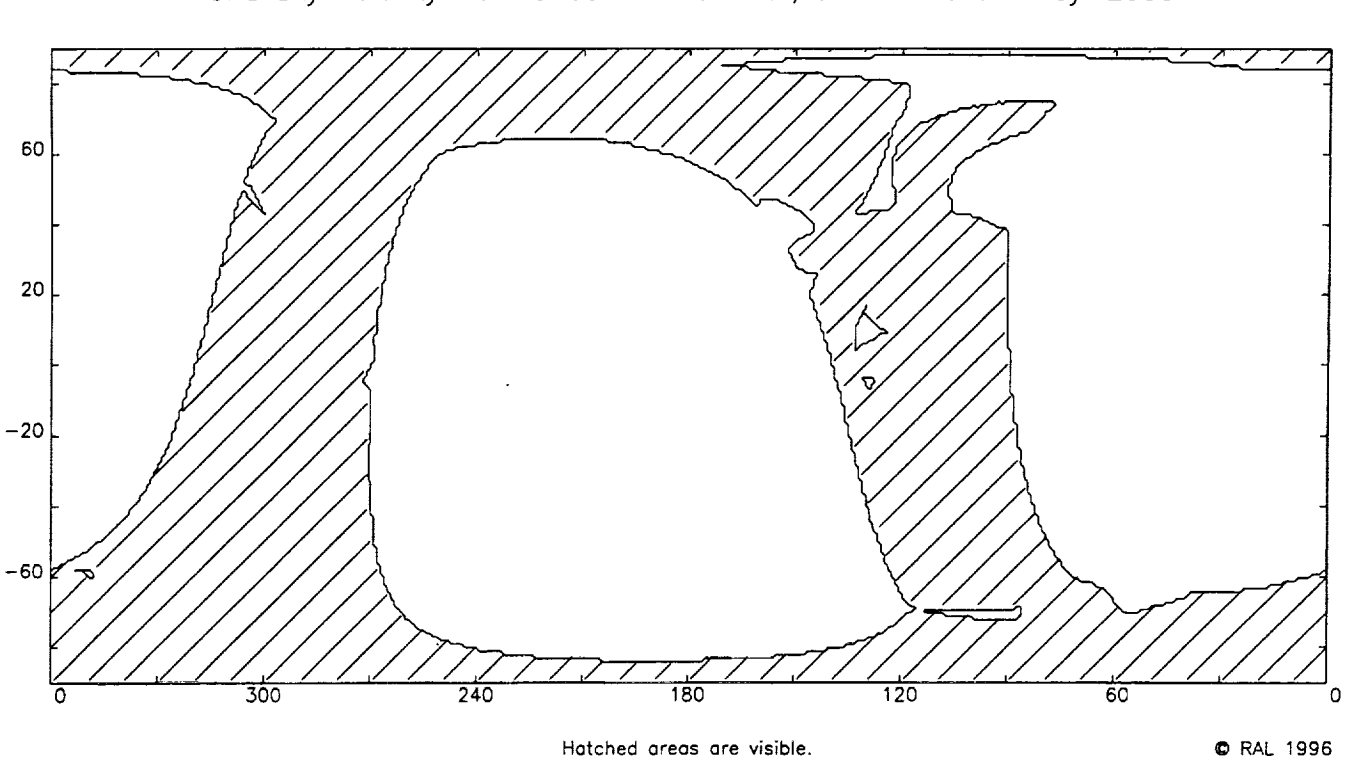

Figure 12: OXS Viewing Opportunities for March & April 2000

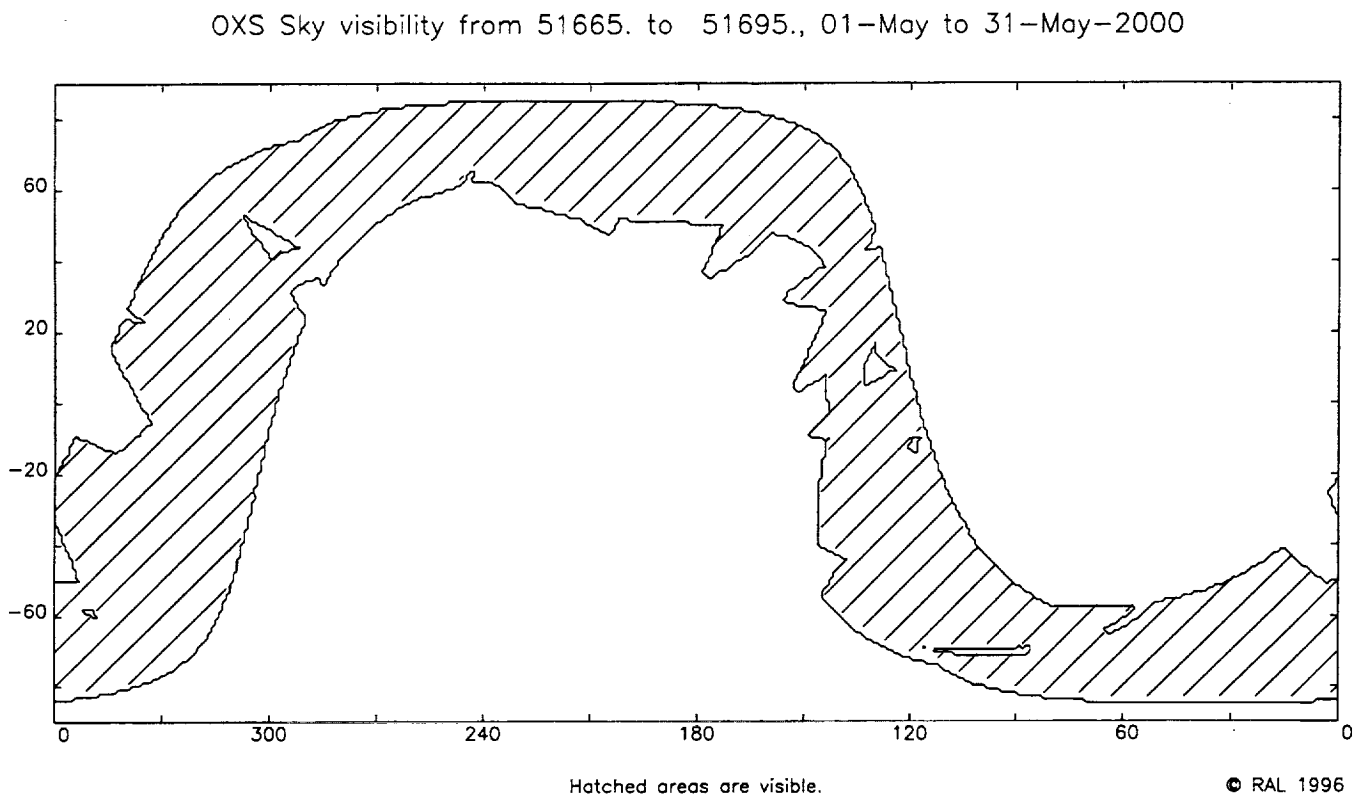

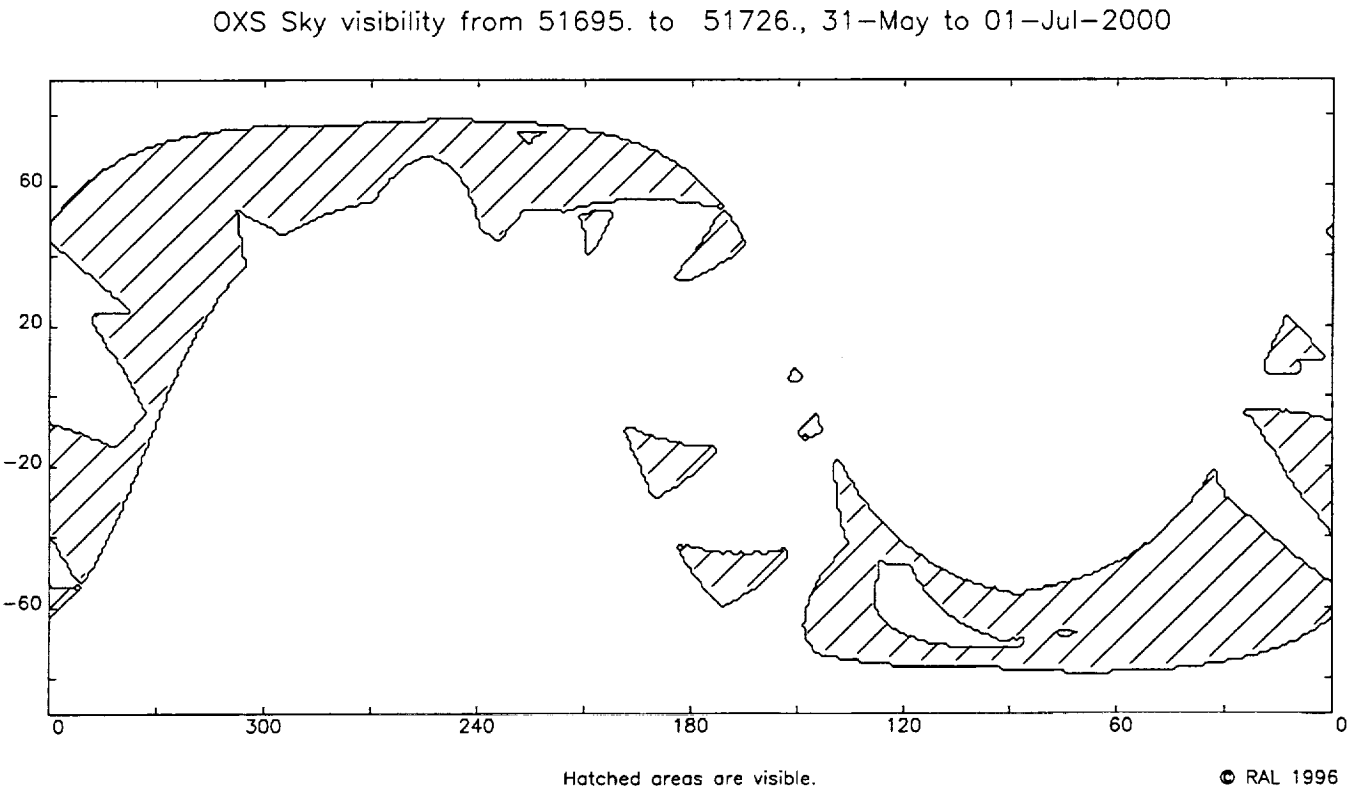

Figure 13: OXS Viewing Opportunities for May & June 2000

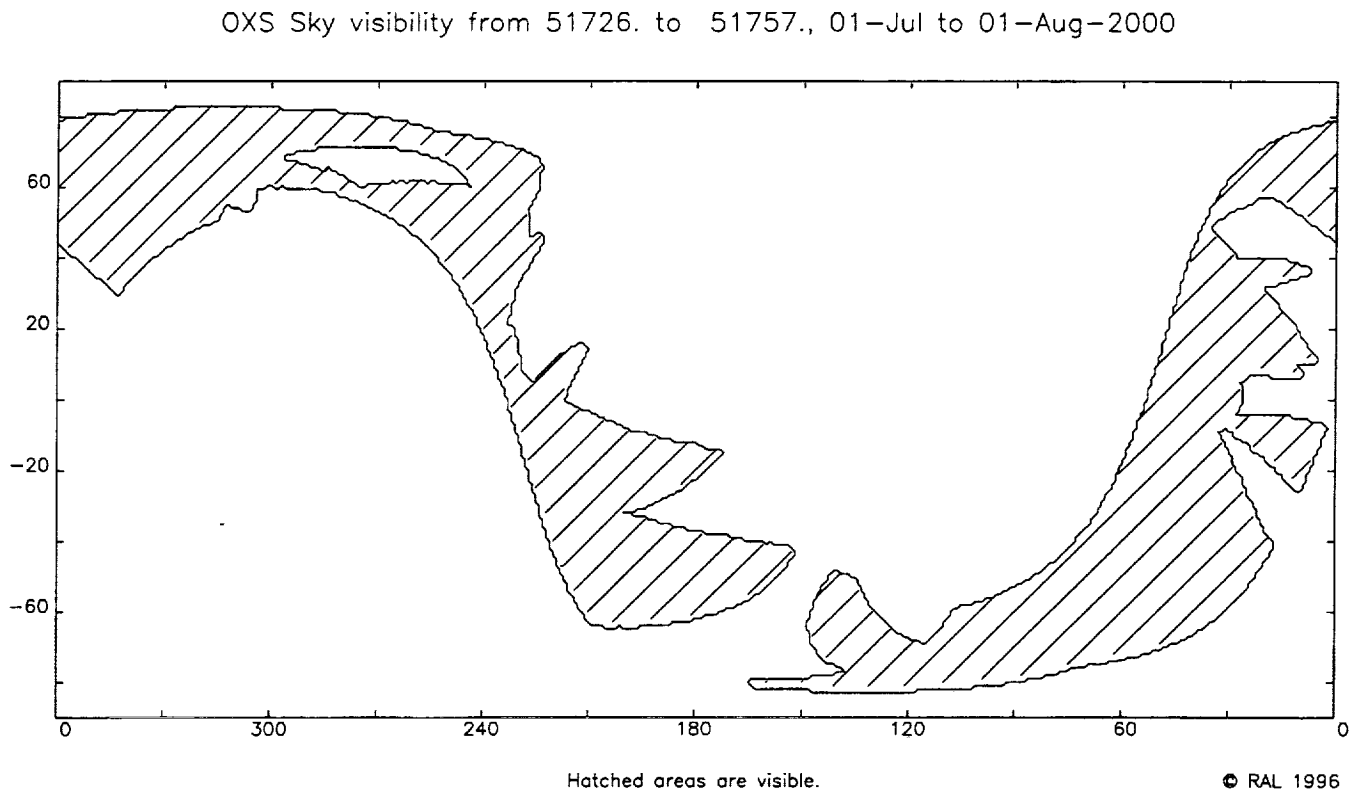

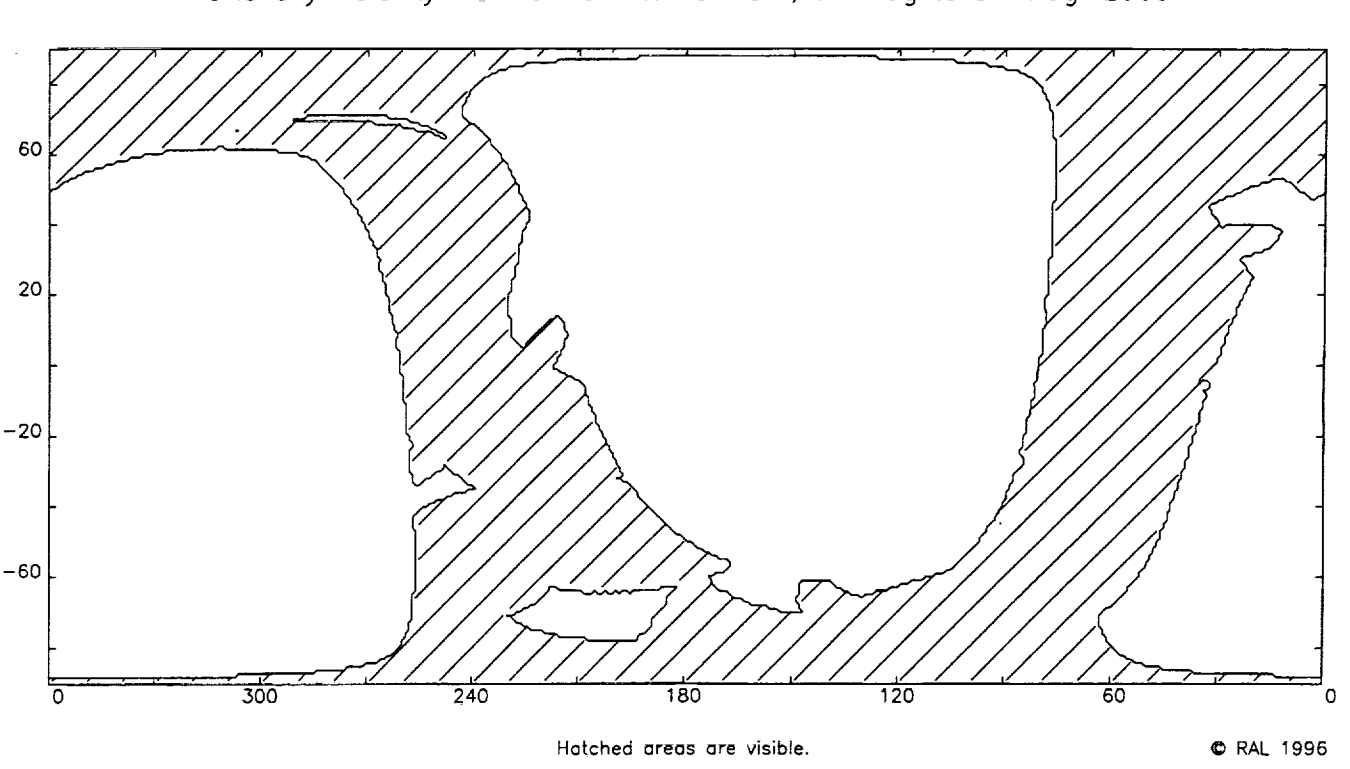

Figure 14: OXS Viewing Opportunities for July & Aug. 2000

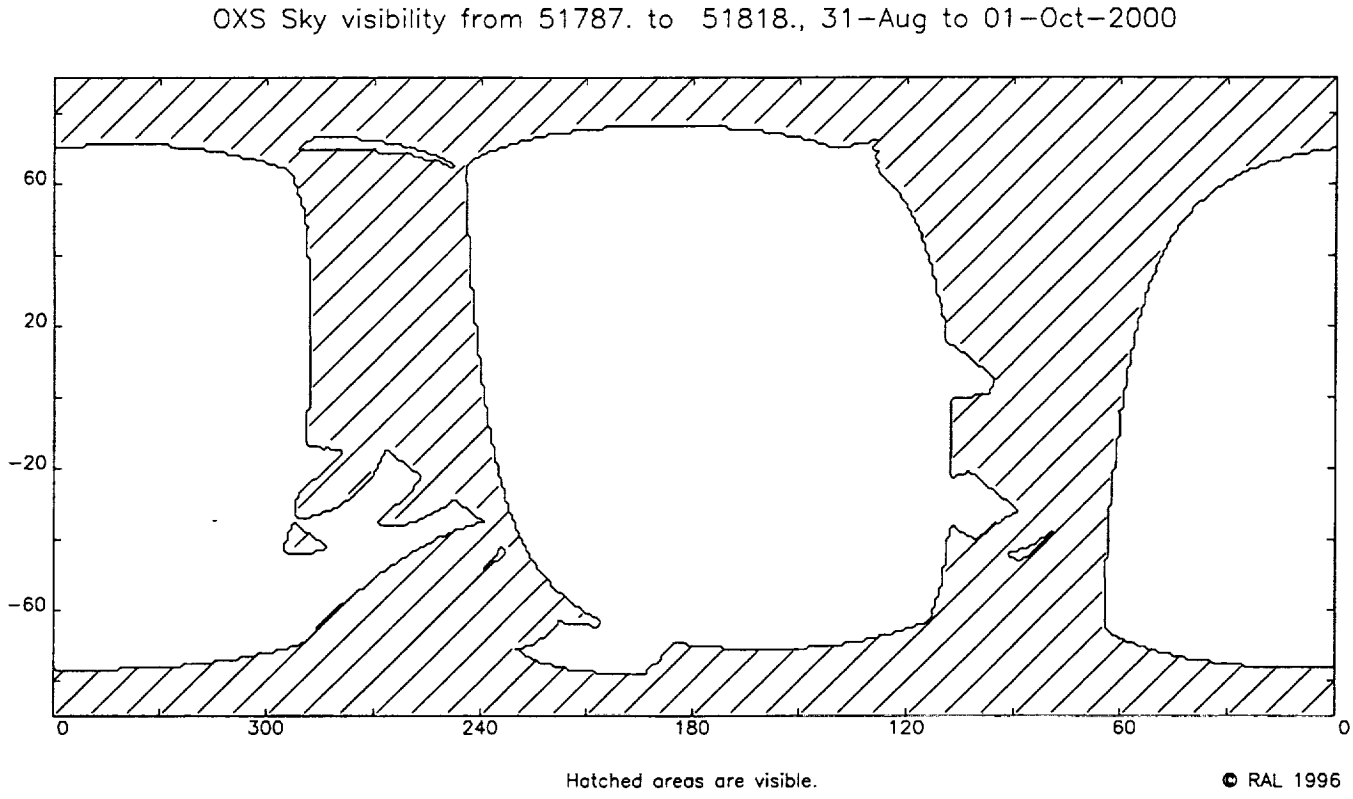

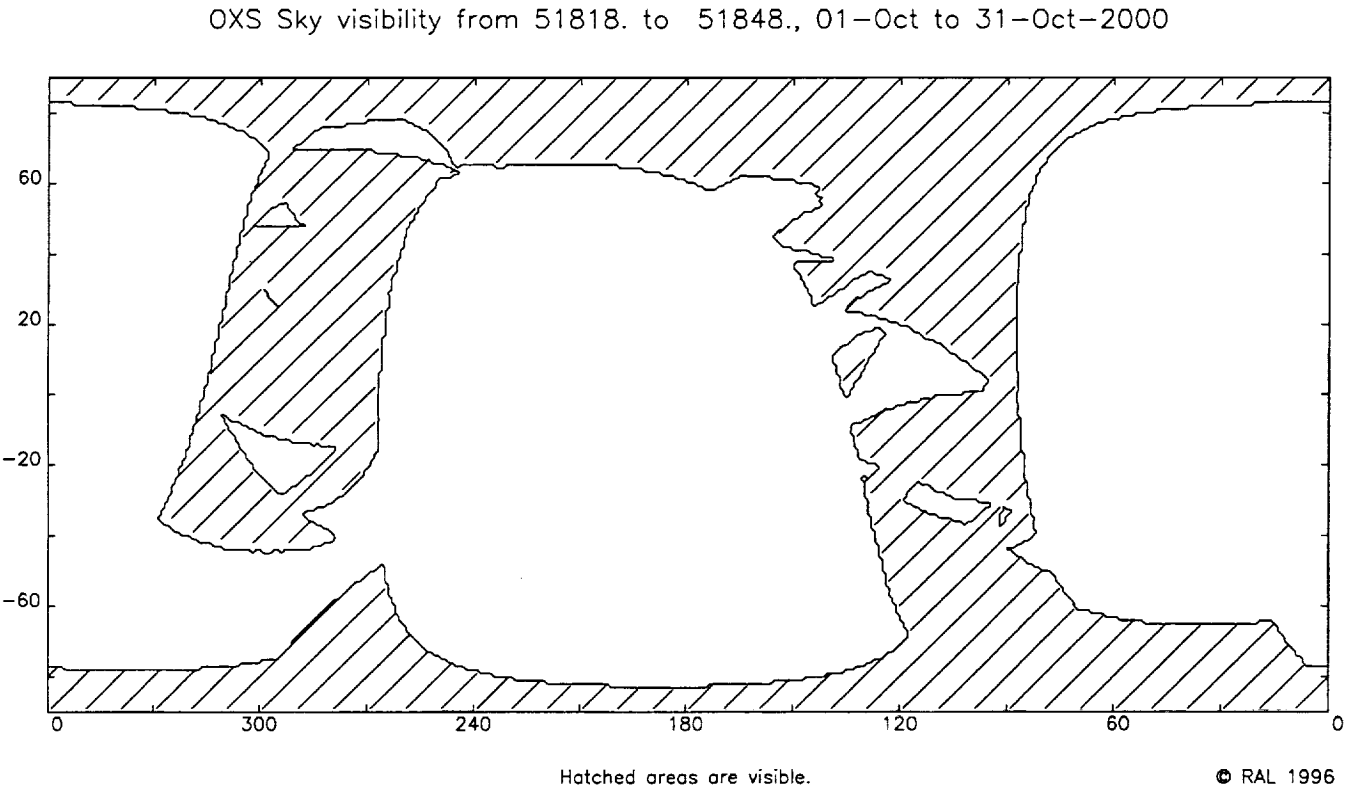

Figure 15: OXS Viewing Opportunities for Sept. & Oct. 2000

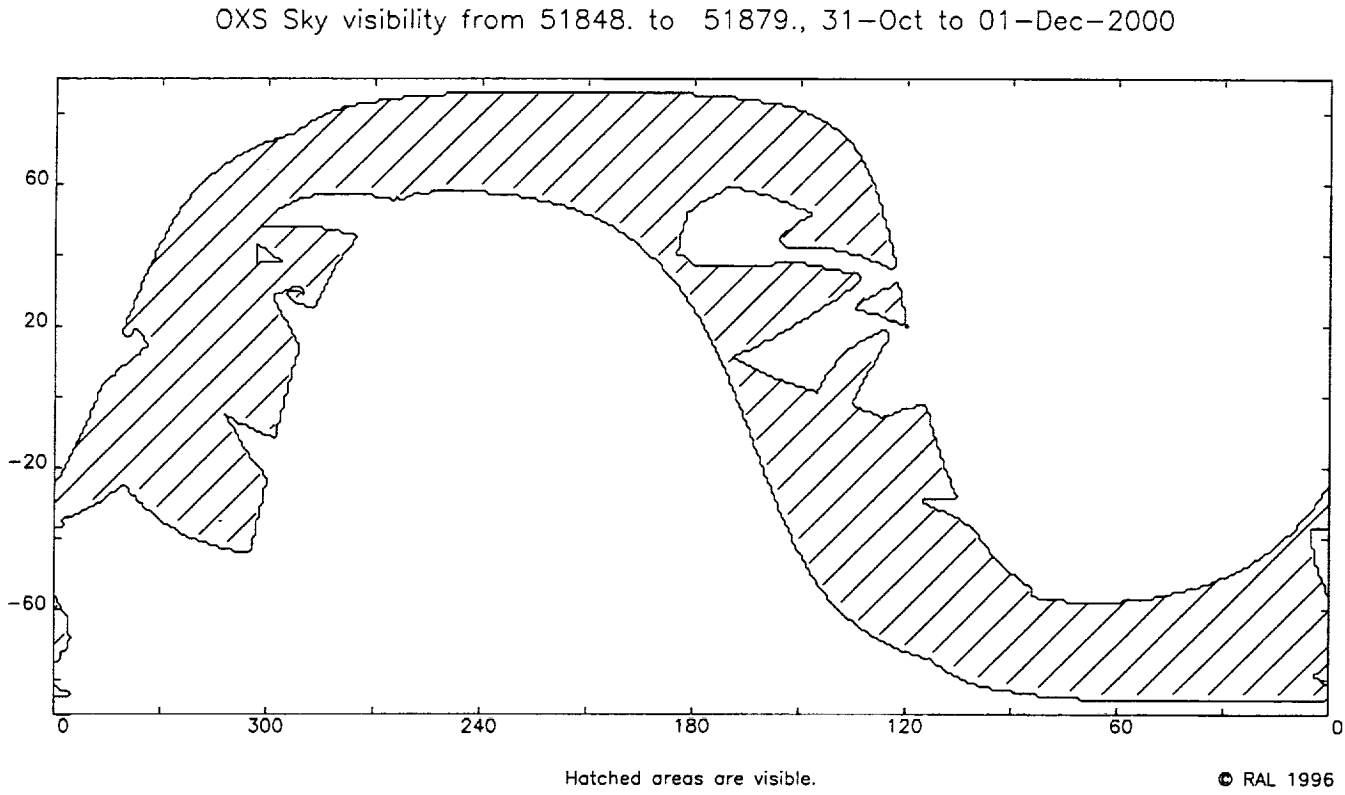

Figure 16: OXS Viewing Opportunities for Nov. & Dec. 2000

3 The SODART Mirror Modules (MM)

3.1 Introduction

The SODART Mirror Modules, designated FM1 & FM2, are two identical, multiply-nested, thin-foil telescopes. The mirror surfaces are conical approximations to a Wolter 1 geometry telescope, and are designed for moderate on-axis spatial resolution and high throughput above ~6 keV. The mirrors are assembled in quadrants and then attached to a support structure to form a complete mirror.

Parameters for each unit are listed in Table 2, and the available instrumentation is listed in Table 3.

Table 2: Mirror Module Parameters

Field of View (diameter)	60 ′
Half Power Diameter	2.5–3 ′
Focal Length	8 m
Inner Shell Diameter	16.32 cm
Outer Shell Diameter	60 cm
Reflecting surface	350 Å gold
Shell material	0.4 mm aluminum
Shell separation (min)	0.52 mm
Shell length	20 cm
Number of shells	143
Mass per telescope	101 kg
Total mirrored surface	62 m^2

Pre-flight calibration of the mirrors has been conducted at the Expanded Beam X-ray Optics Facility at the Daresbury Synchrotron, and is described in detail in Christensen et al. (1997). Their results are summarized here.

Table 3: Mirror Module Instrumentation

FM1	FM2
LEPC-1	LEPC-2
HEPC-1	HEPC-2
KFRD-1	KFRD-2
SIXA	SXRP
	OXS

3.2 Effective Area and Telescope Vignetting

Measurements of on-axis effective areas at energies of 6.627, 8.837, and 11.046 keV, integrated over a 105′ diameter field of view, indicate that the actual effective area is only ~65% of that predicted from ray-tracing studies of an ideal telescope with the SODART design parameters. These results are shown in Figure 17. It is believed that a significant fraction of this effective area reduction is due to the imperfect shape of individual foils near quadrant boundaries.

The relative reduction in effective area for off-axis sources (telescope vignetting) is shown in Figure 18.

3.3 Point Response and Encircled Energy Functions

An image of an on-axis point source at 6.627 keV is shown in Figure 19. The structure in the image is due to the quadrant supports and poorly shaped foils near quadrant boundaries. The azimuthally averaged point response functions measured at 6.627, 8.837, and 11.046 keV, and their integrals, the encircled energy functions, are shown in Figure 20 and Figure 21, respectively. As in section 3.2, the encircled energy is assumed to be 1.0 in a circle of diameter 105′.

Despite the image asymmetry, the azimuthally averaged point response function may be adequately represented by the simple function

$$psf(r) = (a_1/r)\, e^{-0.5(r/b_1)^2} + a_2\, e^{-r/b_2} + a_3\, e^{-r/b_3}$$

where r is expressed in arc-minutes, and the constants have the values shown in Table 4.

Table 4: Point Response Function Model Parameters

Parameter	6.6627 keV	8.837 keV	11.046 keV
a_1	0.01732	TBD	TBD
b_1	1.835	TBD	TBD
a_2	0.0024	TBD	TBD
b_2	2.659	TBD	TBD
a_3	3.047×10^{-5}	TBD	TBD
b_3	14.559	TBD	TBD

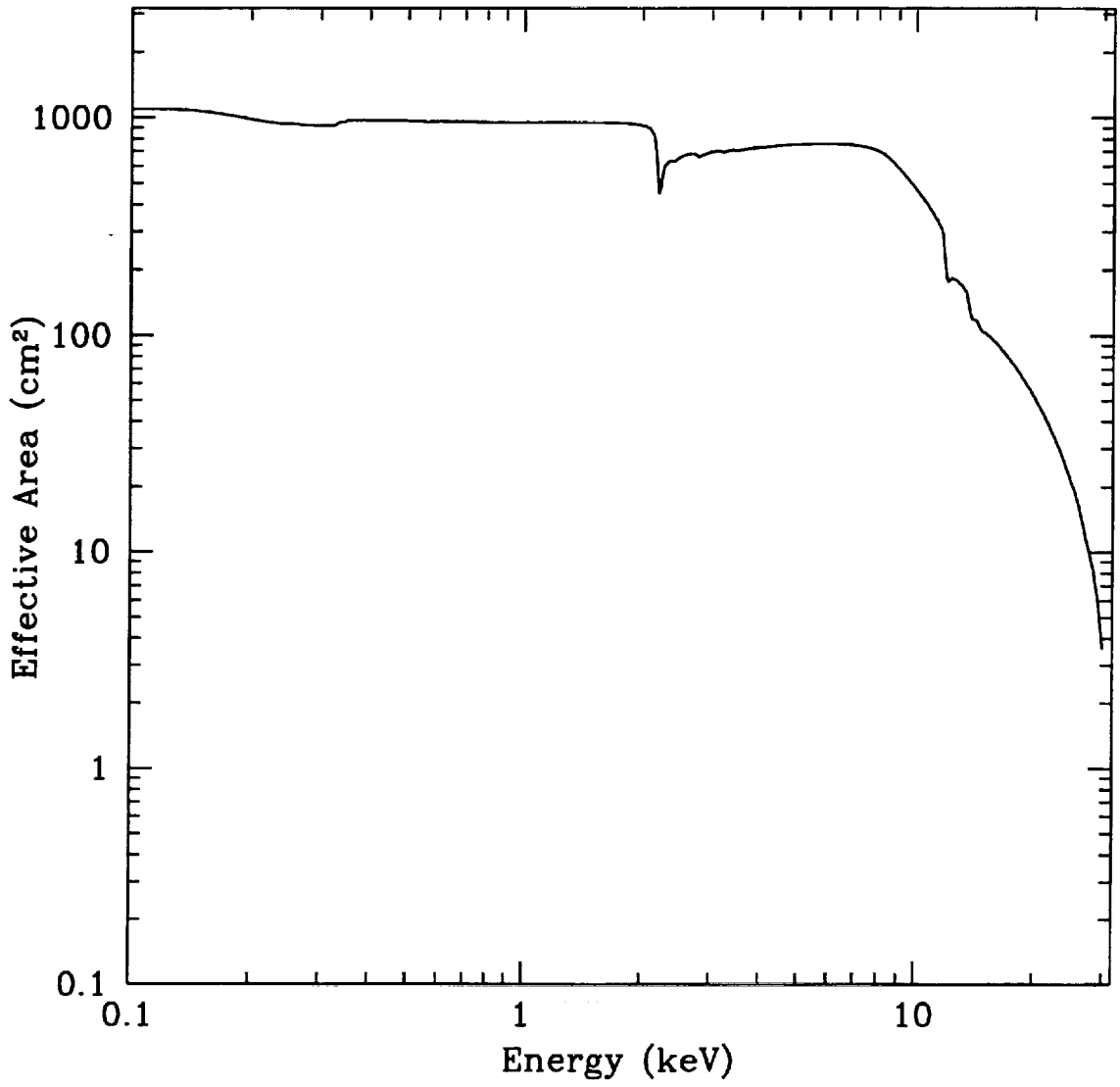

Figure 17: SODART on-axis effective area for a single module. The curve represents the effective area for an ideal x-ray telescope with the SODART parameters, normalized to measured effective areas at energies of 6.627, 8.837, and 11.046 keV.

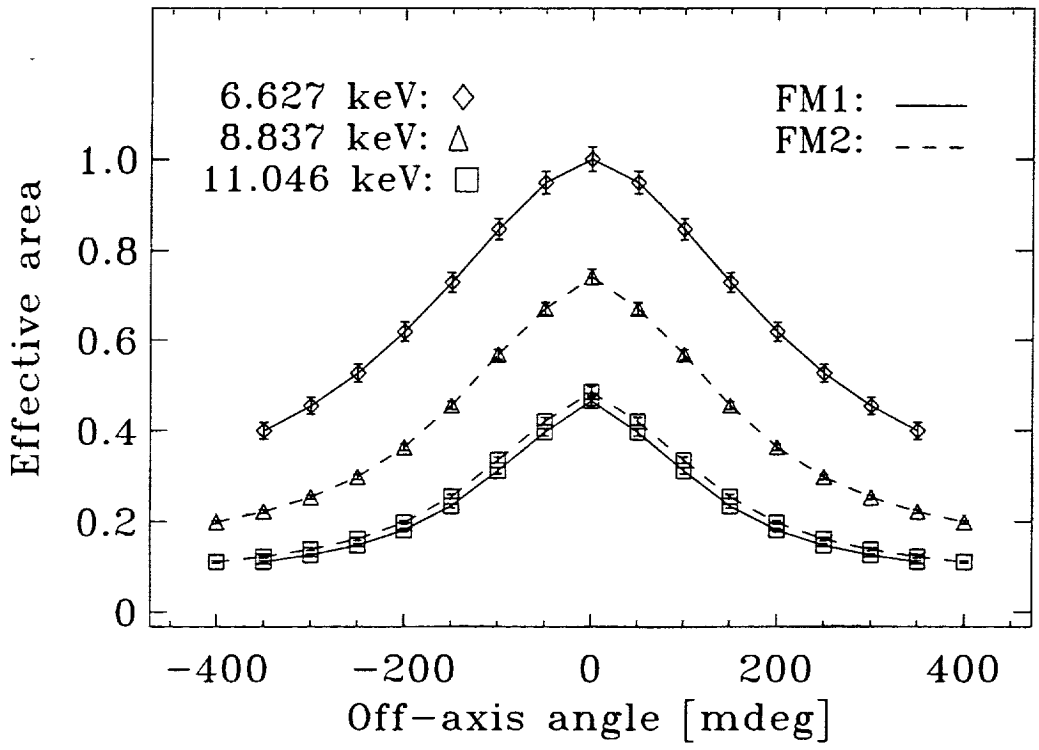

Figure 18: SODART vignetting function measured at three different energies and various off-axis angles. The solid lines are included to guide the eye only, and do not represent a functional fit.

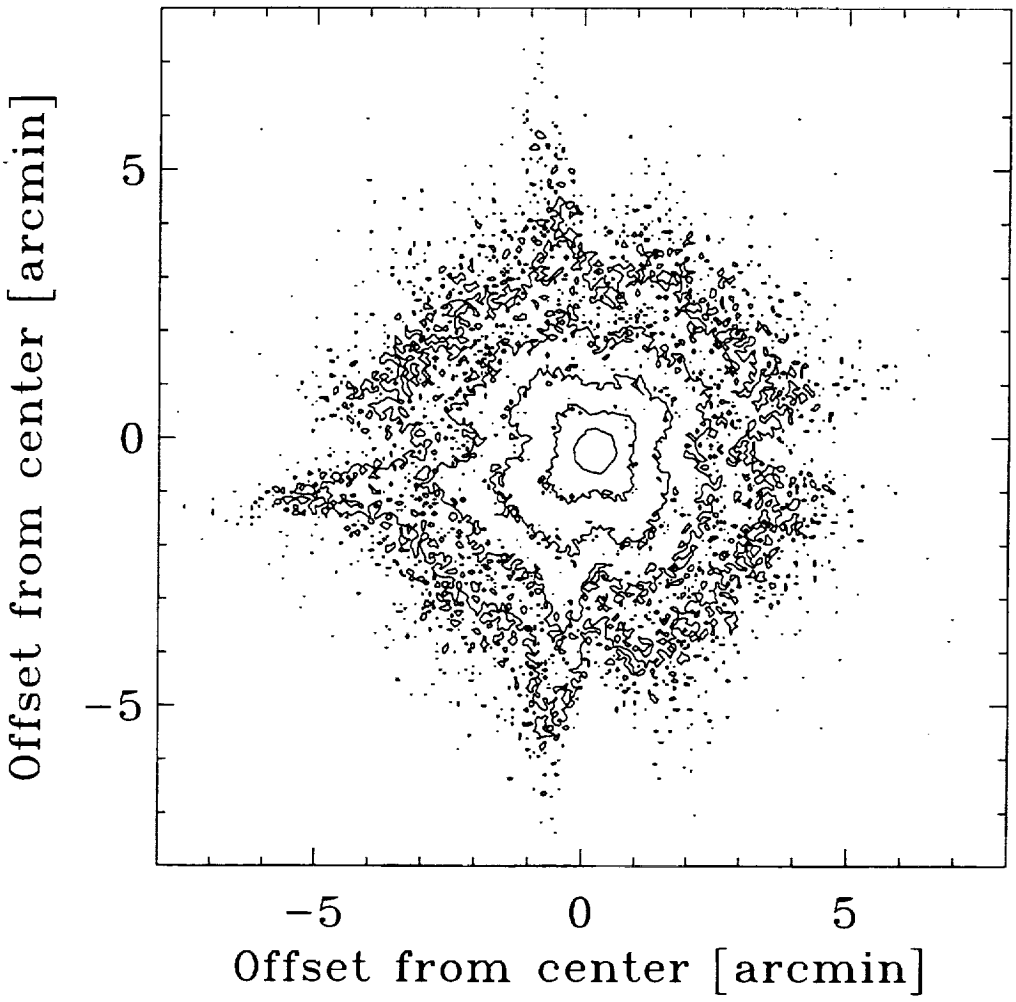

Figure 19: On-axis image of a point source at 6.627 keV in FM1. The data were recorded by an imaging detector similar to LEPC. Adjacent contours are spaced by a factor of e.

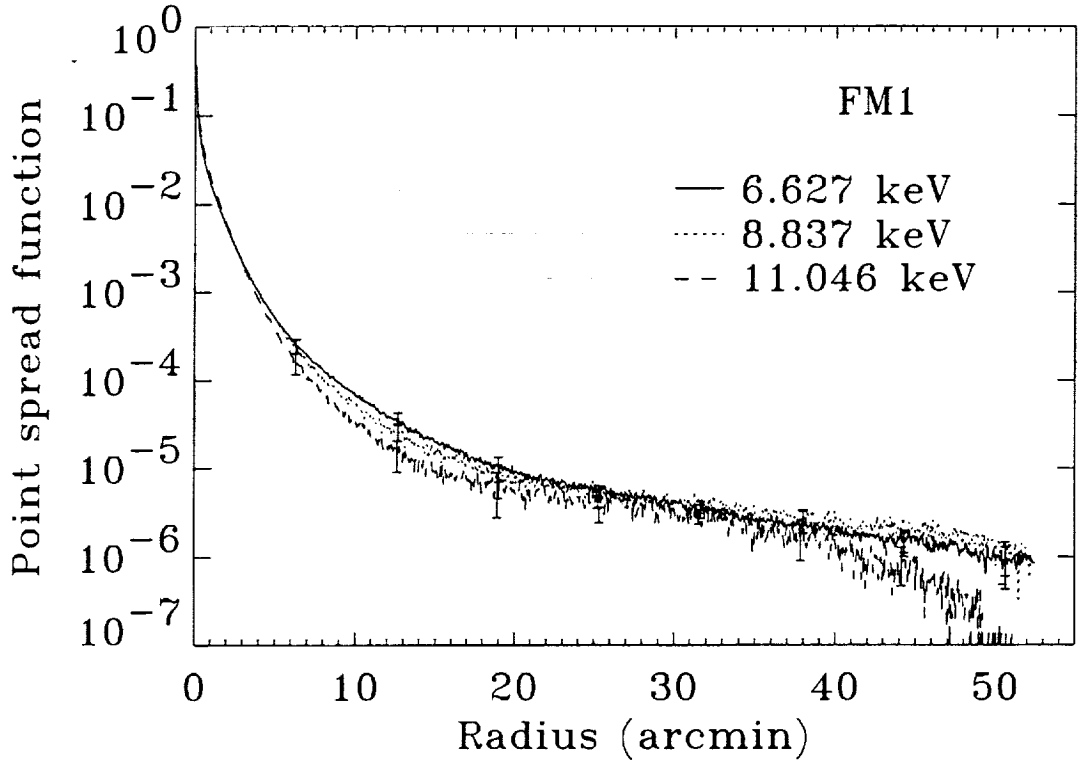

Figure 20: Point Response Function of the SODART MM at three different energies. The function is estimated from the same data used to derive the encircled energy function.

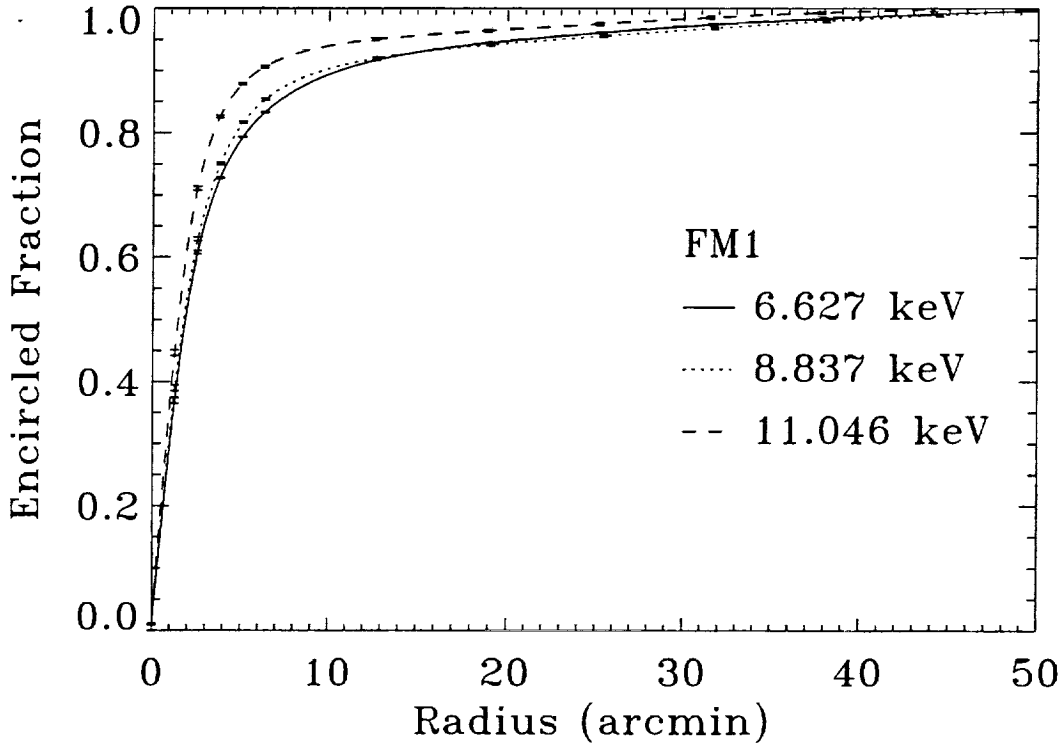

Figure 21: Encircled Energy Function of the SODART MM at three different energies.

4 The High Energy and Low Energy Proportional Counters (HEPC/LEPC)

4.1 Summary Description

The High Energy and Low Energy Proportional Counter (HEPC/LEPC) detectors offer large effective area, good time resolution, and moderate spatial and spectral resolution over a broad energy range. They are well-suited for temporal studies and studies of broad-band spectra. A HEPC/LEPC detector pair will be provided for each telescope. Each detector pair will share a common gas resevoir.

The detectors are microstrip gas proportional counters (MSPC), in which one conventional wire grid plane is replaced by a grid of narrowly spaced conducting microstrips, deposited by photolithographic techniques on an insulating substrate. Pulse shape and amplitude are determined from microstrip anode signals, and positional information from the microstrip cathodes. Positional information in the orthogonal direction is determined from a conventional wire grid, suspended ~1 mm above the microstrip plate. A third electrode, mounted on the rear of the plate, surrounds the useful detector area defined by the counter entrance window. It provides a veto signal for charged particles whose trajectories are nearly parallel to the microstrip plate and which thus mimic the pulse shapes of valid x-ray events. Detailed descriptions of the HEPC/LEPC detectors can be found in Budtz-Jørgensen et al. (1994).

The effective areas of the HEPC & LEPC detectors are shown in Figure 22, and detailed detector parameters are listed in Table 5. The intrinsic spatial resolution of the detectors as a function of energy is shown in Figure 23. The FWHM (or HPD for an assumed Gaussian distribution) is $\lesssim$ 1 mm over most of the operating range of the detectors. In comparison, the HPD of the mirror is $\sim 3'$ (~7 mm for an 8 m focal length telescope). The contribution of the detectors to the overall image resolution is thus negligible. The HEPC/LEPC energy resolution is $\Delta E_{FWHM} = 0.33(E/1\mathrm{keV})^{1/2}$ keV, or ~13% at 6 keV. The detector time resolution depends on the selected data format (see below) and can range from 1 - 400 μsec. Absolute times will be derived post-facto, using regular spacecraft clock-UT calibrations, and are expected to be accurate to ~1 msec.

Charged particle background rejection efficiency, using both pulse shape discrimination and veto information, is expected to be $\gtrsim$ 99.9%. The expected particle background is $< 1 \times 10^{-4}$ cts s^{-1} cm^{-2} keV^{-1}. X-ray–like events will also arise from Compton processes in the counter gas, produced by high energy photons transmitted through the satellite and detector structure. The combined background (excluding the diffuse X-ray background) is expected to be $\sim 5 \times 10^{-4}$ cts s^{-1} cm^{-2} keV^{-1} and is uncertain by a factor of ~2.

4.2 Observing Modes and Data Formats

4.3 Calibration

Each detector contains its own internal ^{55}Fe calibration source, which illuminates an area of the detector outside the field of view with 5.9 keV X–rays. These data will be used to

Table 5: HEPC/LEPC Detector Parameters

	HEPC	LEPC
Field of View	60′	30′
Entrance Window	140 mm diameter circle	70 mm diameter circle
Window Thickness	7.5 μm polyimide, 40 nm Al	0.85 μm polyimide, 40 nm Al
Spatial Resolution	$\lesssim$1 mm	$\lesssim$1–3 mm
Energy Resolution	$\sim$13% @ 6 keV	
Time Resolution	1 – 400 μsec, depending on data format	
Energy Range	2 – 25 keV	0.2 – 8 keV, 0.5 – 16 keV
Gas Thickness	4 cm	4 cm
Gas Pressure	1 atm	0.5 atm
Gas Composition	Xe 90%, CH_4 10%	
Non-X-ray Bgd (2′ dia. circle)	$\sim 2 \times 10^{-3}$ c s^{-1}	$\sim 7 \times 10^{-4}$ c s^{-1}
X-ray Bgd (2′ dia. circle on-axis)	$\sim 1.8 \times 10^{-3}$ c s^{-1}	$\sim 1.1 \times 10^{-2}$ c s^{-1}
Storage Capacity	80 Mbytes per detector	
Maximum Count Rate	$\sim$ 3000 c s^{-1}	

monitor gas gain and energy response. In addition, when not in the telescope focus, the full active areas of the detectors can be illuminated with X–rays from a number of ^{55}Fe sources through a multiple collimator. This produces 62 point-like spots within the central 150 mm of HEPC and 33 point-like spots within the central 70 mm of LEPC. From these data, detector spatial response, energy response, efficiency and background rejection efficiency, and spatial gain variations can be determined. Observers can request out-of-focus calibration exposures before and after their observations.

4.4 Determining the Feasibility of HEPC/LEPC Observations

4.4.1 Background

The HEPC & LEPC detectors will encounter cosmic background from the diffuse x-ray background and scattered solar x-rays, as well as non-X-ray background from charged particles, cosmic-ray-induced secondary radiation from the spacecraft structure, and high energy x-ray background photons which penetrate the spacecraft and detector structures. The total non-X-ray background is estimated to be $\sim 5 \times 10^{-4}$ counts cm^{-2} s^{-1} keV^{-1} for either HEPC or LEPC. In a 2′ diameter circle ($\sim$ 4.7 mm for an 8 m focal length), this corresponds to a rate of $\sim 2 \times 10^{-3}$ counts s^{-1} for HEPC (2 – 25 keV) and $\sim 7 \times 10^{-4}$ counts s^{-1} for LEPC (0.2 – 8 keV).

The diffuse x-ray background in HEPC & LEPC may be estimated using the effective area shown in Figure 22 and a model xrb spectrum. We use the ROSAT spectrum of Wang and McCray (1993) below 3 keV, and the HEAO-1 spectrum of Boldt (1987) above 3 keV, and find

a value of ~ 2 c s^{-1} deg^{-2} for HEPC and ~ 12 c s^{-1} deg^{-2} for LEPC. In a 2′ diameter circle, these correspond to rates of $\sim 1.8 \times 10^{-3}$ counts s^{-1} for HEPC and $\sim 1.1 \times 10^{-2}$ counts s^{-1} for LEPC. Readers should be aware, however, that the soft component of the xrb is dominated by galactic contributions and can vary with viewing direction by as much as a factor of 5. The total xrb in HEPC & LEPC may therefore vary by a large factor.

4.4.2 Estimating HEPC/LEPC Count Rates

Source count rates in HEPC/LEPC can be estimated using HEASARC's multi-mission simulator PIMMS. It is assumed that a spectral model and either an absolute flux or a count rate in another instrument are known. The following dialog illustrates the use of PIMMS to estimate the HEPC/LEPC rate for a source with a $10^{7.4}$ K Raymond-Smith spectrum, cosmic abundances, $N_H = 3 \times 10^{20}$ cm^{-2}, and a 0.5-2.0 keV flux, at the detector, of 9×10^{-14} erg cm^{-2} s^{-1}.

```
sxg-95: pimms
*** PIMMS version 2.3 ***
    1996 Jun 03 release
    (this version does not simulate images)
    Reading mission directory, please wait
* Current model is BREMSSTRAHLUNG, kT=  10.0000 keV; NH =  1.000E+21
   <--- Use 'MODEL' command to change
* By default, input rate is taken to be
 Flux (  2.000- 10.000 keV) in ergs/cm/cm/s
   <--- Use 'FROM' command to change the default
* Simulation product will be
 Count rate in ASCA SIS  (  0.000-  0.000 keV)
   <--- Use 'INSTRUMENT' command to switch to another instrument
PIMMS > from flux erg 0.5-2.0
PIMMS > model rs 2.165 3.0e20
PIMMS > instrument sxg lepc low
PIMMS > go 9.0e-14
* For Raymond Smith model with kT=  2.1645 keV (logT=7.4); NH =  3.000E+20
   and a flux (  0.500-  2.000keV) of  9.000E-14 ergs/cm/cm/s
  (Model normalization =  2.743E-03)
* PIMMS predicts  3.003E-02 cps with SXG LEPC LOW
PIMMS > instrument sxg hepc
PIMMS > go 9.0e-14
* For Raymond Smith model with kT=  2.1645 keV (logT=7.4); NH =  3.000E+20
   and a flux (  0.500-  2.000keV) of  9.000E-14 ergs/cm/cm/s
  (Model normalization =  2.743E-03)
* PIMMS predicts  6.162E-03 cps with SXG HEPC
PIMMS > quit
sxg-96:
```

In Figures 33 – 32, we provide count rate conversion factors from ASCA and ROSAT rates, for power law, bremsstrahlung, and black body spectra, and a range of spectral parameters.

PIMMS may be obtained from the **software/tools** directory in the anonymous ftp node **legacy.gsfc.nasa.gov**. Version 2.0 includes support for SXG instruments. To update earlier versions, users may obtain new mission lists and SXG area files from the directory **/pub/sxg/pimms** in the anonymous ftp node **sao-ftp.harvard.edu**.

4.4.3 Simulating HEPC/LEPC Spectra

HEPC/LEPC spectra can be simulated with the HEASARC XSPEC program. The following dialog illustrates the simulation of the spectrum of a 5 ksec HEPC/LEPC observation of a Raymond-Smith plasma with an emission integral of 10^{60} cm^{-3}, temperature of $10^{7.5}$ K, column density of 10^{21} cm^{-2}, at a distance of 10 kpc.

```
!xspec 13:04:44 21-Mar-96
XSPEC> model raymond wabs
  mo = wabs[2] (raymond[1])
 Input parameter value, delta, min, bot, top, and max values for ...
 Mod parameter  1 of component  1 raymond  kT(keV)
    1.000      1.0000E-02  8.0000E-03  8.0000E-03   64.00        64.00
 2.73
 Mod parameter  2 of component  1 raymond  Abundanc
    1.000     -1.0000E-03      0.          0.        5.000        5.000
 1.0
 Mod parameter  3 of component  1 raymond  Redshift
       0.     -1.0000E-03      0.          0.        2.000        2.000
 0.0
 Mod parameter  4 of component  1 raymond  norm
    1.000      1.0000E-02      0.          0.      1.0000E+24   1.0000E+24
 0.8356
 Mod parameter  5 of component  2 wabs     nH 10^22
    1.000      1.0000E-03      0.          0.      1.0000E+05   1.0000E+06
 0.1
  ------------------------------------------------------------------------
  ------------------------------------------------------------------------
  mo = wabs[2] (raymond[1])
  Model Fit Model   Component     Parameter   Value
  par   par comp
    1     1    1       raymond     kT(keV)    2.73000     +/-       0.
    2     2    1       raymond     Abundanc   1.00000     frozen
    3     3    1       raymond     Redshift         0.    frozen
    4     4    1       raymond     norm       0.835600    +/-       0.
    5     5    2       wabs        nH 10^22   0.100000    +/-       0.
  ------------------------------------------------------------------------
  ------------------------------------------------------------------------
```

```
    3 variable fit parameters
XSPEC> fakeit none
 For fake data, file #  1 needs response file: lepc.rmf
              ... and ancillary response file : none
Use counting statistics in creating fake data? (y)
 Input optional fake file prefix (max 12 chars):
 Override default values for file #    1
 Fake data filename (lepc.fak):
 T, A, Bkg, cornorm ( 1.0000 , 1.0000 , 1.0000 , 0. ): 5000.0
 Net count rate (cts/s) for file   1   360.3    +/-  0.2684
 Chi-Squared =      141.4     using   128 PHA bins.
 Reduced chi-squared =      1.131
XSPEC> fakeit none
 For fake data, file #  1 needs response file: hepc.rmf
              ... and ancillary response file : none
Use counting statistics in creating fake data? (y)
 Input optional fake file prefix (max 12 chars):
 Override default values for file #    1
 Fake data filename (hepc.fak):
 T, A, Bkg, cornorm ( 1.0000 , 1.0000 , 1.0000 , 0. ): 5000.0
 Net count rate (cts/s) for file   1   83.20    +/-  0.1290
 Chi-Squared =      100.2     using   128 PHA bins.
 Reduced chi-squared =     0.8017
XSPEC>
```

Plots of the raw spectra are shown in Figure 51 and Figure 52. The required response matrices, lepc.rmf and hepc.rmf, may be obtained from the directory **/pub/sxg/xspec** in the anonymous ftp node **sao-ftp.harvard.edu**.

XSPEC may be obtained from the **software/xanadu** directory in the anonymous ftp node **legacy.gsfc.nasa.gov**.

4.4.4 Detection of Point Sources

The total background per 2′ diameter sperture in a ∼10 ksec observation is likely to be ≳100 counts for LEPC and ≳30 counts for HEPC. Therefore, Gaussian statistics can be used to estimate the minimum count rate, R_{min}, required to detect a point source at a given count rate significance, as a function of exposure time T. For a point source on-axis, R_{min} is given by the solution to

$$N_\sigma = \frac{R_{min} f T}{\sqrt{R_{min} f T + R_B T}},$$

or

$$R_{min} f T = \frac{N_\sigma^2}{2}\left(1 + \sqrt{1 + \frac{4 R_B T}{N_\sigma^2}}\right).$$

Here, N_σ is the signal-to-noise ratio of the net source counts, expressed as number of σ, f is the encircled energy fraction (0.5 on-axis), and R_B is the total background rate in the

aperture. Results are shown in Figure 53 for LEPC, and Figure 54 for HEPC, for a range of background rates.

Table 6: HEPC/LEPC Data Formats

Format	Event Size	Time Resolution	Event Structure
RAW	24 bytes	1 μsec	Signal from each read–out node of micro strip plate Signal from each read–out node of wire grid Signal from veto electrode 32 bit time from satellite clock in units of μsec
A1	9	10	Derived position on micro strip plate Charge ratio on micro strip plate Derived position on wire grid Charge ratio on wire grid Signal from veto electrode Derived energy Pulse rise time 16 bit time from previous event in units of 10 μsec
A2	7	10	Derived position on micro strip plate Derived position on wire grid Signal from veto electrode Derived energy Pulse rise time 16 bit time from previous event in units of 10 μsec
B1	6	10	Derived position on micro strip plate Derived position on wire grid Signal from veto electrode Derived energy Pulse rise time 8 bit time from previous event in units of 10 μsec
B2	6	400	Derived position on micro strip plate Derived position on wire grid Signal from veto electrode Derived energy Pulse rise time 8 bit time from previous event in units of 400 μsec
I	7	16	Derived position on micro strip plate Derived position on wire grid Signal from veto electrode Derived energy Pulse rise time 16 bit time from previous event in units of 16 μsec
D1	2	10	Derived energy 8 bit time from previous event in units of 10 μsec

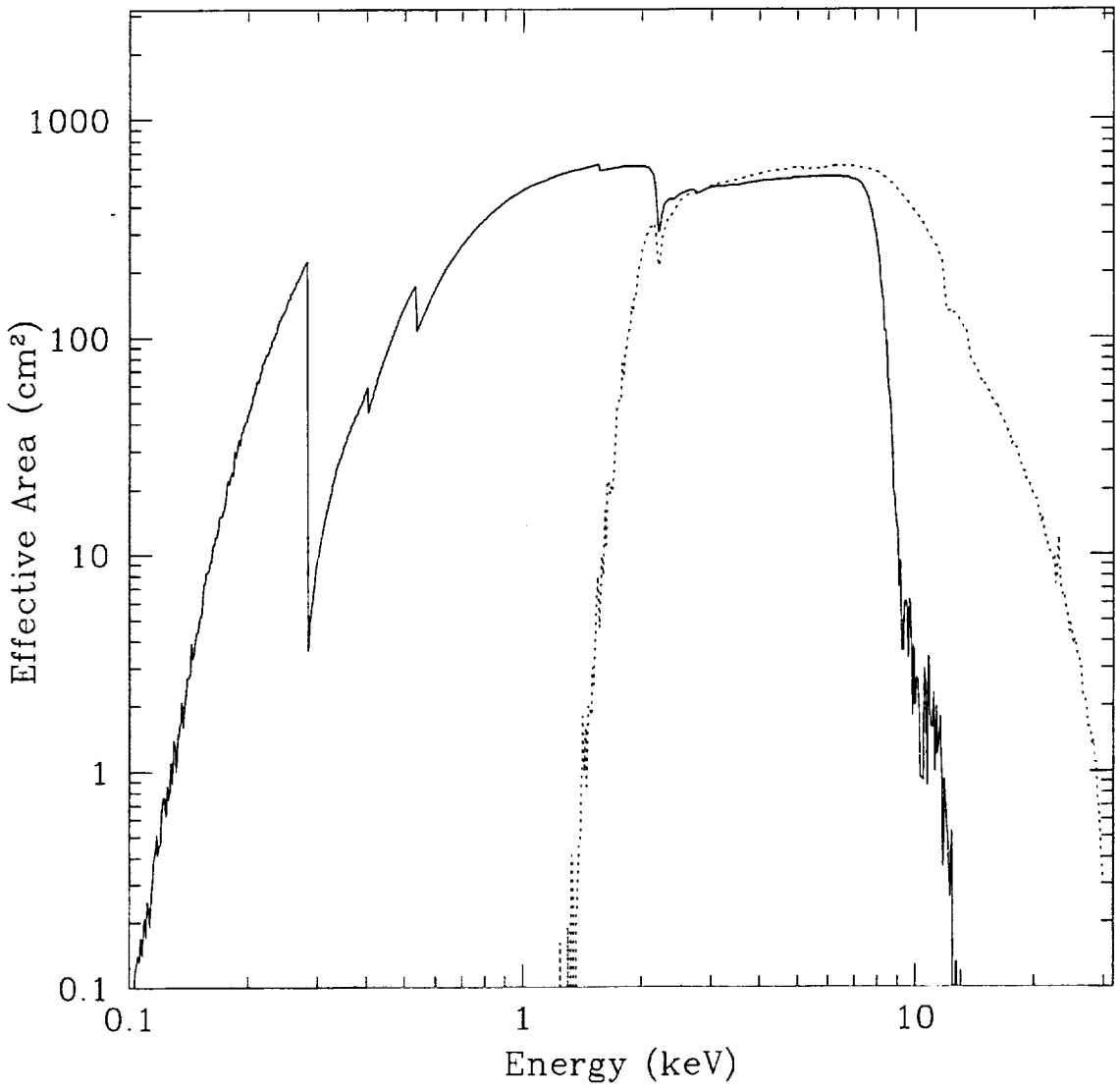

Figure 22: HEPC/LEPC Effective Area. The solid curve shows the effective area of one MM with the LEPC and the dashed curve shows the effective area of one MM with the HEPC.

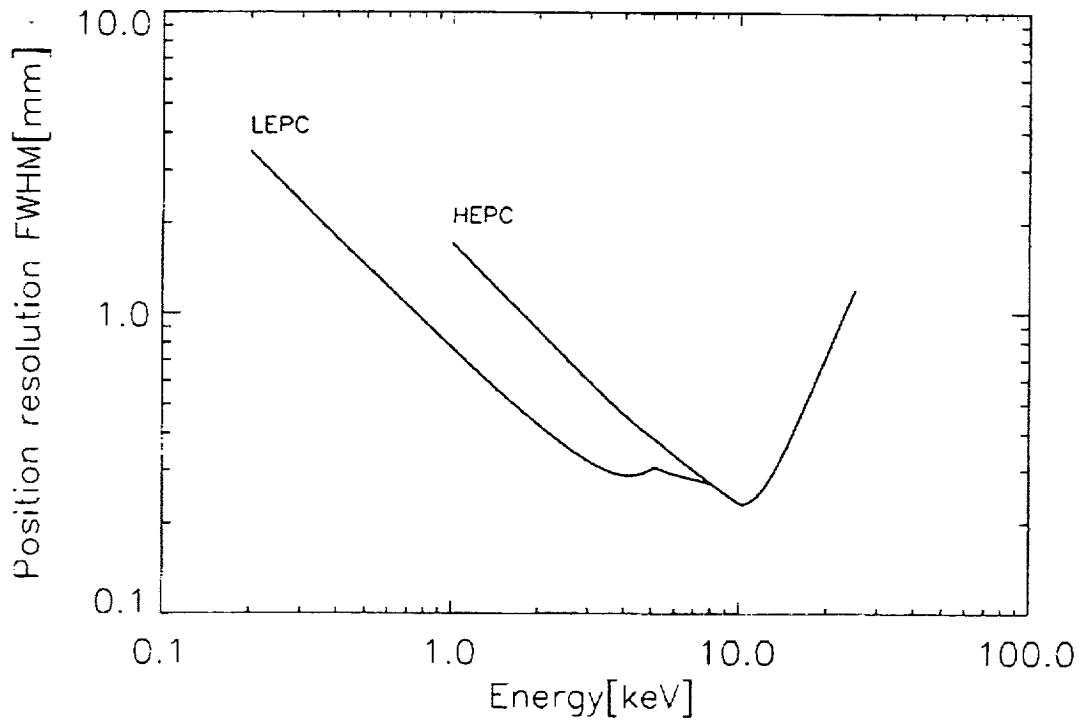

Figure 23: HEPC/LEPC Spatial Response. For an 8 m focal length, 1 mm corresponds to 0.43′.

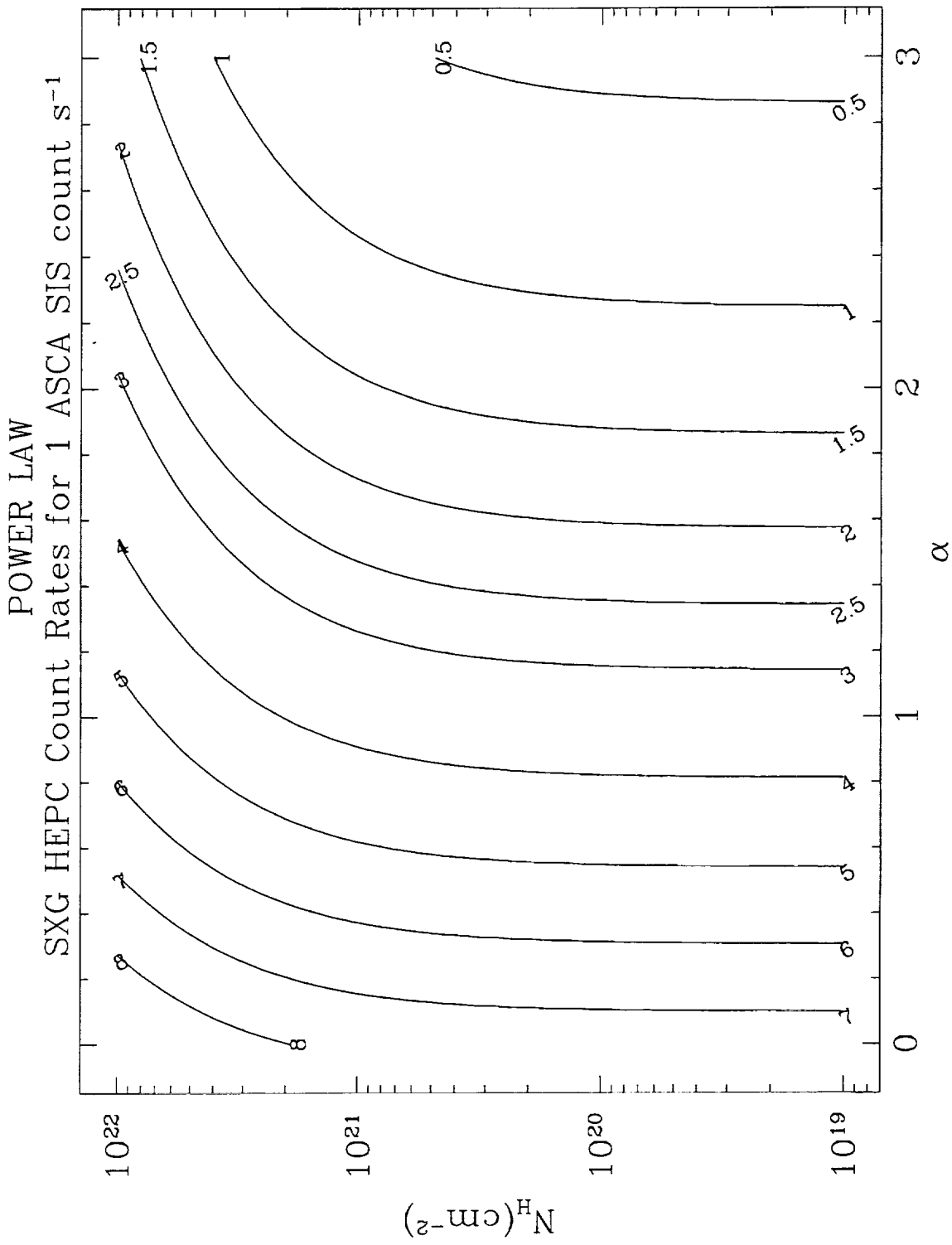

Figure 24: HEPC count rates yielding 1 ASCA SIS c s^{-1}, for a power law spectrum. This and subsequent figures (25 – 50) are contour plots of count rate conversions derived from PIMMS.

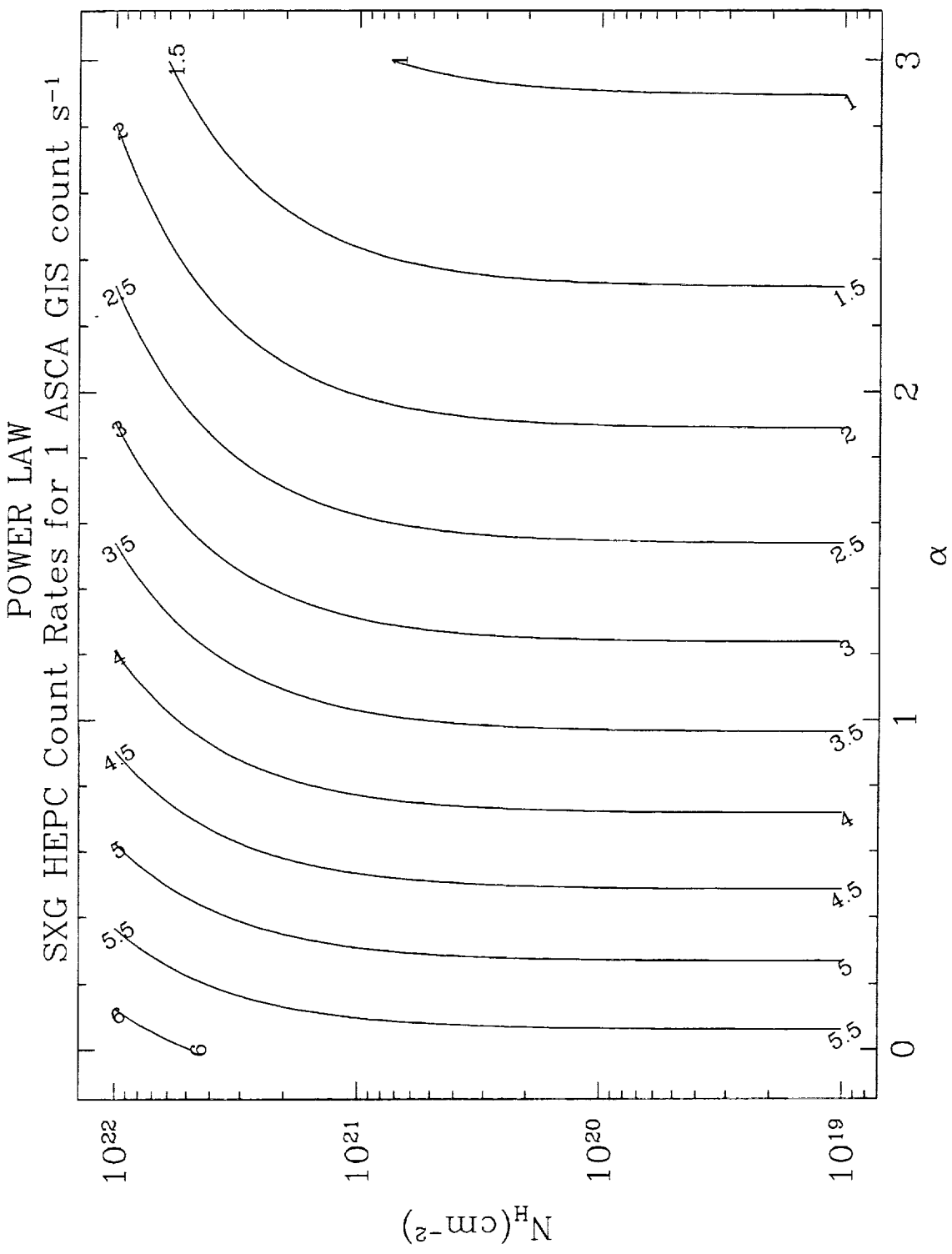

Figure 25: HEPC count rates yielding 1 ASCA GIS c s^{-1}, for a power law spectrum.

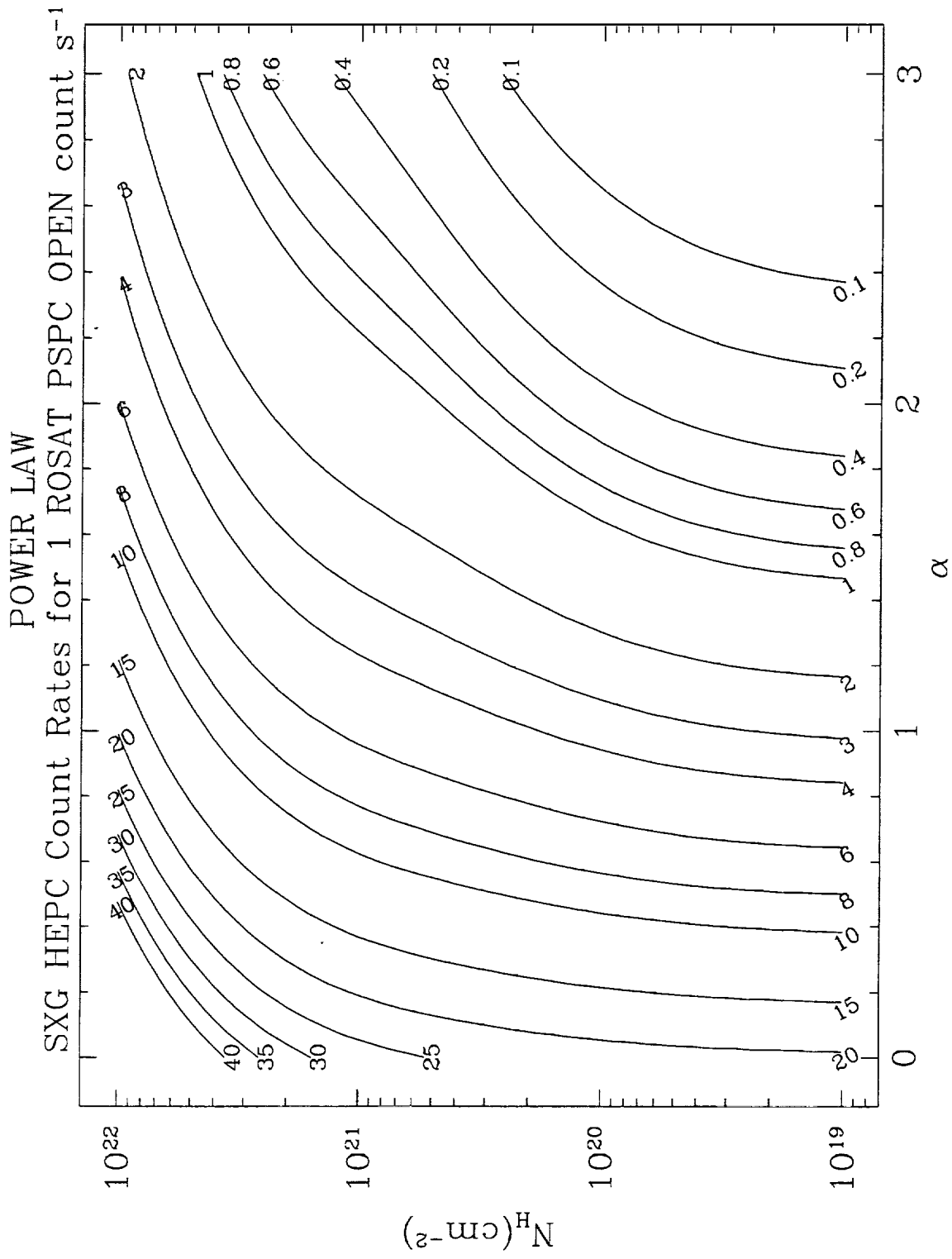

Figure 26: HEPC count rates yielding 1 ROSAT PSPC c s^{-1}, for a power law spectrum.

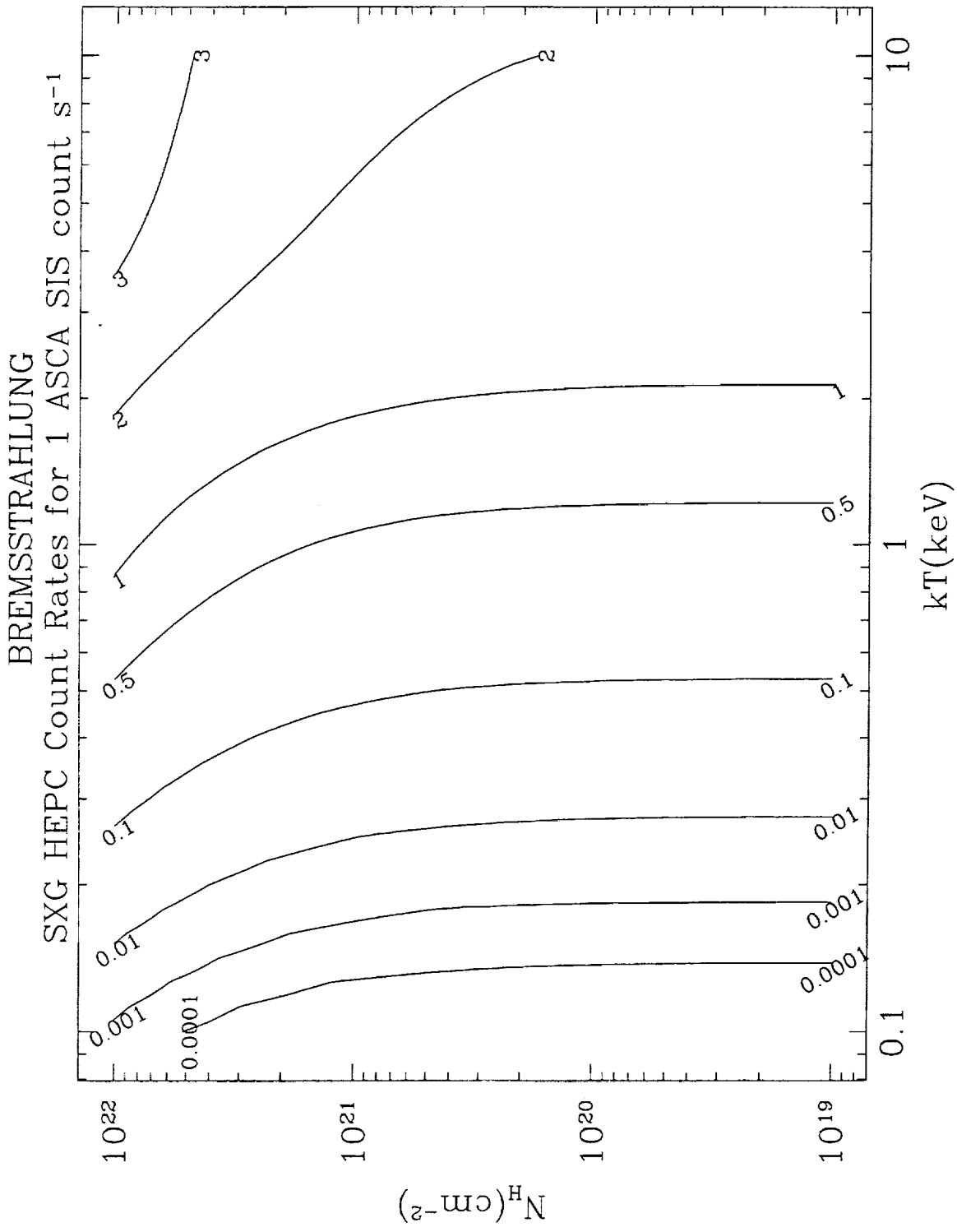

Figure 27: HEPC count rates yielding 1 ASCA SIS c s^{-1}, for a thermal bremsstrahlung spectrum.

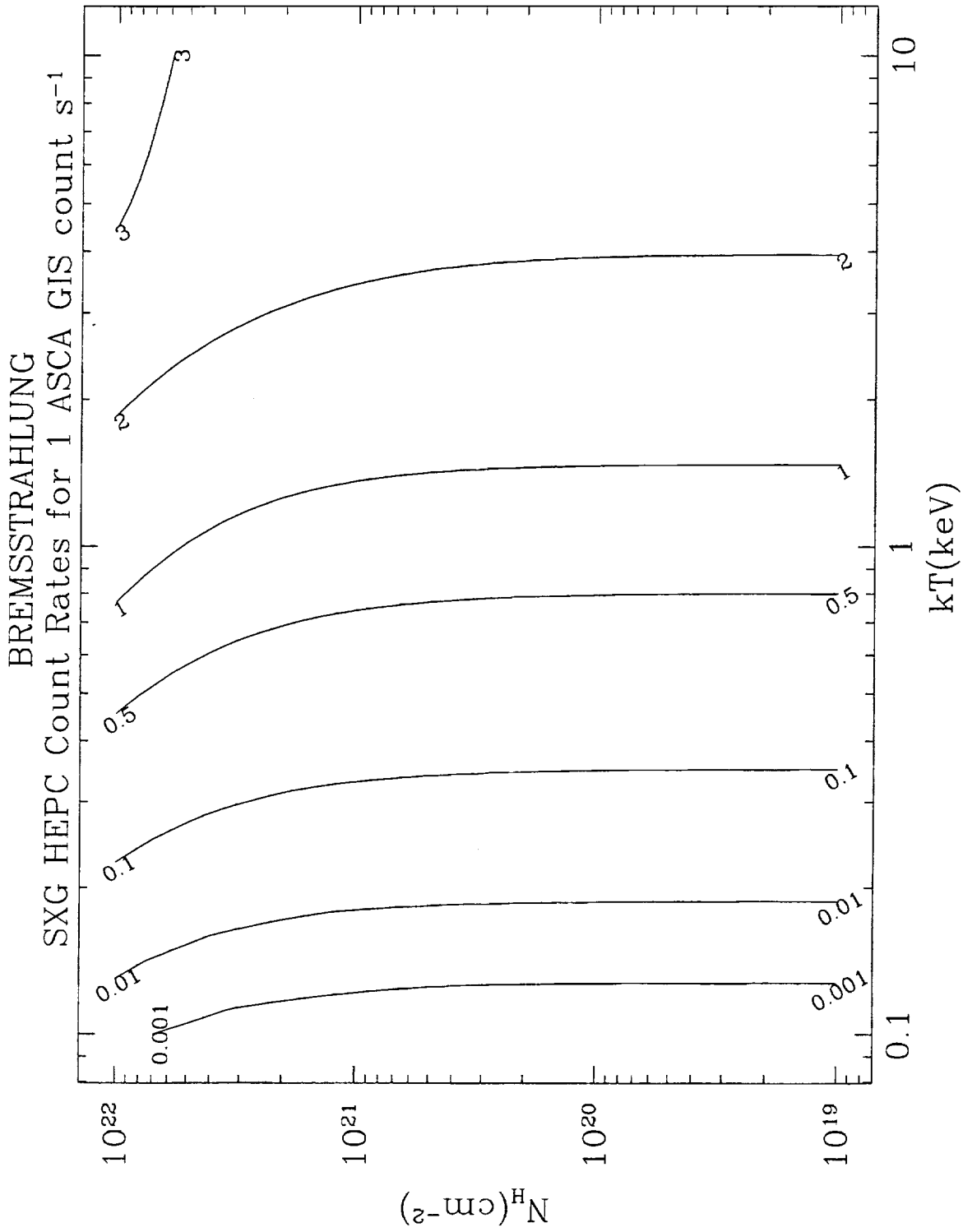

Figure 28: HEPC count rates yielding 1 ASCA GIS c s^{-1}, for a thermal bremsstrahlung spectrum.

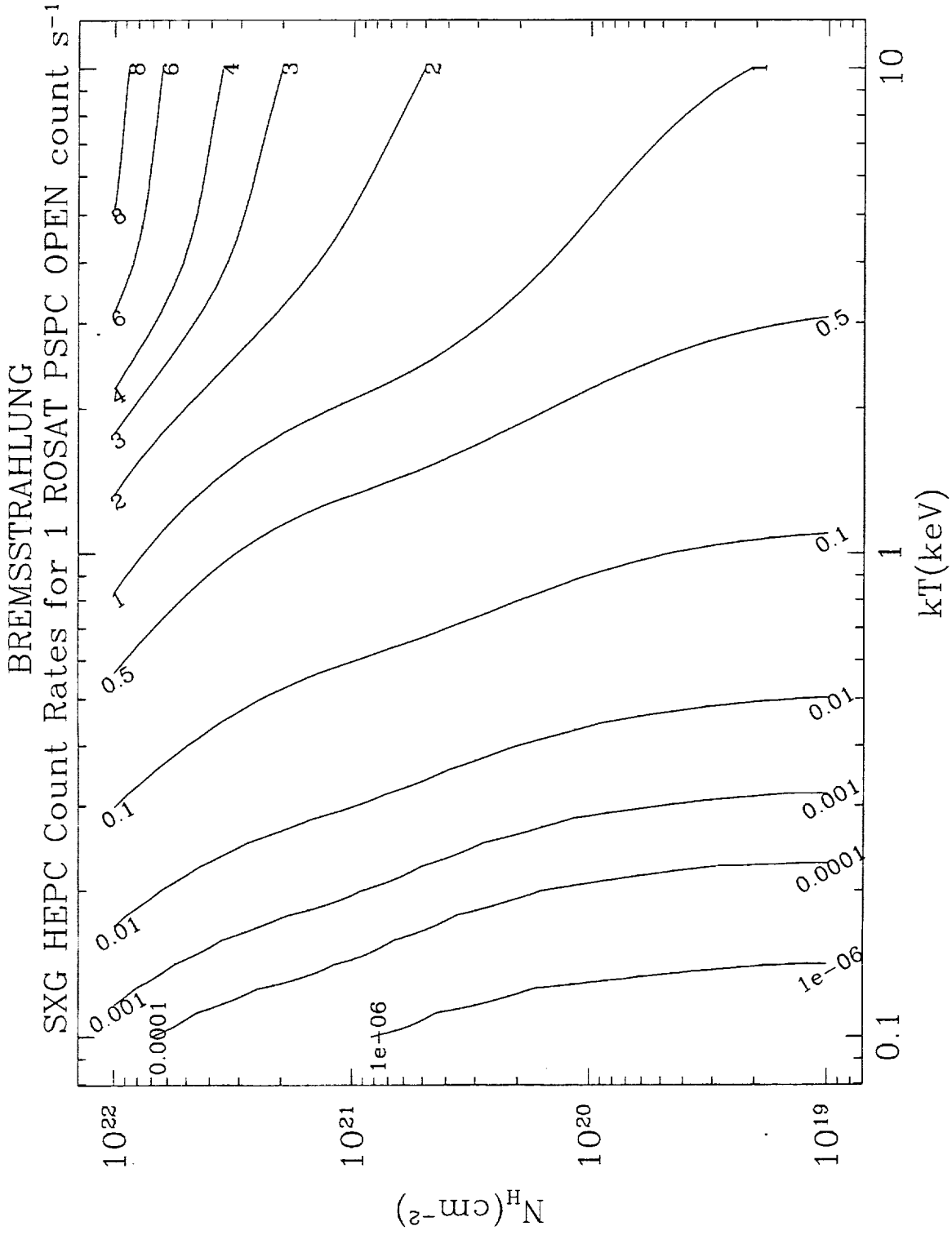

Figure 29: HEPC count rates yielding 1 ROSAT PSPC c s^{-1}, for a thermal bremsstrahlung spectrum.

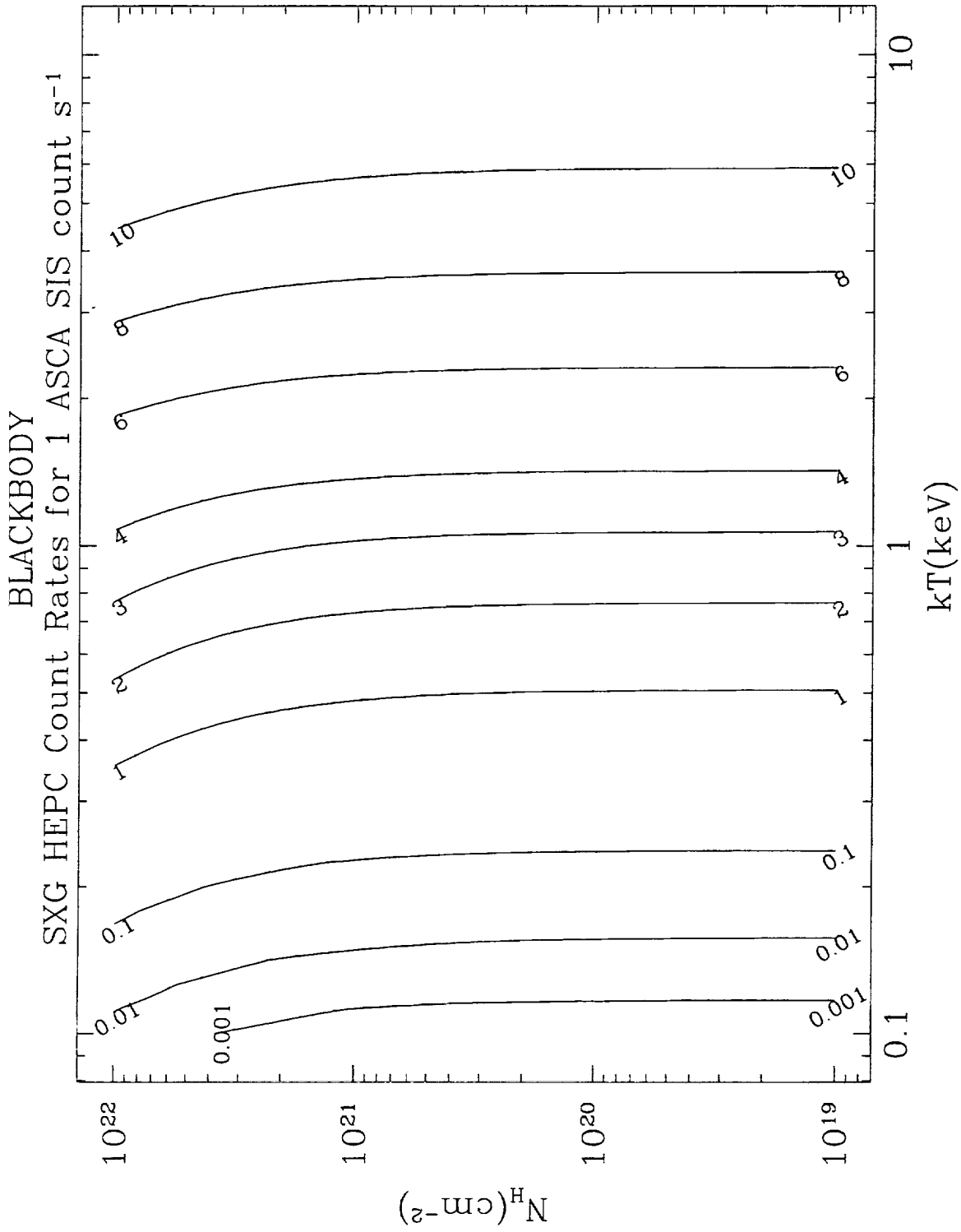

Figure 30: HEPC count rates yielding 1 ASCA SIS c s^{-1}, for a blackbody spectrum.

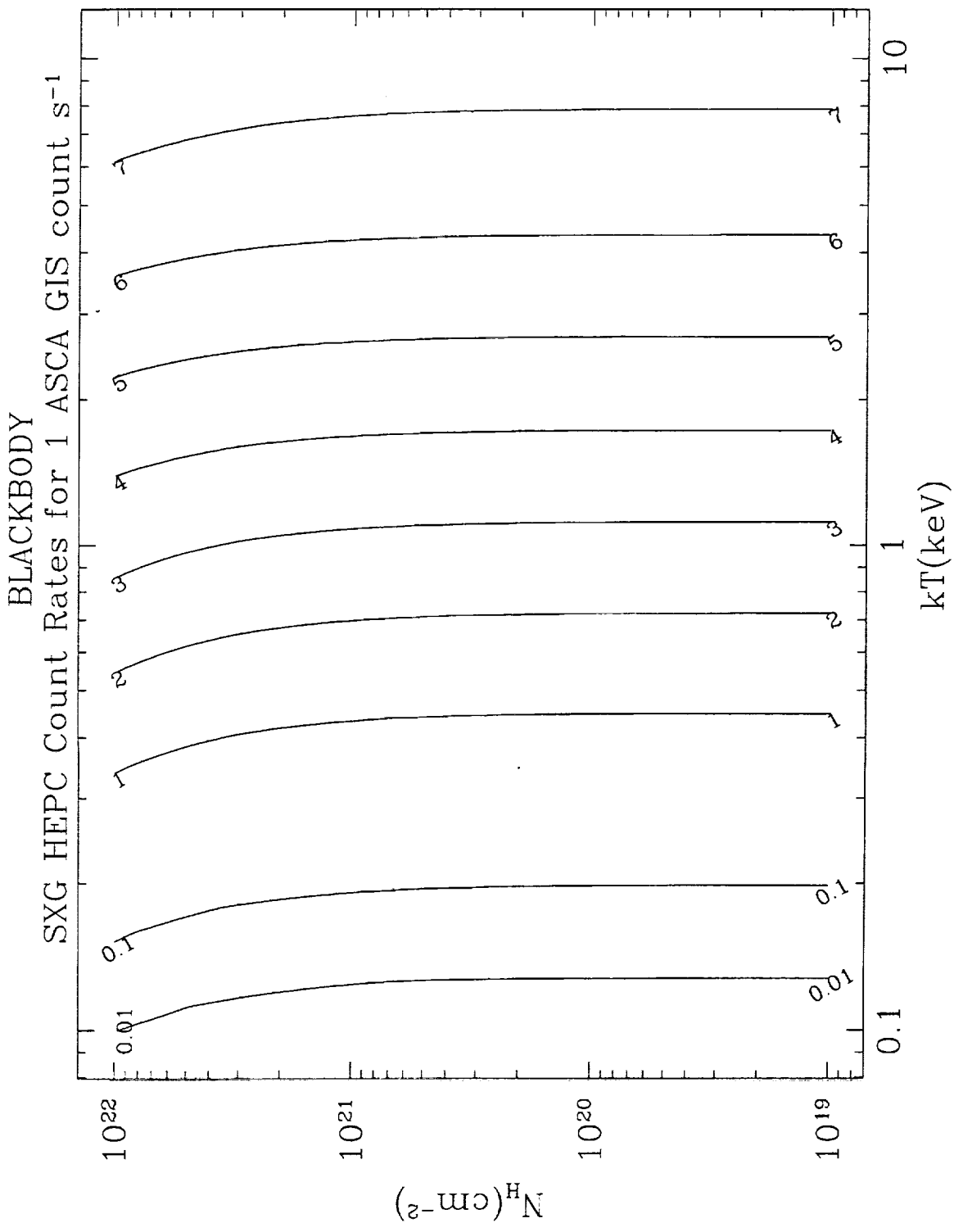

Figure 31: HEPC count rates yielding 1 ASCA GIS c s^{-1}, for a blackbody spectrum.

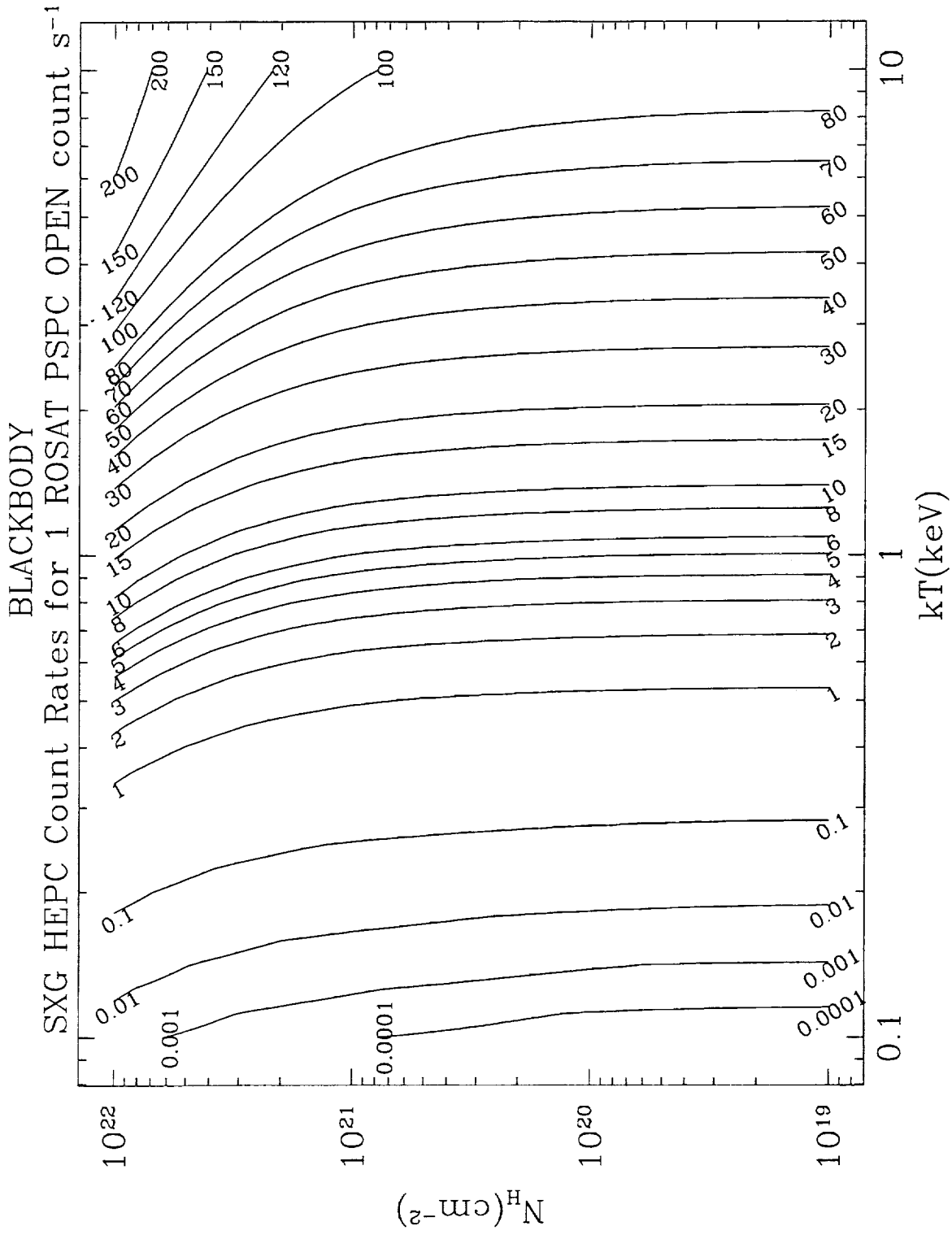

Figure 32: HEPC count rates yielding 1 ROSAT PSPC c s^{-1}, for a blackbody spectrum.

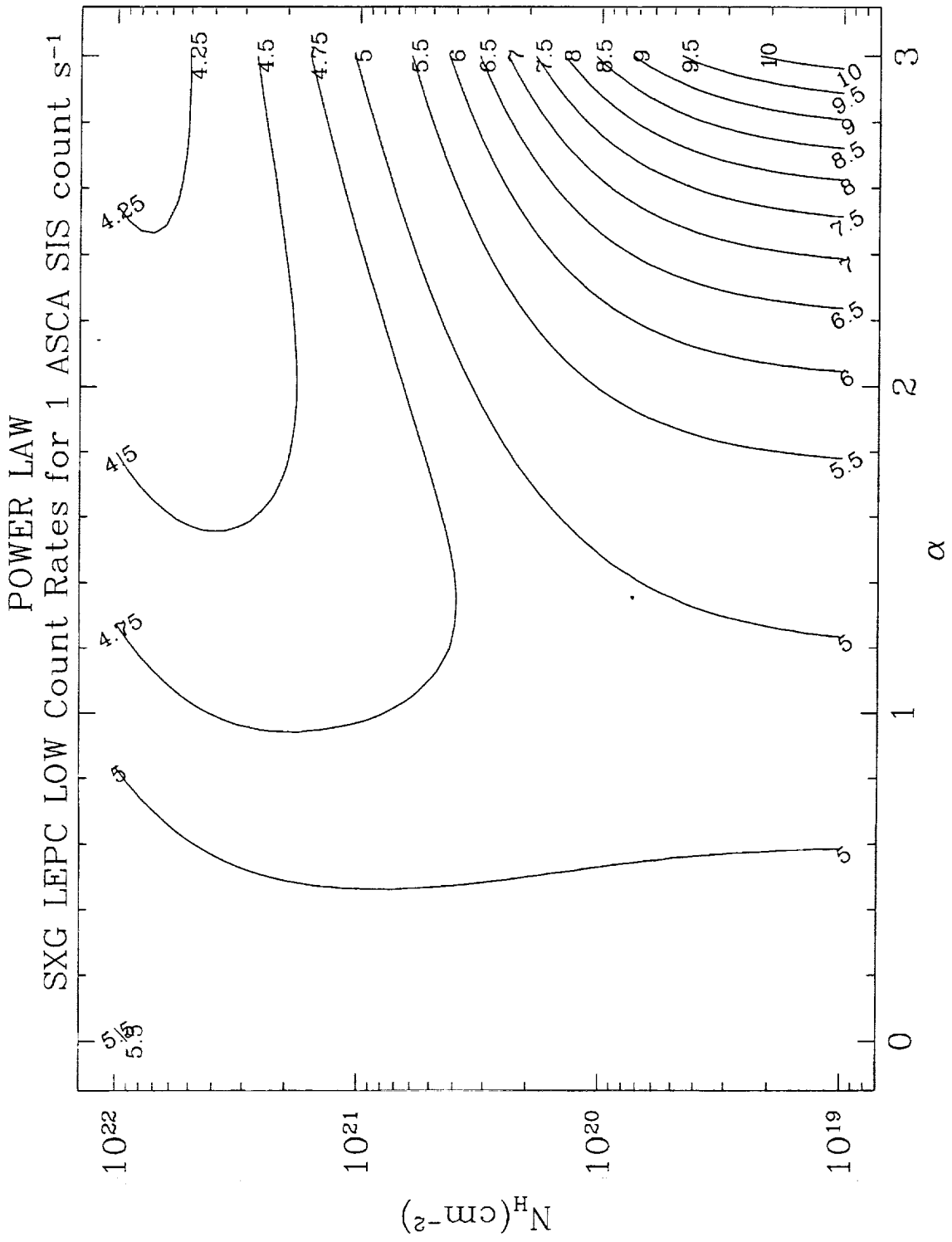

Figure 33: LEPC low-band count rates yielding 1 ASCA SIS c s^{-1}, for a power law spectrum. This and subsequent figures (34 – 41) are contour plots of count rate conversions derived from PIMMS.

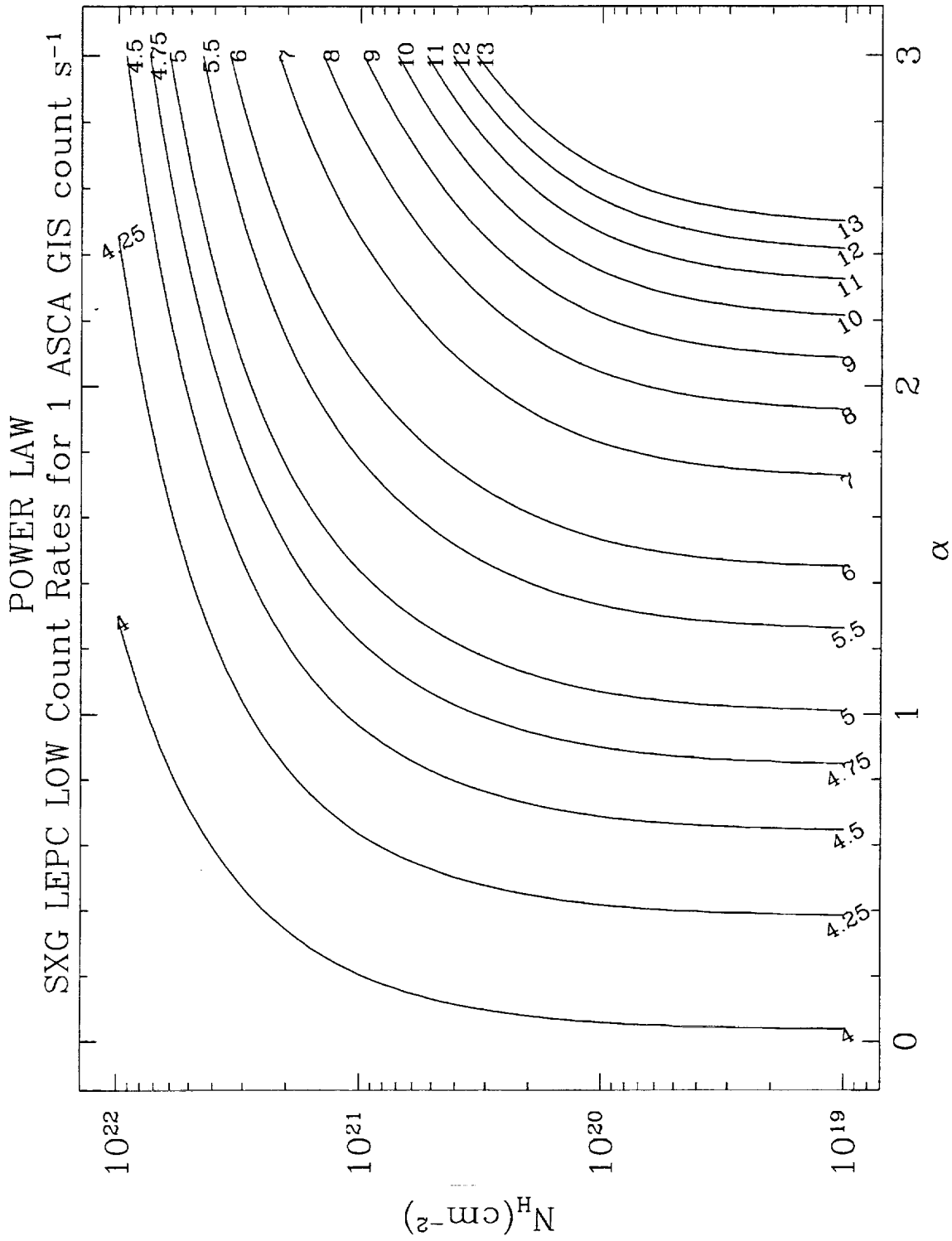

Figure 34: LEPC low-band count rates yielding 1 ASCA GIS c s^{-1}, for a power law spectrum.

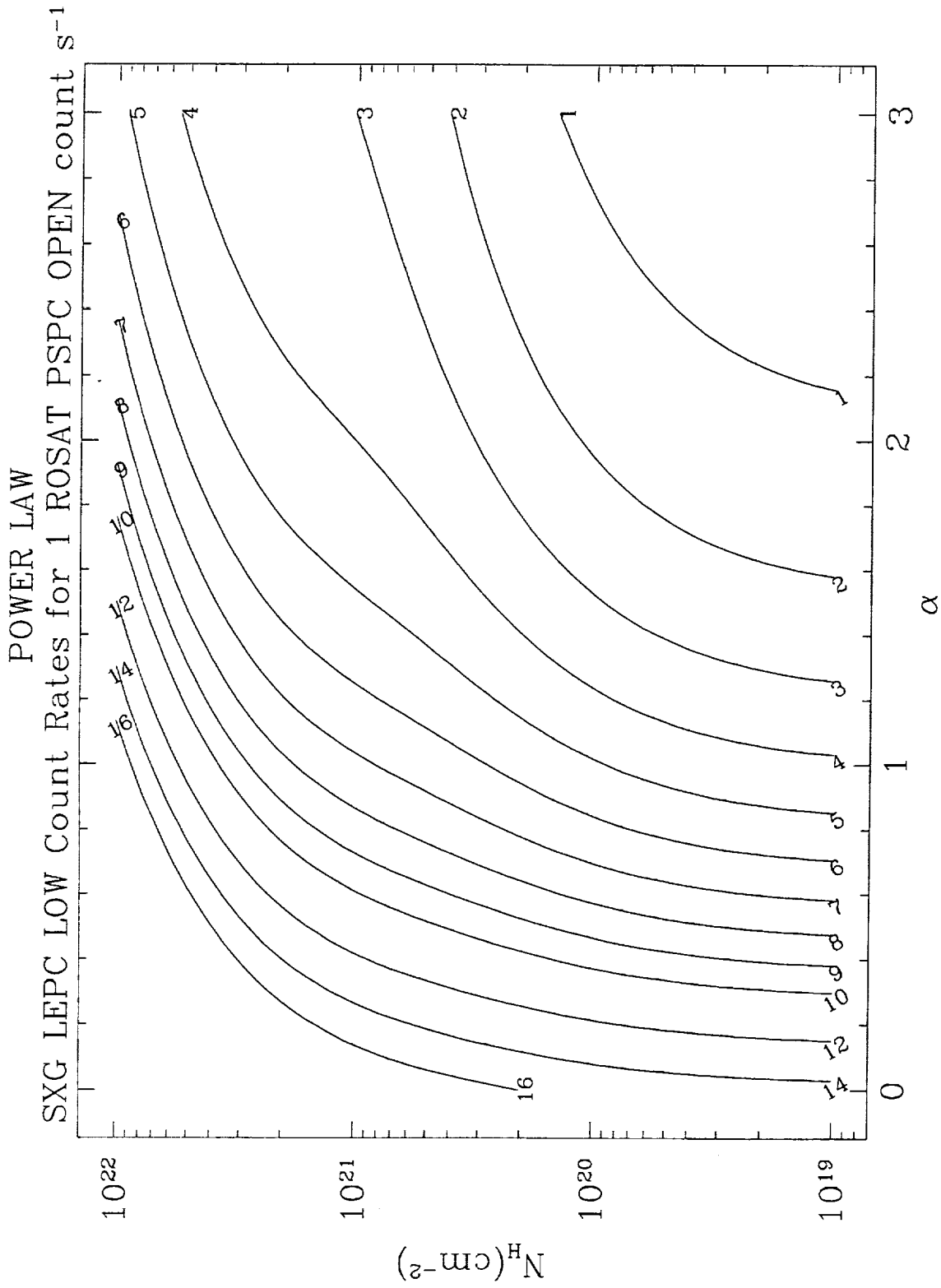

Figure 35: LEPC low-band count rates yielding 1 ROSAT PSPC c s^{-1}, for a power law spectrum.

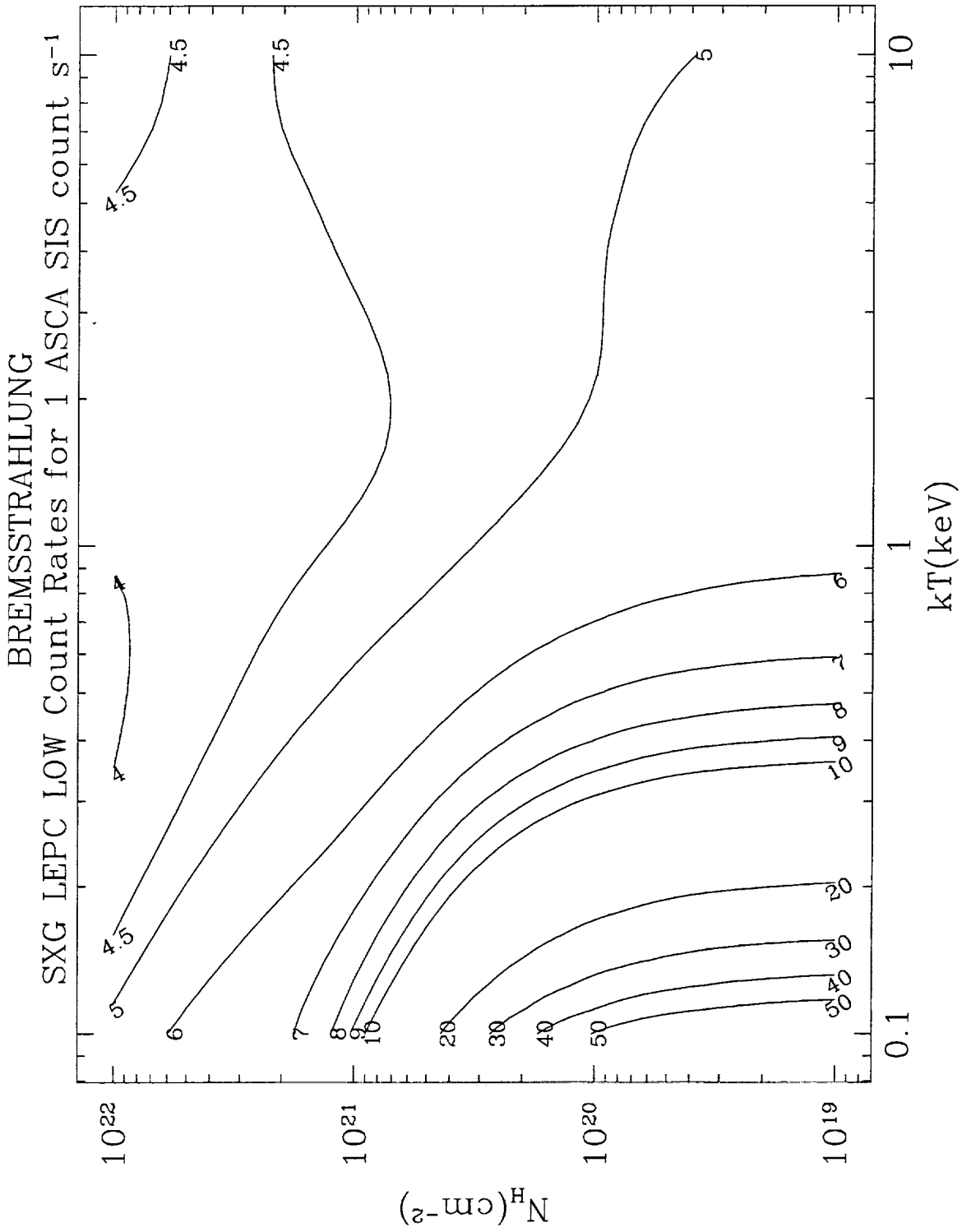

Figure 36: LEPC low-band count rates yielding 1 ASCA SIS c s^{-1}, for a thermal bremsstrahlung spectrum.

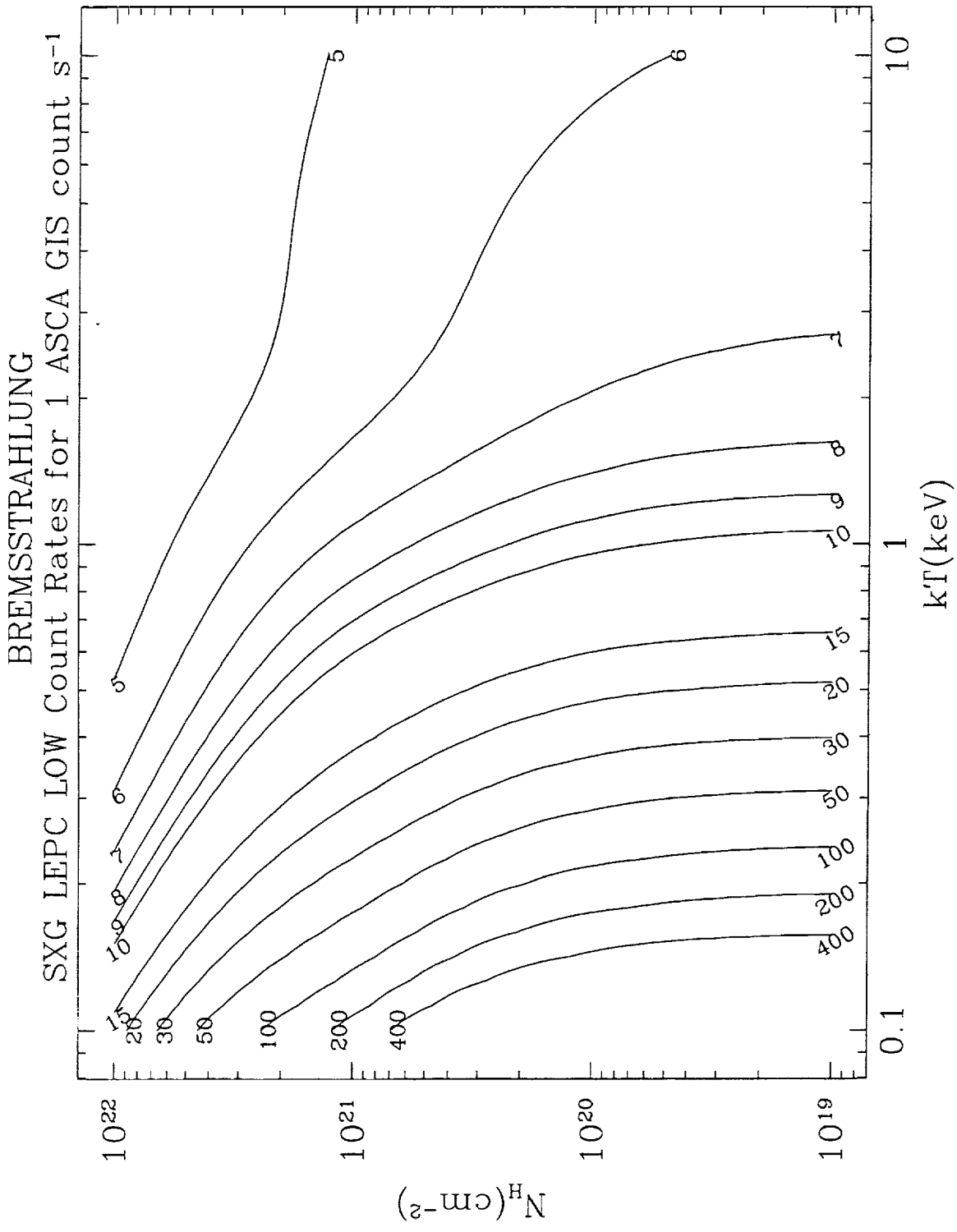

Figure 37: LEPC low-band count rates yielding 1 ASCA GIS c s^{-1}, for a thermal bremsstrahlung spectrum.

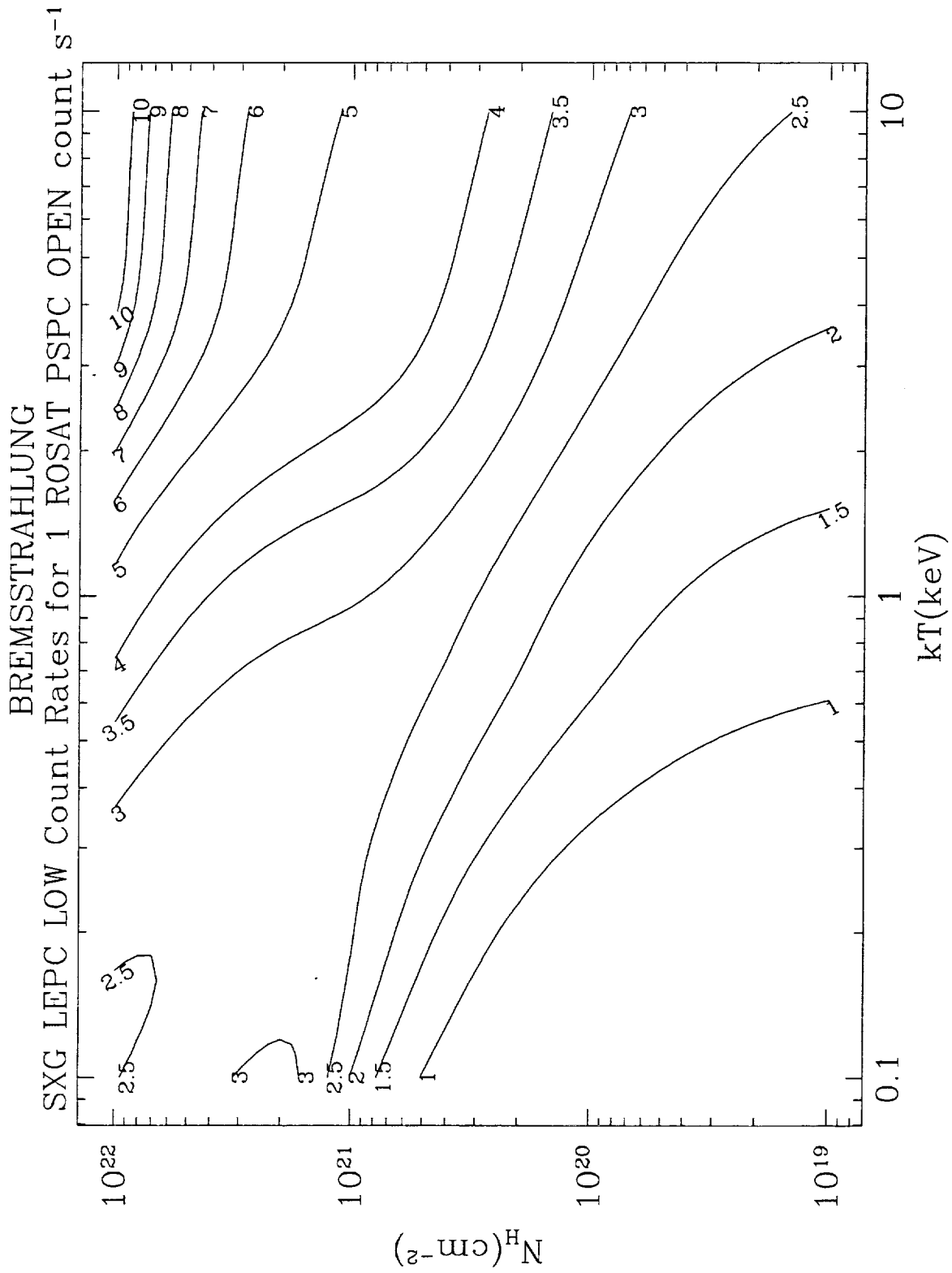

Figure 38: LEPC low-band count rates yielding 1 ROSAT PSPC c s^{-1}, for a thermal bremsstrahlung spectrum.

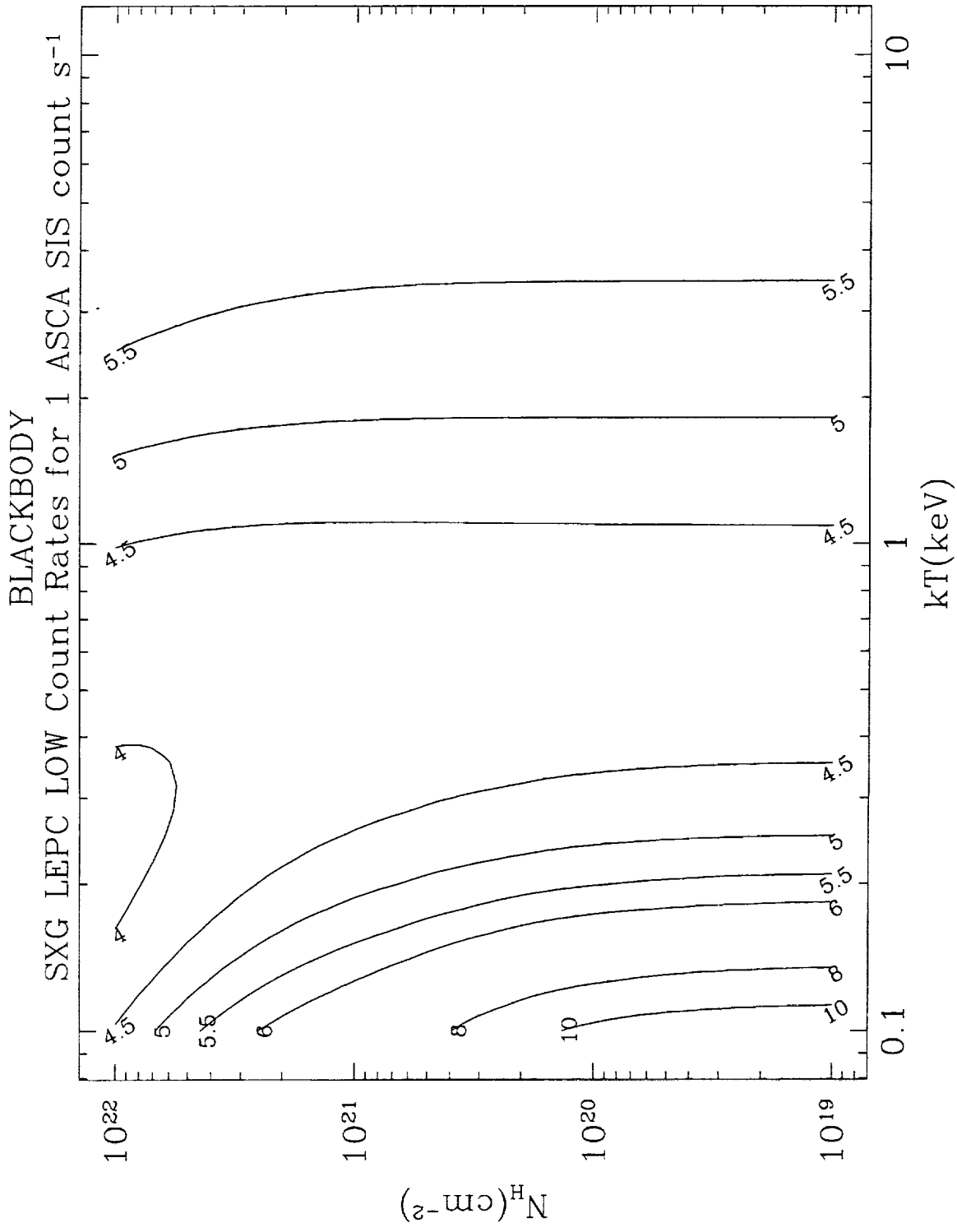

Figure 39: LEPC low-band count rates yielding 1 ASCA SIS c s^{-1}, for a blackbody spectrum.

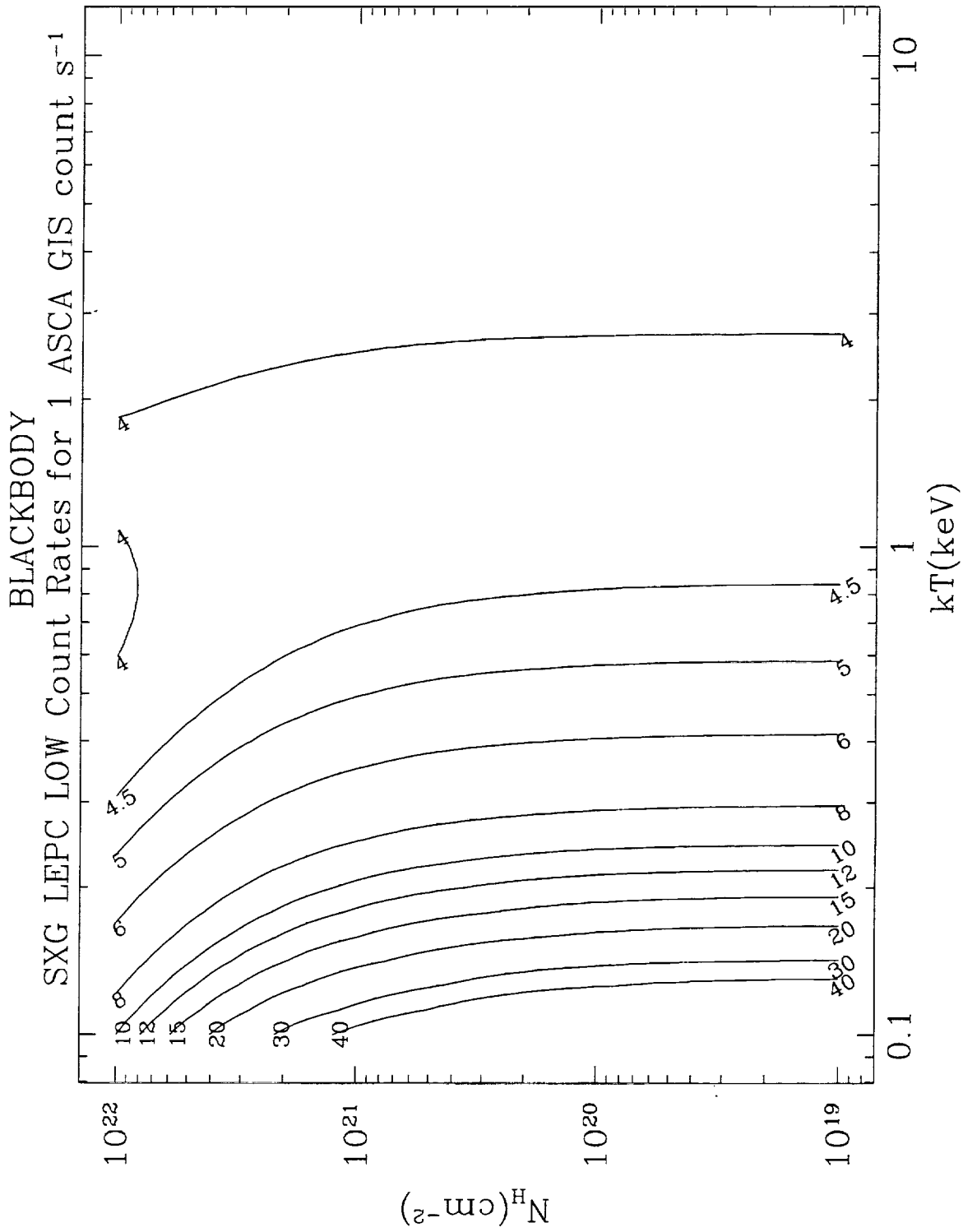

Figure 40: LEPC low-band count rates yielding 1 ASCA GIS c s^{-1}, for a blackbody spectrum.

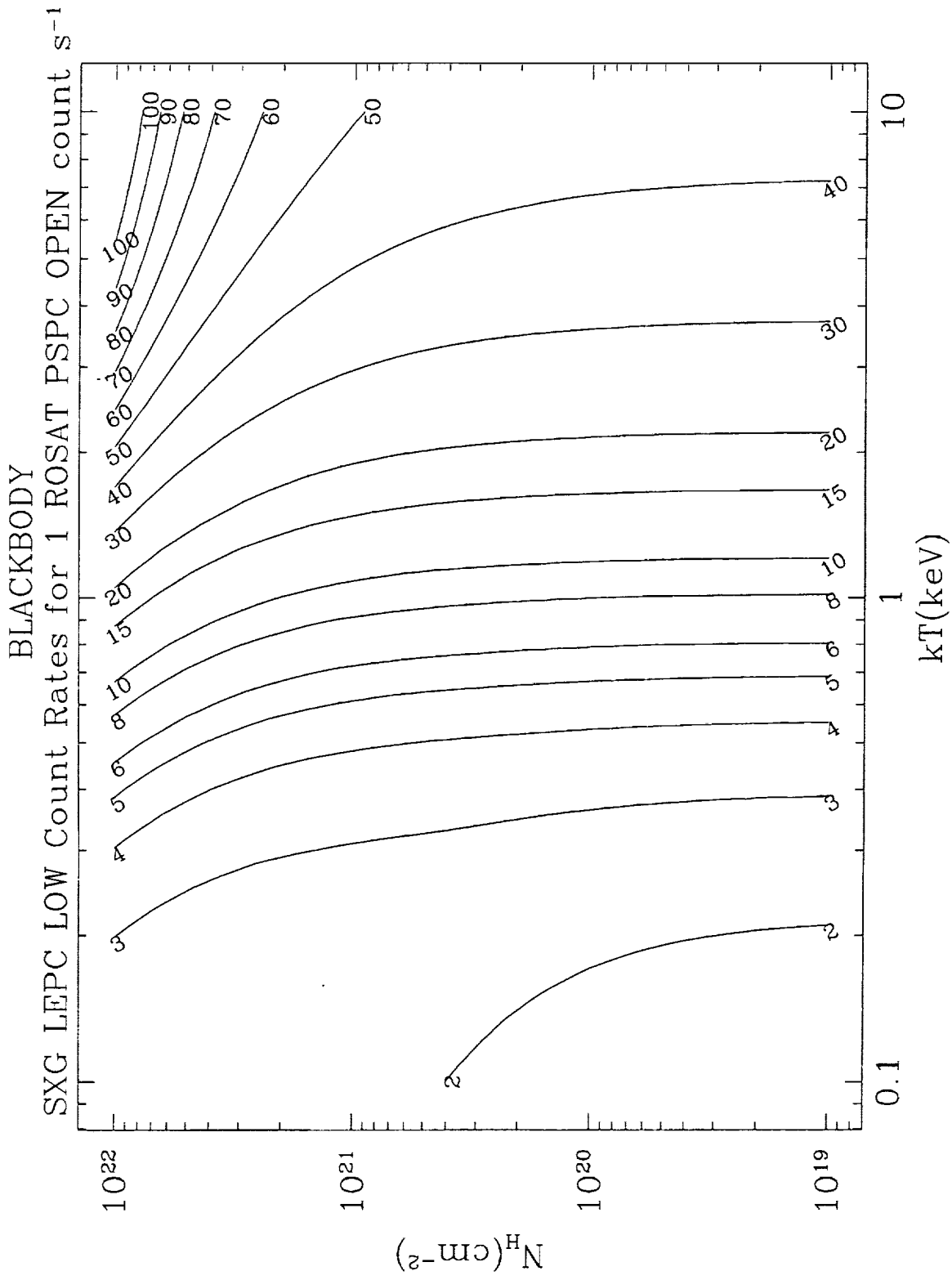

Figure 41: LEPC low-band count rates yielding 1 ROSAT PSPC c s^{-1}, for a blackbody spectrum.

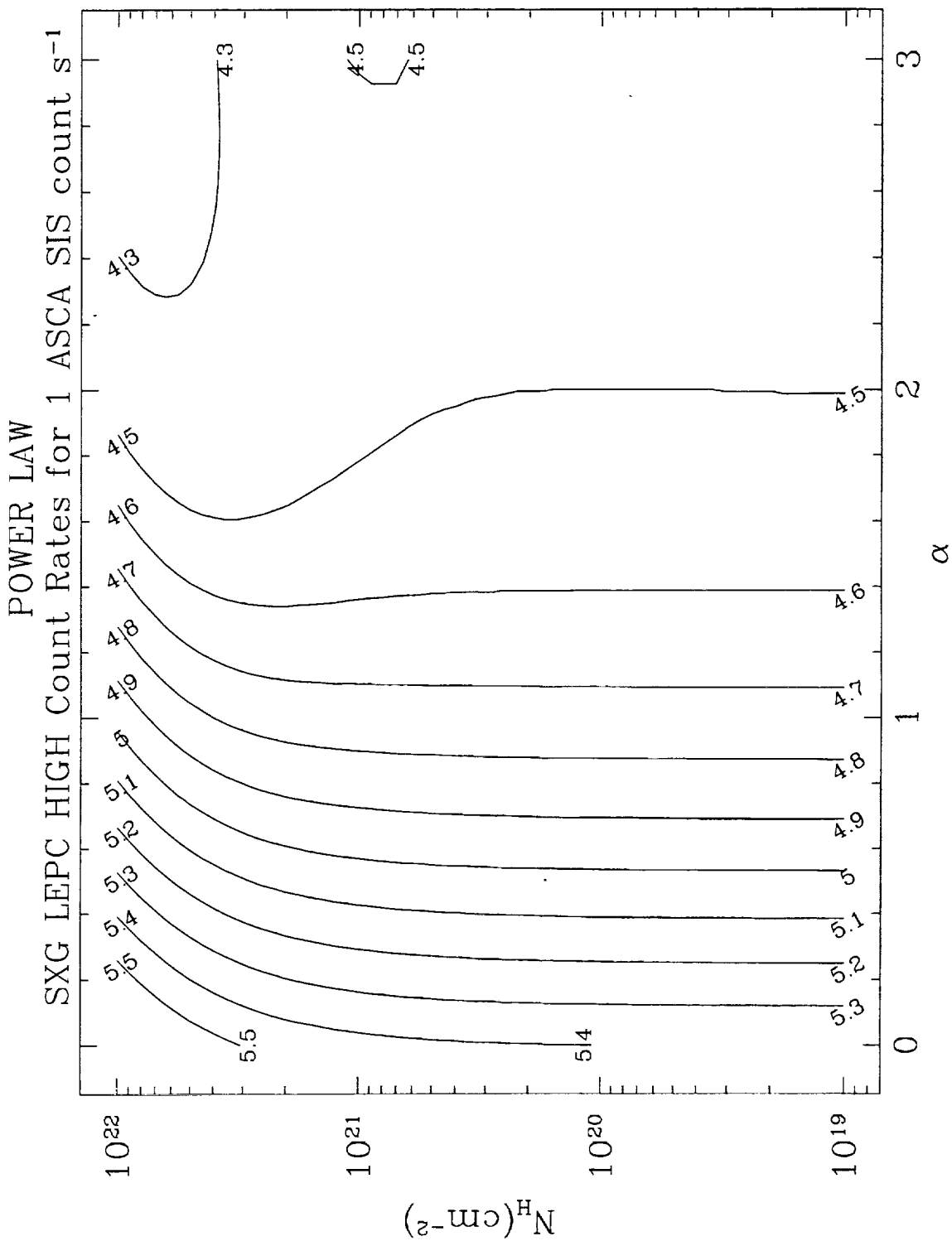

Figure 42: LEPC high-band count rates yielding 1 ASCA SIS c s^{-1}, for a power law spectrum.

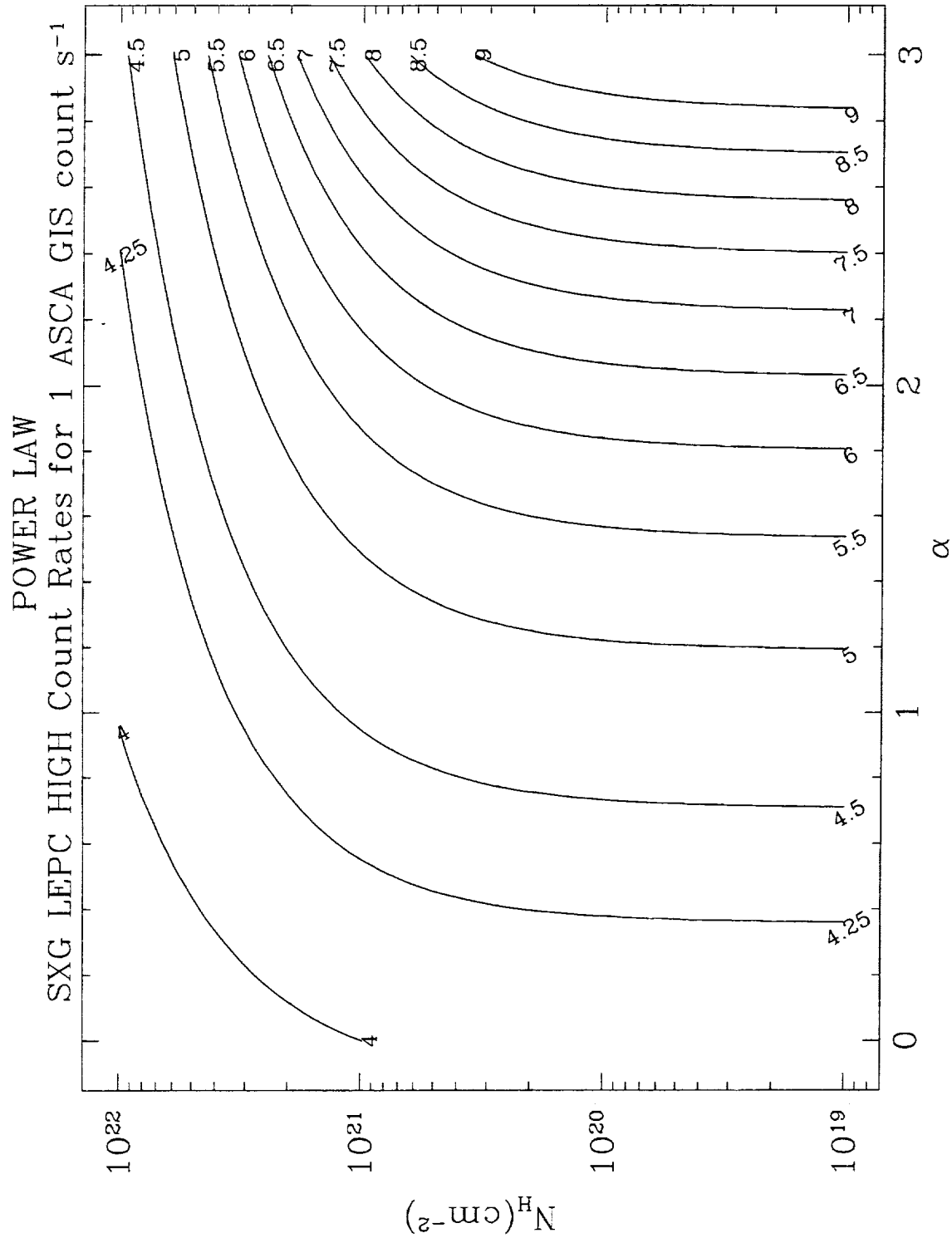

Figure 43: LEPC high-band count rates yielding 1 ASCA GIS c s^{-1}, for a power law spectrum.

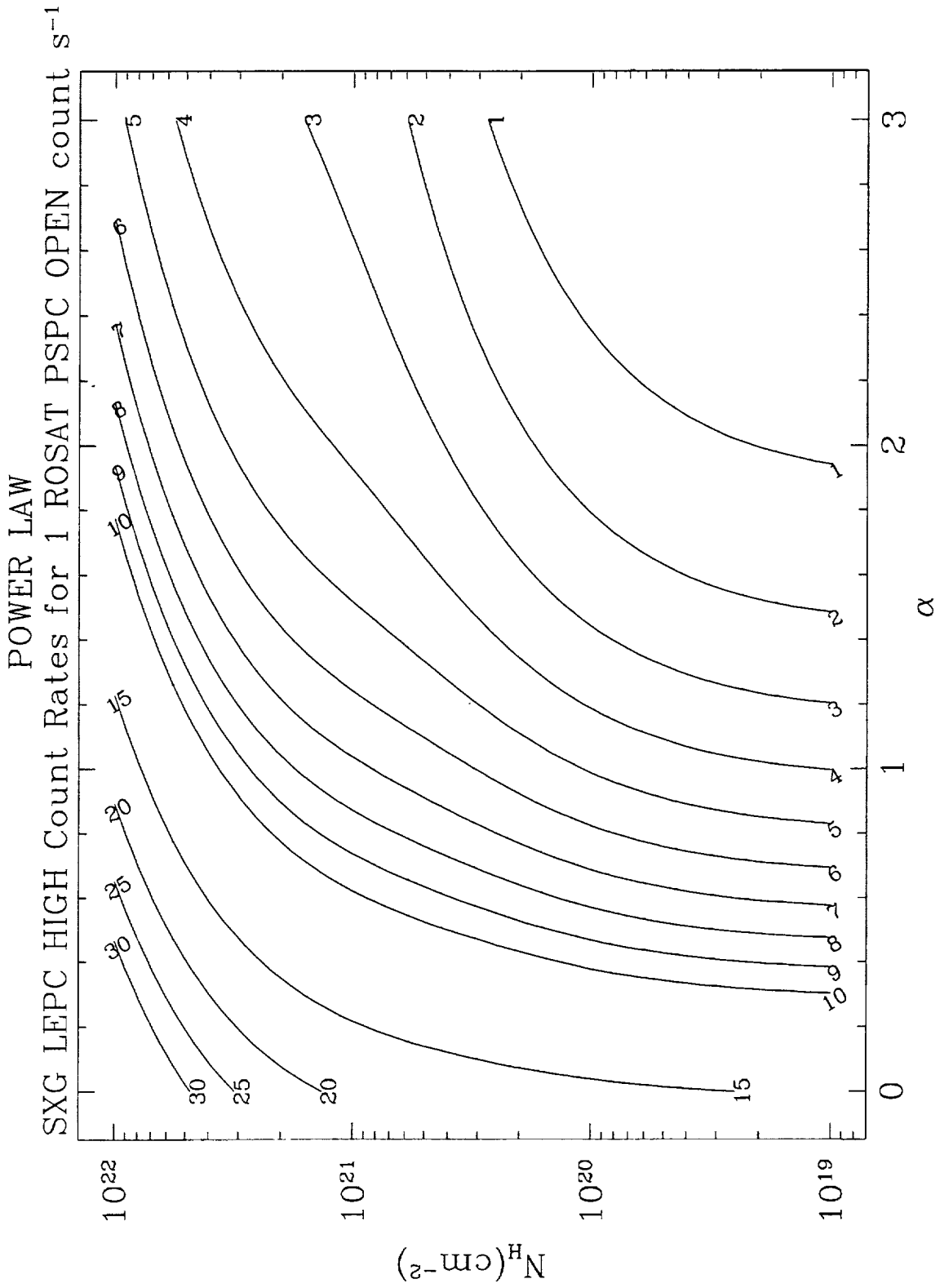

Figure 44: LEPC high-band count rates yielding 1 ROSAT PSPC c s^{-1}, for a power law spectrum.

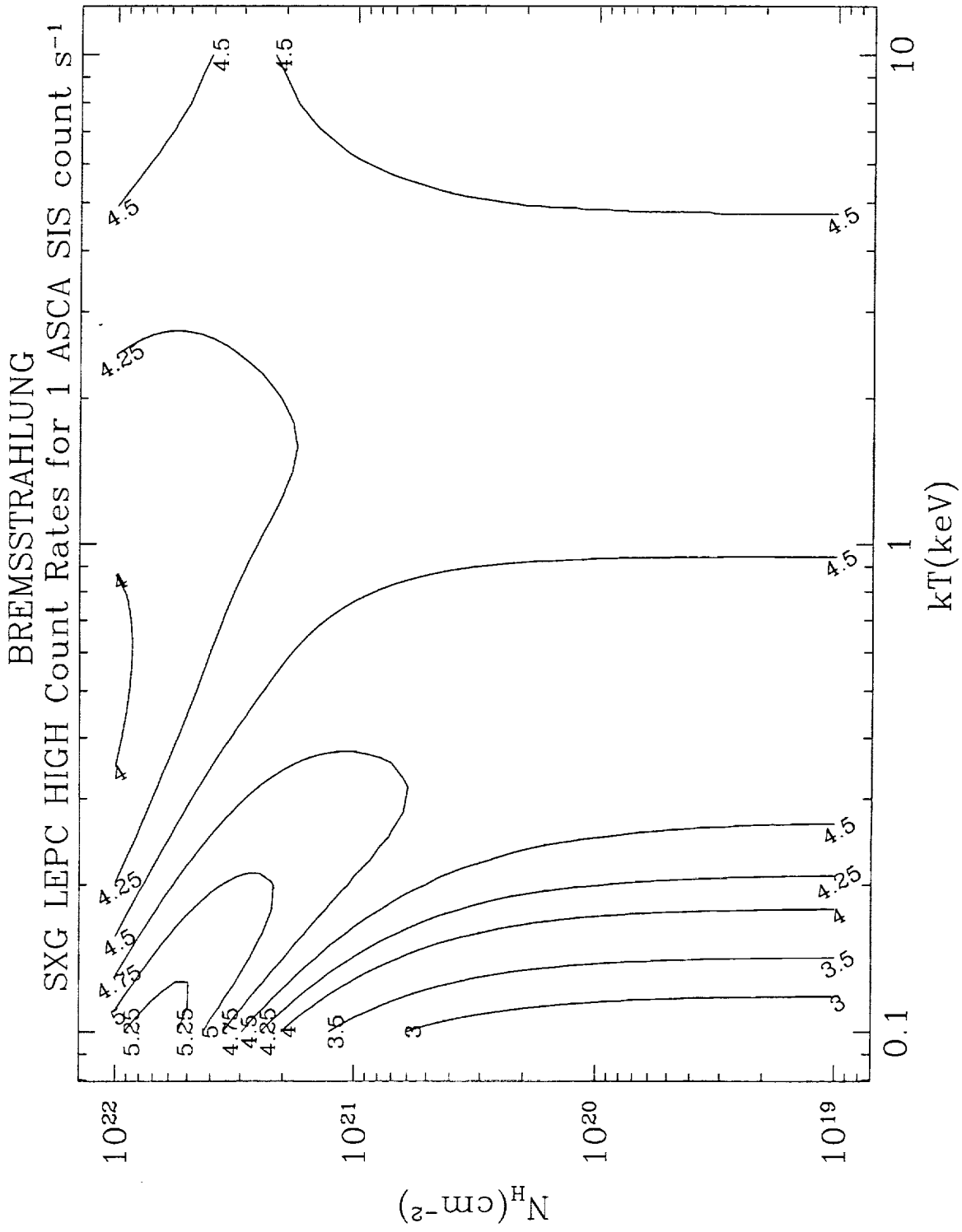

Figure 45: LEPC high-band count rates yielding 1 ASCA SIS c s^{-1}, for a thermal bremsstrahlung spectrum.

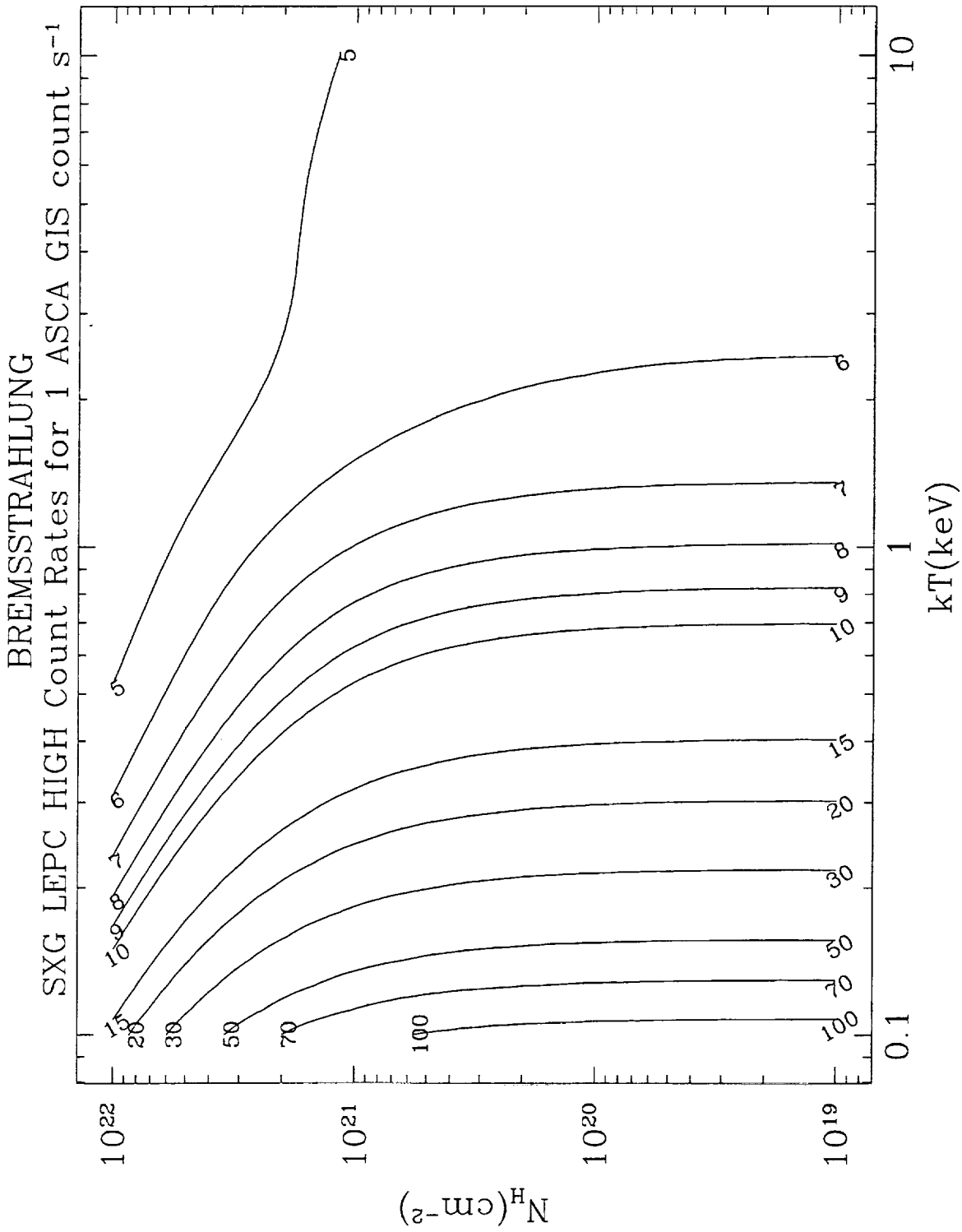

Figure 46: LEPC high-band count rates yielding 1 ASCA GIS c s^{-1}, for a thermal bremsstrahlung spectrum.

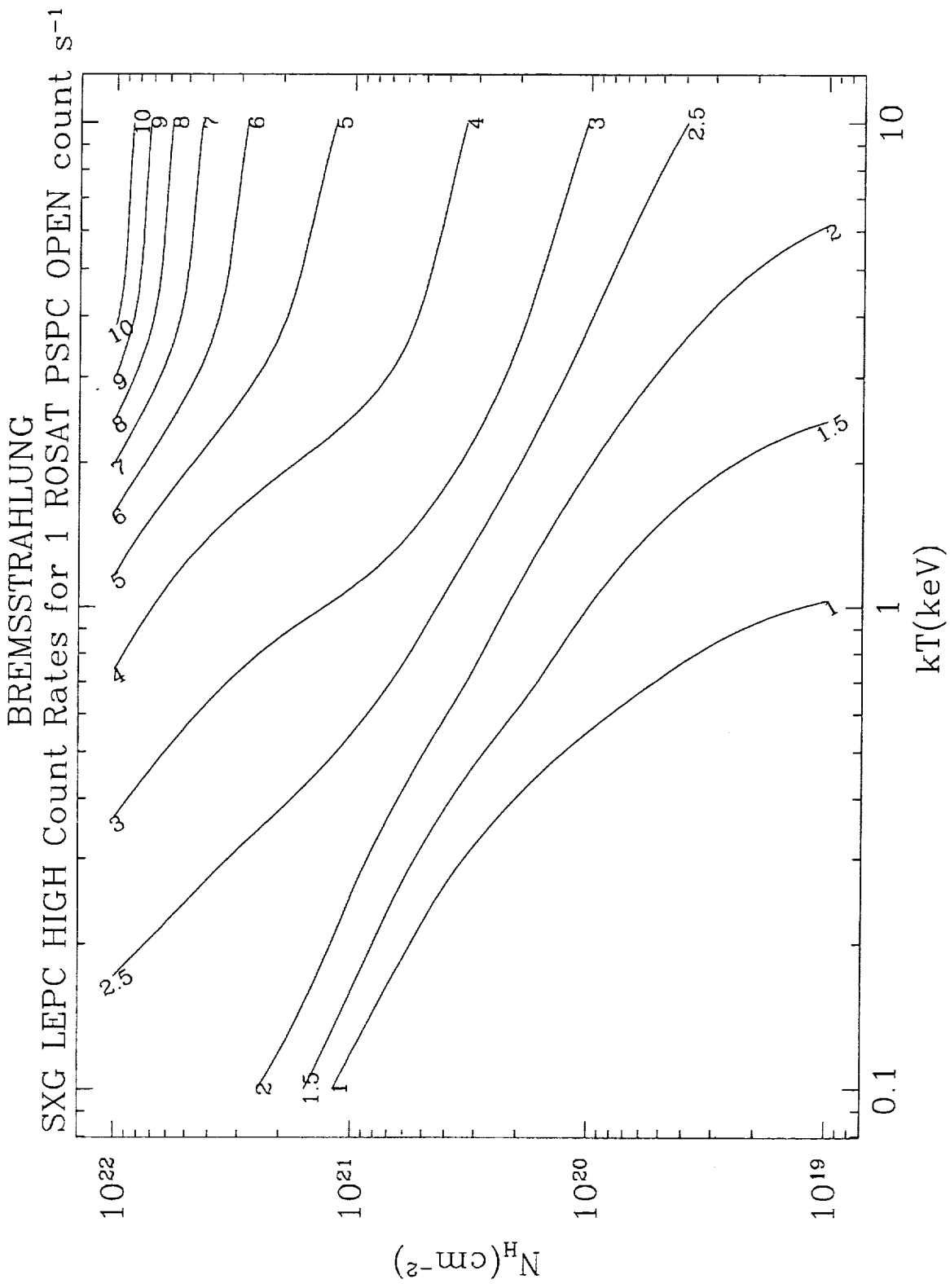

Figure 47: LEPC high-band count rates yielding 1 ROSAT PSPC c s^{-1}, for a thermal bremsstrahlung spectrum.

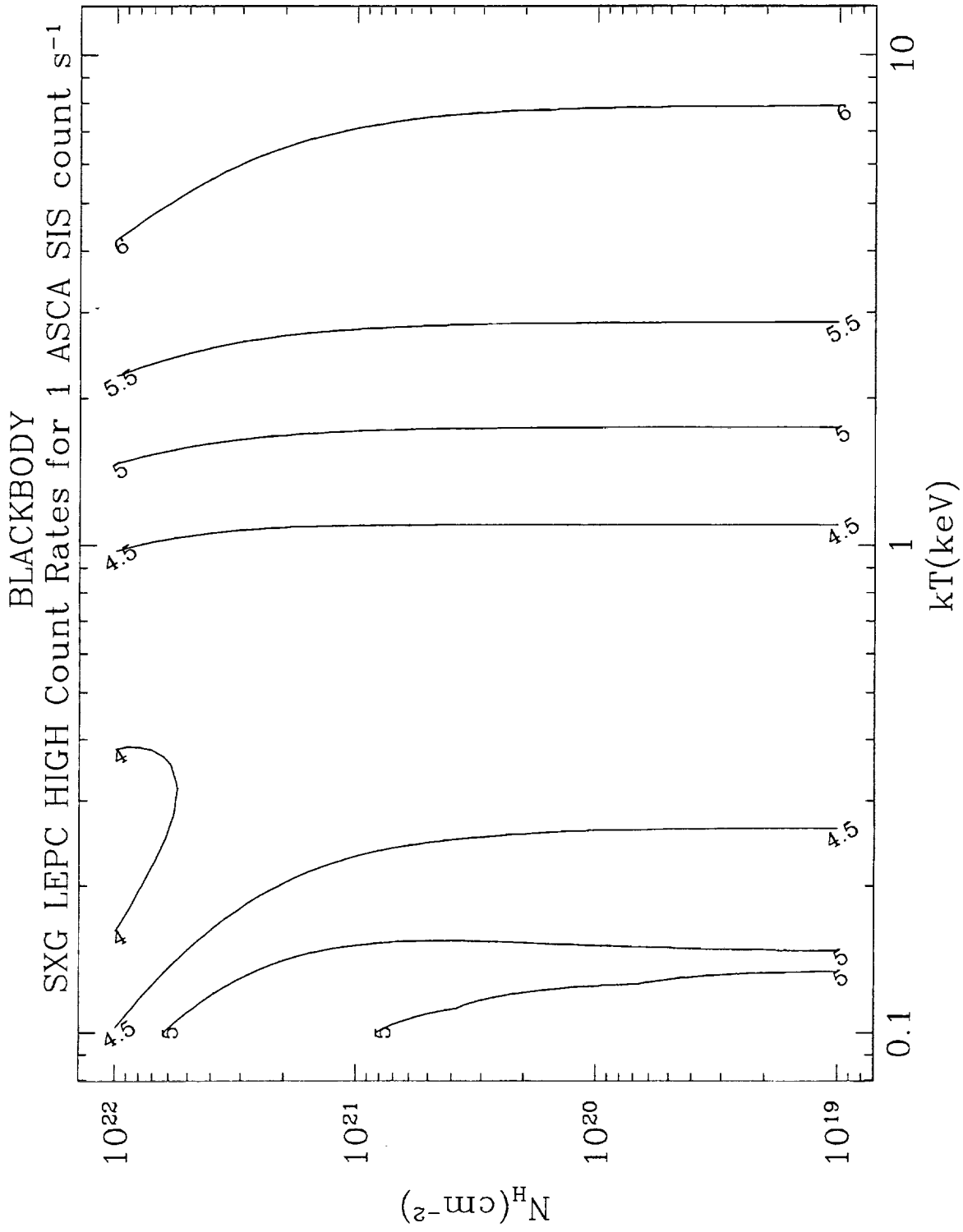

Figure 48: LEPC high-band count rates yielding 1 ASCA SIS c s^{-1}, for a blackbody spectrum.

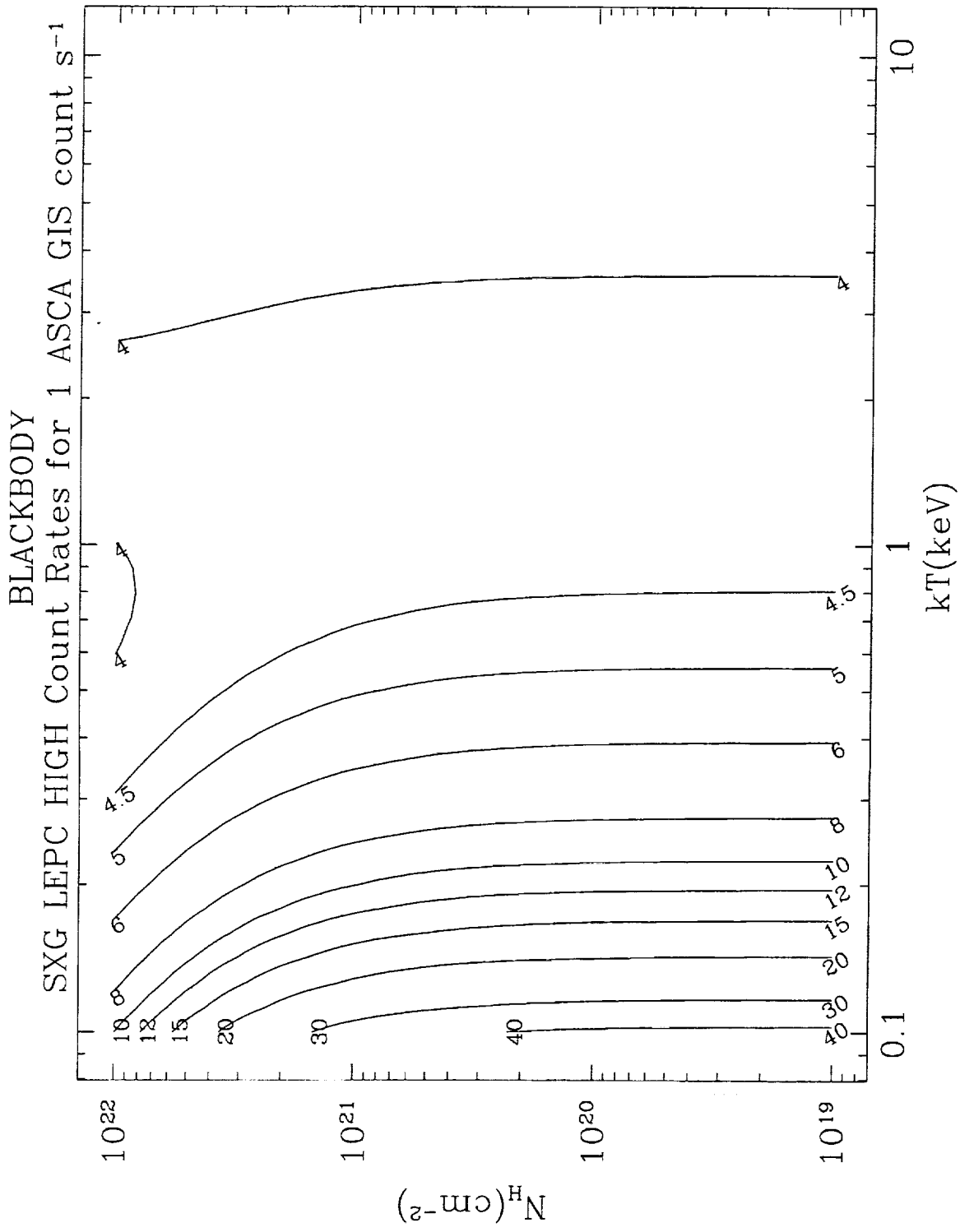

Figure 49: LEPC high-band count rates yielding 1 ASCA GIS c s^{-1}, for a blackbody spectrum.

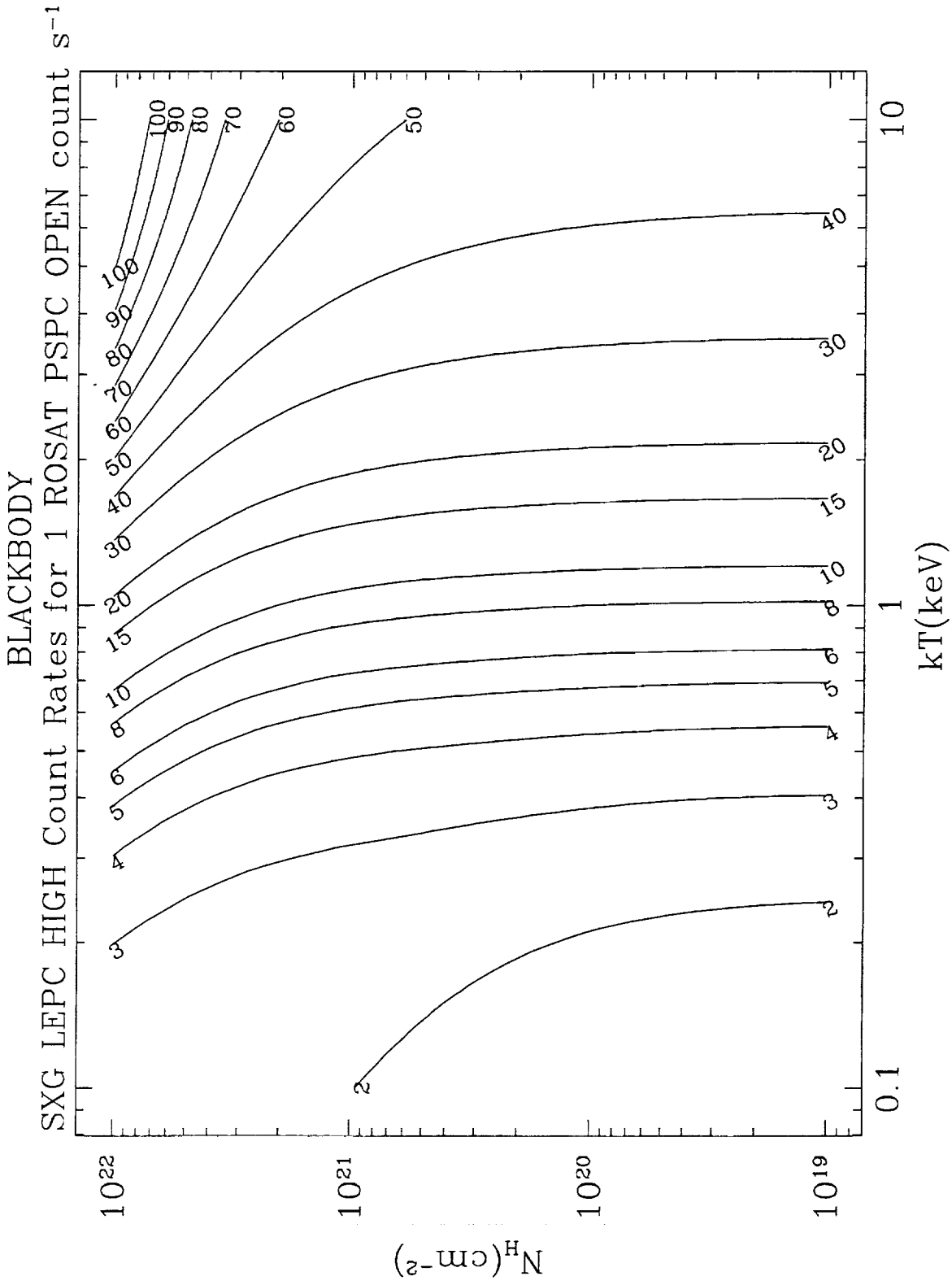

Figure 50: LEPC high-band count rates yielding 1 ROSAT PSPC c s^{-1}, for a blackbody spectrum.

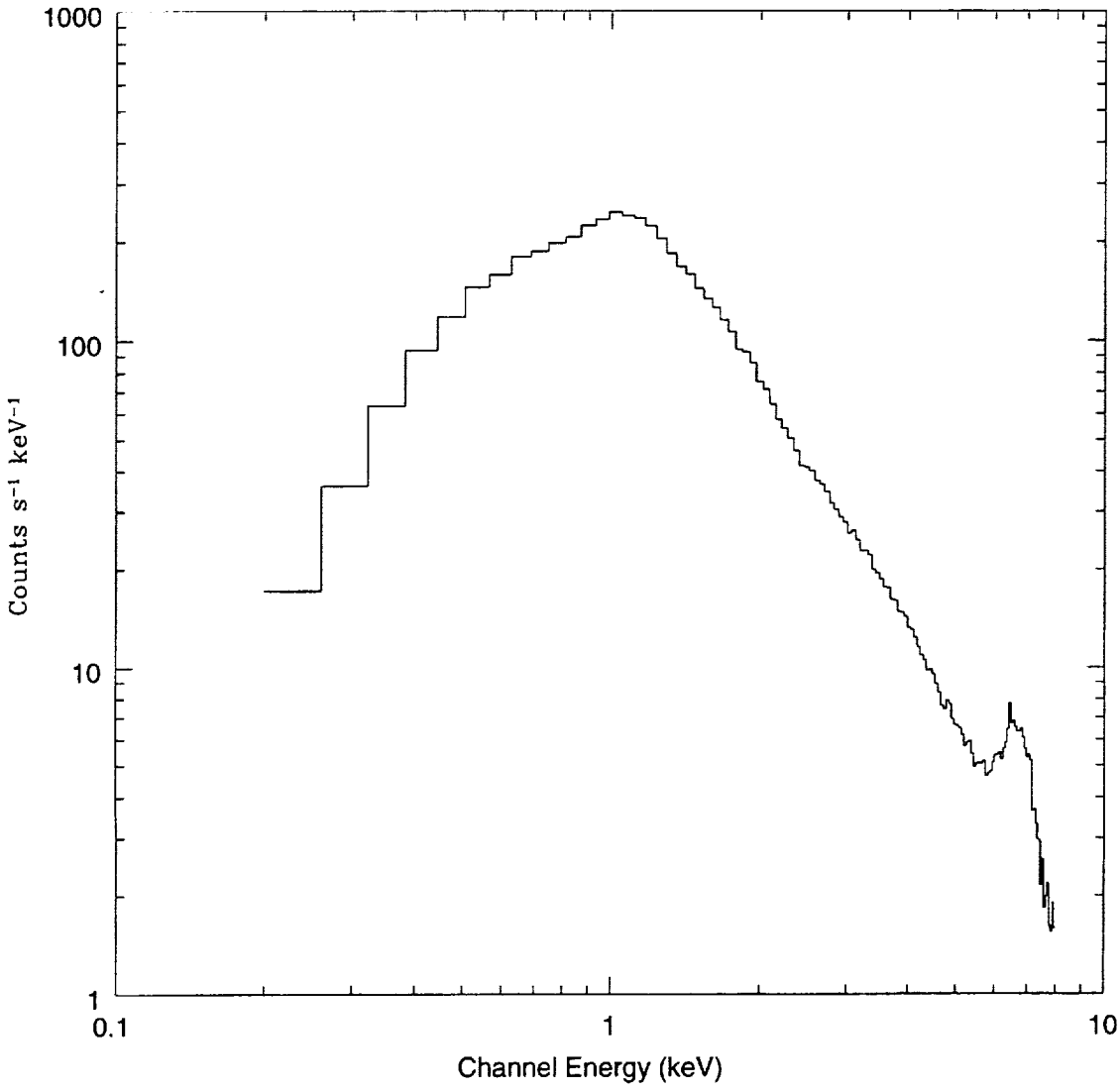

Figure 51: LEPC pulse height spectrum simulated with XSPEC. A 5 ksec LEPC observation of a Raymond-Smith plasma with cosmic abundances, emission integral of 10^{60} cm^{-3}, temperature of $10^{7.5}$ K, column density of 10^{21} cm^{-2}, and distance of 10 kpc is simulated.

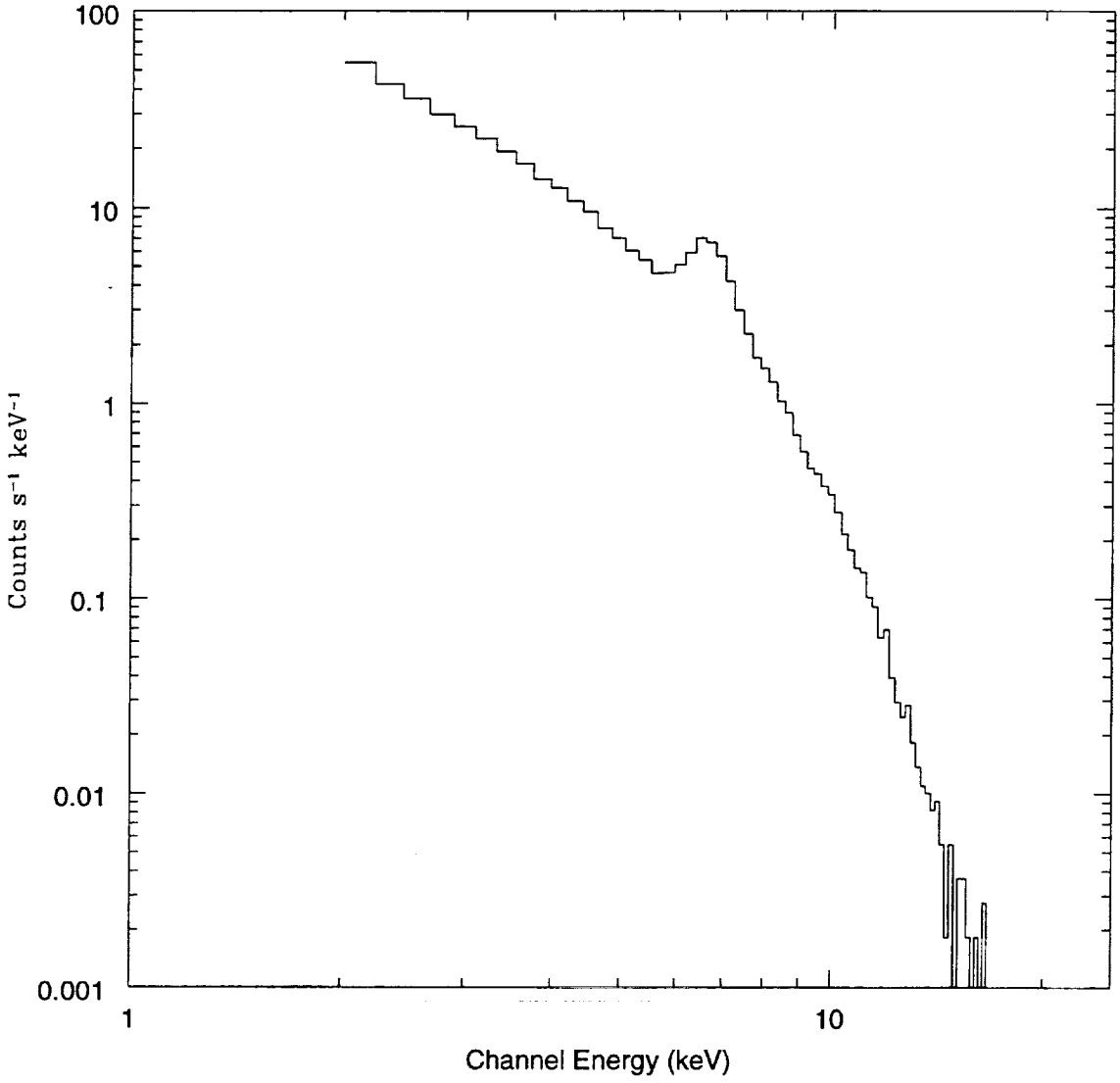

Figure 52: HEPC pulse height spectrum simulated with XSPEC. A 5 ksec HEPC observation of a Raymond-Smith plasma with cosmic abundances, emission integral of 10^{60} cm^{-3}, temperature of $10^{7.5}$ K, column density of 10^{21} cm^{-2}, and distance of 10 kpc is simulated.

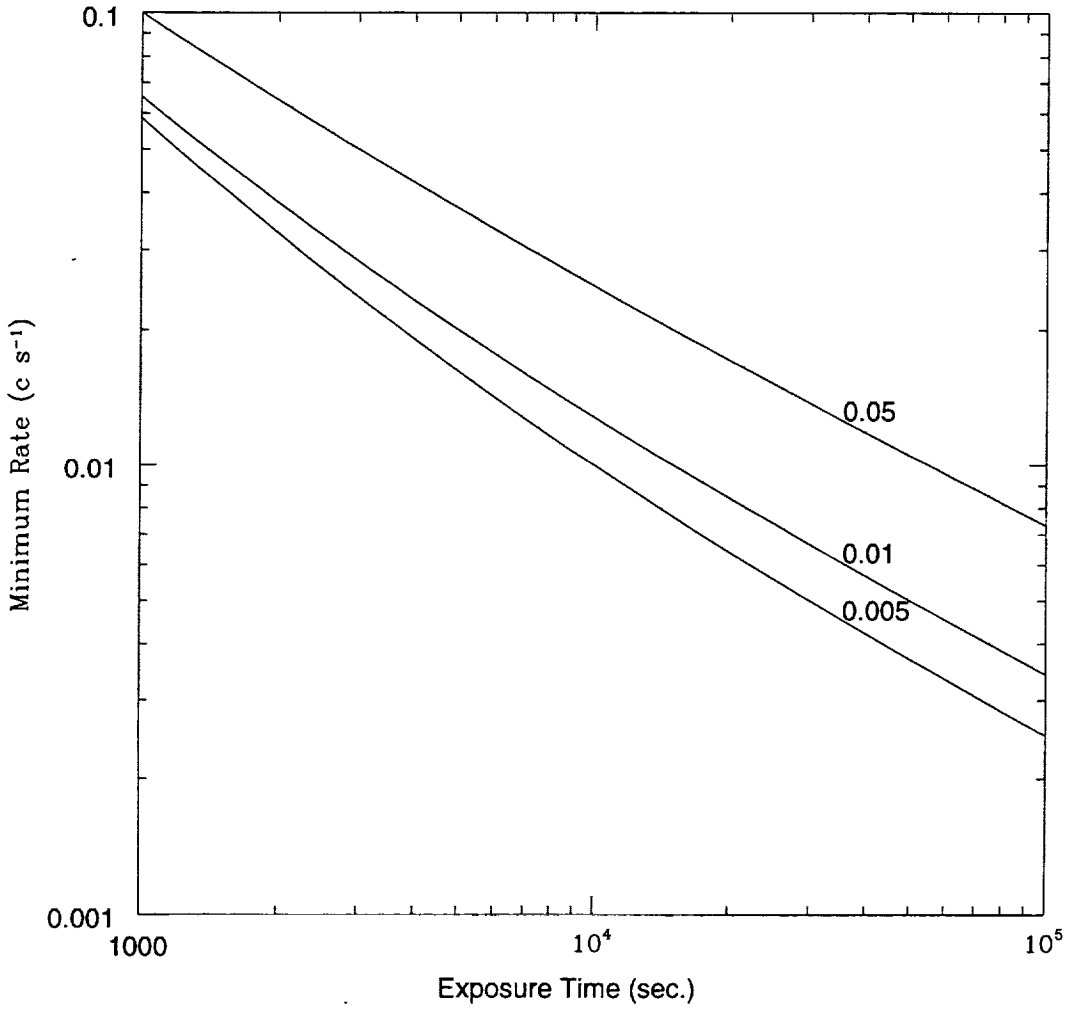

Figure 53: Minimum Count Rate Detectable by LEPC. The minimum count rate for a 5σ count rate significance is plotted as a function of exposure time, for 3 different background rates (in c s^{-1}) in a 2′ diameter aperture on-axis, using the formula given in section 4.4.4.

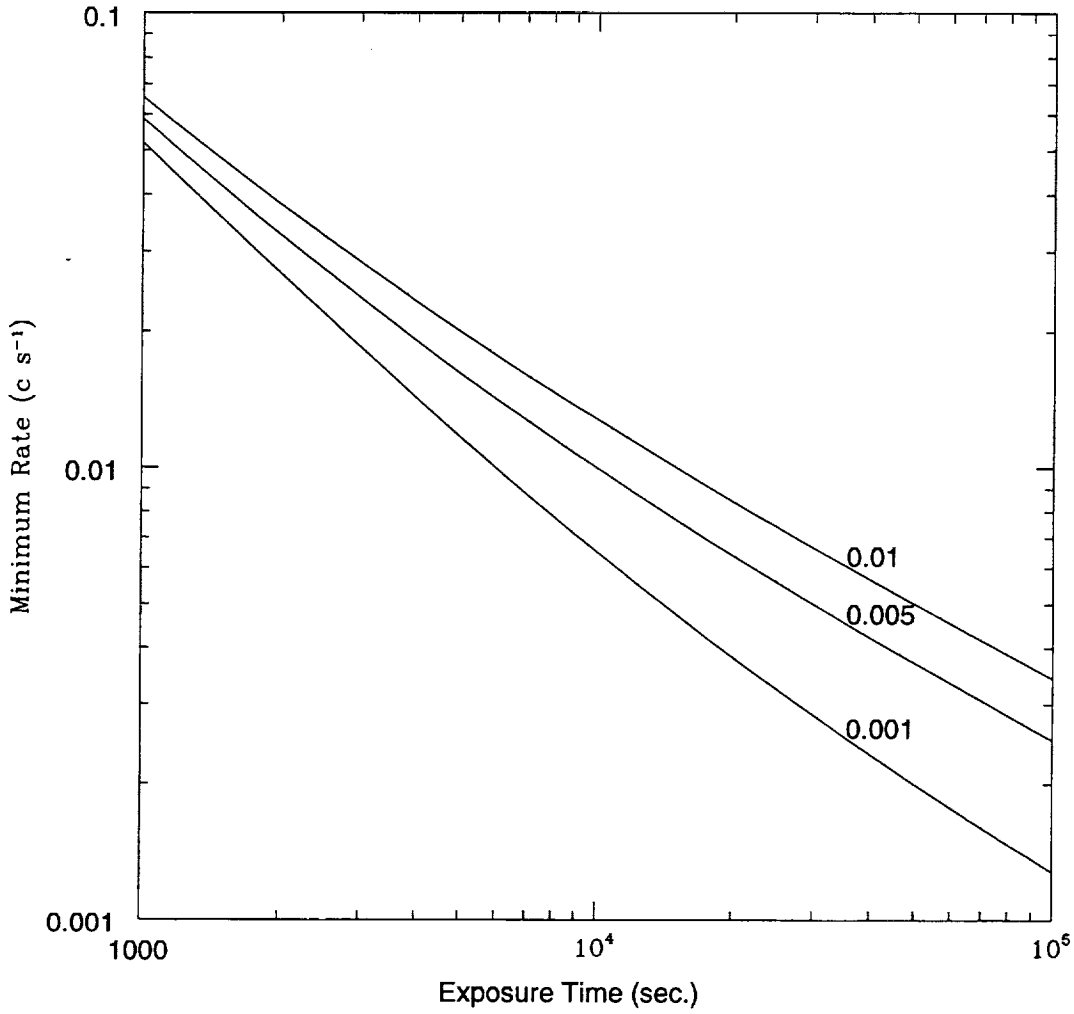

Figure 54: Minimum Count Rate Detectable by HEPC. The minimum count rate for a 5σ count rate significance is plotted as a function of exposure time, for 3 different background rates (in c s^{-1}) in a 2′ diameter aperture on-axis, using the formula given in section 4.4.4.

Table 7: OXS Parameters

Crystal	LiF	Si	RAP	ML
Observable H- & He-like lines	Fe	S & Ar	O	
Bragg angle for He-like lines	41°	50° & 39°	57°	
Wavelength Range (nm)	0.17-0.25	0.27-0.54	1.54-2.26	4.4-7.1
Energy Range (keV)	5.0-7.4	2.3-4.6	0.55-0.81	0.175-0.28
Rocking Curve Width	2.5′	1.6′	7′	40′
Energy Resolution (E/ΔE)	1250	3200	770	80
Peak Reflectivity	21%	35%	2%	12-22%
Non-X-ray Bgd. (c s^{-1} keV^{-1} $pixel^{-1}$)	$\sim 9 \times 10^{-5}$	$\sim 9 \times 10^{-5}$	$\sim 9 \times 10^{-5}$	$\sim 9 \times 10^{-5}$
X-ray Bgd. (c s^{-1} keV^{-1} $pixel^{-1}$)	$\sim 2 \times 10^{-5}$	$\sim 6 \times 10^{-5}$	$\sim 8 \times 10^{-5}$	$\sim 3 \times 10^{-3}$

5 The Objective Crystal Spectrometer (OXS)

5.1 Instrument Description

The OXS is a large, flat Bragg Crystal panel mounted in front of MM No. 1. Different crystals and multilayer coatings provide high-resolution imaging spectroscopy, and allow the study of highly ionized plasmas with appreciable angular extent ($\sim$ 1°) and which emit a broad range of line spectra from oxygen through iron. The spectra of point sources can also be studied with unprecedented resolution.

One side of the OXS panel is completely covered with 23 × 63 mm^2 LiF(220) crystals, while the other side is covered partly with 20 × 60 mm^2 RAP(001) crystals and partly with a multilayer (ML) of 60 × 60 mm^2 Si(111) crystals coated with ~70 periods of Co/C. The coated Si crystals allow simultaneous spectroscopy in two separate wavelength bands: the softer x-ray wavelengths are reflected in the multilayer coatings and the harder x-ray wavelengths are reflected in the substrate (Si-111). Table 7 summarizes the properties of the OXS. The effective area of the OXS, when combined with the LEPC focal plane detector (the normal configuration) is shown in Figure 55.

The OXS concept separates the processes of energy dispersion and imaging. The mosaic panel acts as a narrow bandpass filter and as a mirror. Each pixel in the reflected field of view of the telescope satisfies a specific Bragg angle on the crystal and, therefore, each pixel in the detector can be identified with a particular energy. Scans which involve repositioning of the telescope axis and the angle between the crystal panel and the telescope axis (45° ± 15°) yield either the spectrum of a point source or energy resolved images of an extended source (Figure 56).

5.2 Operating Modes

The OXS will normally be operated in conjunction with the LEPC. During observations with the OXS, the source will be located $\sim 90°$ from the pointing direction of the telescope. To ensure coverage of the full angular extent of diffuse sources over the range of Bragg angles of interest, the telescope will be repositioned several times during the observation. Current expectations are that a typical OXS observation will consist of ~ 10 successive pointings, separated by $\lesssim 10'$, each of 10^4 seconds duration. For observations of point sources, both the telescope pointing direction and the angle between the crystal panel and telescope will be adjusted to keep the source on-axis for the entire observation.

5.3 Scientific Objectives

A major strength of the OXS is its ability to perform high spectral resolution imaging of extended sources, at energies which include several astrophysically important lines. It is thus well-suited for detailed plasma diagnostic studies of bright supernova remnants and clusters of galaxies. It can also be used for precise measurement of the redshifts of cluster gas.

5.4 Determining the Feasibility of OXS Observations

5.4.0.1 Background The OXS will encounter cosmic background from the diffuse x-ray background and scattered solar x-rays, as well as non-X-ray background in the LEPC. The total non-X-ray background in LEPC is estimated to be $\sim 5 \times 10^{-4}$ counts cm^{-2} s^{-1} keV^{-1}. In a $2'$ diameter circle (~ 4.7 mm for an 8 m focal length), this corresponds to a rate of $\sim 9 \times 10^{-5}$ counts s^{-1} keV^{-1}.

The diffuse x-ray background may be estimated using the effective area shown in Figure 55 and a model xrb spectrum. We use the ROSAT spectrum of Wang and McCray (1993) below 3 keV, and the HEAO-1 spectrum of Boldt (1987) above 3 keV, and a pixel corresponding to a $2'$ diameter circle, to determine the values shown in Table 7. Readers should be aware, however, that the soft component of the xrb is dominated by galactic contributions and can vary with viewing direction by as much as a factor of 5. The total xrb in the OXS bands will therefore vary by a large factor.

5.4.0.2 Detection of Spectral Lines Because of the high resolution ($\Delta E \sim 1--5$ eV) of the OXS, the number of events per energy bin in typical 10^4 second OXS scans due to background and source continuum is expected to be $\lesssim 1$. Rough estimates of the total number of events in lines of interest, using effective areas in Figure 55 , can be used to determine the feasibility of OXS observations.

Future tools for determining OXS rates and simulating OXS spectra and energy-resolved images will be available from the WWW sites **http://uhuru.dsri.dk/srg/srg.html** at DSRI and **http://hea-www.harvard.edu/SXG/sxg.html** at the U.S. SXG Coordination Facility.

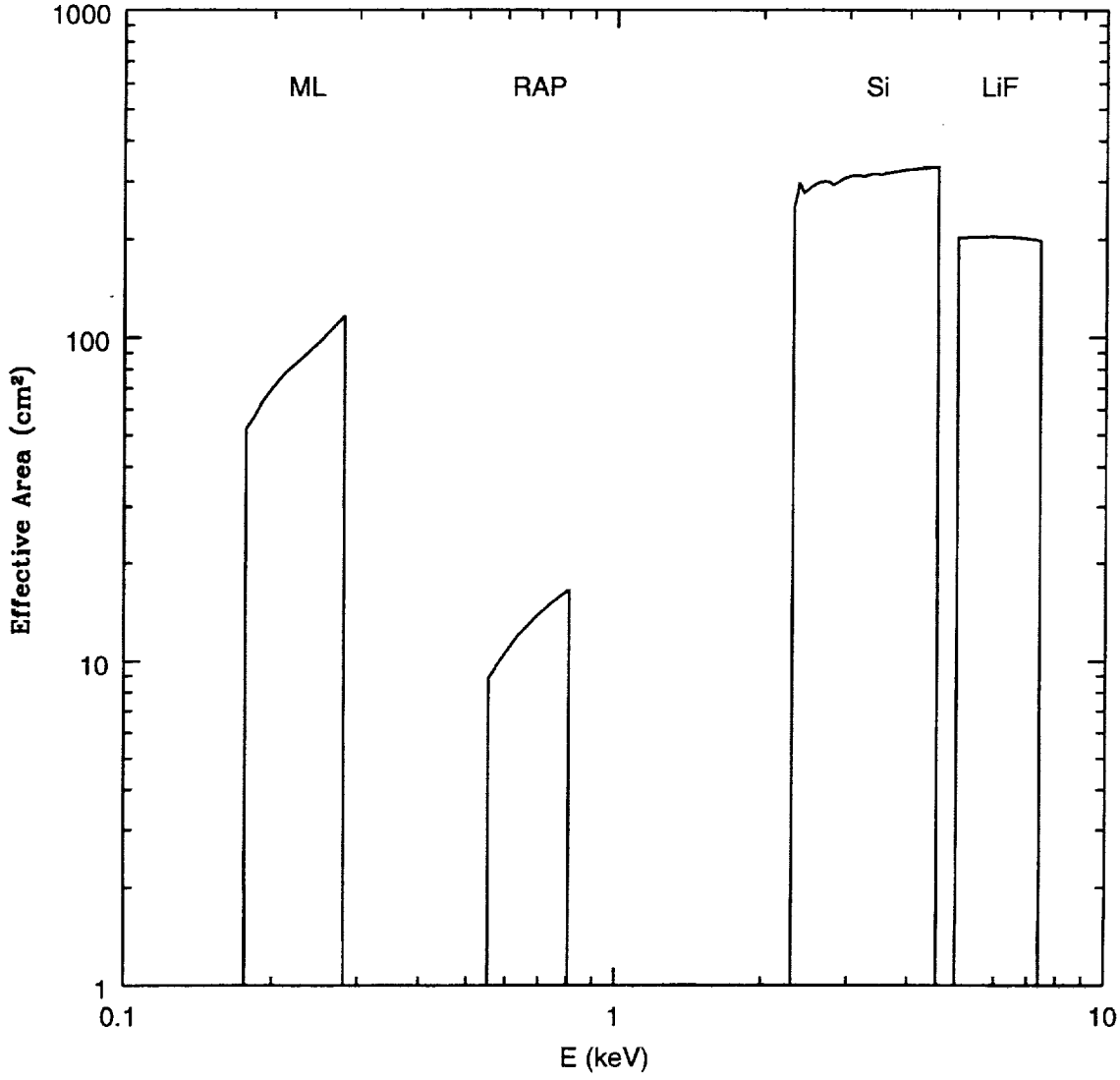

Figure 55: OXS Effective Area

THIS FIGURE IS NOT AVAILABLE YET.

Figure 56: An extended source emitting a He-like line series can be mapped in each spectral feature by combining data from a series of observations, each with a slightly different orientation of the crystal panel and telescope pointing direction. In any one orientation, specific regions of the source, as shown here, will satisfy the Bragg conditions for the Forbidden, Intercombination, and Resonance line energies and thus be imaged into corresponding regions on the detector. Different crystal/telescope orientations will sample different regions of the source.

6 The Silicon X-ray Array (SIXA)

6.1 Instrument Description

SIXA is a multi-element X-ray photon counting spectrometer. It is one of the focal plane instruments for SODART Telescope 2. Its high sensitivity, broad energy range, and good temporal and spectral resolution make it well-suited for obtaining time-resolved spectra and studying spectral lines.

SIXA consists of 19 discrete hexagonally arranged circular elements with a centerline distance of 12 mm (Figure 57). Each element is a 3 mm thick wafer of lithium-drifted silicon (Si(Li)). A radiative cooler is used to bring the detector to the proper operating temperature (120-130 K), and aluminium coated polyimide windows are used to filter out IR/visible/UV light. A number of different observing modes allow the accumulation of individual photon event lists, integrated energy spectra or light curves, or time interval histograms. Table 8 gives a summary of the properties of SIXA. The total response of the SIXA/SODART system is demonstrated in Figure 58.

Diameter of active area	6 cm
Field of view	25′
Number of pixels	19
Total/active pixel diameter	12/9.25 mm (5.16′/3.97′)
Number of energy channels	1024
Width of each channel	20 eV
Effective energy range	0.5-20 keV
Energy resolution (FWHM)	200 eV at 6 keV
Time resolution	30.5 μsec (TIM mode: 12.21 μsec)
Spatial Resolution	4′
Non-X-Ray Background	$\sim 1.3 \times 10^{-2}$ c s^{-1} pixel^{-1}
X-ray Background (on-axis)	$\sim 1.7 \times 10^{-2}$ c s^{-1} pixel^{-1}
Depletion depth	3 mm
Operating temperature	120-130 K

Table 8: SIXA Detector Parameters

6.1.1 Entrance Window

An X-ray entrance window will be placed between the telescope and the detector. The window is transparent to X-rays and opaque to the optical background, functioning at the same time as an optical filter and a part of the cooler shield. The window consists of two similar filters, both fabricated of a polyimide substrate (0.3 microns) supported by a hexagonal polyimide grid, and coated on both sides with aluminium (30 nm), where the aluminium acts as the optical filter. The total thickness of each filter is 18 microns, and

the total thickness of Al for the window system is 120 nm. In addition, the transmission is affected by the thin contact layer (Au/Pd; thickness 30 nm) on the detector.

The thickness of aluminium is determined so that the UV, optical and IR flux from the source and background will be reduced to a negligible level for any reasonable source brightness. The filter attenuates the flux by at least 10^{-9} from IR to UV; thus the noise from, e.g. Sirius (-1.4 mag) would be less than 0.01 eV. For a zero magnitude star the respective noise would still be only about 0.3 eV.

6.1.2 Cooler and Electronics

The detector is connected to the radiative cooler (Passive Cooling System) and to the control electronics unit. The cooler is an $\sim$ 1 m long tube with weight of about 100 kg, directed vertically to the optical axis. The dimensions of the electronics box are 560 $\times$ 317 $\times$ 277 mm, and the total weight of the electronics and detector system is 33 kg.

Each detector element has its own front-end electronics channel which includes a charge-sensitive preamplifier with transistor reset feedback and a linear amplifier. The first stages of the preamplifiers (JFETs) are positioned in the detector body in order to cool them and thus reduce the noise of the FETs, which will be a dominant factor determining the energy resolution. In addition to energy signal outputs, the linear amplifiers have fast timing outputs for time-interval measurements.

The front-end electronics is grouped on three cards, and one multiplexer is used for the energy outputs from each group. The multiplexers also provide anticoincidence functions and pile-up rejection. The pulse height analyzers linked to each multiplexer use Gatti sliding scale construction.

The resulting digital information is processed by digital electronics including two independent processors (DPUs) that share the control of the available observing modes, which are described later in "Operating modes". The permanent programs and parameters are stored in an EEPROM, and the system has 4 MBytes of RAM and (at least) a 40 Mbyte hard disk for the science data.

6.1.3 Time Resolution

The time resolution for the system is 30.512 μsec for event characterization (SEC, ESM, WCM), and 12.21 μsec for time interval (TIM) spectra. The maximum continuous count rate is 5000-10000 cts/s, which limit is determined by the capacity of the DPUs with the actual load by various software tasks. The upper limit is close to 2 Crabs (one Crab is about 3500 cts/s with SIXA).

The analog electronics part of the system can separate events with a much higher time resolution than indicated above, which property is used by hardware for coincidence and pile-up rejection. X-ray bursts caused by, for example, cosmic radiation hitting the satellite will thus be filtered out effectively before they enter the digital counters. Direct hits of high energy cosmic rays will also be rejected because they exceed the energy range of SIXA.

The dead time correction for SIXA countrates can be estimated from the total countrates in the 3 subgroups of detector pixels (see Figure 57), using a time constant of 12.21 microsec for the TIM mode, and 30.512 microsec for all the other modes. For a 300 cps/group

source the dead time correction would be about 1%, and for a 3000 cps/group source about 10%. The pile-up effect (signal of two or more events combined into one detected event) is significant only for very large countrates (about 10000 cps or more).

6.1.4 Spatial Resolution

The spatial resolution of SIXA is determined by the point spread function of the SODART telescope (~2.5′–3′ HPD on-axis, decreasing with increasing energy). One SIXA pixel corresponds to a single detector element. The active diameter of 9.25 mm corresponds to ~ 4′ for an $f = 8m$ telescope. The encircled energy in the central SIXA pixel is ~57%–~65% (6.6–11 keV) for a point source on-axis. The corresponding encircled energies, accounting for the dead area between pixels, are ~73%–76% for the central 7 pixels, and ~76%–79% for all 19 pixels.

6.2 Operating Modes

For each session between ground contacts (18-33 hours) SIXA will be programmed using a series of operation commands sent from the ground station to the satellite. If the device is not in use, it will normally be powered down (off). When switched on, the DPUs perform first a sequence of standard power-up tests. After this SIXA enters the STANDBY operating mode. All service functions are performed in the standby mode. After receiving the parameters in the standby mode, and warming up in the MEASUREMENT mode, the device is ready to start observing or calibration. When SIXA is in the measurement mode, the analog electronics is on. Other OPERATING MODES are DUMPING and DATA RETENTION modes. During, for example, reorientation it is in the data retention mode, refreshing data stored in RAM. Science data is transferred to the satellite in the dumping mode.

There will be a selection of six OBSERVING MODES available: three different SEC (single event characterization) modes, Energy-Spectrum Mode (ESM), Window-Counting Mode (WCM), and Time-Interval Mode (TIM). The control over the modes is shared between two processors, so that one DPU runs the SEC modes, and the other DPU the three other modes. The ESM, WCM and TIM can be run in parallel with one SEC mode (maximum of four modes simultaneously), and any of the modes can be switched off. The starting and ending times of each spectrum are stored with a 10 ms accuracy. The time resolution in SEC, ESM and WCM is about 30.5 μsec, and in TIM it is 12.21 μsec.

In the SEC modes the detector acts as a photon counter, and an event list is obtained. Every event is stored in a four-byte word (photon energy, arrival time, and id. of pixel). SEC 1 measures the events in all 19 elements and all energy channels. SEC 2 measures only events in the 7 central elements and within two energy windows. SEC 3 is similar to SEC 2 but the window limits are not applied. The arrival time is stored by a counter with units of about 30.5 μsec.

In ESM an energy spectrum is obtained. The integration time (10ms, 1 s - 33 h) is specified by the user. During this interval the events in each of the 1024 channels are counted (corresponding to the energy range about 0.5-20 keV). The optimal integration time depends on the source strength. At least several thousand events have to be recorded before a useful spectrum is obtained.

In WCM an X-ray light curve is obtained in two energy bands. The user selects the sampling time (time bin) and the two energy bands within which the events are summed in each of the seven central elements separately. Typically, the energy bands could be 0.5-2 keV (soft), 2-10 keV (medium), 10-20 keV (hard) and 6-7.5 keV (the iron line). For hardware requirements, ESM and WCM are coupled, so that the time bin is a fixed (1/1024, 2/1024, 4/1024, ..., 1) fraction of the integration time in ESM.

In TIM a time interval spectrum is obtained. The seven central elements act as one, and the time intervals between every other event (i.e. t2-tl, t4-t3, ...) caught by them is stored. The time unit for the intervals is 12.21 μsec, and there are 8192 channels, each corresponding to one time interval (n $\times$ 12.21 μsec, n=1,2,3,...,8192). When a time interval matching an interval in the range from 12.21 to (8192 $\times$ 12.21) μsec is registered, the corresponding counter is incremented. TIM mode is therefore suitable for searching short time periodicities in astronomical objects.

WCM and SEC 2 modes use common energy windows defined in the measurement program for each target separately. Energy windows for TIM, however, are independent of these and more permanent, but can also be redefined with a separate parameter command.

6.3 Scientific Objectives

The high sensitivity, broad energy range, and the spectral resolution of SIXA will enable observations of time-resolved X-ray spectra for a variety of astronomical objects. Potential observing programs include stellar coronae, molecular clouds, cataclysmic variables and X-ray binaries; accretion discs and coronae of neutron stars and black hole candidates; supernova remnants, active galactic nuclei, clusters of galaxies and the diffuse cosmic X-ray background.

The energy range of SIXA (0.5-20 keV) contains many K-shell transitions. Detailed analysis of these spectral features will permit the determination of the physical characteristics of the emitting region and its environment. The ratio of the strength of the helium-like (Fe XXV) to the hydrogen-like (Fe XXVI) lines is a measure of the plasma temperature. A temperature measure that is independent of the equilibrium assumption is the ratio of the K-alpha and K-beta line intensities. All these can be separated with SIXA.

In accretion-powered X-ray sources (X-ray binaries and AGN's) the X-ray emitting plasma is often optically thick, with FWHM almost 1 keV. With the resolution of SIXA (200 eV), line profiles can be measured, giving an opportunity to study the line broadening mechanisms and the geometry of the emitting regions.

The SIXA detector will be suitable for studies in a wide variety of time scales. Galactic sources of variable X-ray emission include accretion disks, active stars with variable X-ray emission (X-ray flares), and mass accreting compact stars in close binary systems (X-ray bursts on white dwarfs and neutron stars). These exhibit variations in timescales from fractions of a second to days.

Stars of almost all spectral types possess X-ray coronae with luminosities in the range $10^{26} - 10^{34}$ erg s^{-1} and with mean coronal temperatures $10^6 - 10^8$ K. Spectroscopic study of stellar coronae can provide crucial information on a number of interesting physical processes, such as the generation of magnetic fields by dynamo action, the conversion of non-radiative energy into thermal energy and plasma heating, and the processes that cause mass and

angular momentum loss in stars. With SIXA, a 5σ detection can be made in 2×10^4 s at distances d = $50 \times (L/10^{27}\ erg\ s^{-1})^{\frac{1}{2}}$ pc for the continuum and $d = 5 \times (L/10^{27}\ erg\ s^{-1})^{\frac{1}{2}}$ pc for the Fe-line. Spectroscopy with a few minutes time resolution gives an opportunity to model flare dynamics of most active stars.

X-ray emission is a fundamental property of active galactic nuclei (AGN). Measurement of the X-ray time variability and spectra of these objects give us the closest look at the central energy source. X-ray active AGN's typically have strong soft excesses and canonical power-law spectra. In some cases, a broad iron line has been detected. The resolution and through-put of SIXA are sufficient for searching for e.g. the relativistic (two-horn) effects in line profiles.

Especially suitable targets for the geometry and field-of-view of SIXA are clusters of galaxies (especially those with cooling flows) and supernova remnants.

6.4 Determining the Feasibility of SIXA Observations

6.4.1 Background

The SIXA detectors will encounter cosmic background from the diffuse x-ray background and scattered solar x-rays, as well as non-X-ray background from charged particles, cosmic-ray-induced secondary radiation from the spacecraft structure, and induced radioactivity. The main contributors to the non-X-ray background are expected to be induced radioactivity and bremsstrahlung from charged particles. The total non-X-ray background is estimated to be $\sim 10^{-3}$ counts cm^{-2} s^{-1} keV^{-1}, or $\sim 1.3 \times 10^{-2}$ counts s^{-1} pixel^{-1}, from 0.5 – 20 keV.

The diffuse x-ray background in SIXA may be estimated using the effective area shown in Figure 58 and a model xrb spectrum. We use the ROSAT spectrum of Wang and McCray (1993) below 3 keV, and the HEAO-1 spectrum of Boldt (1987) above 3 keV, and find a value of ~ 5 c s^{-1} deg^{-2} or $\sim 1.7 \times 10^{-2}$ c s^{-1} pixel^{-1}, on-axis. Readers should be aware, however, that the soft component of the xrb is dominated by galactic contributions and can vary with viewing direction by as much as a factor of 5. The total xrb in SIXA may therefore vary by a factor of 2-3.

6.4.2 Estimating SIXA Count Rates

Source count rates in SIXA can be estimated using HEASARC's multi-mission simulator PIMMS. It is assumed that a spectral model and either an absolute flux or a count rate in another instrument are known. The following dialog illustrates the use of PIMMS to estimate the SIXA rate for a source with a 5 keV thermal bremsstrahlung spectrum, interstellar absorption of 5×10^{20} cm^{-2}, and an ASCA SIS rate of 1 c s^{-1}:

```
*** Small PIMMS version s2.03 (XTE compatible) ***
    1994 Dec 27 release
    (this version does not simulate images)
    Reading mission directory, please wait
* Current model is BREMSSTRAHLUNG, kT=  10.0000 keV; NH =  1.000E+21
   <--- Use 'MODEL' command to change
* By default, input rate is taken to be
```

```
 Flux (  2.000- 10.000 keV) in ergs/cm/cm/s
   <--- Use 'FROM' command to change the default
* Simulation product will be
 Count rate in XTE PCA
   <--- Use 'INSTRUMENT' command to switch to another instrument
pimms > instrument sxg sixa
pimms > from asca sis
pimms > model brem 5.0 5.0e20
pimms > go 1.0
* For thermal Bremsstrahlung model with kT=  5.0000 keV;
  NH =  5.000E+20 and  1.000E+00 cps in ASCA SIS
  (Model normalization =  5.374E-03)
* PIMMS predicts  6.618E+00 cps with SXG SIXA
pimms >
```

In Figures 59 – 67, we provide count rate conversion factors from ASCA and ROSAT rates, for power law, bremsstrahlung, and black body spectra, and a range of spectral parameters.

PIMMS may be obtained from the **software/tools** directory in the anonymous ftp node **legacy.gsfc.nasa.gov**. Version 2.0 includes support for SXG instruments. To update earlier versions, users may obtain new mission lists and SXG area files from the directory **/pub/sxg/pimms** in the anonymous ftp node **sao-ftp.harvard.edu**.

6.4.3 Simulating SIXA Spectra

SIXA spectra can be simulated with the HEASARC XSPEC program. The following dialog illustrates the simulation of the spectrum of a 5 ksec SIXA observation of a Raymond-Smith plasma with an emission integral of 10^{60} cm^{-3}, temperature of $10^{7.5}$ K, column density of 10^{21} cm^{-2}, at a distance of 10 kpc.

```
!xspec 13:27:26 12-Feb-96
XSPEC> model raymond wabs
  mo = wabs[2] (raymond[1])
 Input parameter value, delta, min, bot, top, and max values for ...
 Mod parameter  1 of component  1 raymond  kT(keV)
    1.000      1.0000E-02  8.0000E-03  8.0000E-03   64.00       64.00
 2.73
 Mod parameter  2 of component  1 raymond  Abundanc
    1.000     -1.0000E-03      0.          0.       5.000       5.000
 1.0
 Mod parameter  3 of component  1 raymond  Redshift
       0.     -1.0000E-03      0.          0.       2.000       2.000
 0.0
 Mod parameter  4 of component  1 raymond  norm
    1.000      1.0000E-02      0.          0.     1.0000E+24  1.0000E+24
 0.8356
```

```
Mod parameter  5 of component  2 wabs      nH 10^22
   1.000      1.0000E-03      0.           0.      1.0000E+05  1.0000E+06
0.1
 ------------------------------------------------------------------------
 ------------------------------------------------------------------------
 mo = wabs[2] (raymond[1])
 Model Fit Model   Component     Parameter   Value
 par   par comp
   1    1    1       raymond     kT(keV)    2.73000     +/-      0.
   2    2    1       raymond     Abundanc   1.00000     frozen
   3    3    1       raymond     Redshift       0.      frozen
   4    4    1       raymond     norm      0.835600     +/-      0.
   5    5    2       wabs        nH 10^22  0.100000     +/-      0.
 ------------------------------------------------------------------------
 ------------------------------------------------------------------------
   3 variable fit parameters
XSPEC> fakeit none
 For fake data, file #  1 needs response file: sixa.rmf
              ... and ancillary response file : none
Use counting statistics in creating fake data? (y) y
 Input optional fake file prefix (max 12 chars): appe
 Override default values for file #    1
 Fake data filename (appesixa.fak):
 T, A, Bkg, cornorm ( 1.0000 , 1.0000 , 1.0000 , 0. ): 5000.0,1735.0
 Net count rate (cts/s) for file   1   242.6    +/-  0.2203
 Chi-Squared =      842.6     using  1007 PHA bins.
 Reduced chi-squared =     0.8392
XSPEC>
```

A plot of the raw spectrum in the energy range from 0.5 – 10 keV (channels 1 – 500) is shown in Figure 68. The required response matrix, sixa.rmf, may be obtained from the directory **/pub/sxg/xspec** in the anonymous ftp node **sao-ftp.harvard.edu**.

XSPEC may be obtained from the **software/xanadu** directory in the anonymous ftp node **legacy.gsfc.nasa.gov**.

6.4.4 Detection of Point Sources

The total background per SIXA pixel in a ~1 ksec observation is likely to be $\gtrsim$30 counts. Therefore, Gaussian statistics can be used to estimate the minimum count rate, R_{min}, required to detect a point source at a given count rate significance, as a function of exposure time T. For a point source on-axis, R_{min} is given by the solution to

$$N_\sigma = \frac{R_{min} f T}{\sqrt{R_{min} f T + R_B T}},$$

or

$$R_{min} fT = \frac{N_\sigma^2}{2}\left(1 + \sqrt{1 + \frac{4R_B T}{N_\sigma^2}}\right).$$

Here, N_σ is the signal-to-noise ratio of the net source counts, expressed as number of σ, f is the encircled energy fraction (0.57–0.65 on-axis), and R_B is the total background rate per SIXA pixel. Results are shown in Figure 69 for a range of background rates.

6.4.5 Detection of Spectral Lines

Given the good spectral resolution of SIXA and the high throughput of the SODART mirrors, it is expected that one of the principal uses of SIXA will be in the study of spectral lines. In this case, exposure times sufficient for simple source detection will not be adequate. Rather, the required exposure time will depend on the line strength, continuum, and background. Line strength is expressed in terms of Equivalent Width, W, defined as the ratio of the net counts in the line (summed over some energy range ΔE) to the continuum (in counts keV^{-1}) at the line centroid,

$$W = \frac{n_{line}}{CA_{eff}T}.$$

Here, C is the continuum spectrum, in photons cm^{-2} s^{-1} keV^{-1}, and A_{eff} is the effective area at the line energy. The required exposure time is then given by the solution to

$$\frac{W}{\sigma_W} = N_\sigma,$$

where

$$\sigma_W^2 = \frac{\sigma_{n_{line}}^2}{(CA_{eff}T)^2} = \frac{n_{line} + CA_{eff}T\Delta E + B_{x-ray}A_{eff}T\Delta E + B_{inst}A_{geom}T\Delta E}{(CA_{eff}T)^2}.$$

Here, B_{x-ray} and B_{inst} are the cosmic and non-X-ray backgrounds (in counts cm^{-2} s^{-1} keV^{-1}), and A_{geom} is the active geometric area of a SIXA pixel (0.67 cm^2). The minimum detectable Equivalent Width is then

$$W_{min} = \frac{N_\sigma^2}{2CA_{eff}T}\left(1 + \sqrt{1 + \frac{4(CA_{eff}T\Delta E + B_{x-ray}A_{eff}T\Delta E + B_{inst}A_{geom}T\Delta E)}{N_\sigma^2}}\right).$$

Typical results for Fe K lines are shown in Figure 70, for a range of exposure times.

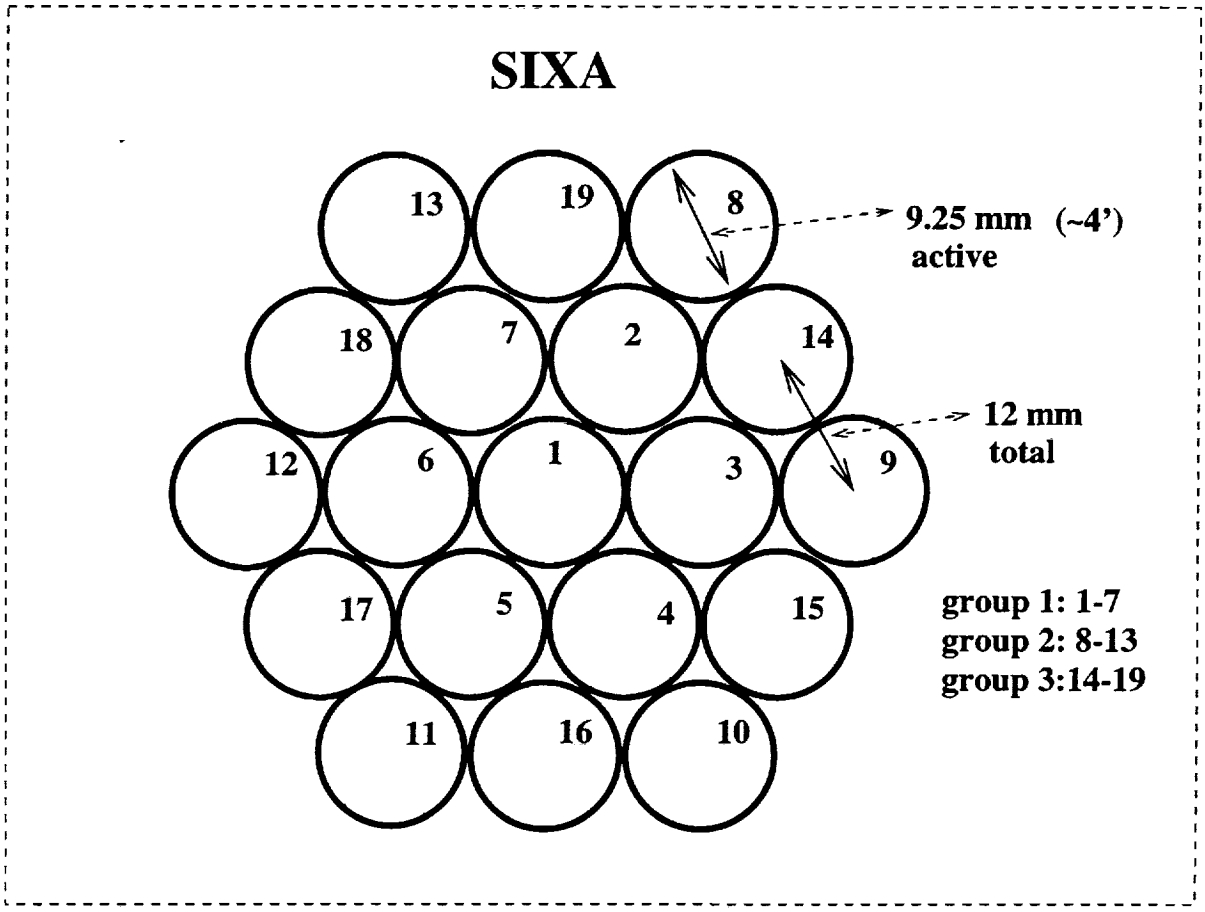

Figure 57: Array of 19 SIXA Detector Elements. Individual detector elements are labelled with SIXA pixel numbers.

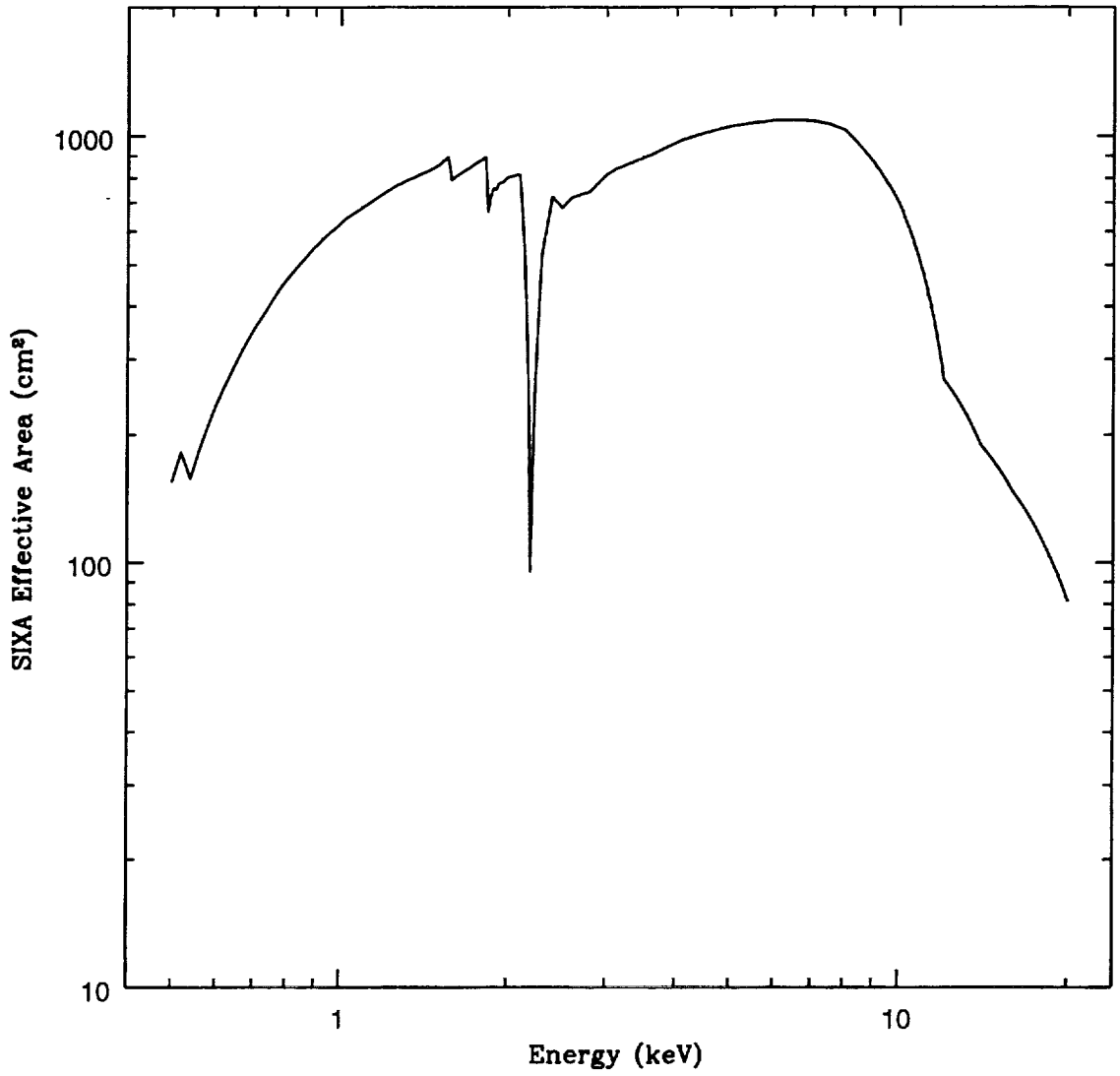

Figure 58: SIXA Effective Area

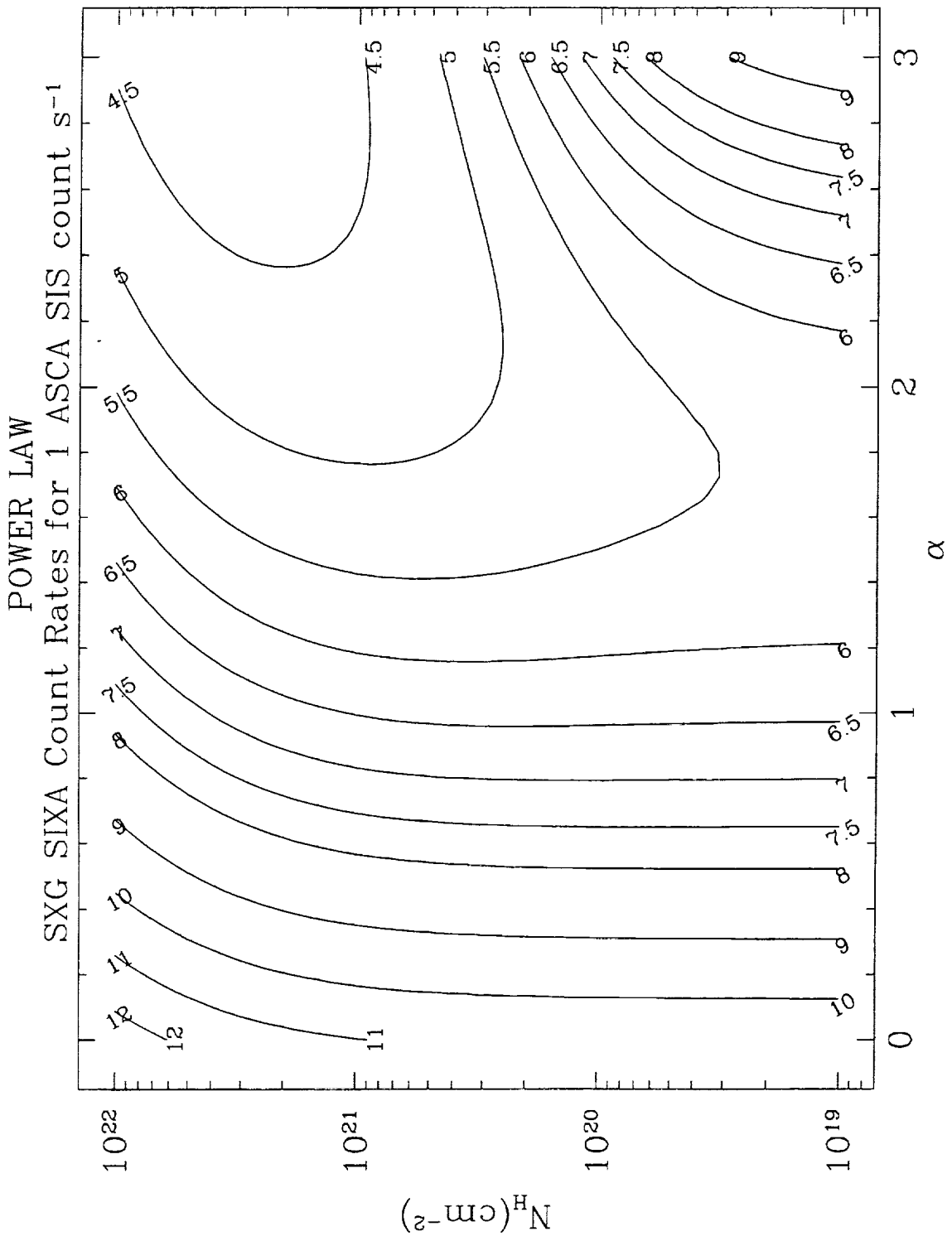

Figure 59: SIXA count rates yielding 1 ASCA SIS c s^{-1}, for a power law spectrum. This and subsequent figures (60 - 67) are contour plots of count rate conversions derived from PIMMS. For conversion factors less than 1, one contour per decade is displayed. For factors greater than 1, contour intervals differ by ~30%, on average.

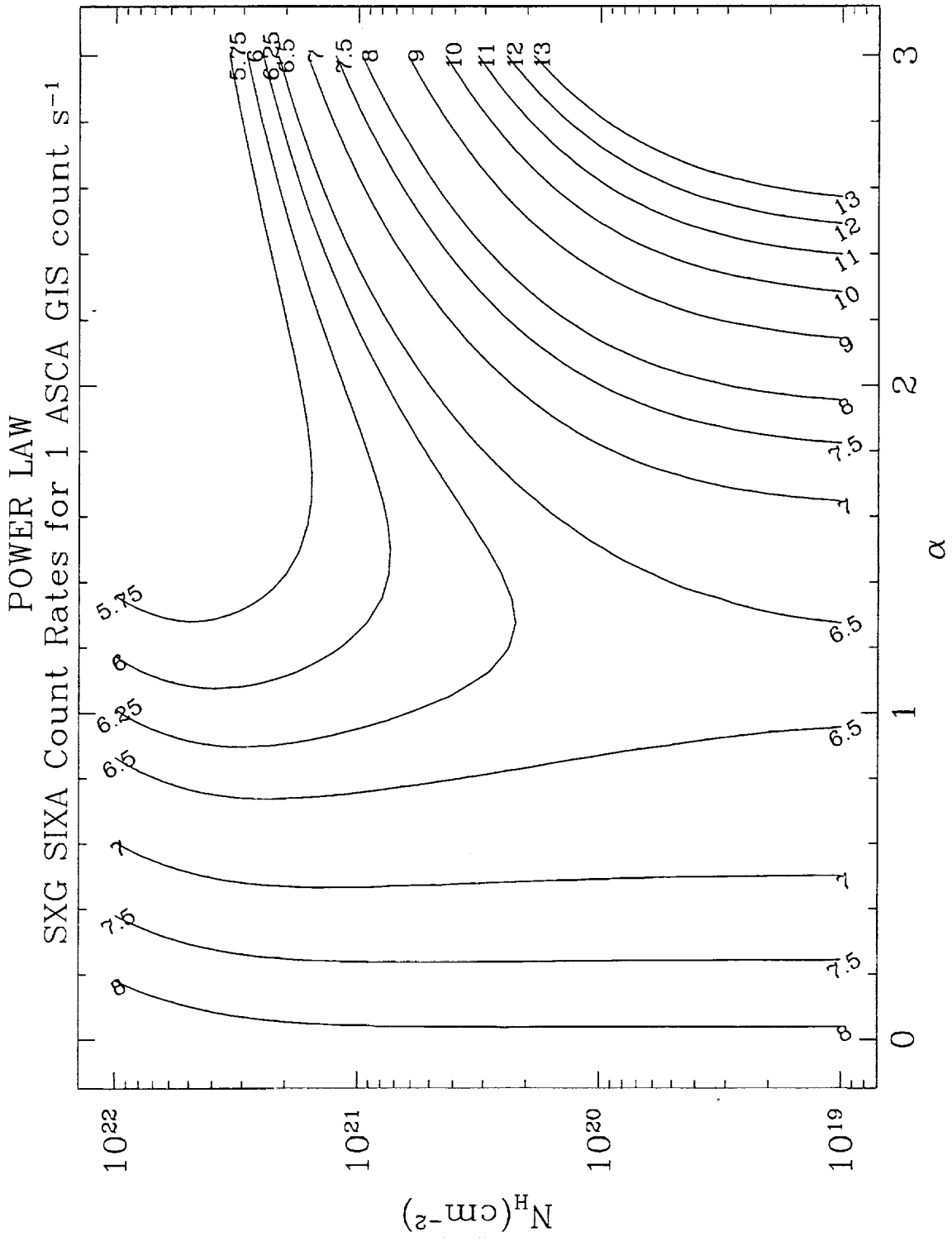

Figure 60: SIXA count rates yielding 1 ASCA GIS c s^{-1}, for a power law spectrum.

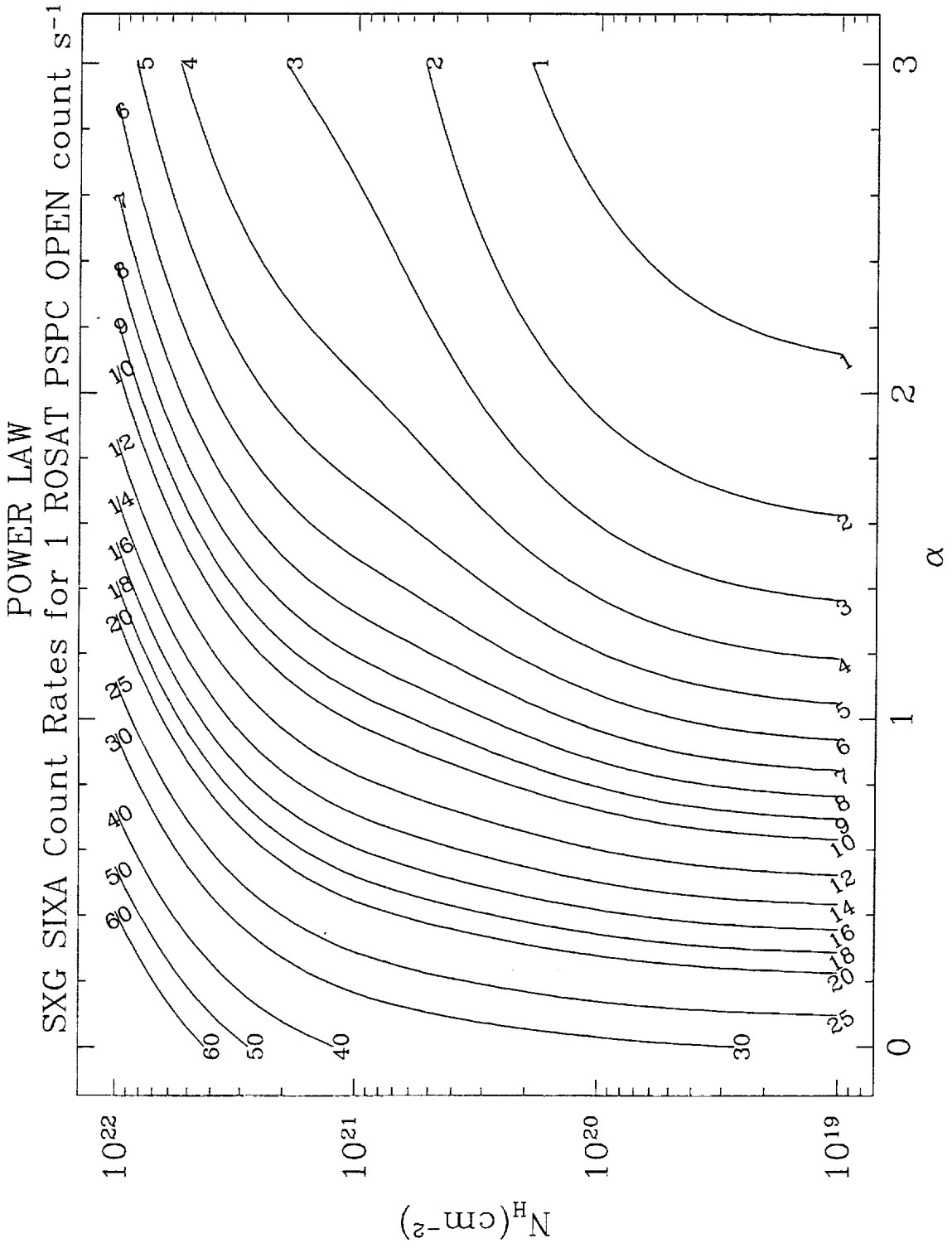

Figure 61: SIXA count rates yielding 1 ROSAT PSPC c s^{-1}, for a power law spectrum.

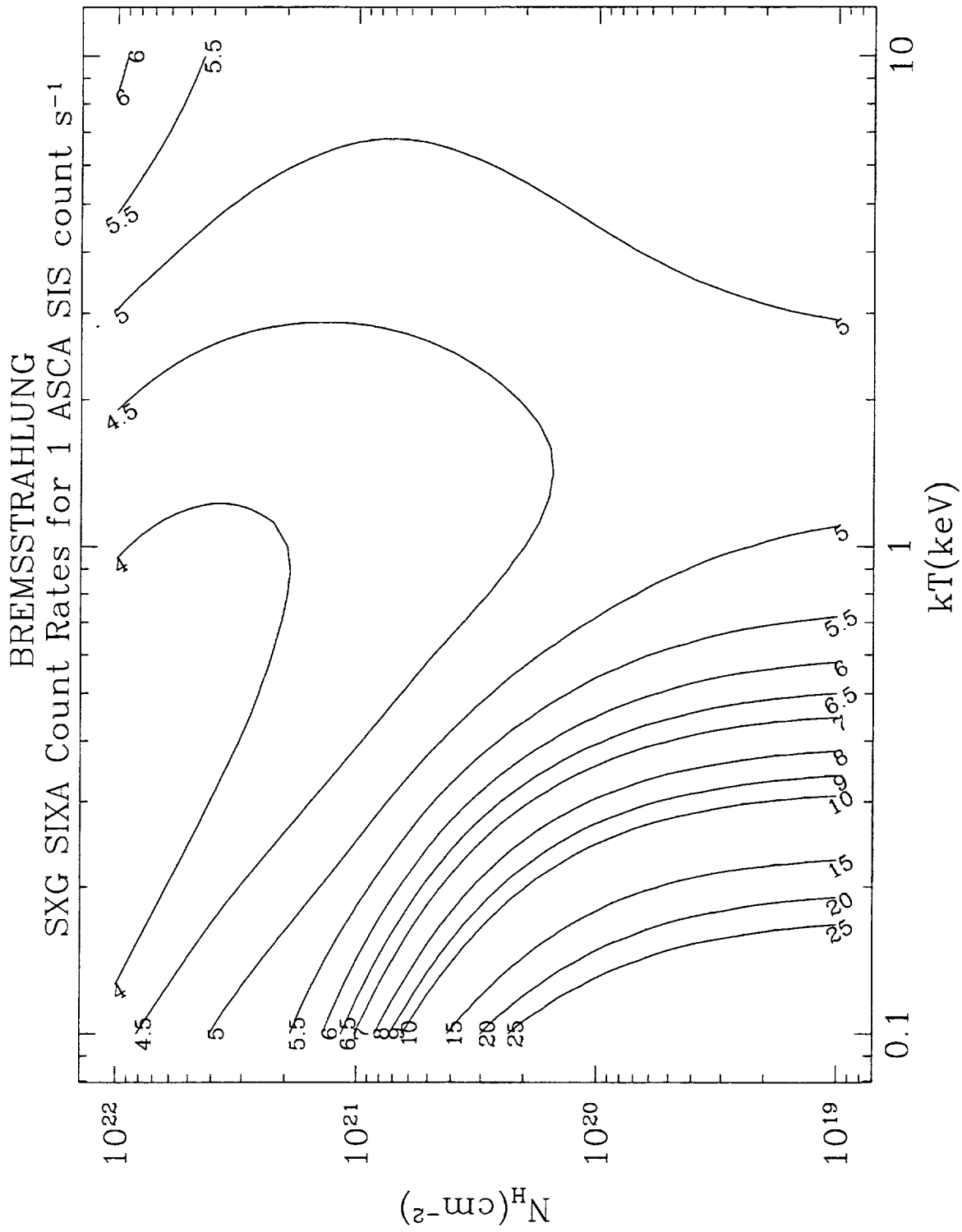

Figure 62: SIXA count rates yielding 1 ASCA SIS c s^{-1}, for a thermal bremsstrahlung spectrum.

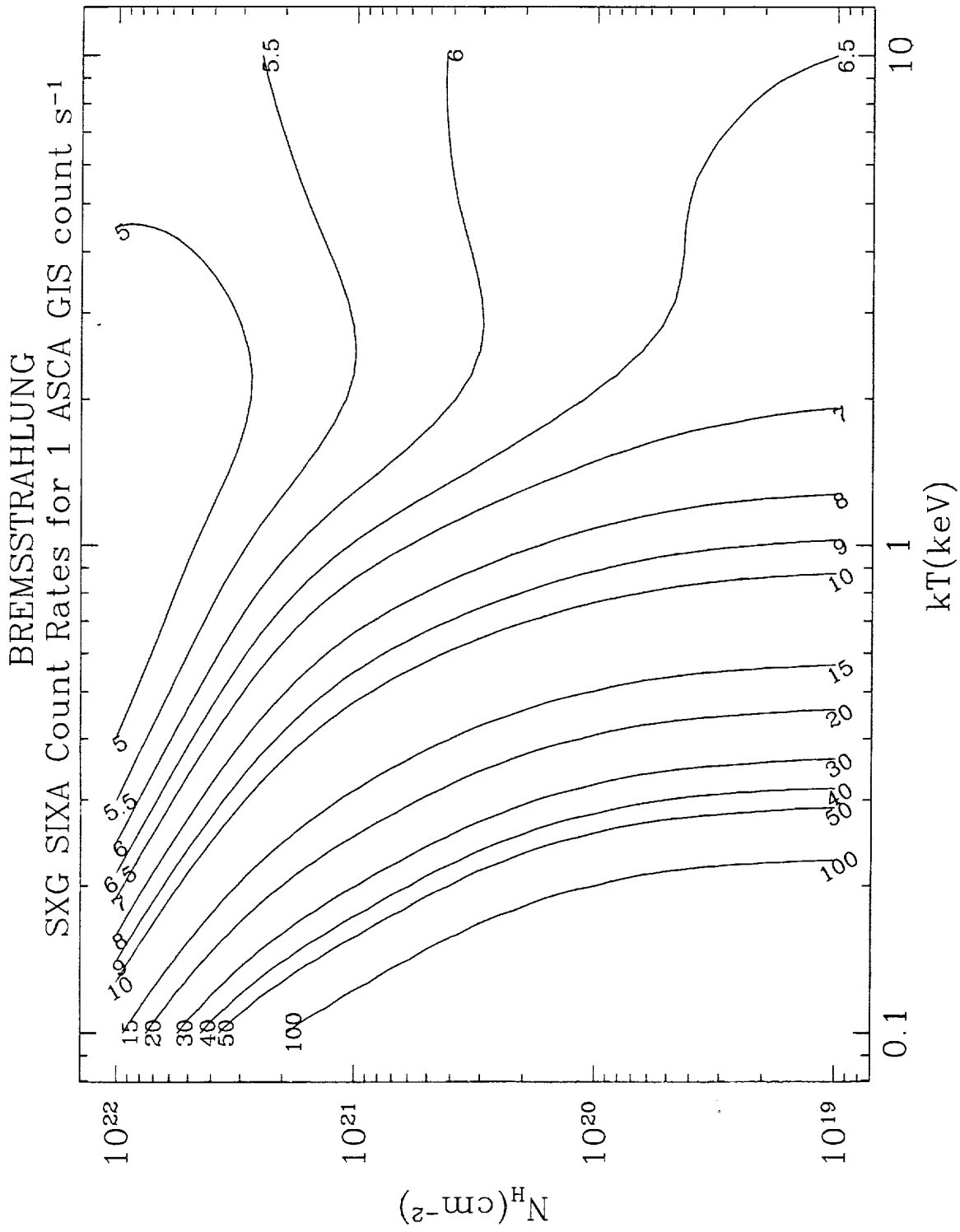

Figure 63: SIXA count rates yielding 1 ASCA GIS c s^{-1}, for a thermal bremsstrahlung spectrum.

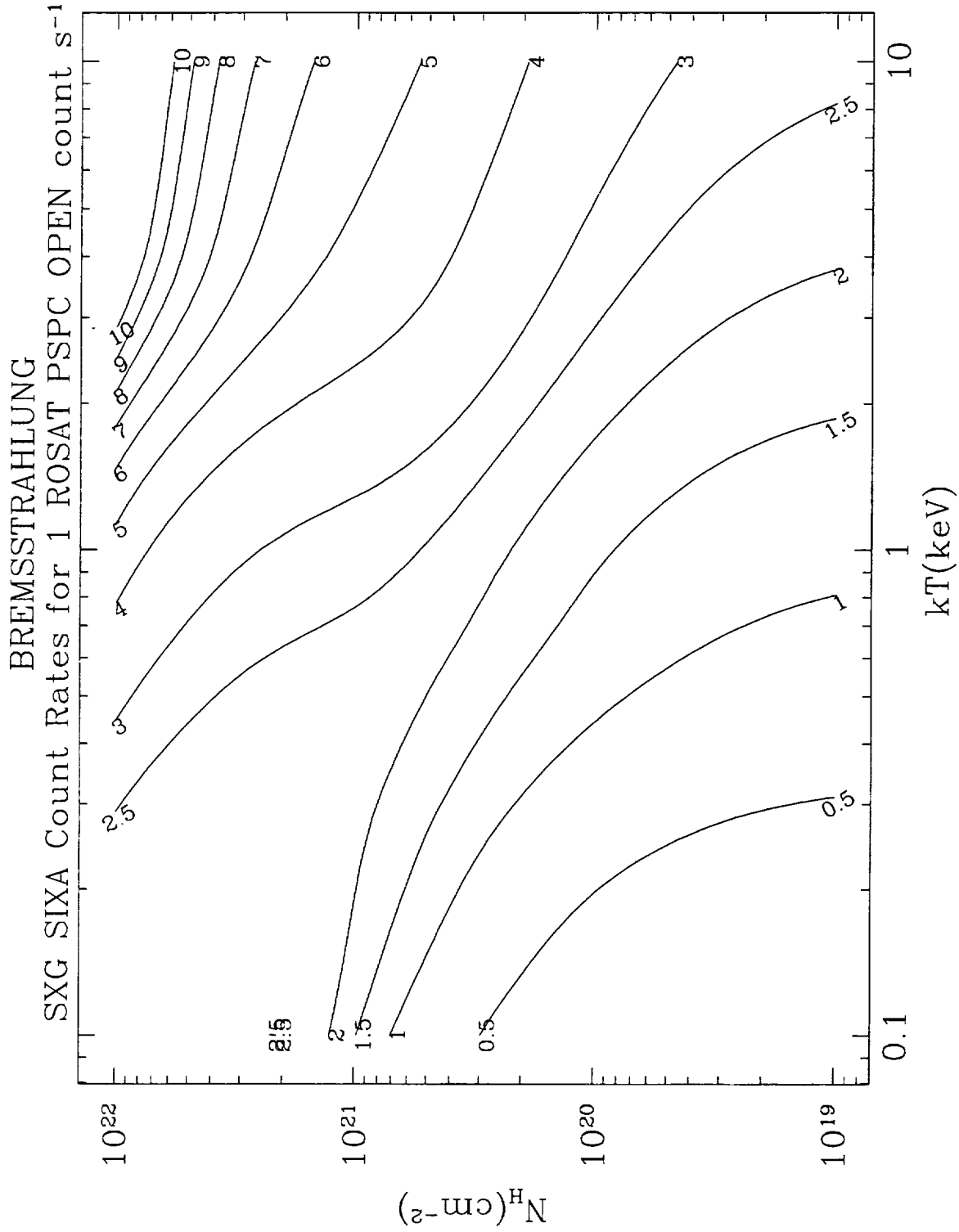

Figure 64: SIXA count rates yielding 1 ROSAT PSPC c s^{-1}, for a thermal bremsstrahlung spectrum.

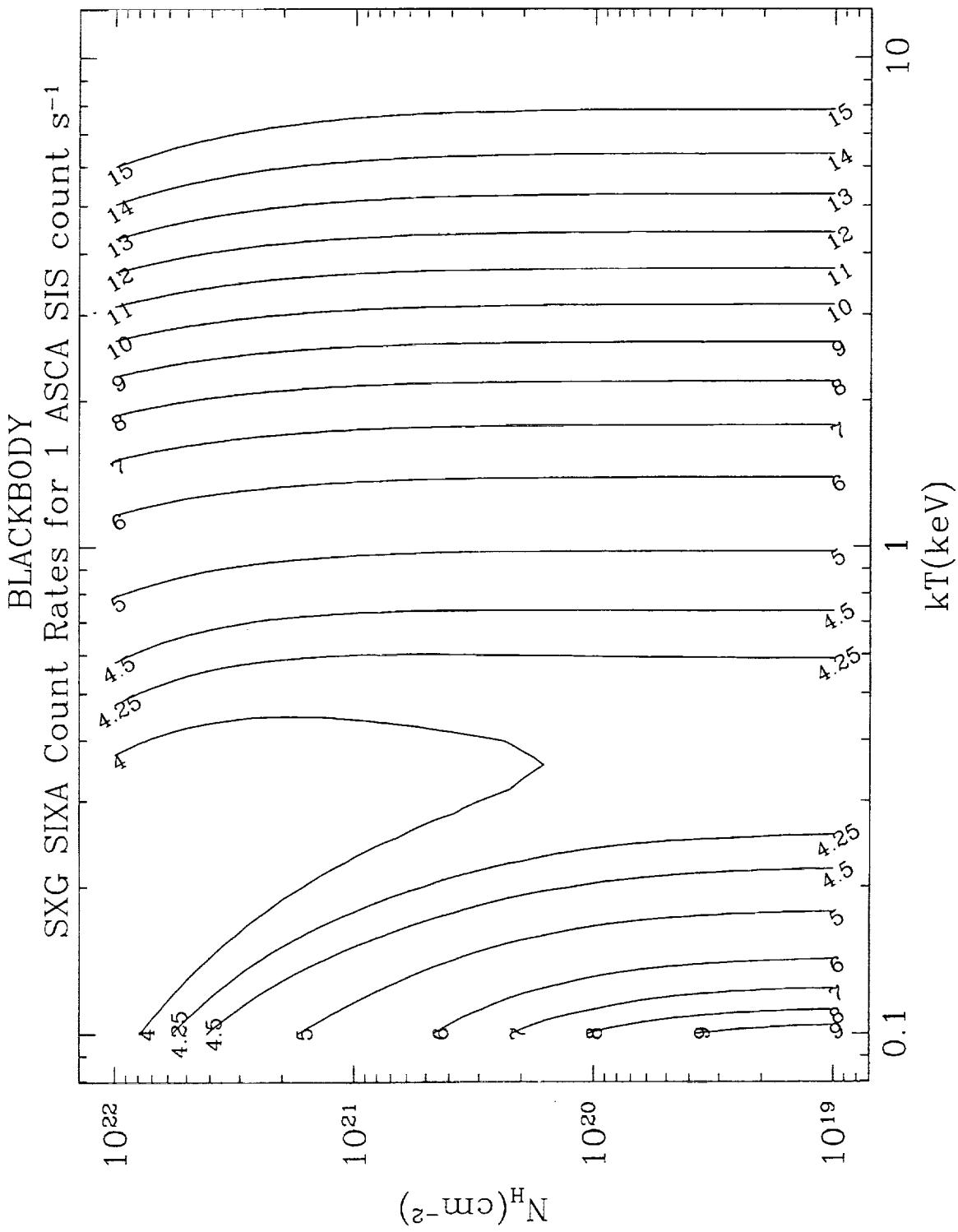

Figure 65: SIXA count rates yielding 1 ASCA SIS c s^{-1}, for a blackbody spectrum.

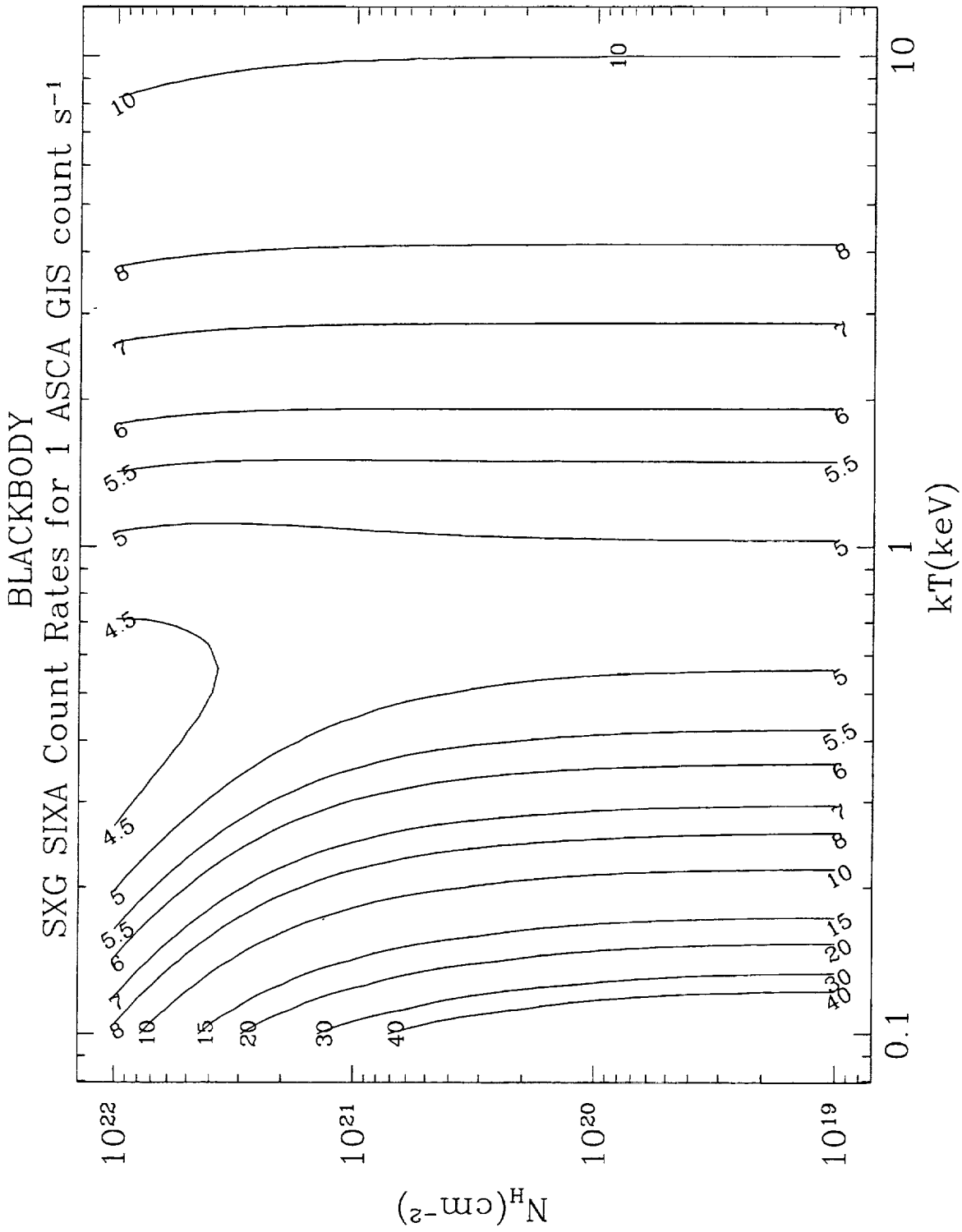

Figure 66: SIXA count rates yielding 1 ASCA GIS c s^{-1}, for a blackbody spectrum.

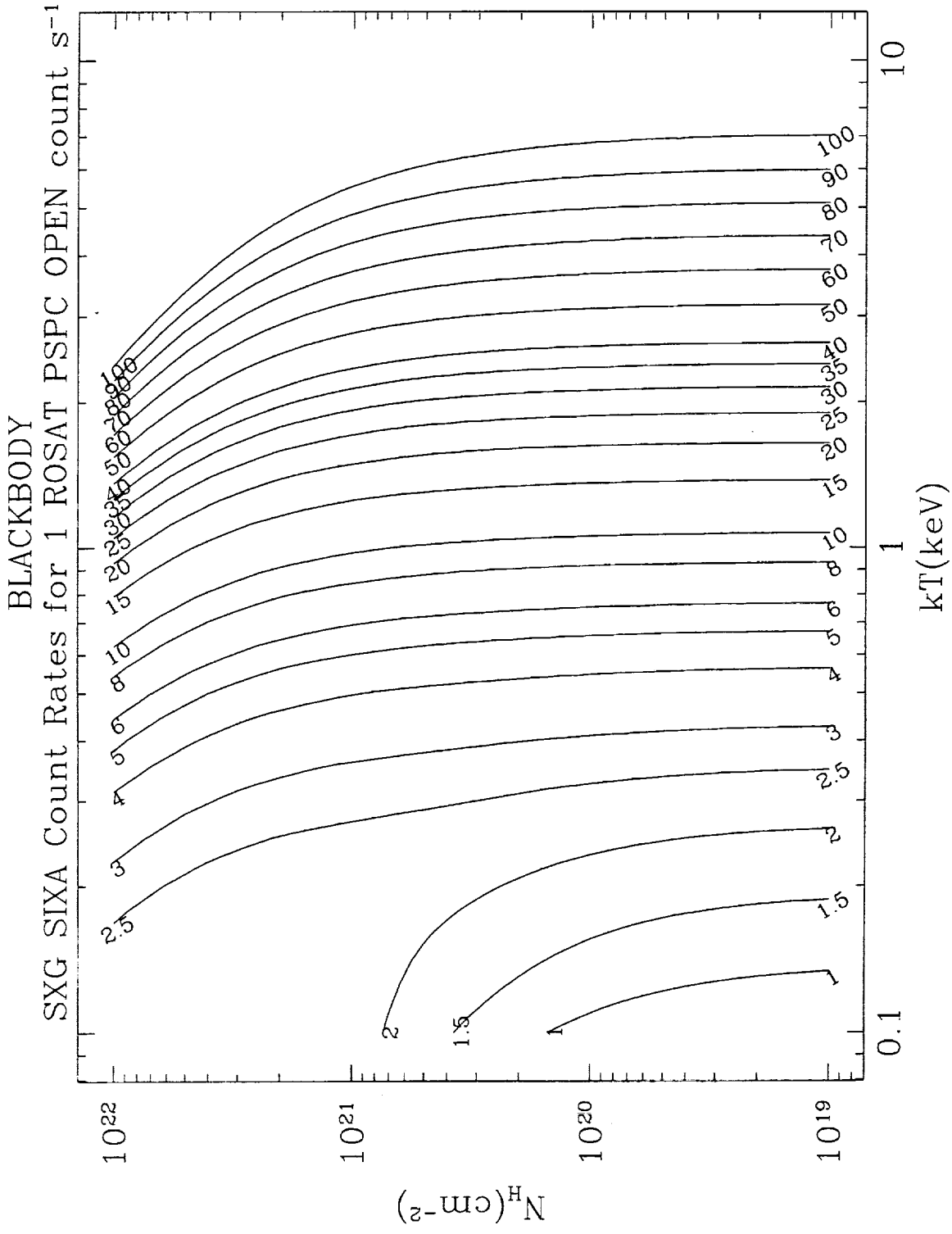

Figure 67: SIXA count rates yielding 1 ROSAT PSPC c s^{-1}, for a blackbody spectrum.

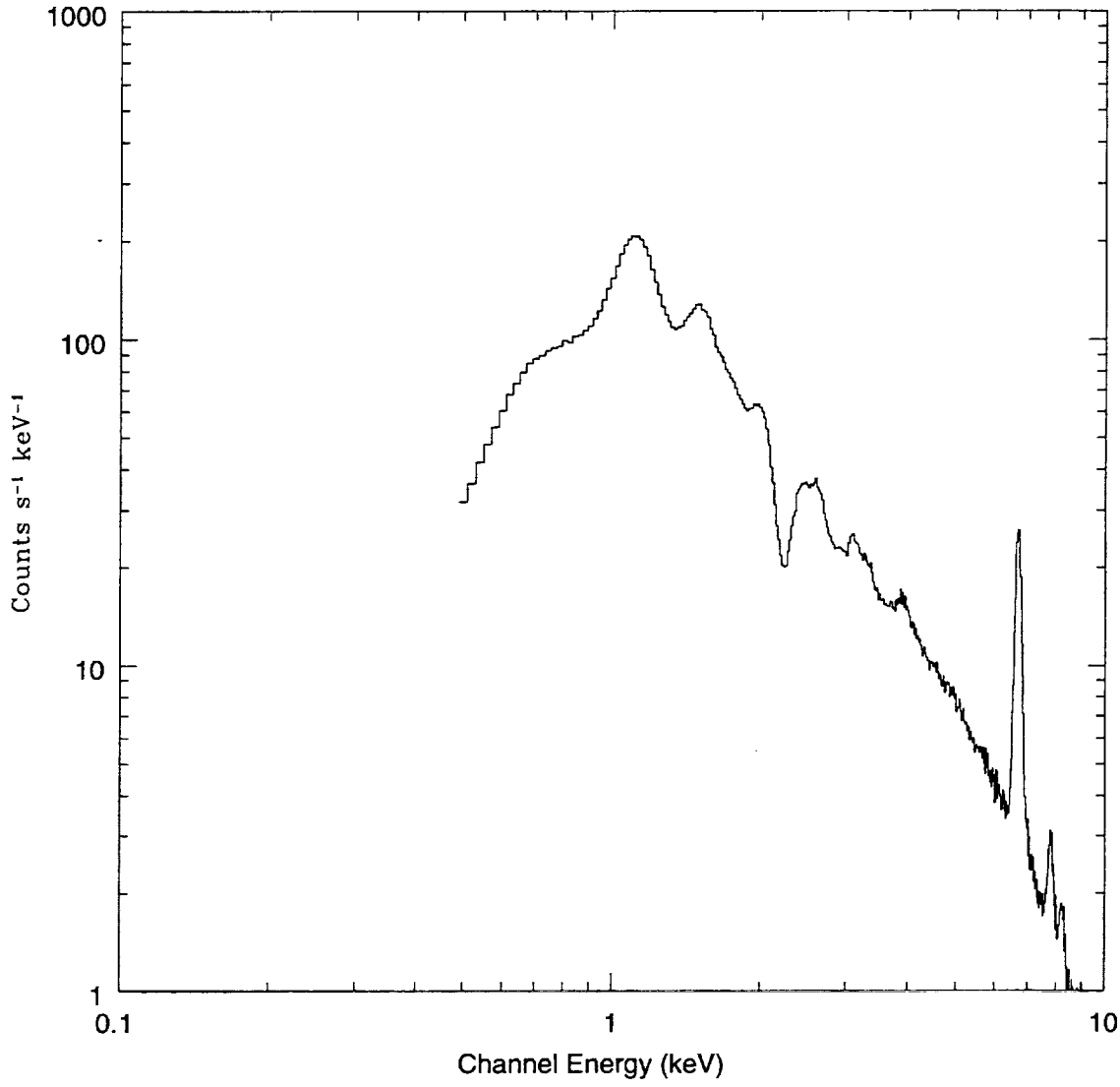

Figure 68: SIXA pulse height spectrum simulated with XSPEC. A 5 ksec SIXA observation of a Raymond-Smith plasma with cosmic abundances, emission integral of 10^{60} cm^{-3}, temperature of $10^{7.5}$ K, column density of 10^{21} cm^{-2}, and distance of 10 kpc is simulated.

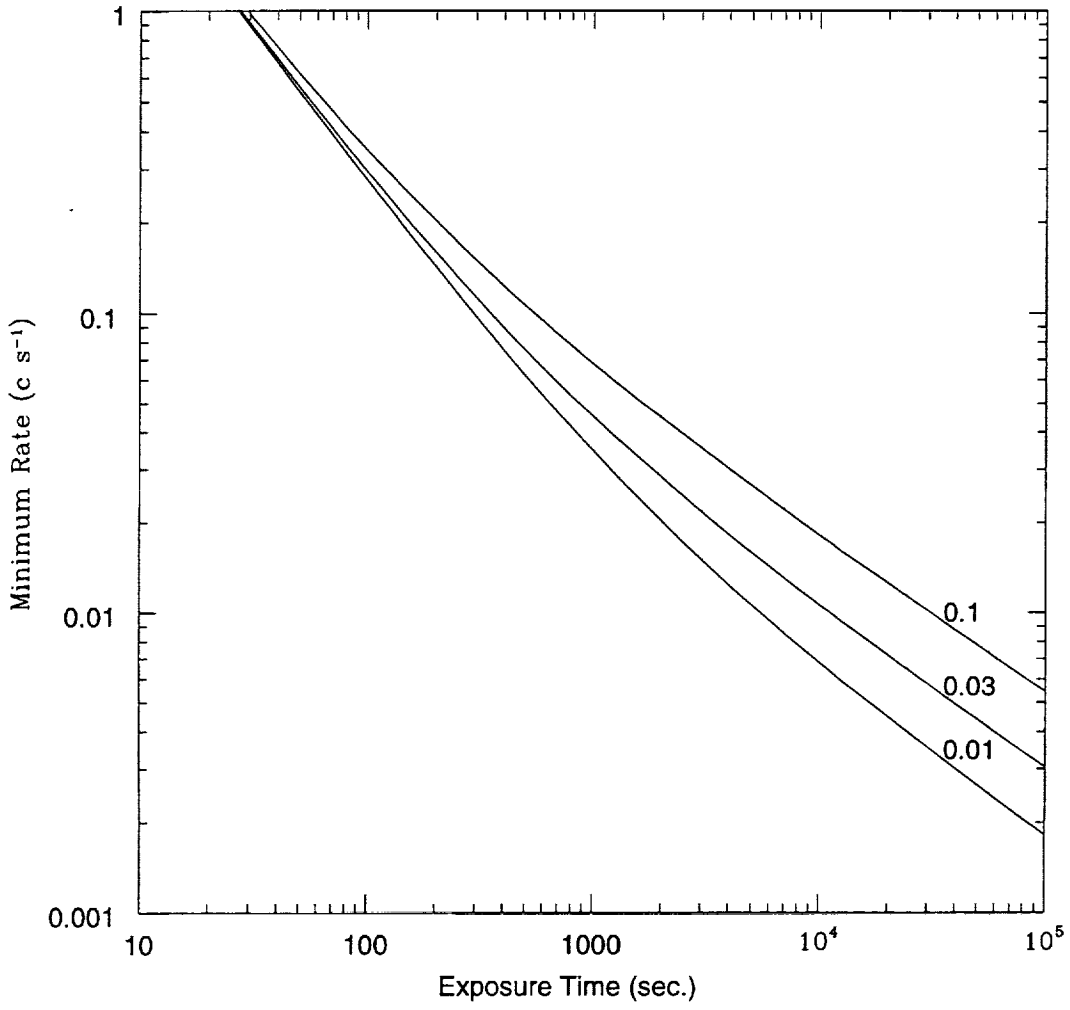

Figure 69: Minimum Count Rate Detectable by SIXA The minimum count rate for a 5σ count rate significance is plotted as a function of exposure time, for 3 different background rates (in c s^{-1}) in the central SIXA pixel, using the formula given in section 6.4.4.

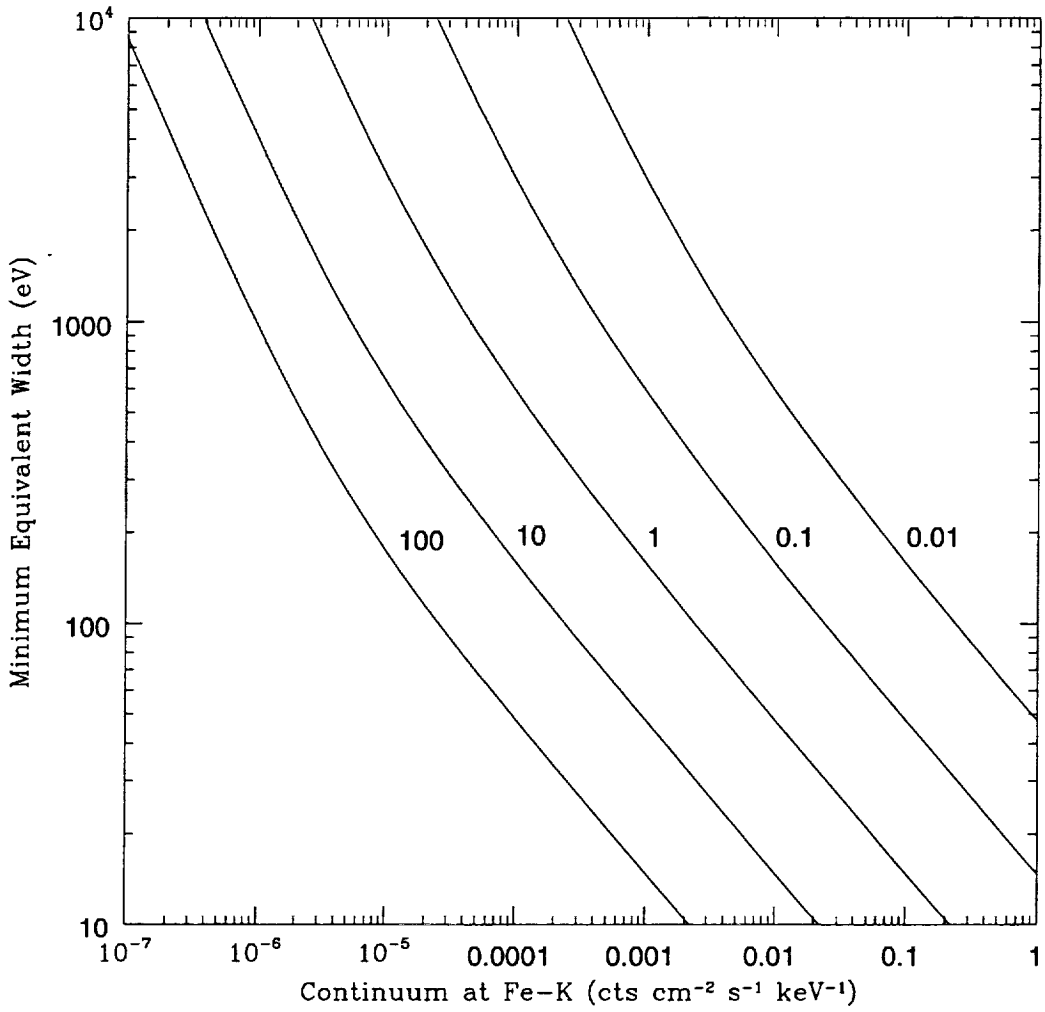

Figure 70: Minimum Equivalent Width at 6 keV detectable by SIXA The minimum detectable equivalent width at 6 keV is plotted as a function of source continuum, for 5 different exposure times in ksec, using the formula given in section 6.4.5. A 5σ significance is required and background rates of 3×10^{-3} counts cm^{-2} s^{-1} keV^{-1} (instrumental) and 6.6×10^{-7} counts cm^{-2} s^{-1} keV^{-1} pixel^{-1} (cosmic) are assumed.

7 The Stellar X-ray Polarimeter (SXRP)

7.1 Instrument Description

SXRP consists of two separate polarization analyzers: a thin mosaic graphite crystal that makes use of the polarization dependence of Bragg reflection, and a metallic lithium target that exploits the polarization dependence of Thomson scattering. The graphite crystal and lithium target are surrounded by four imaging proportional counters that detect the Bragg reflected and the Thomson scattered x-rays. The entire polarimeter assembly rotates about the optical axis of the telescope.

The Bragg polarization analyzer consists of a thin graphite crystal mounted above the lithium scattering target. A graphite crystal oriented at 45 degrees with respect to an incoming x-ray beam will reflect only those x-rays with energies satisfying the Bragg condition and with electric vectors lying in the plane of the crystal. If the incident beam is polarized, the intensity of the reflected beam will be modulated at twice the rotation frequency of the polarimeter. The Bragg polarimeter is sensitive in two narrow energy bands, the first order and second order Bragg peaks at 2.6 and 5.2 keV.

The angular distribution of x-rays scattered from the lithium target depends on the polarization of the incident x-ray according to the Thomson scattering cross-section. Maximum scattering occurs when the photon is scattered through an azimuthal angle perpendicular to the photon electric vector. Therefore, the intensity of scattered radiation for a polarized beam is, again, modulated at twice the rotation frequency. The energy band pass for the lithium polarimeter extends from 5 keV, limited by photoelectric absorption, up to 15 keV, limited by the reflectivity of the SODART telescope.

The IPCs are part of the scattering polarimeter subassembly of the SXRP and are used to detect x-rays which have passed through a polarization analyzer, either reflected from a graphite crystal or scattered in a metallic lithium target. There are four IPCs, forming a box which surrounds the graphite crystal and lithium scattering target. X-rays reflected from the graphite crystal fall on a small part of one of the IPCs. There is a small thin window which is devoted to imaging x-rays reflected from the graphite crystal. The remainder of the window area on each counter is used to detect x-rays scattered from the lithium.

To match the energy band pass of the graphite and lithium polarization analyzer, the IPCs must be efficient in an energy band extending from 2 to 15 keV. The x-ray energy is not significantly changed by Thomson scattering or Bragg reflection. Therefore, the accuracy with which we can measure the energy of incoming x-rays is determined by the energy resolution of the IPCs.

Since photons are scattered from the lithium over all angles, the detectors must intercept a large fraction of the solid angle; also, the distance from the target to the detector window must be at least 90 mm in order to reduce false polarization signatures due to spacecraft pointing errors. These two conditions lead to an active area requirement of 100 cm^2 for each counter, leading to a total active area of 400 cm^2.

A multiwire proportional counter with a single amplification stage, a wedge and strip cathode for position sensing, and a rear anticoincidence region are used. Each counter has an active area of 10 cm by 11 cm sealed with a beryllium window to eliminate the need for a gas system. The drift region is 3 cm. To have good efficiency up to 15 keV, the gas mixture

contains a large fraction of xenon – 50% Xenon - 40% Argon - 10% Methane.

Position sensing of the X-rays scattered by the lithium increases the effective modulation factor because it leads to more accurate determination of the scattering angle. Non-imaging detectors used in the same geometry would decrease the polarization sensitivity by a factor of 3. In addition, imaging allows continuous measurement of the background and its possible polarization signature.

A crucial parameter of the IPCs is their background rejection efficiency. The use of a polarization analyzer, Bragg crystal or Thomson scattering target, greatly reduces the number of detected X-rays. Low count rates imply a corresponding increase in sensitivity to background. For the lithium scattering polarimeter, the large active area required further increases the deleterious effects of the background. A low background rate is crucial for the operation of a sensitive polarimeter. The detectors employ five sided anticoincidence (rear and four sides) and anode pulse shape discrimination to reduce the background count rate.

The entire SXRP is contained in a single package with an envelope of 470 cm by 604 cm by 400 cm (not including the aperture cover) and an estimated total mass of 60 kg. The polarization analyzers and the four detectors are mounted on a rotating platform within the SXRP instrument. During normal observations, this platform under goes continuous rotation at a typical rate of 0.5 rpm. In the case of failure of a drive motor, a parafin actuator can be used to change the rotation platform drive to a redundant motor.

All of the preamps, signal processing and digitization electronics, and high voltage power supplies are mounted on the rotating platform. Only low voltage power and digital signal are passed, via a slip ring, between the rotating and non-rotating sections of the SXRP.

The non-rotating section of the SXRP contains a 96 MB mass memory, BIUS interface and control microprocessors, the rotation drive motors, and the low voltage power supplies. The SXRP electronics is divided into two separate, but non redundant parts. Each half of the electronics processes the data from two of the four IPCs. The rotation drive can be operated from either half of the SXRP. Both halves of the SXRP must function to provide optimal performance. However, if either half fails the SXRP will still function but with reduced performance. This design greatly reduces the potential for single point failures of the entire instrument.

7.2 Scientific Objectives

The Stellar X-Ray Polarimeter (SXRP) is the only orbiting X-ray polarimeter currently scheduled to be flown. It will be the only instrument available in the next decade able to extend x-ray observations to the full parameter space of the radiation. The primary processes which lead to polarized x-ray emission are non-thermal radiation and electron scattering of thermal x-rays in non spherically symmetric geometries. The degree and position angle of polarization from a source is highly dependent on the geometry of some feature of the source, (the feature can be the magnetic field, the scattering disk, etc.). Thus, polarization measurements provide a direct probe of the source geometry. Because the SXRP provides unique information about x-ray emission, it will enable us to make important statements about the properties of a variety of astrophysical sources.

Binary X-ray pulsars X-ray polarimetry will allow the study of the accretion geometry at the polar caps of magnetized neutron stars. Using the scattering polarimeter of the SXRP,

we will be able to measure the x-ray polarization of Her X-1 in five pulse phase bins and three energy bins with an average minimum detectable polarization of 5distinguish between the pencil and fan beam geometries. In addition, we will be able to measure the average polarization of a number of other X-ray binaries (Cen X-3, GX1+4, 4U1626-67, ...) to a level of a few percent in individual 105 second observations.

Supernovae remnants The only statistically significant (19 sigma) measurement of X-ray polarization of an astrophysical object was the 19which verified the synchrotron nature of the emission. SXRP can extend this measurement to other supernova remnants.

Accretion disk sources

Compton scattering from an accretion disk can lead to X-ray polarization. Polarimetry can provide information on the disk geometry.

Black hole candidates Inertial frame dragging around a rotating black hole (Lense-Thirring effect) can lead to a polarization vector that rotates with energy. Observation of such an effect could lend support the presence of a black hole and test a previously untested prediction of general relativity.

Radio pulsars X-rays from radio pulsars are believed to be due to a synchrotron radiation. The emission mechanism for optical pulses is unknown. X-ray polarization measurements would allow a comparison with optical measurements, providing information on the optical emission mechanism.

Soft X-ray transients A large fraction of soft X-ray transients are black hole candidates. X-ray polarization measurements could help determine the nature of these sources.

7.3 Operating Modes

There are four basic operating modes of SXRP:

1. Memory Mode - When the SXRP instrument is turned on, it comes up in the memory mode. In this mode, only the mass memory processor is operating; this processor is responsible for accepting and responding to commands on the BIUS interface and for maintaining data in mass memory (either from SXRP or from another scientific instrument on SRG). In this mode all detectors and high-volta- ge power supplies are turned off as are the stepper motors that operate the rotating platform. Power in this mode has been measured to be approximately 4 Watts for the engineering model (EM) SXRP. In the flight model (FM), total power should be 8 Watts.

2. Observation Mode - This is the normal operating mode of the instrument. In this mode, all normal subsystems are turned on including all detectors, all high-voltage power supplies, all processing electronics, and the motor that rotates the rotating platform. The Observation Mode is established by executing a series of BIUS commands from the Memory Mode. In the Observation Mode, detectors are operating in their normal configuration and scientific is being generated and accumulated in mass memory. Power in this mode was measured to be 20.4 Watts for EM, which contains approximately half of the electronics of the FM. The power dissipation of the FM, with one rotation drive motor operating in 0.5 rpm, is estimated to be 38 Watts.

3. Motor Transfer Mode - If one motor fails, it is possible to disengage that motor and engage a backup motor. This process involves powering a mechanical actuator based on the expansion of paraffin wax. This process is accomplished in the Motor Transfer Mode.

Note that this mode is only used in case of emergency and is not a normal operating mode. In this mode, motors are operating and energy is supplied to the paraffin actuators for approximately 3 minutes. High-voltage power supplies are turned off.

4. Graphite Transfer Mode - Normally, the graphite crystal is oriented so that incoming X-rays are reflected to one detector. If that detector fails, a motor can be commanded to rotate the crystal to reflect to an adjacent detector. This process is accomplished in the Graphite Transfer Mode. Note that this mode is only used in the case of emergency and is not a normal operating mode. Power during this mode has been measured to be about 25.5 Watts for the EM. This number should be roughly the same for the FM.

7.4 Calibration Programs

The SXRP flight model will be calibrated at Lawrence Livermore National Laboratory, with both a polarized and unpolarized X-ray source, prior to being shipped to Moscow. Individual detectors are also calibrated at Columbia University before integration with SXRP.

In-flight, each detector has, imbedded in the titanium strong back of the beryllium window, a small Fe-55 radioactive source. These sources were produced with an activity of 10 microCuries each in the autumn of 1992; by the autumn of 1995 the sources will have decayed and be producing a count rate of approximately 1 count per second in each detector. The 5.9 keV line of Fe-55 allows the gains of the detectors to be monitored throughout the flight.

SXRP has four on-board Fe-55 sources placed in the window of the detectors. Each source was approximately 10 microCuries in August 1992. The sources are imbedded in the detectors and emit no radiation detectable outside the SXRP.

7.5 Requirements on Operations

During observation mode SXRP will require 38 Watts of power. For a typical 24 hour observation, approximately 60 megabytes of data will be accumulated and stored in SXRP's mass memory.

A total pointing error (spacecraft pointing plus telescope alignment) of no more than 1 arcmin is required to reduce systematic errors in the polarization measurement to below the 1errors will necessitate the use of detailed modeling of systematic effects to extract the polarization information.

During radiation belt passage, the HV power supplies will be shut down.

In eclipse mode, SXRP will be put into memory mode.

7.5.0.1 Operation Requirements on Other Instruments Aspect data from Tauvex will be critical to achieve the best performance of the SXRP. Observations of bright point sources made with the HEPC or FRD in the same SODART tube as the SXRP, i.e. while the SXRP is not operating, will be needed to correlate the Tauvex aspect solution with the true SODART aspect. During the performance verification phase the SXRP will be used with the HEPC in the other SODART tube to monitor the SRG/SODART aspect.

For scientific observations, SXRP will be most effective if used in conjunction with MART and with SIXA, to monitor the complex time-dependent spectral evolution exhibited by

sources like Her X-1. If required by limitations in the SODART aspect control, the SXRP will be used with the HEPC in the other SODART tube to monitor the aspect.

7.6 Instrument Performance and Sensitivity

The performance of the SXRP is critically dependent on the effective area of the SODART telescope. Detailed evaluation of the performance of the SXRP will be presented after the SODART design is finalized.

The instrument sensitivity has been described in detail in a paper by Kaaret et al. (1994; SPIE, 2010, 22). Polarized radiation from a source will produce a modulation in the detected source count rate at twice the frequency of rotation of the polarization analyzers. THe count rate can be decomposed into a Fourier series in azimuthal angle given by

$$N(\phi) = \Sigma a_n \cos[n(\phi - \phi_n)]. \quad (1)$$

The magnitude of the polarization of the source is then given as $P = a_2(r+b)/a_0\mu r$ where μ is the modulation factor, r is the source counting rate, and b is the background counting rate. The modulation factor for is the modulation in the rate for 100% linearly polarized X-rays in the absence of background. The position angle of the polarization is given by ϕ_2. In a time T, the minimum detectable polarization, MDP, that can be detected at 99% confidence can be expressed as:

$$\text{MDP} = \frac{4.29}{\mu r}\sqrt{((r+b)/T}. \quad (2)$$

The MDP given above corresponds to a 2.6σ detection.

The expected and measured telescope effective areas and detector efficiencies can be used to estimate MDP. The effective area of the lithium polarimeter has a maximum of 65cm^2 at 9keV. The modulation factor, *mu*, varies from 0.77 at 6keV to 0.71 at 20keV. The detector efficiency is calculated to be 79% at 2.6keV and 97% at 5.2 keV. For the Bragg crystal polarimeter, the modulation factor μ exceeds 99%. A spectrum of $10E^{-2.05}$cm-2 photons cm-2 sec-1has been assumed along with an interstellar absorption of 3×10^{21} cm-2. This spectrum yields a flux of 2.4×10^{-8} ergs cm-2 sec-1 in the 2-10 keV band. The background was assumed to be 3×10^{-3} cts cm-2 sec-1 keV-1. For the graphite polarimeter, the background was integrated over an image diameter of 14 arcminutes. For the lithium polarimter, the signal was integrated over an energy band of 6-12 keV. Note that a single integration will produce three polarization measurements: two in narrow energy bands at 2.6keV and 5.2keV and a broad band measurement from 6-12keV which in principle can be resolved in energy if sufficient statistics are available.

Figure 71: Drawing of Stellar X-ray Polarimeter
This figure is a drawing of the functional components of the SXRP.

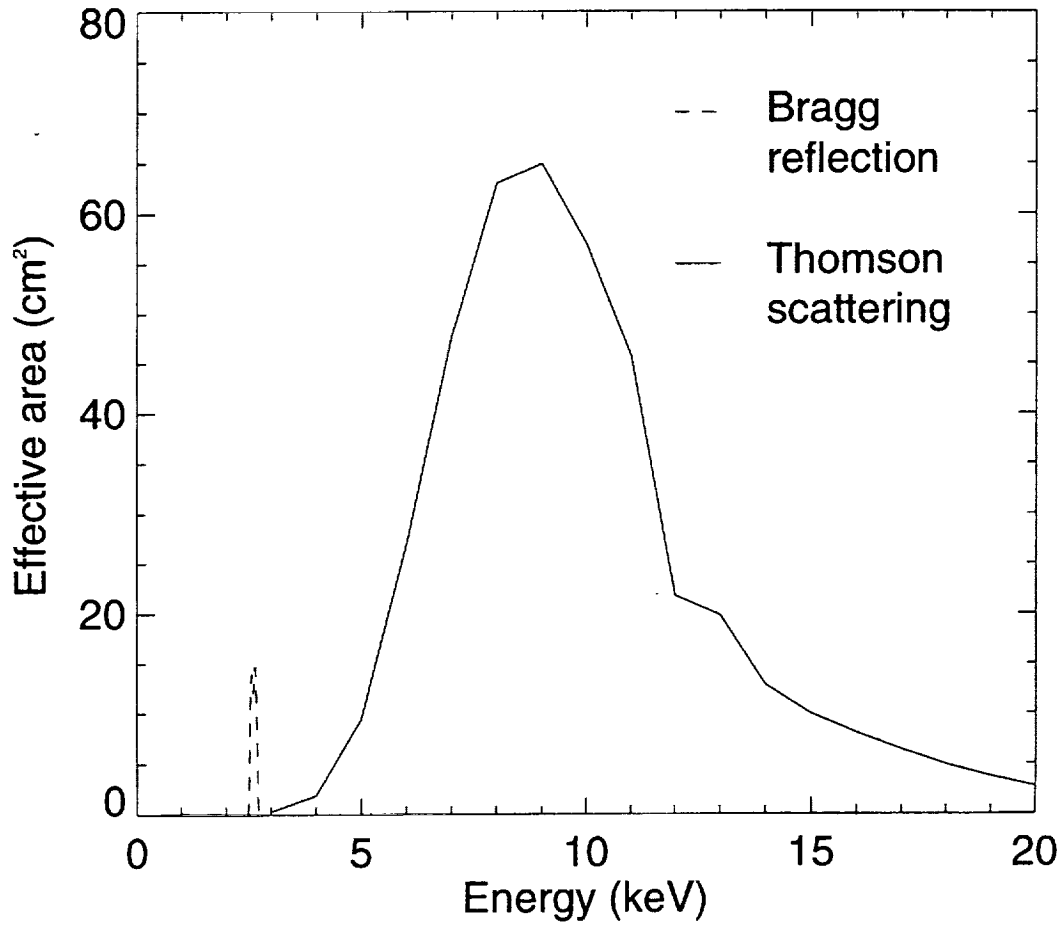

Figure 72: SXRP Effective Area
This figure shows the calculated effective area of SXRP which lies behind one of the SODART mirror modules.

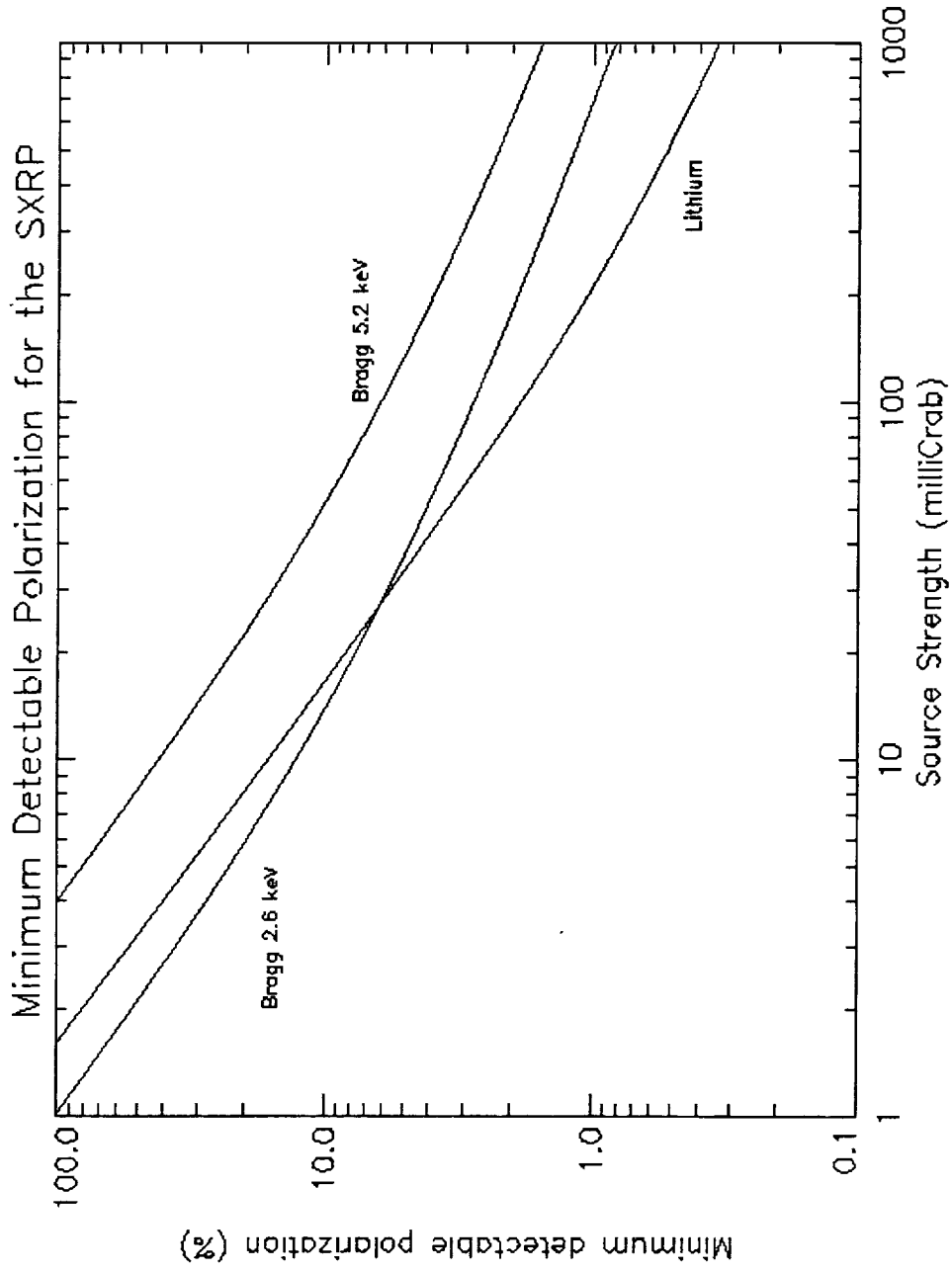

Figure 73: SXRP Minimum Detectable Polarization
The minimum detectable polarization for the two Bragg energy bands and for the broad Lithium energy band is shown.

Table 9: KFRD Detector Properties

Detector MWPC	filled with 85%Xe+10%Ar+- 5%CO2 at pressure 1.3 atm
Energy band	2 - 25 keV
Entrance window	120 mm diameter
Window Thickness	50 μm Be
Efficiency/effective area	0.98/1100 cm2 at E=5.9 keV 0.44/ 35 cm2 at E=22.1 keV
Energy resolution	17% at E=5.9 keV 9% at E=22.1 keV
Spatial resolution	0.5 mm at E=5.9 keV (10 arc sec in focal plane)
Angular resolution	2 arc min (limited by mirrors)
Timing	1/4096 ; $\sim$ 250μsec
Dead time	50μsec

8 Focal Plane X-ray Detectors (KFRD)

8.1 Instrument Description

KFRD consists of two instruments FRD-A (sled 1) and FRD-B (sled 2). Instruments FRD-A and -B are two identical and independent position sensitive x-ray spectrometers.

Position Sensitive Detector System (PSDS) includes: a Multi-Wire Proportional Counter (MWPC); Pulse Processing System (PPS) includes front-end electronics, discriminators and pulse shaping amplifiers, produces control pulses; Secondary Power Supply and High Voltage Supply (SPS-HVS) provide necessary voltage for PSDS and PPS; Information Conversion System (ICS) transforms analog pulses into digital code; Data Processing System (DPS) forms arrays of scientific and housekeeping information suitable for transmitting via the on-board information system (BIUS), receives and decodes commands, clock and synchropulses coming to KFRD; Output Channels System (OCS) maintains link with BIUS and telemetry systems of the spacecraft (receives relay commands and transmits analog information).

8.1.0.2 Design of the MWPC Internal volume of the MWPC is a cylinder 55 mm in height and 340 mm in diameter. The size of the position sensitive area of the MWPC is - 150x150 mm. The diameter of the entrance Be window is 120 mm. The support frame is installed on the window for compensation of internal gas pressure. X-ray calibrations sources, Fe-55 (5.89 keV) and source Cd-109 (22.1 keV), are integrated into the Ti body of the chamber beyond the entrance window zone over the sensitive area.

The system of electrode planes forms two layers. The first layer is position sensitive and spectrometric, the second one - only spectrometric. The second layer is also used for the anticoincidence system with the aim to reduce the charge particle background in the MWPC. All electrode planes are mounted on ceramics frames.

The first layer includes an amplification zone of 12 mm depth formed by the anode plane A and cathode planes K1 and K2 and two drift zones of 16 mm depth placed above and

under the amplification zone. A second layer of 6 mm depth is formed by the anticoincidence plane AC and the grounded plane D. The second cathode is formed from the AC-layer at the bottom of the chamber. The AC-layer has only an amplification zone.

Tungsten-rhenium gold wire is used for the anode planes and has a diameter 20 mm. The wire pitch in both layers is 3 mm. Anode wires of each layer are combined in two groups and connected with preamplifiers. The guard wires have diameter 100, 150 and 200 mm and are placed on the edge of the electrode planes for smoothing the edge plane influence.

Cathodes K1 and K2 and drift D planes are made of wire with diameter 100 mm, pitch - 1 mm, material - Be bronze. The delay line on discrete elements is used for determination of coordinate x-ray photon detection.

8.2 Calibration Programs

In-flight calibrations All calibration will be carried out for FRD-A and FRD-B (mode 1 and 2). Targets for calibration include:

1. Crab Nebula - 45 points covering the detector area in a "serpent"-shape with 100 sec observation per point plus 5 minutes for s/c maneuver.
   Expected Time Duration: 4 hours
   Aim: efficiency calibration
   Data Expected: 45-50 Mbyte

2. Point Source of the order 50 mCrab (type TBD)
   45 pointings covering the detector in a "serpent"-shape for 100 sec observation per point plus 5 minutes for s/c maneuver.
   Time Duration: 4 hours
   Aim: PSF calibration
   Data Expected: 10-15 Mbyte

3. Source of the order 50 mCrab (type LMC, SMC)
   Time Duration: 4 hours
   Aim: efficiency calibration
   Data Expected: 10-15 Mbyte

4. Source of the order 2 mCrab (type 3C273, 3C390.3, M82)
   Time Duration: 4 hours
   Aim: efficiency calibration
   Data Collected Amount: 1-2 Mbyte

5. Field without known sources
   Time Duration: 4 hours
   Aim: efficiency calibration and background determination

Data Collected Amount: 1-2 Mbyte

6. Out of the focus
   Time Duration: 4 hours
   Aim: background determination
   Data Collected Amount: 1-2 Mbyte
   Other Instrument: nearest DSRI Detector (for FRD-A) SXRP (for FRD-B)

8.3 Scientific Objectives and Feasibility of KFRD Observations

The KFRD detectors are similar to the HEPC detectors and hence have comparable scientific objectives and sensitivity. While the KFRD system has a somewhat better instrumental point response than HEPC, the SODART telescope system dominates the overall PSF determination. Therefore, for the purposes of this NRA, the KFRD detectors should be treated identically to HEPC. For detailed sensitivity calculations, see the sections on HEPC in this document. Count rate estimates may be made using the HEPC area and response in PIMMS and XSPEC.

REPORT DOCUMENTATION PAGE

Form Approved
OMB No. 0704-0188

1. AGENCY USE ONLY *(Leave blank)*	2. REPORT DATE	3. REPORT TYPE AND DATES COVERED
	August 1999	Contractor Report

4. TITLE AND SUBTITLE
The U.S. Spectrum X Gamma Coordination Facility
(Final Report for the period 10/11/94 – 4/30/1999)

5. FUNDING NUMBERS
NAS5-32779

6. AUTHOR(S)
PI: Dr. William R. Forman

7. PERFORMING ORGANIZATION NAME(S) AND ADDRESS (ES)
Smithsonian Institute
Astrophysical Observatory
Cambridge, MA 02138

8. PEFORMING ORGANIZATION REPORT NUMBER

9. SPONSORING / MONITORING AGENCY NAME(S) AND ADDRESS (ES)
National Aeronautics and Space Administration
Washington, DC 20546-0001

10. SPONSORING / MONITORING AGENCY REPORT NUMBER
NASA/CR-1999-209487

11. SUPPLEMENTARY NOTES
GSFC COTR: Dr. Donald West, Code 681

12a. DISTRIBUTION / AVAILABILITY STATEMENT
Unclassified–Unlimited
Subject Category: 90 89
Report available from the NASA Center for AeroSpace Information,
7121 Standard Drive, Hanover, MD 21076-1320. (301) 621-0390.

12b. DISTRIBUTION CODE

13. ABSTRACT *(Maximum 200 words)*

Spectrum-X-Gamma (SXG) provides for US participation in a first-class international x-ray mission. Despite launch delays, SXG will provide unique scientific opportunities due to its capability for all-sky monitoring, polarimetry, high resolution spectroscopy, and broad wavelength range–from the ultraviolet (TAUVEX and FUVITA), through the x-ray (SODART and JET-X), to the hard x-ray (MART), and gamma-ray burst detectors. Before describing our completed work, we review the unique properties of SXG and provide some examples of the scientific importance of SXG in the Chandra, XMM, and ASTRO-E era.

14. SUBJECT TERMS	15. NUMBER OF PAGES
Spectrum-X-Gamma, x-ray, Chandra, XMM. ASTRO-E, all-sky monitoring,	106
	16. PRICE CODE

17. SECURITY CLASSIFICATION OF REPORT	18. SECURITY CLASSIFICATION OF THIS PAGE	19. SECURITY CLASSIFICATION OF ABSTRACT	20. LIMITATION OF ABSTRACT
Unclassified	Unclassified	Unclassified	UL